Technology Collaboration Programme
by iea

December 2024

IEA Wind TCP Task 39 Phase 2

Final Technical Report

iea wind

Final Technical Report

IEA Wind TCP Task 39 – Phase 2
Quiet Wind Turbine Technology

Franck Bertagnolio **DTU Wind Energy (DK)**
Eoin King **University of Galway (IE)**

December 2024

Disclaimer:
IEA Wind TCP functions within a framework created by the International Energy Agency (IEA). Views, findings, and publications of IEA Wind do not necessarily represent the views or policies of the IEA Secretariat or of all its individual member countries. IEA Wind is part of IEA's Technology Collaboration Programme (TCP).

Executive Summary of IEA Wind TCP Task 39 Phase 2

Phase 2 of the IEA Wind Task 39 project was officially kicked-off in September 2021. Five countries officially participated to this second phase, and more than 50 engineers and scientists actively participated to the various collaborating activities. The latter were divided into four main work packages, each of which addressing a specific issue related wind turbine noise, from engineering to socio-psychological aspects. A fifth work packaged focused on dissemination.

The collaborative work was relatively fruitful due to the numerous interactions between the participants. This is illustrated by a significant number of publications directly related to the Task 39 activities. The numerous meetings that took place as part of the Task were also a platform for communication and dissemination. The main technical results and publications directly resulting from the task activities are provided as appendices.

Preface

This document is the Final Technical report for the 2nd phase of Task 39 – Quiet wind turbine technology, that was kicked-off in September 2021 and consequently terminated officially in September 2024, according to the maximum 3 years duration of IEA Wind TCP Tasks. The role of Operating Agents and management for this Task were shared between DTU (Denmark) and University of Galway (Ireland).

Numerous experts from many different countries did attend the Task meetings. A restricted list of countries formally participating to Task 39, as well as institutions or organizations in these respective countries from which experts have been participating to actual Task activities, are reported in Table 1.

Table 1 - IEA Wind Task 39 Participants during the period 2021-2024.

Country	Contracting Party	Active Organizations
Denmark	Danish Energy Agency (Energistyrelsen)	DTU, FORCE technology, Vestas
Germany	Forschungszentrum Jülich Gmbh	DLR, Uni. Stuttgart, Uni. Siegen, PTB, LUH, GE, Enercon, MS Hamburg
Ireland	Sustainable Energy Agency of Ireland	Uni Galway, SEAI, RPS Group
The Netherlands	Rijksdienst voor Ondernemend	TNO, TU Delft, Uni Twente
Sweden	Swedish Energy Agency (Energimyndigheten)	KTH

Table of Contents

Executive Summary 3
Preface 4
1. Background Information and Objectives of Task 7
1.1 WP1 - Interdisciplinary Education and Guidance 7
1.2 WP2 - Analysis and Reduction of Wind Turbine Noise Emissions 8
1.3 WP3 - Noise propagation modelling 8
1.4 WP4 - Assessing and Managing the Noise Effects on Health, Wellbeing and Consent 8
1.5 WP5 - Characterising non-noise influences on Noise Perception and its effects 9
2. WP1 – Interdisciplinary Education and Guidance 9
2.1 Fact Sheets 9
2.2 Expert group study report 9
2.3 A roadmap for required technological advancements to further reduce onshore wind turbine noise impact on the environment 9
2.4 International wind turbine noise regulation catalogue 10
2.5 Other disseminations 10
3. WP2 – Analysis and Reduction of Wind Turbine Noise Emissions 11
3.1 Wind turbine noise prediction code benchmark 11
3.2 Serration benchmark 11
3.3 Tip noise investigation 14
3.4 Low-Frequency Noise (LFN) study 15
4. WP3 – Noise Propagation Modelling 15
5. WP4 – Assessing and Managing the Noise effects on Health, Wellbeing and Consent 16
6. WP5 – Characterising non-noise influences on Noise Perception and its effects 17
7. Key Conclusions/Recommendations 18
References 18
Appendices 19
Appendix WP1 20
Annexes 1-3
Appendix WP2 54
Annexes 1-5
Appendix WP3 210
Annexes 1-5
Appendix WPs 4 and 5 272
Annex 1

List of Figures

Figure 1 - Turbulent inflow (Left) and Trailing edge (Right) noise model results from all participants for the test turbine.

Figure 2 – Four of the 5 wind tunnel facilities used in the project (Top left: DTU-PLC; Top right: DLR-AWB; Bottom left: TU Delft-LTT; Bottom right: TU Delft A-Tunnel).

Figure 3 – Two types of serration geometry tested in the project.

Figure 4 – Scaling of the $\Delta SPL\_1/3$ with flapped sawtooth serrations with the displacement thickness based Strouhal number at an effective angle of attack of 0 deg.

Figure 5 - Blade tip measured in DTU PLC wind tunnel

Figure 6 - Spatial distribution of Loudness levels in the study area

Figure 7 - Spatial distribution of Loudness levels in the study area

Figure 8 - Behavioural laboratory layout

List of Tables

Table 1 - IEA Wind Task 39 Participants during the period 2021-2024

1. Background Information and Objectives of Task

In additional to technical issues, societal acceptance is key to the wider deployment of wind energy in the future electricity production network. In some jurisdictions, there are concerns about the potential impact of wind turbine noise. The goal of Task 39 is to accelerate the development and deployment of quiet wind turbine technology and consolidate understanding of wind turbine sound emissions. The Task convenes an international expert panel to discuss and identify best practices in the prediction, measurement and assessment of noise and its environmental impact, as well as investigate regulatory aspects.

The target audience is rather broad. In a first place, dissemination work is meant to inform the public about the specificites of wind turbine noise in a non-technical language. In additions, more specialized documents aim at informing professionals working in related fields but not necessarily having the technical background, such as engineers, consultants, regulators or decision-makers. The main activities are centered around scientific collaborations and experts from all participating countries are invited to join the on-going collaborative efforts. During the 2nd phase of this task, numerous meetings were organised with different panel discussion, and a number of collaborative activities also took place.

This report is gathering the technical results obtained as part of the international collaborations conducted in the framework of Task 39 Phase 2, including some dissemination documents that have been published during this period.

The 2nd phase of Task 39 work programme was divided into five work packages:

- WP1: Interdisciplinary Education and Guidance
- WP2: Analysis and reduction of wind turbine noise emission
- WP3: Noise Propagation Modelling
- WP4: Assessing and Managing the Noise effects on Health, Wellbeing and Consent
- WP5: Characterising non-noise influences on Noise Perception and its effects

The main objectives of these specific WPs are explained, and more details about the specific activities conducted in these WPs are reported, in the following. Various technical reports and documents are included in the appendices. These have been drafted in collaboration with the experts contributing to these activities and their names are acknowledged as authors.

1.1 WP1 - Interdisciplinary Education and Guidance

These questions of how wind turbine noise affects people and how best to quantify the effects are not yet fully answered. Much work has been conducted at an international level across disciplines including engineering, regulations, physiology, psychology and sociology. This work package supports interdisciplinary discussions, as well as dissemination to the broader public. Communication within and across work packages are facilitated by this work package. The aim is for a consensus with robust, scientific and widely accepted knowledge, and transparent metrics for the effects of wind turbine noise. This work package has received outputs from the other work packages to facilitate dissemination of best practices.

A number of documents are published as a results of the present work package.

1.2 WP2 - Analysis and reduction of wind turbine noise emissions

This WP focuses upon the methods that are applied to analyzing, measuring, quantifying and qualifying, the generation of wind turbine noise. In the first phase of Task 39, WP2 has focused on modelling of WTN emission using prediction models and wind tunnel measurements. A wind turbine noise prediction code benchmark and a serration noise measurement benchmark activities were initiated. In Phase 2 of the Task, these efforts were continued with more active participants and more thorough investigations. In addition, activities related to specific noise generation mechanisms were initiated. Tip noise was investigated experimentally, and some efforts also concerned the issue of the Low-Frequency Noise content in wind turbine noise emission.

1.3 WP3 - Noise Propagation Modelling

This WP addresses noise propagation from the turbine to the receiver. There are many different empirical approaches to modelling the propagation of wind turbine noise ISO 9613, Nord2000 and other country specific approaches. These approaches have been validated for predicting wind turbine noise and generally work well, for frequency bands in the range from 63 Hz to 8000Hz, in rather flat and homogeneous terrain. With the advent of larger turbines and increasing offshore deployment some distance from shore, there is no internationally agreed method for predicting noise levels inland from offshore turbines. Noise from offshore turbines arising onshore need to be assessed for environmental impacts. Likewise, the known empirical approaches of wind turbine noise propagation on-shore fail in complex (forested, hilly) terrain and over extended distances. A number of comparison studies between task participants have been initiated to gain better knowledge on noise propagation over different surfaces and under different meteorological conditions. Those studies have been based on measurement data sets, like Utgrunden offshore noise propagation measurements (by KTH, Sweden), WEA-Akzeptanz project (by LUH, Germany), or the Perdigão-2017 campaign in Portugal (by DLR, Germany).

1.4 WP4 - Assessing and Managing the Noise Effects on Health, Wellbeing and Consent

This WP includes a programme of activities designed to assess the contribution of wind turbine sound to noise perception, annoyance, and the effects of these on health, wellbeing, and consent. Activities in this task include both lab and field-based psycho-acoustic annoyance testing, as well as exploring the possibility of using auralization and stimulus synthesis in annoyance assessments. Laboratory tests involve presenting calibrated wind farm noise samples under controlled conditions, potentially with additional visual or auditory stimuli, to measure annoyance thresholds, cognitive effects, and physiological responses. It was hoped that online testing might also be piloted to explore large-scale, high-fidelity data collection methods. .

1.5 WP5 - Characterising non-noise influences on Noise Perception and its effects

Social acceptance of wind turbines is driven to some extent by noise produced by wind turbines, but there is evidence of an effect in the reverse direction. That is, sensitivity to wind turbine noise may be driven partly by social acceptance, with lower acceptance driving greater sensitivity to such noise. To explore this complex relationship, proposed activities include a joint conference with Task 28 to build a network of researchers focused on the interaction between social acceptance and noise perception. Additionally, in parallel with the online tools of WP4, the task would hope to investigate online methods for assessing public consent by allowing individuals to sample projected wind turbine noise at various locations and distances.

2. WP1 - Interdisciplinary Education and Guidance

2.1 Fact sheets

A Fact Sheet about Low-Frequency Noise has been drafted during the 2nd phase of the task (see Appendix 1 - Annex 1). As a controversial subject and also a sensitive topic for the public, this document has undergone multiple reviews by various experts in order to reach a consensus about its content, or more precisely its correctness, conciseness and relevance.

In additions, a Fact Sheet concerning the issue of mechanical/tonal noise has also been circulated between participants, and has been released at the end of this project in Appendix 1 - Annex 2

2.2 Expert group study report

An expert group study report practice document addressing a priori technical requirements when conducting outdoor noise measurement of wind turbine noise has been produced by participants of WP3. This document is mainly addressed to researchers and engineers who may be relatively new to the field of outdoor acoustic measurement in general, and of wind turbine noise in particular. It does not intend to replace or be a substitute for the widely used IEC 64100-11 standard. The present document is available in Appendix 1 - Annex 3.

2.3 A roadmap for required technological advancements to further reduce onshore wind turbine noise impact on the environment

The aim is to identify the current needs in term of technology, and what it implies for the near/mid-term future scientific research goals, in order to close the scientific and technological gaps in the state-of-the-art knowledge of wind turbine noise for further reducing the noise impact. The content of the associated document, that has been drafted in collaboration as part of Task 39, stems from the discussions held during the forums on ‘Future Design of Low Noise Wind Turbines’ and ‘Source Prediction’ which took place at the Wind Turbine Noise conference in Lisbon, 2019. It has further been reviewed by numerous experts in the field.

This document is providing guidance on the most relevant research directions from an engineering perspective, namely: simulation methods, wind tunnel testing, and wind turbine design. Each topic is addressed separately and specific scientific challenges are identified. Future research directions that may improve our physical understanding of wind turbine noise, as well as facilitate the deployment of wind energy, are outlined. It is concluded that future scientific research on the topic of wind turbine noise should be conducted in a multi-disciplinary context to maximize its impact. The suggested topics shall be seen as a collection of what is seen as the most relevant topics across research and product development but shall not be seen as exclusive nor interlinked with specific development plans.

The resulting article has been published in WIREs journal and is freely available online following this link:
https://wires.onlinelibrary.wiley.com/doi/10.1002/wene.469

2.4 International wind turbine noise regulation catalogue

An important dissemination activity was initiated in the early phase of the project. It is concerned with a review of international wind turbine noise regulations. The goal is to gather noise limit regulatory schemes related to wind turbines in an exhaustive number of jurisdictions worldwide (at least where such exists) in the form of a catalogue. From there, an analysis is conducted in order to classify the various choices and their specific practical implementations in policies.

It is believed that this document should provide guidance to decision-makers and/or politicians in countries that are in the phase of developing or increasing wind energy integration in their energy system, but facing inadequate noise regulations for this purpose.

The document has been drafted with contributions from various worldwide experts in the field providing data. The information are integrated as an online database, as part of the OSF (Open Science Foundation) and can be consulted online following this link:
https://osf.io/2u58w/

It is meant as an interactive tool and the information can be updated in the future by international experts in the field, so that this document remains a state-of-the documentation on wind turbine noise regulations.

2.5 Other disseminations

Different Task 39 activities were presented at various conferences. These contributions are reported below and the conference papers are available in Appendices

Note: WP4 and WP5 are concerned about the psycho-acoustic aspects of wind turbine noise. Both groups are populated by experts from the fields of engineering and psychology. It was highlighted earlier that the group might need to develop an efficient knowledge exchange programme, so experts from different backgrounds could can communicate effectively. For example, annoyance is an important concept to both fields, but depending on one's background the discussions on annoyance might deviate into another field. To address this issue, a seminar featuring presentations from experts in both Engineering and Psychology was held, and followed by an open discussion forum. This seminar is available for all Task Members to view. This knowledge exchange will through a shared working

document (hosted on the Open Science Framework https://osf.io) to enable effective collaboration and joint definitions of technical concepts.

3. WP2 - Analysis and reduction of wind turbine noise emissions

3.1 Wind turbine noise prediction code benchmark

The aim of this benchmark is to compare and validate wind turbine rotor noise codes that are developed by the participants of Task 39. This benchmark is joined to a similar effort conducted as part of Task 29. Task 29 is mainly concerned with aerodynamic and aeroelastic features but it also has a WP dedicated to acoustics. Here, the focus is on aerodynamic noise generation, hence mechanical noise as well as long range propagation effects are not considered, at least in the first phase of this benchmark.

The main conclusion of the study is that all wind turbine noise prediction codes more or less falls into the 2dB margin error of standard IEC noise measurements of wind turbines, making it difficult to favouritize a specific degree of fidelity at a first glance. However, some trends were observed between low and high-fidelity methods. This could also indicate that better accuracy is needed in term of noise source measurement techniques in order to reduce these errors. Task 39 activities also included comparisons at airfoil levels in order to cross-validate models among participants, and to investigate some specific mechanisms at airfoil levels that reflects on the overall wind turbine noise emission (e.g. directivity).

The description of this project (benchmark definition) and the technical report are provided in Appendix 2 - Annex 1. In addition, the results of the overall study were presented at a conference (see Appendix 2 - Annex 2). An example of the results obtained during this study is displayed in Figure 1.

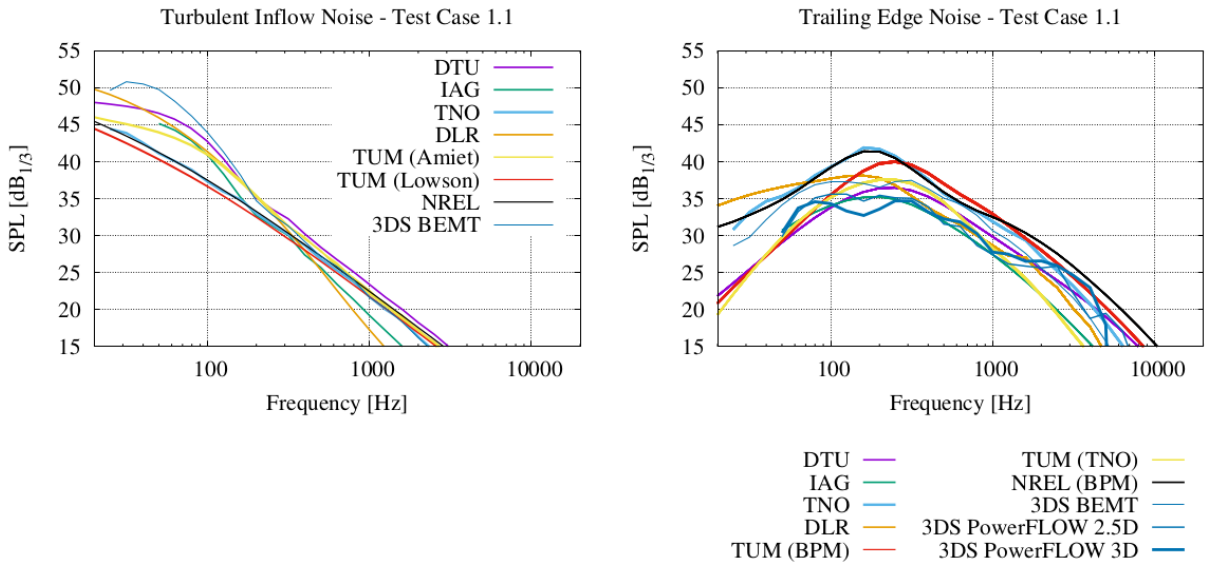

Figure 1 – Turbulent inflow (Left) and Trailing edge (Right) noise model results from all participants for the test turbine.

3.2 Serration benchmark

Trailing edge serrations have been widely used to reduce trailing edge noise of wind turbine blades. However, large uncertainties in terms of analytical and computational modelling as well as testing do persist. The challenges in wind tunnel testing are found in the low signal to noise ratio, because an aerofoil equipped with trailing edge serration is very quiet and background noise in the aeroacoustic test setup can become dominant.

Three leading groups working with aeroacoustics (5 wind tunnel test facilities in total, see Figure 2) in Europe joined forces to quantify these uncertainties in testing. The participating institutions are: Technical University of Denmark (DTU, DK), German Space Agency (DLR, DE), and Delft University of Technology (TU Delft, NL). During Phase 2 of Task 39, University of Twente (NL) and University of Berlin (DE) (also NREL (USA) as an observer, since USA are not officially part of Task 39[*]) joined this effort.

The strategy was to test the same aerofoil model in the different facilities in order to compare results and quantify the spread of the data. In order to achieve these objectives, two models of the same aerofoil shape but of different size were tested in 5 different facilities. Exchanging the same model reduces the uncertainty in geometry that is usually present when manufacturing different models with the same theoretical geometry. The model were equipped with exactly defined serration geometries that were also produced at one place and shipped to the different facilities (see Figure 3).

All measurement campaigns (in the 5 test facilities) planned for the present study have been collected. A collaborative effort for the analysis and cross-comparisons of the different results has been conducted. As an illustration of this, results from 2 separate wind tunnels (DTU/TU Delft) could be analyzed and compared using noise emission scaling rule, so that the comparisons can make sense, in Figure 4. A good agreement between the 2 set of results is observed in a given frequency range. This also illustrates the fact that different facilities can contribute to investigate noise emission (from serration or other devices) as they can focus on different part of the mechanism. The fact that the scaled results agree within the overlapping range of the two frequency domains is paramount to ensure the validity of the results.

A results of the study were published at the AIAA/CEAS 2022 conference (see Appendix 2 - Annex 3) and a journal article is being drafted (at the time of writing of the present report). Further conclusions about the project are reported in Appendix 2 - Annex 4.

[*] Note that NREL is managing a similar effort about acoustic wind tunnels' assessment, and Task 39 was also a platform for participating to this effort and coordinating the activities respective to each project.

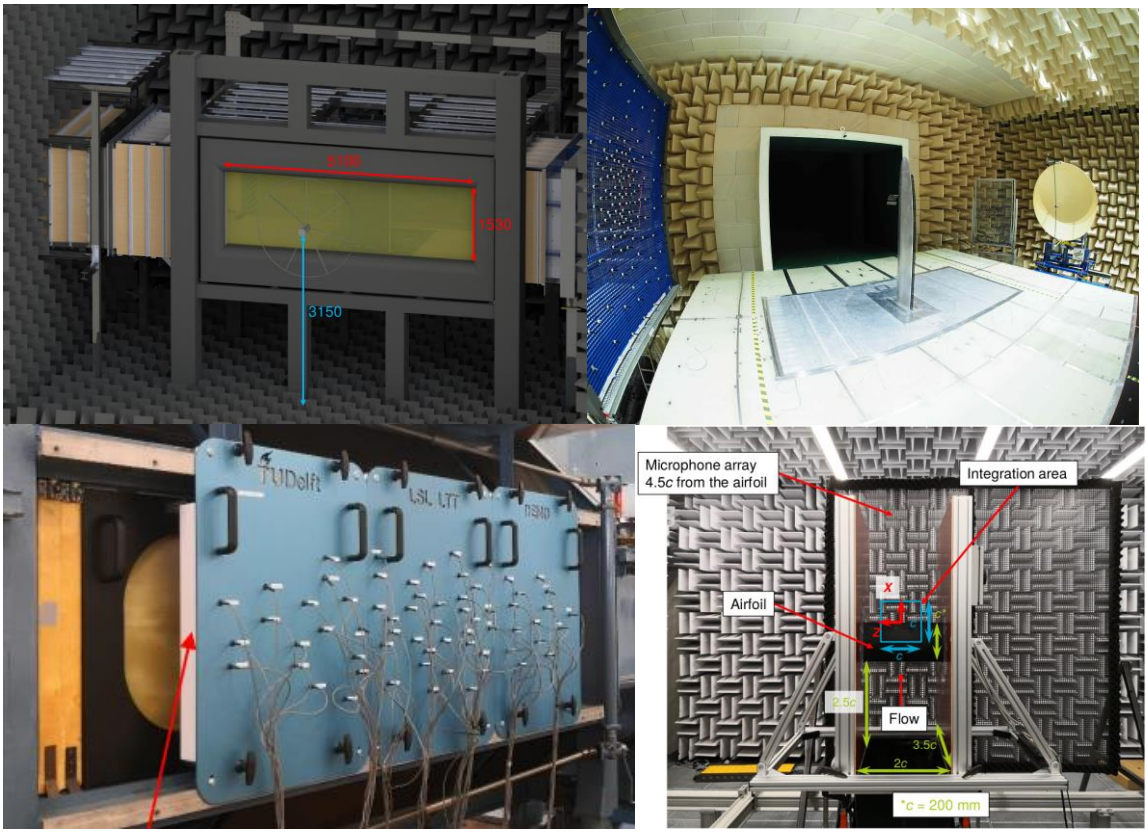

Figure 2 – Four of the 5 wind tunnel facilities used in the project (Top left: DTU-PLC; Top right: DLR-AWB; Bottom left: TU Delft-LTT; Bottom right: TU Delft A-Tunnel).

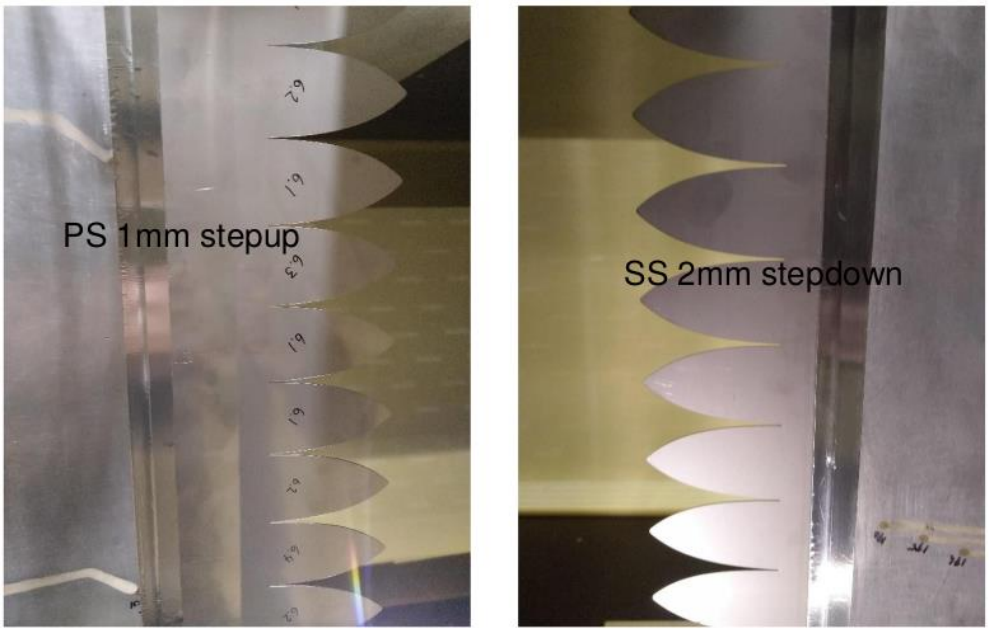

Figure 3 – Two types of serration geometry tested in the project.

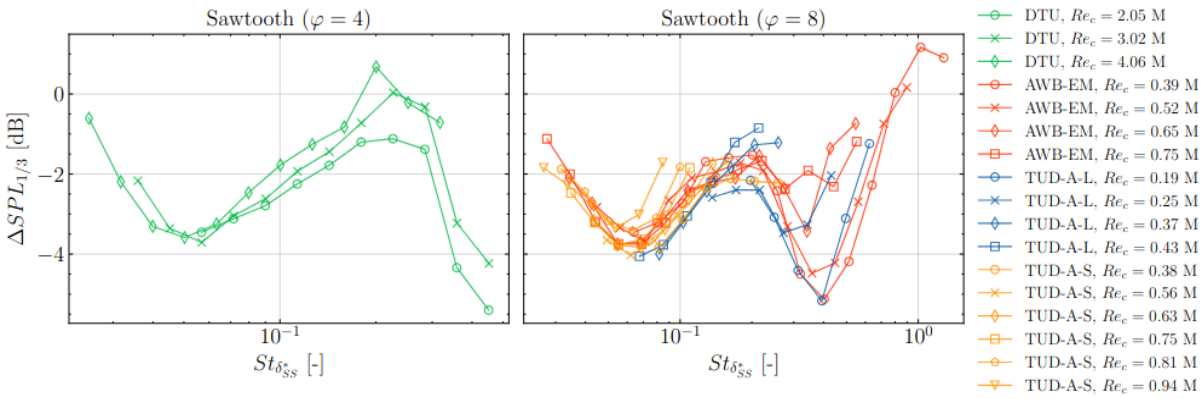

Figure 4 – Scaling of the Δ*SPL*_1/3 with flapped sawtooth serrations with the displacement thickness based Strouhal number at an effective angle of attack of 0 deg.

3.3 Tip noise investigation

In parallel with the evolution of wind turbine design, it appears possible that winglets may be applied at the tip of future wind turbines (in the same way that it is now current on commercial airplanes). To the best author's knowledge, some winglets have already been tested on MW side wind turbines. The tip of the blades being the part that emits most of the aerodynamic noise, it can be expected that tip design should also consider noise emission in the future.

The present activity is centered on establishing an experimental database. Wind tunnel noise measurement of an unconventional tip were conducted at the DTU PLC wind tunnel facility. The database is being processed to be released publicly in the near future. In addition, some ongoing work addresses the improvement of engineering tip noise models, which are currently very questionable in terms of accuracy.

A picture of the wind tip model mentioned above, as measured in the DTU PLC wind tunnel is provided in Figure 5.

Preliminary of the study were presented at the WTN2023 conference (see Appendix 2 - Annex 5).

Figure 5 - Blade tip measured in DTU PLC wind tunnel

3.4 Low-Frequency Noise (LFN) study

The initial plan was a collaboration with IEA Wind Task 40 (Downwind turbine). Downwind turbine are well known to produce high levels of (essentially low-frequency) noise. Before the start of this 2nd phase of Task 39, there was ongoing negotiations between Hitachi (Japan) and participants of Task 40 to share some noise measurement data acquired on some of their operating turbines. Unfortunately, later Hitachi withdrew its offer and it was not possible to conduct the initially planned activities based on these measurements as part of the present task.

At the time of writing, DTU is developing an engineering numerical framework to predict LFN from the interaction between blade and tower. The final goal is to validate the results obtained by other Task participants (IAG Stuggart) showing that this blade-tower interactions is actually the dominating part of LFN as far as large wind turbines are concerned.

4. WP3 - Noise Propagation Modelling

This WP aims at assessing the reliability and accuracy of current state-of-the art modeling frameworks for wind turbine noise propagation. The work was mainly divided into two parts. A first part concentrates on flat terrain (including offshore, see Appendix 3 - Annex 4) and the second on complex terrain (see Appendix 3 – Annex 1). In both cases, two strategies are implemented in order to validate the models: either conduct code-2-code comparisons, or confront the model predictions with actual field measurements.

The project results shows that noise propagation predictions are very sensitive to the numerical solution methods. Due to the inherent complexity of the phenomenon, it is also

sensitive to the environmental conditions, many of which are difficult to monitor (e.g. atmospheric turbulence and other wind homogeneities).

The project results were published in two conference papers drafted by Task 39 participants, and presented at Forum Acusticum 2023 and DAGA 2024 (see Appendix 3 – Annexes 3 and 5). An overall and extensive technical report for this WP is also available in Appendix 3 – Annex 2.

5. WP4 - Assessing and Managing the Noise effects on Health, Wellbeing and Consent

The technological advances from WP4 focused on enhancing the understanding and assessment of wind turbine noise impacts through innovative methods and tools. Key advancements include the development of noise annoyance maps and listening experiments to model and assess wind turbine noise, with a focus on community response. The objective was to map factors that may influence annoyance instead of simply plotting a noise level alone.

Figure 6 plots the loudness levels surrounding a candidate wind farm. It is possible to plot a variety of sound quality indicators (such as loudness, sharpness, roughness, fluctuating strength), instead of a traditional noise level (in terms of L_{Aeq}, or L_{90} for example). Then by considering results from controlled listening tests, it is possible to link these sound quality metrics to % of people who may experience annoyance (Figure 7).

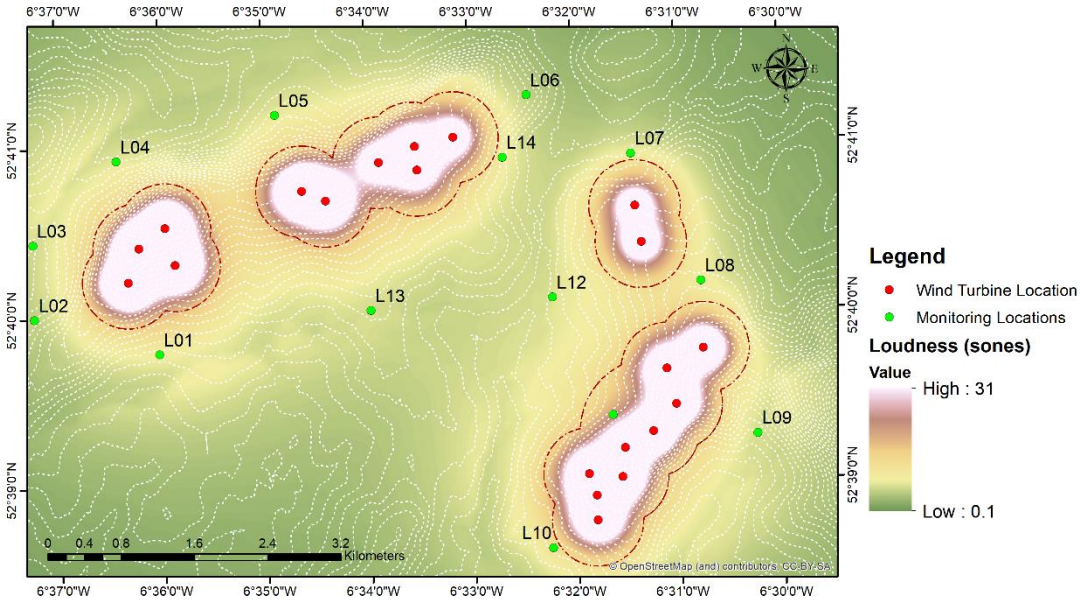

Figure 6 - Spatial distribution of Loudness levels in the study area.

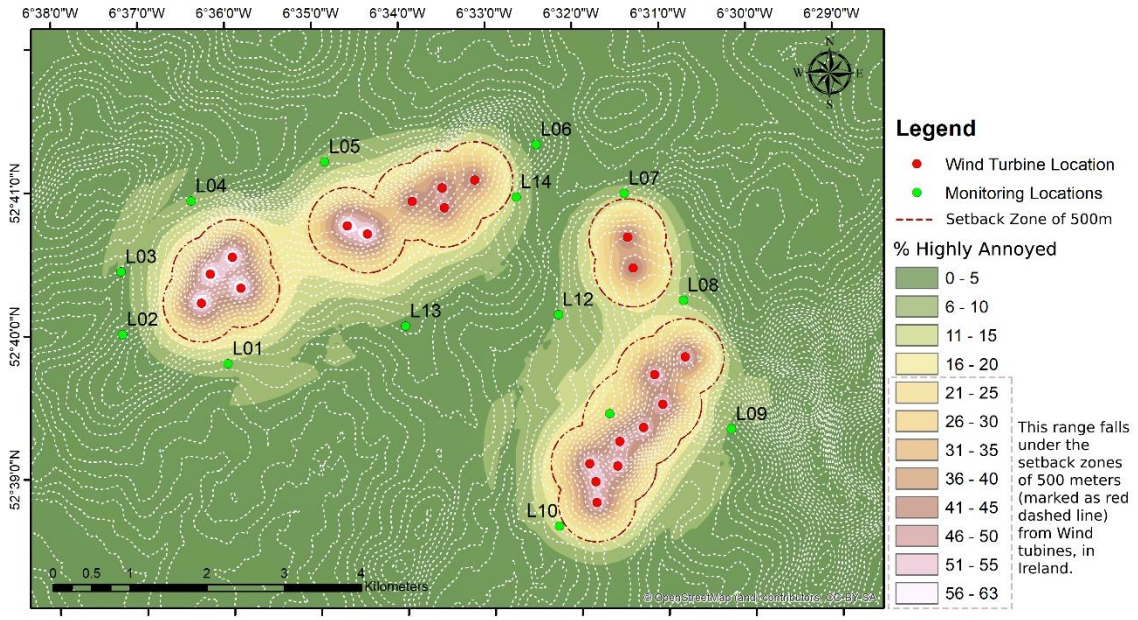

Figure 7 - Spatial distribution of Loudness levels in the study area.

The above approach was applied to a candidate Wind Farm in Ireland. A relationship between Loudness and the percentage annoyance was developed, while exploring the method to map the annoyance levels spatially. The findings reveal that Loudness is the primary factor contributing to WTN-related annoyance, while other psychoacoustic indicators have a limited role in explaining this perception. However, fluctuation strength, particularly with an amplitude modulation range of 0.5–20 Hz and a peak around 4 Hz, emerges as a promising indicator for further investigation, despite WTN typically having a modulation of amplitude closer to 1 Hz.

Efforts in interdisciplinary collaboration have also led to enhanced noise measurement frameworks, integrating meteorological, acoustic, and operational data to better understand the relationship between noise characteristics and annoyance. A journal article describing the annoyance map is forthcoming, with a separate article describing some listening tests that were conducted to assess the accuracy of various sound quality indicators in predicting annoyance.

6. WP5 - Characterising non-noise influences on Noise Perception and its effects

One study conducted through this Task assessed the effects of concurrent wind turbine sound on memory performance to investigate such effects. 46 participants were recruited for the study and each completed 304 memory trials under varying conditions of wind-turbine sound. Participants performed as expected in the memory task, with greater memory load reducing recognition accuracy, but there were no effects of wind turbine sound properties on performance. Subjective annoyance by wind turbine sound was low, but it was consistently related to acoustic properties of the sound samples, specifically loudness, sharpness,

roughness and fluctuation strength. Note: preliminary research plans of this study were pre-registered via the Open Science Framework (OSF) site associated with the project.

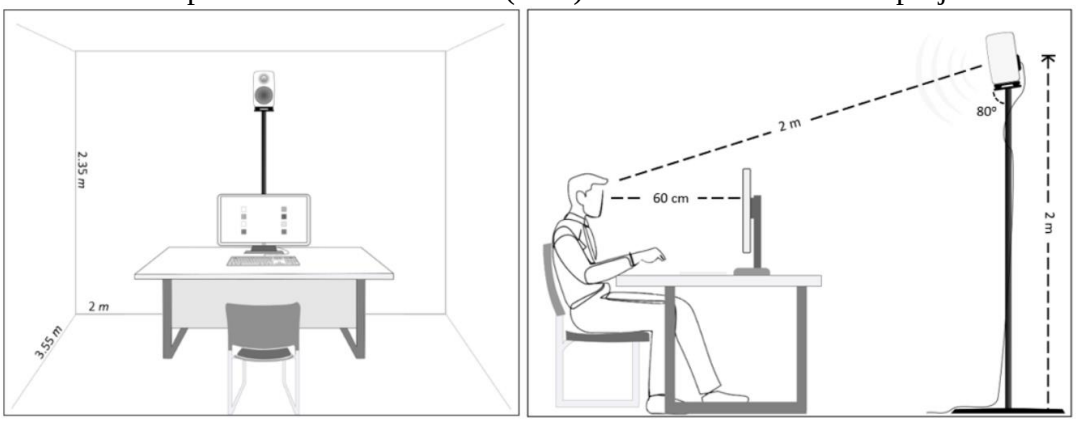

Figure 8 - Behavioural laboratory layout

Finally, WP5 involved coordination with the activities of Task 28, which included a proposed joint conference with this other Task. While this was not achieved during the timeframe of Task 39, it is scheduled to go ahead in June 2025 at the Wind Energy Science Conference 2025 in Nantes France. A micro-symposium has been organized in close coordination with Task 62 (which is the next task continuing from that activities of Task 28).

7. Key Conclusions/Recommendations

Most of the collaborative research activities conducted as part of Task 39 are still on-going. It is thus too early to draw firm and assertive conclusions from these works, as the analysis and findings need to be consolidated. There is a lot to be benefited by collaborating between institutes in order to advance physical knowledge about noise generation mechanisms at airfoil level.

Significant advancements were made in understanding wind turbine noise annoyance through lab and field-based testing, with key findings to be published in 2025, while coordination efforts with related tasks have set the stage for collaborative events in 2025. Moving forward, activities should focus on addressing challenges in sound reproduction validation for lab and online testing and strengthening international collaboration to advance research methodologies.

References

Note: All Task 39 technical reports and dissemination documents are collated in the Appendices at the end of the present document.

Appendices

Content:

Appendix 1: WP1 - Interdisciplinary Education and Guidance……. 20
Annex 1 - Fact Sheet on Low-Frequency Noise
Annex 2 - Fact Sheet on Tonal Noise
Annex 3 - A priori requirements for wind turbine noise propagation measurement data to be used for model validation (toward "Best Practices")

Appendix 2: WP2 - Analysis and reduction of wind turbine noise emission ……..... 54
Annex 1 - Report on WTN code benchmark
Annex 2 - Conference proceedings on comparisons between wind turbine noise code prediction models and measurement data
Annex 3 - Conference proceedings on comparisons of serration noise measurements in various facilities
Annex 4 - Presentation of the serration benchmark main results
Annex 5 - Conference proceedings on measurement of tip noise

Appendix 3: WP3 - Noise propagation modelling ……..... 210
Annex 1 - Definition of noise propagation codes benchmark for complex terrain
Annex 2 - Report on noise propagation code benchmark for complex terrain
Annex 3 - Conference proceedings on noise propagation codes benchmark for complex terrain
Annex 4 - Definition of noise propagation codes benchmark for flat terrain and offshore conditions
Annex 5 - Conference proceedings on noise propagation codes benchmark on flat terrain

Appendix 3: WP 4 - Assessing and Managing the Noise Effects on Health, Wellbeing and Consent & WP5 - Characterising Non-Noise Influences on Perception and its Effect ……272
Annex 1 – Conference proceedings on summary of WP meetings and workshops' discussions

IEA Wind Task 49
Final Technical Report

APPENDIX - WP1
Interdisciplinary Education and Guidance

Contents

1 Introduction **2**

2 Fact sheets **2**

3 Study report **2**

4 Review article **3**

5 WP1 / Annex 1 - Fact Sheet on Low-Frequency Noise **4**

6 WP1 / Annex 2 - Fact Sheet on Tonal Noise **16**

7 WP1 / Annex 3 - A priori requirements for wind turbine noise propagation measurement data to be used for model validation (toward "Best Practices") **26**

1 Introduction

WP1 is focused on dissemination of the Task 39 activities and findings.

In this document, the output documents from this WP are provided.

2 Fact sheets

In addition to the a Fact Sheet on amplitude modulation of wind turbine noise that was published in Phase 1 of the Task 39, two additional Fact Sheets were published during Phase 2:

1. Fact Sheet on Low-Frequency Noise (see Section 5/Annex 1)
2. Fact Sheet on Tonal (mechanical) Noise (see Section 6/Annex 2)

3 Study report

As part of the activities coordinated during the WP3 (Noise Propagation) meetings, a series of discussions on how to conduct outdoor wind turbine noise measurements were held. These yielded to a document in the form of an Expert Group Study Report, in the IEA Wind terminology. This report in available in Section 7/Annex 3 below in the present document.

Note that this document is not an attempt to replace existing and recognized standards for wind turbine noise measurements (e.g. the broadly used IEC 61400-11), but rather to provide general tips to the less experienced practitioners.

4 Review article

An article entitled "A Roadmap for Required Technological Advancements to Further Reduce Onshore Wind Turbine Noise Impact on the Environment" initiated and drafted by Task 39 participants has been published.

This article is freely available online by following this link:
https://doi.org/10.1002/wene.469

5 WP1 / Annex 1 - Fact Sheet on Low-Frequency Noise

Technology Collaboration Programme
by iea

June 2022

IEA Wind TCP Task 39

Low Frequency Noise from Wind Turbines – Fact Sheet

iea wind

IEA Wind TCP - Task 39
Quiet Wind Turbine Technology

Low Frequency Noise from Wind Turbines – Fact Sheet

Forewords

This document summarizes a number of facts concerning low-frequency noise emissions from wind turbines, and related issues such as human perception and regulations. It is addressed to non-specialists in the field of acoustics and wind turbine noise in general. Attempts have been made to define most of the technical concepts introduced in this document. A number of references to various scientific articles, reviews and reports are provided. However, in some cases their contents are very technical and may be more difficult to grasp for the layman. This document has been drafted with contribution from scientists and engineers working in scientific fields related to wind turbine sound issues.

Disclaimer

The IEA Wind Technology Collaboration Programme (TCP) is organised under the auspices of the International Energy Agency (IEA) but is functionally and legally autonomous. Views, findings and publications of the IEA Wind TCP do not necessarily represent the views or policies of the IEA Secretariat or its individual member countries.

Low Frequency Noise from Wind Turbines – Fact Sheet

What is Low Frequency Noise (LFN)? General considerations

The human perception of sound arises from the ability of the auditory system in the ear, and subsequently the brain, to detect acoustic waves travelling in the air. However, it must be emphasized that the audibility of different frequencies (or pitches), i.e. the intensity at which they are subjectively perceived relative to their actual physical intensity or energy content, varies with frequency. Whereas an ideal microphone with a constant sensitivity at all frequencies can measure the actual acoustic energy content or noise level of all these frequencies, the human ear has indeed a specific frequency response. It is most sensitive to sound waves in a frequency interval ranging *approximately* from 1 kHz to 5 kHz[1]. Below and above this frequency range, the ear sensitivity progressively decreases. In other words, for an equal amount of physical acoustic energy or actual noise level, the loudness of the noise will appear to a listener increasingly quieter as the frequency of the emitted noise decreases below 1 kHz, or increases above 5 kHz. In other words, in order to be perceived equally loud by the human ear, a noise source emitting at a frequency outside the above frequency interval therefore needs to have more physical energy content than a noise source emitting at a frequency within this interval.

Generally speaking, LFN refers to the low frequency end of the audible sound spectrum. Conventionally, sound at frequencies below 20 Hz is referred to as infrasound (IS). LFN is usually referring more specifically to sound waves above 20 Hz and below 200 Hz. Below 20 Hz, acoustic waves may be perceived provided that the noise level, i.e. their energy content, is high enough. As an example, the average[2] human audibility threshold for a sound at 8 Hz is around 100 dB [Watanabe & Madsen, 1990; Møller & Pedersen, 2004], compared to 20 dB at 200 Hz (i.e. a sound with 100 million times less energy), and 0 dB at 2000 Hz (i.e. 10,000 million times less energy), as displayed in Figure 1.

[1] Some sources mention a peak sensitivity ranging from 2 to 4 kHz. For reference, normal voice speech typically ranges from 100 Hz to 1000 Hz. A male with a deep bass voice can reach below 70 Hz, while a female soprano above 1200 Hz (a female high-pitched scream to 3000 Hz). A tuba brass instrument can play notes down to around 50 Hz and a cathedral pipe organ down to 8 Hz, while a piccolo flute can play up to 5 kHz and higher pitches can be obtained with cymbals or triangles.

[2] Note that the measure of audibility varies from one person to the other, including factors such as age, and that it can be measured using several methods for which the results may also differ.

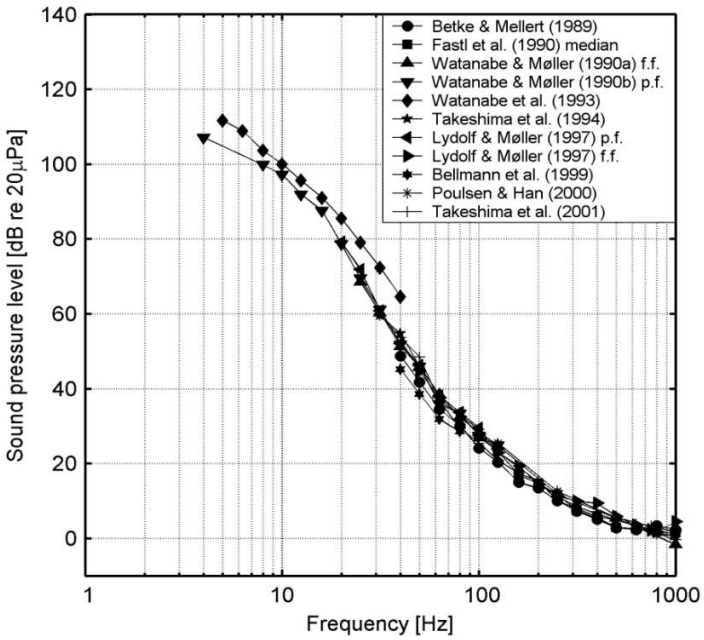

Figure 1 - Low-frequency hearing threshold measured between 1989 and 2001 [Source: Pedersen PhD thesis, 2008]

It is also important to note that sound levels decrease as the distance from their source increases, a phenomenon called `geometric spreading' which applies similarly to all frequencies. In addition, acoustic waves are dissipated when travelling through the air due to `air absorption'. This dissipation is increasingly efficient at higher frequencies. Therefore, LFN propagates from the source more easily compared to high-frequency noise.

Since noise levels decrease with the distance from the source. At a certain distance these levels will be masked by, and eventually become negligible compared to other natural (wind-induced noise in the vegetation, birds, etc) and/or anthropogenic (traffic noise, industrial activities, etc) noise sources. Probably, the most critical issue concerning LFN is a proper assessment of the distance at which this masking occurs.

How wind turbines create LFN?

In the context of WTN, it is usual to segregate the two main sources of noise: aerodynamic noise and mechanical noise. As these designations indicate, the former is related to aerodynamic features of the flow around the wind turbine blades as they rotate. In the latter case, noise is generated by the rotating and vibrating machinery of the drive-train, such as the generator and gearbox, produces sound waves during the operation of a wind turbine. Fans from cooling devices also emit noise, even during periods of stand-still. Accordingly, these two mechanisms are reviewed separately below.

Aerodynamic noise

As far as aerodynamic noise is concerned, a first contribution to LFN stems from the interaction of the atmospheric turbulence with the blade surfaces as they rotate. As the blades move through the air at

relatively high speed (in particular in the tip region), atmospheric inhomogeneities inherent to the turbulent wind flowfield generate pressure fluctuations on the blade surfaces. These fluctuations subsequently radiate as sound waves away from the turbine. The contribution of atmospheric turbulence to noise emissions is largest in the low frequency range due to the blade velocity and the size of the inhomogeneities involved. In addition, most of the sound energy is generated toward the tip of blades because the radial velocity is highest there. This type of noise is called broadband, in the sense that sound is emitted over a large range of continuous frequencies corresponding to the various sizes of the turbulent vortices contained in the atmospheric wind. It is estimated that the turbulent inflow impinging on the rotor blades generates broadband sound in the low frequencies with a maximum at 10 Hz [VanDenBerg2005].

Other aerodynamic phenomena create LFN by the same basic physical principle described above, but through different mechanisms. Flow disturbances and inhomogeneities can be created by the wind turbine itself (e.g. the turbine tower does alter the incoming wind flowfield) and these can interact with the blades. In the case of an upwind rotor concept (see Fig. 2 (left)), the tower slows down the flowfield upstream of itself, which influence can be felt by the blades as they pass by the tower at each rotation. More significantly, in the case of a downwind rotor concept (see Fig. 2 (right)), the flowfield disturbances are even stronger in the form of a downstream tower wake. When the blades pass through these disturbances, blade surface pressure fluctuations arise and sound waves are generated (similarly to the effect of the atmospheric turbulence above). In this latter case, the noise emission is `impulsive' in the sense that the noise wave emissions occur at each passage of a blade near the tower. Note that wind turbines with a downwind rotor configuration have been discarded from utility-scale commercial use since the 80's [Hubbard90], partly because it became clear that this configuration was an important source of LFN. In the same way that the tower flow disturbances create pressure fluctuations on the blade, radiating as noise, the passing blades reciprocally generate pressure fluctuations on the tower surface (mostly in the case of a cylindrical steel tower) which also radiate as noise. Recent studies have shown that this mechanism may contribute substantially to infrasound emissions [Klein2018, Zajamsek2019]. This type of blade-tower interaction may occur for upwind rotor concepts when the wake of the blade(s) hit the rotor as illustrated in Fig. 2 (left), but can also be the result of the impact on the tower of the air displacement caused by the passing blade which occurs both for upwind and downwind rotor concepts. It is not clear yet which of these two phenomena dominate.

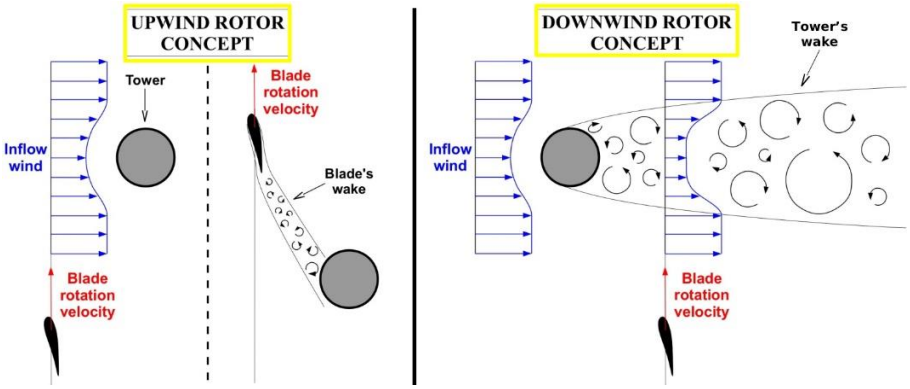

Figure 2 - Sketch of upwind (left) and downwind (right) wind turbine rotor concepts as seen from a cross-section in a plane perpendicular to the tower, and visualizing the airfoil section from one of the blades passing in front of, or behind respectively, the tower.

Mechanical noise

Because some of the structural vibrations originating from the drive train or other components (e.g. cooling system) can generate noise at relatively low frequencies, these mechanical noise sources may fall in the category of LFN. However, they have the peculiar property of being tonal, i.e. noise is emitted only at a specific frequency associated with the rotating speed of the mechanical components and/or the resonance frequencies of the structure. Tonal noise, if loud enough, easily stands out from the broadband noise and is therefore more noticeable, thus potentially more annoying. Note that the wind turbine nacelle may contain equipment or machinery that emit noise without structural vibrations (e.g. humming of electricity converters or cooling fans). Mechanical sound sources can usually be considerably attenuated, e.g. by using proper insulation of the nacelle or dampening devices at critical structural locations.

Propagation

Because LFN can travel further away than high frequency sound waves (see above), some studies have reported that LFN from wind turbines could be measured at quite large distances [Bolin2014, Zajamšek2016], although this may occur in specific weather conditions. Nevertheless, it has also been found that, at normal residential distances, measured LFN from a single turbine, or even from a wind turbine cluster, rarely exceeds the natural ambient background noise or other LFN sources, even in a quiet environment such as the country side [Ratzel2016, JapanMoE2016, JapanMoE2017]. Although very low frequencies, which travel further away, can be measured at slightly higher levels than ambient ones, at these distances these are again far below the hearing threshold.

Another mean of propagating noise away from a vibrating structure, in particular in the LFN and IS range, is by ground-borne noise. In this case, the medium that conveys the acoustic energy is not the air, but the ground itself. This may cause other structures at distances from the noise source to vibrate and/or emit noise on their own because of the energy transmitted to them through this mechanism. This has been investigated mostly in the case of rail and road traffic, but to our best knowledge, this has been very rarely reported for wind turbines [Sjöström2014] and the amount of energy communicated to the ground by

this mechanism is far lower than what can be produced by a train on a railway or other heavy industrial machinery. Consequently, the recorded levels are below the threshold of perception [HayesMcKenzie2006, Gastmeier2008, Nguyen2020].

Measuring LFN

It can be challenging to measure LFN, and even more so infrasound, emitted from a wind turbine accurately. Firstly, as the distance from the turbine increases, the noise immission[3] will rapidly become of the same order of magnitude as the ambient noise already present in the environment and the actual turbine noise can easily be drowned in this background noise. To segregate the background noise from wind turbine noise, it is necessary to compare the noise measured when the wind turbine is operating and shutdown periods. However, background noise vary significantly between day and night, but time of the day, atmospheric conditions, and possibly other factors, play significant roles. Therefore, it is recommended to conduct these measurements during extensive time-periods over several weeks or even months [Bluemendeller2020].

Secondly, measuring sound waves presents some specific difficulties at the lower end of the frequency range. Microphones are usually designed and optimized to measure sound in the human audible range say from 10 Hz up to 10 kHz or much higher. Their performances can deteriorate toward lower frequencies depending on the microphone technical specifications. Although so-called IEC 61672 Class 1 microphones should be able to measure with sufficient accuracy, some microphones are specifically designed for LFN measurements. More importantly, setting a microphone in the open-air also creates noise because of the wind interacting with the microphone itself, a phenomenon denoted as wind-induced noise which is predominant at low-frequencies. Foam and/or fur wind shields are used to minimize this effect (see pictures in Fig. 3). These wind shields are effective in the audible range but perform poorly at low frequencies and sometimes it is the wind-induced noise in the wind shield which is being measured, not wind turbine or ambient noise. There are ongoing investigations to improve wind shields for very low frequency measurements or placing them below ground level to avoid wind effects [Zajamšek2014, D'Amico2019, Bluemendeller2020].

Finally, when considering noise inside dwellings, low-frequencies are influenced by the noise emission levels, but the building itself (e.g. its structure) plays also an important role [Hansen2017]. If possible, outdoor noise measurements in front of the building should be correlated with indoor measurements providing more information [Søndergaard20XX, Thorsson2018, Maijala2020]. Note that also the measurement location inside a building or a room is a significant factor, making it difficult to obtain a unbiased quantitative measure of indoor LFN levels.

[3] In contrast to noise emission which characterizes the sound source, noise immission refers to the sound levels that can be measured or perceived at a listener position at a given distance from the source, possibly inside a dwelling.

Figure 3 – Top left picture: Outer fur wind screen, with inner foam wind screen for extra protection, shielding a microphone from the wind for outdoor noise measurements [Source: FORCE Technology, Denmark] - Bottom picture: Foam outer (left) and inner (middle) wind screens with the inner assembly contains the microphone (right) [Source: Norsonic AS, Norway] – Top right: Microphone (with foam wind screen) placed in a wooden box at the ground level to minimize wind effect [Source : Blumendeller2020]

Perception and impact on humans

Psycho-medical studies have reported that, at high enough levels of LFN, like for any other sound at high levels, humans can be affected in the form of annoyance, stress, irritation, unease, fatigue, headache, possible nausea and disturbed sleep [Hansen2020]. However, it must be remembered that the LFN emissions from a wind turbine, when heard at residential locations at a few hundred meters, are comparable with, or often below, the natural ambient levels. Although LFN can be measured in the immediate vicinity of a wind turbine and sometimes far away as well, there is no evidence that wind turbine noise can cause direct physical effects on people living nearby, considering the low levels involved at distances equal or larger than the typical minimum legal distances between wind turbines and dwellings. Typically, LFN and infrasound from wind turbines falls well below the level of audibility [ONeal2009, Howe2010, Ewans2013, Ratzel2016, Maijala2020]. A resident's attitude to wind turbines is an important factor in their response to them and annoyance certainly plays a role here [VanKamp2018, Leventhall2019, Maijala2020].

Metrics for quantifying LFN and regulations

Noise levels are commonly measured in decibels (dB) although other units do exist. As sound waves are characterized by air pressure fluctuations, a sound pressure level (SPL) in dB provides a measure of the amplitude of these fluctuations. A specific SPL can be associated with each of the measured sound frequencies[4]. For standard noise level assessment over the whole audible frequency range, noise is measured in dB(A), namely A-weighted decibels. A-weighting is a filter of the measured sound levels at all frequencies which is adapted to reflect human hearing in order to create a realistic metric for noise levels. Its effect is to attenuate the contribution of frequencies associated with lower audibility for humans, say below 1000 Hz and above 5000 Hz as discussed in the Introduction. Thus, quantifying LFN and infrasound require different metrics, so that they can be used for legislating. Note that noise regulations concerning LFN from wind turbines are not enforced in all jurisdictions. However, when they are, fixed limits on quantitative metrics of LFN can be applied, or these metrics can be included as an additional penalty to the standard noise limits in regulatory schemes.

The International standard (ISO) for quantifying infrasound is called G-weighting [IEC 61672-1] which, in the same way as for A-weighting, filters out the contributions outside of the frequency range from 10 to 30 Hz (e.g. as used in Denmark). Germany has its own standard by comparing A- and C-weighting. The latter filter being more orientated toward low-frequency sound than the former, it is possible to enhance the contribution of LFN to the overall noise using this metric. In Denmark, two specific metrics are used for noise regulations. Infrasound is evaluated using the G-weighted noise levels. Separately, LFN is evaluated based on A-weighting but restraining the summation to frequencies between 10 to 160 Hz. Furthermore, different limits are applied for day and night, and residential or working areas.

Final words

For further details about low-frequency noise from wind turbine, the reader is referred to the extensive reviews by Leventhall [Leventhall2009] and Howe [Howe2010].

Acknowledgments

This document was written and reviewed by scientists and engineers working in the field of wind turbine acoustics.

[4] Conventionally, the SPLs are summed up over what is called octave bands. The latter define consecutive frequency intervals with center frequencies increasing exponentially. This is a mean to cover a large range of frequencies, from very low to very high, with a relatively small number of discrete center-frequencies.

References

[Blumendeller2020] E. Blumendeller, I. Kimmig, G. Huber, P. Rettler, and P.W. Cheng, "Investigations on Low Frequency Noises of On-Shore Wind Turbines", Acoustics, Vo.2(2) pp.343-365, 2020. https://doi.org/10.3390/acoustics2020020

[Bolin2014] K. Bolin, M. Almgren, E. Ohlsson and I. Karasalo, "Long term estimations of low frequency noise levels over water from an off-shore wind farm", Journal of the Acoustical Society of America, Vol. 135 (3), pp.1106-1114, 2014.

[D'Amico2019] S. D'Amico, T. Van Renterghem and D. Botteldooren, "Measuring infrasound from wind turbines : the benefits of a wind-shielding dome", Wind Turbine Noise 2019 (Conference proceedings), Lisbon, Portugal, 2019.

[Evans2013] T. Evans, J. Cooper and V. Lenchine, "Infrasound levels near windfarms and in other environments", Report from Resonate Acoustics, For the Environment Protection Authority, Adelaide, SA, Australia, 2013. https://www.epa.sa.gov.au/files/477912_infrasound.pdf

[Hubbard90] H. Hubbard and K. Shepherd, "Wind Turbine Acoustics", US Department of Energy/NASA, NASA Technical Paper 3057 – DOE/NASA/20320-77, 1990. Retrieved from: https://ntrs.nasa.gov/archive/nasa/casi.ntrs.nasa.gov/19910007366.pdf

[Hansen2019] "Prevalence of wind farm amplitude modulation at long-range residential locations", K. L. Hansen, P. Nguyen, B. Zajamšek, P. Catcheside, C. H. Hansen, Journal of Sound and Vibration, Vol. 455, pp.136-149, 2019. https://doi.org/10.1016/j.jsv.2019.05.008

[Hansen2020] C. Hansen and K. Hansen, "Recent Advances in Wind Turbine Noise Research", Acoustics, Vol.2(1), pp.171–206, 2020. https://doi.org/10.3390/acoustics2010013

[HayesMcKenzie2006] Hayes McKenzie Partnership Ltd., "The Measurement of Low Frequency Noise at Three UK Wind Farms", UK Department of Trade and Industry (DTI) contract number: W/45/00656/00/00, 2006. Retrieved from: https://webarchive.nationalarchives.gov.uk/20090609065010/http://www.berr.gov.uk/files/file31270.pdf

[Howe2010] B. Howe, "Low frequency noise and infrasound associated with wind turbine generator systems – A literature review", Ontario Ministry of the Environment RFP No. OSS-078696, 2010. Retrieved from: https://docs.wind-watch.org/HGC-LFI-wind-turbine-lit-rev.pdf

[JapanMoE2017] "Notice of Guideline for the Wind Turbine Noise", Notification No. 1705261 of the Air Environment Division, Ministry of Environment, Government of Japan, 2017. Retrieved from: https://www.env.go.jp/en/air/noise/windturbine190208.pdf

[JapanMoE2016] "Investigation, Prediction and Evaluation of Wind Turbine Noise in Japan - Final Report by Expert committee on Wind Turbine", Office of Odor, Noise and Vibration, Ministry of Environment, Government of Japan, 2016. Retrieved from: https://www.env.go.jp/en/air/noise/windturbine.pdf

[Klein2018] L. Klein, J. Gude, F. Wenz, T. Lutz and E. Krämer, "Advanced CFD-MBS coupling to assess low-frequency emissions from wind turbines", Wind Energy Science, 2018. https://doi.org/10.5194/wes-2018-51

[Leventhall2009] G. Leventall, "Review: Low Frequency Noise. What we know, what we do not know, and what we would like to know", Journal of Low Frequency Noise, Vibration and Active Control, 28(2), pp.79–104, 2009. https://doi.org/10.1260/0263-0923.28.2.79

[Maijala2020] P. Maijala, A. Turunen, I. Kurki, L. Vainio, S. Pakarinen, C. Kaukinen, K. Lukander, P. Tiittanen, T. Yli-Tuomi, P. Taimisto, T. Lanki, K. Tiippana, J. Virkkala, E. Stickler and M. Sainio, "Infrasound Does Not Explain Symptoms Related to Wind Turbines", Publications of the Government's analysis, assessment and research activities, Prime Minister's Office, Finland, 2020. http://urn.fi/URN:ISBN:978-952-287-907-3

[Nguyen2020] D. P. Nguyen, K. Hansen, B. Zajamsek, "Human perception of wind farm vibration", Journal of Low Frequency Noise, Vibration and Active Control, Vol.39(1), pp.17-27, 2020. doi:10.1177/1461348419837115

[ONeal2009] R. D. O'Neal, R. D. Hellweg and R. M. Lampeter, "A Study of Low Frequency Noise and Infrasound from Wind Turbines", Report No. 2433-01, Prepared for: NextEra Energy Resources, LLC Juno Beach, FL, Prepared by: Epsilon Associates, Inc., Maynard, MA, July 2009.

[Ratzel2016] U. Ratzel, O. Bayer, P. Brachat, M. Hoffmann, K. Jänke, K.-J. Kiesel, C. Mehnert and Dr. C. Scheck (Editors), "Low-frequency noise incl. infrasound from wind turbines and other sources", LUBW Ministry for the Environment, Climate and Energy of the Federal State of Baden-Wuerttemberg, Germany, 2016.

[Sjöström2014] A. Sjöström, C. Novak, H. Ule, D. Bard, K. Persson; G. Sanberg, " Wind Turbine Tower Resonance", Inter-Noise 2014 (Conference proceedings), Melbourne, Australia, 2014.

[Thorsson2018] P. Thorsson, K. Persson Waye, M. Smith, M. Ögren, E. Pedersen and J. Forssén, "Low-frequency outdoor–indoor noise level difference for wind turbine assessment", The Journal of the Acoustical Society of America, Vol.143(3), 2018. https://doi.org/10.1121/1.5027018

[VanDenBerg] G. P. Van Den Berg, "The beat is getting stronger: The effect of atmospheric stability on low frequency modulated sound of wind turbines", Journal of Low Frequency Noise Vibration and Active Control, Vol. 24(1), pp.1-24, 2005. https://doi.org/10.1260/0263092054037702

[VanKamp2018] I. Van Kamp and F. Van Den Berg, "Health Effects Related to Wind Turbine Sound, Including Low-Frequency Sound and Infrasound", Acoustics Australia, Vol. 46, pp.31–57, 2018. https://doi.org/10.1007/s40857-017-0115-6

[Zajamšek2014] B. Zajamšek, K. L. Hansen and C. H. Hansen, "Identification of low frequency wind turbine noise using secondary windscreens of various geometries", Noise Control Engineering Journal, Vol. 62(2), 2014. DOI: 10.3397/1/376207

[Zajamšek2016] B. Zajamšek, K. L. Hansen, C. J. Doolan and C. H. Hansen, "Characterisation of wind farm infrasound and low-frequency noise", Journal of Sound and Vibration, Vol. 370, pp.176–190, 2016. http://dx.doi.org/10.1016/j.jsv.2016.02.001

[Zajamsek2019] B. Zajamsek, Y. Yauwenas, C. J. Doolan, K. L. Hansen, V. Timchenko, J. Reizes and C. H. Hansen, "Experimental and numerical investigation of blade–tower interaction noise", Journal of Sound and Vibration, Vol. 443, pp.362-375, 2019. https://doi.org/10.1016/j.jsv.2018.11.048

6 WP1 / Annex 2 - Fact Sheet on Tonal Noise

Technology Collaboration Programme
by iea

January 2023

IEA Wind TCP Task 39

Wind Turbine Tonalities –

Fact Sheet

iea wind

IEA Wind TCP - Task 39
Quiet Wind Turbine Technology

Wind Turbine Tonalities – Fact Sheet

Forewords

This document summarizes a number of facts concerning tonal noise emissions from wind turbines, and related issues such as human perception and regulations. It is addressed to non-specialists in the field of acoustics and wind turbine noise in general. Attempts have been made to define most of the technical concepts introduced in this document. A number of references to various scientific articles, reviews and reports are provided. However, in some cases their contents are very technical and may be more difficult to grasp for the layman. This document has been drafted with contribution from scientists and engineers working in scientific fields related to wind turbine sound issues.

Disclaimer

The IEA Wind Technology Collaboration Programme (TCP) is organised under the auspices of the International Energy Agency (IEA) but is functionally and legally autonomous. Views, findings and publications of the IEA Wind TCP do not necessarily represent the views or policies of the IEA Secretariat or its individual member countries.

Wind Turbine Tonalities – Fact Sheet

What is structure-borne sound?

Every piece of machinery with moving parts emits, to some degree, sound, some loud, noisy and disturbing, some less prominent and almost inaudible. When the machine starts to vibrate, e.g. due to internal friction or unbalanced rotating parts, these vibrations are transmitted through the housing surface into the air. A sound is emitted.

Wind turbines, being some of the largest machinery ever built, are no exception. The components of the drive train, like gear boxes or generators, cause excitations of quite significant amplitude. Moreover, the expansive, thin walled surfaces of the rotor blades, the nacelle cover or the tower can easily resonate, increasing sound emittance almost like a large-scale loudspeaker. Characteristic for this so-called vibroacoustic, or structure-borne sound is its tonal appearance, meaning that it is dominated by only a few, sharp, and often annoying frequencies in the audible spectrum.

Because the human hearing is particularly sensitive to tonal noise, the international certification regulations for wind turbines set strict limits for tonal exposure. It is therefore the task of the turbine designer - and the wind farm operator - to minimize the vibroacoustic footprint of a wind turbine for residents.

Wind turbine noise generation

The audible sound profile surrounding wind turbines has several different sourcing mechanisms, as shown in *Figure 1*, and consequently has very different auditory characteristics. Most recognizable in immediate proximity of the turbine is a broadband, alternating 'swish' sound. This sound is caused by an interaction of the wind and flow characteristics at the blade with its surface. Because of a wide range of involved flow structures the noise generated by this interaction is broadband in nature, with a frequency ranging from about 20 Hz well into the kHz.

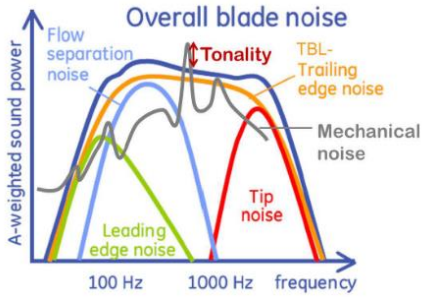

Figure 1: Contribution of different noise sources to the overall wind turbine noise spectrum including a tonal component (Note that the respective quantitative contributions may differ from turbine to turbine, and this graph should only be considered as a qualitative examplei [Source: vanHoellebeke].

The broadband nature of airfoil noise is important for the audibility of tonal noise sources as it effectively masks other noise sources of the turbine, see *Figure 1*. Tonal noise components only become

audible to the human ear if the sharp frequency peak stands out significantly above the masking spectrum. The masking spectrum itself is composed of the airfoil noise on the one hand, and everything that contributes to 'background' noise on the other. In many locations, infrastructure such as traffic and industry, provide a significant contribution to the local sound emissions. More importantly the wind itself is a major noise source to the human ear, due to turbulent structures carried within the moving air. In the case of strong and gusty wind, the wind noise will be the predominant and only audible sound surrounding a wind turbine. Tonality as such will, therefore, only be an issue if the blade noise of a wind turbine is low (which is every intention of a turbine manufacturer), and the wind speed is relatively low and constant in time. Under these conditions, the machine borne tonalities are no longer hidden behind the masking noise, and can become audible or in some cases even annoying.

Tonal noise generation on wind turbines

Noise audible to the human ear is the final element in a chain of physical processes. One divides machine noise generation in *excitation, transmission, radiation, propagation* and *immission. Excitations* within the drive train are the primary source for machine noise, but other mechanical devices can also be the source of a tonal acoustic footprint:

- Gearbox induced vibrations
  Wind turbines make use of gear boxes to adjust the rotational frequency of the electrical generator with the demanded grid frequency. Gear boxes of modern-day wind turbines consist of multiple planetary and spur-gear stages. As the contact between the teeth of gear wheels is unsteady (varying between zero and full contact), the transmitted forces between two gear wheels are subject to undulations. These time-varying contact forces are the primary reason for gear box vibrations. The frequency of a harmonic gear pair excitation is proportional to the rotational speed of the wind turbine rotor: if the speed increases, so does the frequency of the tone. The actual pattern of excited gear box frequencies is a function of gear teeth number in the individual gear box stages. The resulting excitation profile usually is a rather complex, fan-type pattern, as shown in *Figure 2*. It consists of the principal and higher harmonic orders associated to multiple gear pair contacts within a multi-stage gear box configuration.

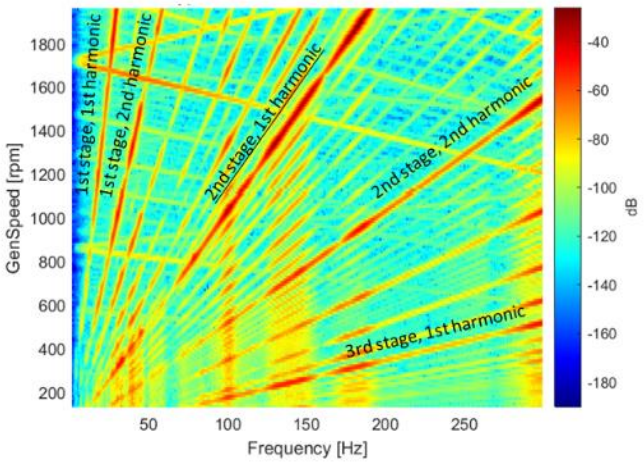

Figure 2: Typical response pattern of a geared wind turbine.

- Generator induced vibration
  The wind turbine generator is equally a source for structural vibrations, and for gearless wind turbines it is the most significant one. The passing of rotor poles and stator windings result in periodic variations of the electromagnetic forces in the airgap, commonly known as the cogging torque. Like in gear boxes, the generator internal excitation is characterized by the principal and higher harmonics, and comparably this leads to a fan type excitation pattern. Generator induced vibrations are particularly relevant for the design of tonality-free direct drive wind turbines, as the corresponding forcing magnitude as well as the resonating generator structures are large.
- Power electronics
  Power electronics components serve to match the generated electrical frequency and voltage levels to the grid demands. The electrical switching frequency in those devices, rectifiers, and transformers in particular, can translate into narrow-banded vibrations and direct tonal noise. Power electronics in modern day wind turbines are usually installed directly within the nacelle to reduce cable losses. Noise and vibrations must be shielded adequately to avoid a tonal character of the noise spectrum.
- Cooling fans
  Some wind turbine types operating in hot climatic conditions require an external, fan-driven cooling system to exchange excess heat. The noise of those fans can be tonal in character and is strongly correlated to the fan rotational speed, not necessarily the turbine rotational speed. Fan related tones can thus become increasingly apparent at low wind speeds or close to turbine standstill when the aerodynamic masking noise is low. The primary measures to reduce fan induced tonality are noise shielding and redirecting.
- Aerodynamic tonal noise
  As described by [Dawson2014] and others, aerodynamic effects on wind turbines can produce tonal type sounds. The underlying effect is so-called laminar-boundary-layer-vortex-shedding, a local flow phenomenon at the rotor blades unrelated to vibroacoustic emissions. The appearance of aerodynamic tonality points to inadequate blade performance, potentially due to degradation or icing. These effects can be easily avoided or mitigated if occurring.

Vibrations created within the drive train are transferred within the entire turbine structure, passing between individual components via bearings and fixations, see *Figure 3*. Along this **transfer path**, most oscillations will be absorbed by structural damping or lead to internal noise emissions. In both cases they are no longer relevant for external noise emission. Tower and blades, along with the nacelle housing, are the primary radiation surfaces of wind turbines. Being thin walled, large structures, the surfaces of these components can easily resonate with a wide range of excitation frequencies. If resonance occurs, the structure starts to amplify the vibrations of certain frequencies. A potential resonance within the frequency window of a critical excitation, thus, must be avoided to keep tonality levels low.

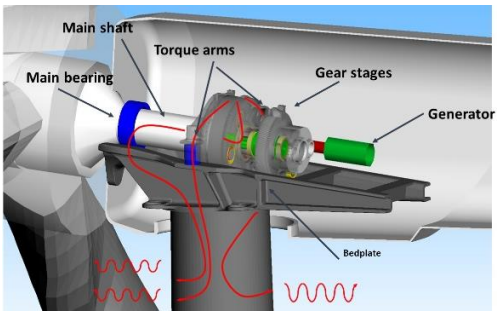

Figure 3: Vibration transfer and radiation within a wind turbine.

Tones emitted via tower or blade surfaces can potentially occur in very low frequency ranges below 20 Hz, due to the large dimensions of the radiating components. The highest tonal frequencies may be observable around 600 Hz, depending on the source. The most common range for drive train borne tones is from 60 Hz to 200 Hz.

Tonal noise assessment and regulations

Tonal noise from wind turbines may be addressed differently in different jurisdictions. However, many regulatory frameworks make use of the well-known IEC 61400-11 standard, in which tonal noise measurement is a part of the regular noise measurement of wind turbines. This part of the standard is shortly summarized below.

A measurement campaign is conducted with one or multiple microphones positioned in a sector downwind of the turbine. The microphone distance corresponds to the tower height plus half the rotor diameter. Narrow-banded spectra of sound pressure levels are obtained for 10s measurement periods. All 10s band spectra are categorized by the corresponding measured mean wind speed. This ensures that a wind turbine is assessed for all wind speeds individually.

Generally, a tone is defined in a spectrum when a local maximum stands out significantly compared to the neighboring bands. In order to identify the potential tones in a spectrum the following method is applied:

- Identify the local maxima in the narrow-banded spectrum.
- Calculate the background noise level as the average energy level of the *critical frequency band*, centered around the local maximum, excluding the identified local maximum and its two neighboring bands. Except for tones between 20 and 70 Hz, the width of the critical frequency band Δf_c increases with increasing tonal frequency f_c, according to the following formula:

$$\Delta fc = 25 + 75 \left(1 + 1.4 \left[\frac{f_c}{1000}\right]^2\right)^{0.69}$$

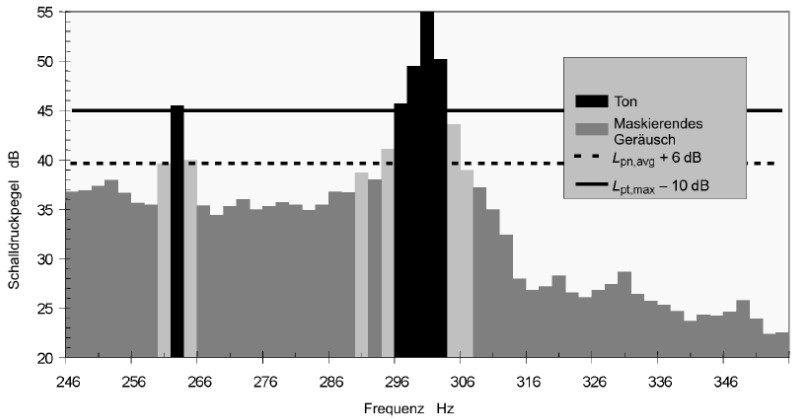

Figure 4: Classification of spectral lines for tone identification. [IEC 61400-11]

- A *potential tone* is identified if the local maximum exceeds the average level of the masking noise within the critical frequency band by at least 6dB.
- The spectral bands are classified into masking bands, neutral bands and tonal bands. The *tonal audibility* is calculated relating the sound pressure levels of the tonal bands to the average levels of the masking bands. After factoring in a frequency dependent perceptibility term (around +2dB for the most common wind turbine tonal frequencies), a *perceivable tone* is declared if the perceived tone level exceeds the masking noise level by 3 dB.

Local regulations may vary, but usually a perceivable tone is accounted for by a noise penalty on the overall turbine noise level when assessing compliance.

Tonal noise perception

The human ear and the cognitive system interpreting sounds is not a neutral receptor. Humans' hearing is adapted to perceive certain frequency ranges better than others, specifically those frequencies related to speeches and whisper. Similarly, humans can focus on particular noise phenomena apparent within a broad background noise, such as impulsiveness, modulation and tones. Perception and annoyance of noise in general are not equivalent to each other, but both correlate to the hearing's sensitivity [Pedersen2004].

Laboratory and field studies have confirmed that a tonal component in a sound spectrum is perceived as more annoying than constant, broadband, or steady noise, even if the overall sound pressure level is maintained constant [Hongisto2018, Landström1994]. Further studies have shown that the working performance of individuals can suffer due to the presence of tonal sounds, even at very low ambient levels [Lee2017]. Psychoacoustic annoyance due to tones is generally correlated to the **frequency** (higher tonal frequencies imply higher annoyance) and the **loudness of the tone**. **Multiple tones** in a spectrum can cause significantly higher annoyance. Frequency impact, loudness as well as multitude of tones are all evaluated and penalized in the guiding international standards. Further research on residential annoyance can help to draft more specific regulations for wind turbines, for example accounting for typical background characteristics and low-frequency tones.

Tonal noise mitigation

Due to the advances made in reducing the aerodynamic blade noise, tonality of wind turbines has become an increasing concern for manufacturers. Because machine borne sound is no longer necessarily hidden behind the curtailed aerodynamic masking noise, wind turbine developers nowadays devote significant resources to identify and mitigate the tonal impact. The challenge for the engineers is the complex combination of variable speed operation, variations in wind conditions, site specific requirements as well as local regulations and residential concerns. This requires an integrated system engineering approach in the concept and design phase of the turbine. High-fidelity numerical models are widely used throughout the engineering pipeline, to capture the essential physics of the acoustic chain:

- **the sources of excitation**
  Possible countermeasures consist of smoothing and mitigation of gear pair forces, minimizing and manipulating electro-magnetic forces in generators, shielding and damping transformers, and others.
- **the mechanisms of vibration transfer**
  Support structure and housing properties need to be adapted, joint and bearing characteristics modified or additional damper elements introduced.
- **noise propagation**
  Numerical tools capture variations in air temperature and density, account for directivity, doppler-effect, etc, helping estimating noise immission levels at residential area.

Subcomponent testing and prototype noise measurements are a crucial step in the product development process in the run-up to certification. The latest wind turbines on the market are now equipped with advanced monitoring systems. Several sensors inside and outside the turbine capture critical vibrations and noise emissions. Concepts for machine learning in combination with virtual sensing are in an infant stage but have the potential to contribute to both tonality-free design and operation of wind turbines in the future.

Summary

Tonality is one specific aspect of wind turbine noise emissions into the environment. The general mechanisms from which it originates are well understood, but it can still be difficult to control. State-of-the-art engineering allows to reduce or damp this type of noise. Nevertheless, in some cases, counter-measure packages are needed to address the problem on site on an individual basis, e.g. when the tonal noise emissions do not comply with the local noise regulations. This is an active field of research, as broadband wind turbine noise emissions have been considerably reduced in the past decade (e.g. with the widespread use of serration), making tonal noise emerging more clearly from the overall wind turbine noise emission.

Acknowledgments

This document was written and reviewed by scientists and engineers working in the field of wind turbine acoustics. In particular, Birger Luhmann has been the main contributor in writing this document.

References

IEC 61400-11:2012+AMD1:2018. Wind turbine generator systems – Part 11: Acoustic noise measurement techniques.

Vanhollebeke, Frederik. (2015). Dynamic Analysis of a Wind Turbine Gearbox Towards Prediction of Mechanical Tonalities.

Landström U, Kjellberg A, Söderberg L, Nordström B. Measures Against Ventilation Noise – which tone frequencies are least and most annoying? Journal of Low Frequency Noise, Vibration and Active Control. 1994;13(3):81-88. doi:10.1177/026309239401300301

Hongisto, Valtteri & Saarinen, Pekka & Oliva, David. (2019). Annoyance of low-level tonal sounds – A penalty model. Applied Acoustics. 145. 358-361. 10.1016/j.apacoust.2018.09.023.

Lee, Joonhee et al. "How tonality and loudness of noise relate to annoyance and task performance." Noise Control Engineering Journal 65 (2017): 71-82.

Dawson, B. & Mackenzie, N.. (2014). Tonal characteristics of wind turbine drive trains. INTERNOISE 2014 - 43rd International Congress on Noise Control Engineering: Improving the World Through Noise Control.

Pedersen E, & Persson Waye K, "Perception and annoyance due to wind turbine noise—a dose–response relationship", Journal of the Acoustic Society of America, 116(6): 3460-3470 (2004), DOI: 10.1121/1.1815091

7 WP1 / Annex 3 - A priori requirements for wind turbine noise propagation measurement data to be used for model validation (toward "Best Practices")

EXPERT GROUP STUDY REPORT – TASK 39

A priori requirements for wind turbine noise propagation measurement data to be used for model validation (toward “Best Practices”)

Authors: Task 39 participants (Work Package 3)

Editor: F. Bertagnolio (Operating Agent)

September 12, 2023

FOREWORD

The International Energy Agency Implementing Agreement for Co-operation in the Research, Development and Deployment of Wind Energy Systems (IEA Wind) is a vehicle for member countries to exchange information on the planning and execution of national, large-scale wind system projects and to undertake co-operative research and development projects called Tasks or Annexes.

As a final result of research carried out in the IEA Wind Tasks, Recommended Practices, Best Practices, or Expert Group Reports may be issued. These documents have been developed and reviewed by experts in the specialized area they address. They have been reviewed and approved by participants in the research Task, and they have been reviewed and approved by the IEA Wind Executive Committee as guidelines useful in the development and deployment of wind energy systems. Use of these documents is completely voluntary. However, these documents are often adopted in part or in total by other standards-making bodies.

A Recommended Practices document includes actions and procedures recommended by the experts involved in the research project.

A Best Practices document includes suggested actions and procedures based on good industry practices collected during the research project.

An Experts Group Studies report includes the latest background information on the topic as well as a survey of practices, where possible.

Previously issued IEA Wind Recommended Practices, Best Practices, and Expert Group Reports can be found at https://iea-wind.org.

PREFACE

Publisher/Authors and Context

This document is published as part of the collaborative work taking place in the IEA Wind TCP (Technology Collaboration Program) Task 39 "Quiet wind turbine technology". The latter convenes experts in the field of wind turbine noise. More specifically, this document has been drafted by the participants of Task 39 - WP3, which focuses on wind turbine noise propagation issues.

Target audience

This document is mainly addressed to researchers and engineers who may be relatively new to the field of outdoor acoustic measurement in general, and of wind turbine noise in particular. It could also be used as a kind of checklist for more experienced individuals. It is assumed that the reader has some basic understanding of wind turbine noise and acoustic measurements.

Objectives

This document aims at providing technical guidance for measuring wind turbine noise, focusing on noise propagation effects. It is however not a step-by-step technical guide on how to conduct a wind turbine noise measurement campaign. Rather, it takes the form of an exhaustive list of information that should be documented in addition to the acoustic measurement data themselves. These information are categorized into a number of topics. The objectives are to improve the content of the resulting measurement dataset (e.g. by increasing its completeness), as well as prepare and facilitate the post-processing of the measured data and their interpretation during a subsequent scientific analysis. Some specifications for the measuring equipment is also provided that should also contribute to the latter objectives.

Scope and Limitations

This document is concerned with the measurement of wind turbine noise in a broader sense, however with a particular focus on validation of models for noise propagation effects. It may also partly be used in the context of the study of the wind turbine noise emission itself, when noise propagation effects can be neglected. It may be a reasonable assumption if measuring sufficiently close to the turbine. Nevertheless, for the measurement of wind turbine noise (e.g. for the purpose wind turbine certification), the reader is referred to the IEC 61400-11 standard[1], which has been approved by a broader international standardization committee. This latter document also describes the measurement technical set-up in more details.

NOTICE:

IEA Wind Task 39 functions within a framework created by the International Energy Agency (IEA). Views, findings and publications of IEA Wind Task 39 do not necessarily represent the views or policies of the IEA Secretariat or of all its individual member countries.

[1] International Standard IEC 61400-11: Wind Turbines - Acoustic noise measurement techniques (Ed. 3), International Electrotechnical Commission (CH), 2012.

TABLE OF CONTENTS

	Page …
FOREWORD	… 2
PREFACE	… 3
TABLE OF CONTENTS	… 4
1. INTRODUCTION	… 5
2. GENERAL INFORMATION ABOUT THE TEST SITE	… 5
3. ATMOSPHERIC CONDITONS	… 5
4. CHARACTERIZATION OF THE NOISE SOURCES	… 6
5. NOISE MEASUREMENT SET-UP	… 7
6. LOGBOOK	… 7
7. CONCLUSIONS	… 8

1. INTRODUCTION

Wind turbine noise emission and propagation through the atmosphere is a complex phenomenon, with various physical processes interacting with each other (e.g. atmospheric turbulent flow, air temperature, wind turbine as a noise source with its own specificities). The measurement of wind turbine noise in itself is challenging, as most outdoor acoustic measurements for characterizing a noise source are plagued by ambient background noise which deteriorates the "signal-to-noise" ratio (where "signal" refers here to the noise from the wind turbine and "noise" to the perturbing ambient noise, like vegetation, animals, road traffic, etc). This is notoriously difficult for wind turbine noise in the far-field, where wind turbine noise levels are often of the same order of magnitude as the background noise.

The subsequent analysis of the measured data is also challenging. The complexity of the interacting phenomena mentioned above makes it difficult to isolate the influence of the different physical parameters influencing the measurement data. Therefore, it is important to have access to as much information as possible about the experimental conditions in order to enable a more reliable analysis of the data.

In the following, a series of topics that should be considered for designing a wind turbine noise measurement campaign are reviewed. For each of these, a number of specific details that should be addressed, recorded, and/or documented are provided. Some basic explanation for the necessity of these procedures are provided.

2. GENERAL INFORMATION ABOUT THE TEST SITE

Wind turbine noise propagation will be influenced by the surrounding environment. It is always informative for the person processing the data a-posteriori to be able to have access to as much as possible of the details, in particular if that person has not been participating to the measurement campaign. These include:

- Definition of terrain (elevation map, roughness class)
- Surface cover description (ground impedance if possible)
- Description of the (audio-)surrounding (e.g. presence of nearby roads, trees, etc)

3. ATMOSPHERIC CONDITONS

The main physical factors influencing outdoor noise propagation are related to the atmospheric conditions. These should be measured with appropriate sensors. It is often not possible to obtain a full picture of the three-dimensional atmospheric field, but again, collecting as much as possible of its features is desirable.

- Definition of meteorological conditions:
    - Wind speed and direction
    - Wind and temperature gradient (preferably up to a height of at least 1/10 of propagation distance), wind veer
    - Atmospheric stability

    - Humidity and temperature
    - Turbulence level (possibly at several heights)
    - Using met mast(s) and/or Lidar(s) (specify height of sensor for each measured quantity)
    - General and specific information about atmospheric conditions (e.g. sunny day, windy day, day/night measurement periods, stable/unstable atmospheric conditions…)
    - Specify time-frame for the above information if longer measurement campaign (e.g. if these conditions change significantly)
- Synchronization of noise measurements and meteorological data (specify relation between measurement periods and actual time-stamps)

4. CHARACTERIZATION OF THE NOISE SOURCE(S)

When interested in characterizing wind turbine noise and its propagation (e.g. to the nearby dwellings), it is natural to also collect information on the noise source itself.

- Characterization of the wind turbine noise emission, e.g.
    - IEC-type noise measurements for 1 turbine
    - Noise directivity pattern if possible
    - Noise curve, e.g. SWL as function of wind speed
- If measuring a wind farm, same as above for each turbine
- Characterization of the background noise (e.g. using regular shutdown of the turbine(s)) at the time of measurements
- "Reasonable" Signal-to-Noise Ratio (min. +3dB, 6dB preferable)
- If measuring a wind turbine, position of potential nearby turbines/farms (possibly causing spurious noise)
- If measuring farm (position of all turbines ./. mics.), and position of potential nearby farms/turbines (possibly causing spurious noise)
- Wind turbine geometry:
    - Hub height
    - Rotor diameter
    - More if available (e.g. blade planform, required for higher fidelity noise emission models)
- Blade add-ons (serration, VGs, etc)
- SCADA data from turbine(s)
    - Rpm
    - Power
    - Yaw position
    - Yaw off-set (in connection with wind direction, see Atmospheric conditions)
    - More if available (e.g. blade pitch)
- Synchronization of noise measurements and SCADA data (time-stamping details)
- If several turbines are involved, possibility of characterizing possible wake interactions

5. NOISE MEASUREMENT SET-UP

All sensors are subjected to measurement uncertainties. Therefore, the audio equipment quality will affect the findings and conclusions that can be drawn from a subsequent analysis of the measured noise data, which is the main quantity of interest in the present context. Details about the acoustic sensors and their installation should be provided.

- Specifics about the microphone measurements:
    - Microphone type (Class 1 preferable)
    - Calibration (frequency response and limits)
    - Directivity properties
    - Height above ground (and installation characteristics, e.g. documented with a picture)
    - Wind screen types (and insertion losses)
    - Acquisition system characteristics
    - Time resolution of raw data
    - Specifications of the stored data (e.g. Leq in time intervals, SPL in octave bands, Z/A-weighted, etc)
- Positioning of microphones relative to turbine(s)

6. LOGBOOK

It is strongly advised (if not compulsory) to record all the details about the measurement set-up, timing of the measurements, specific or unusual/unexpected conditions, etc, in a concise way in a so-called "logbook" document. With this document, it is clear for anyone using the measured dataset what were the specific conditions at the time, and possibly during the different phases, of the measurement period. It should contain (when/if possible):

- Details about the instruments (e.g. serial number, exact location)
- Starting-, end- and down-time of measurement systems
- Running and down-time for the turbine(s)
- Timing for calibration of instruments (e.g. microphones with calibrator)
- Timing and details about events that could affect the quality of the data
    - either specific to the measurement system
    - or in the surrounding (e.g. rain, traffic)

It is also recommended to take pictures of the experimental set-up and surrounding to get a good overview of the experimental conditions, in particular for those who did not participate to the measurement campaign. Note that such logbook is not only aimed at informing persons who would not have been attending to the measurement campaign themselves. It is very useful for those who have been conducted the measurements as well, as it is virtually impossible to remember the whole sequence of events, especially during long term measurement campaigns.

7. CONCLUSIONS

A list of items to consider for the design and the completion of a wind turbine noise measurement campaign is provided in the present document. This list is meant to be as exhaustive as possible, and can surely not be implemented in reality as the requirements would be too great to be all met at the same time. Nevertheless, this can be used as a guidance for conducting such experiment. Indeed, all these items, if feasible/achievable, are aiming at facilitating and improving the quality of the analysis of the acoustic measurement data at a later stage.

Note that the topic of the curation of the acquired experimental data has not been addressed in the present document. It is advised here to comply with the FAIR Guiding Principles as initially published by Wilkinson et al (2016)[2]. This effort has been followed by further collaboration work on the topic (see, e.g., https://www.go-fair.org).

The next step in the editing of the present document would be to prioritize some elements over the others. The suggestions for conducted an experiment are only listed here, without evaluating their respective actual impact on the intrinsic quality of the measurement dataset.

Finally, the present document would need further additions in order to be considered as a Recommended Practices or Best Practices document. In particular, more specific procedures should be provided for the different items that were identified as important in the present document. Nevertheless, many of them could be addressed by referring to earlier work and existing standards.

[2] Wilkinson, M., Dumontier, M., Aalbersberg, I. et al. The FAIR Guiding Principles for scientific data management and stewardship. Sci Data 3, 160018 (2016). https://doi.org/10.1038/sdata.2016.18

IEA Wind Task 49
Final Technical Report

APPENDIX - WP2
Analysis and reduction of wind turbine noise emissions

Contents

1 Introduction **2**

2 Wind turbine noise codes benchmark **2**
2.1 Benchmarking of WTN codes and directivity 2
2.1.1 Completion of the Wind Turbine Noise Code benchmark . . . 3
2.1.2 Comparison of Amiet turbulent inflow noise model 3
2.1.3 Investigation of trailing edge noise directivity 4
2.1.4 Effect of airfoil shape and trailing edge bluntness on noise . . 7
2.2 Comparisons with Wind Turbine Noise measurements 9
2.2.1 DANAERO NM80 turbine 9
2.2.2 MEXICO turbine 9

3 Serration benchmark **13**

4 Tip noise **14**

5 WP2 / Annex 1 - Report on WTN code benchmark **15**

6 WP2 / Annex 2 - Conference proceedings on comparisons between wind turbine noise code prediction models and measurement data **76**

7 WP2 / Annex 3 - Conference proceedings on comparisons of serration noise measurements in various facilities **98**

8 WP2 / Annex 4 - Presentation of the serration benchmark main results **123**

9 WP2 / Annex 5 - Conference proceedings on measurement of tip noise **144**

1 Introduction

WP2 consist of a series of activities resolving about the generation of wind turbine noise. It focuses on aerodynamic noise sources (see Appendix WP1 in which a Fact Sheet on tonal/mechanical noise is available).

The activities can be divided into three main parts:

1. Wind turbine noise generation code benchmarks
2. Serration noise
3. Tip noise

which are all continuations of the initial work conducted during the first phase of Task 39.

These activities are reported in 3 corresponding sections. A number of publications are also reported as Annexes as reported further down in the present document.

2 Wind turbine noise codes benchmark

This section has two main objectives:

1. Terminate the code-2-code benchmark comparison initiated in the first phase of Task 39.
2. Conduct new benchmarks using actual wind turbine noise measurements for comparisons with the various noise prediction codes from the Task participants.

2.1 Benchmarking of WTN codes and directivity

The results of these activities are reported below. It consists of the completion of the code-2-code comparison, and two additional activities that took place as part of this WP. These activities relate to noise emission at airfoil levels. Indeed, correctly modeling airfoil noise is a preriquisite to be able to model wind turbine blade/rotor noise. Therefore, in concertation with Task 39 participants the three following investigations were conducted:

1. Comparison of Amiet turbulent inflow noise model, including directivity.
2. Investigation of trailing edge noise directivity with a higher fidelity model and verification of a standard model.
3. Investigation of the effect of airfoil geometry on trailing edge noise.

2.1.1 Completion of the Wind Turbine Noise Code benchmark

This work is a continuation of work initiated during the Phase 1 of Task 39 (2018-2020). The goal was to compare different wind turbine noise prediction codes using the same reference turbine. The NM80 2.3 MW turbine used in the DANAERO project is considered. Indeed, its geometry and operational conditions can be shared with IEA Wind Task participants.

The final report for this activity is available in Section 5/Annex 1, to be found later in the present document.

2.1.2 Comparison of Amiet turbulent inflow noise model

In order to assess the correctness of the turbulent inflow models, a few Task 39 participants (DTU, TUM and NREL) decided to engage in a detailed comparison of the so-called Amiet turbulent inflow (TI) noise model. It is the standard model that is used to predict that specific noise source in nearly (if not all) engineering applications. The main results can be summarized in Fig. 1 which displays the models prediction of the TI noise spectra by each of the partner's Amiet model implementation. Note that this calculation test-cases were meant to reproduce the results from the original article by Amiet. A very good agreement between the different predictions is found, which confirms the fact that the three participants indeed implemented the model correcly.

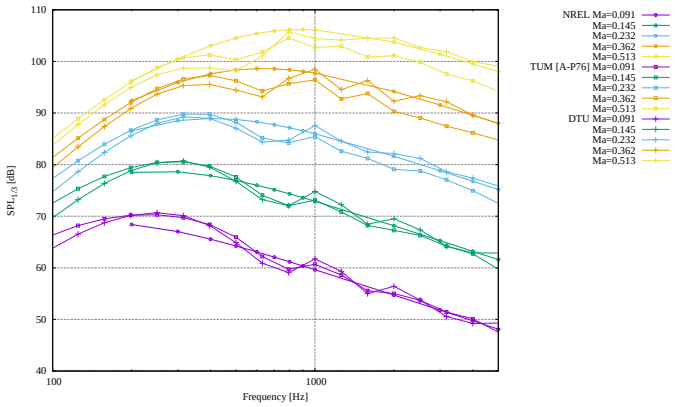

Figure 1: Comparison of TI noise model predictions for three different implementation of Amiet model.

2.1.3 Investigation of trailing edge noise directivity

In this exercise, the Task participants agreed to investigate further the directivity of trailing edge (TE) noise (which is the dominant part of wind turbine noise emission in the audible range). Investigations are performed for the overall wind turbine (see Section 2.2), but the issue of the validity of the model at airfoil level remains, as far as directivity pattern predictions are concerned. In order to assess the directivity of an airfoil section, a spherical coordinates system (as illustrated in Fig. 2) is defined for specifying the observer position with respect to the airfoil section.

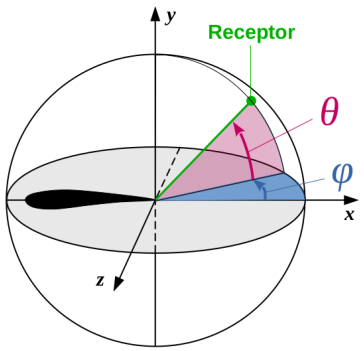

Figure 2: Spherical coordinates system with two angles for assessing TE noise directivity for an airfoil section TE noise directivity.

The investigation starts by displaying the TE noise directivity of the Amiet TE noise model in the 2D airfoil section plane, see Fig. 3, and in the airfoil transverse plane, see Fig. 4 [1]. As expected, the model predicts directivity patterns which are symmetric with respect to the axis defined by the airfoil chord, for both figures. The cardioid pattern characteristic of TE noise is also recovered at higher frequency in Fig. 3, while the airfoil behave more like a dipole a low frequencies as expected.

In order to address the validity of the directivity predictions by the Amiet model, calculations were conducted with a Boundary Element Method (BEM) developed by DTU. This framework can accurately predict the directivity effects of TE noise (although only in the airfoil plane is this 2D implementation of the BEM). The results were compared with the standard Amiet model in Fig. 5. The directivity patterns differ quite significantly toward larger frequencies and it can only be surmised that the Amiet model is less reliable here.

[1] Note that the present Amiet TE noise model should not be confused with Amiet turbulent inflow (TI) noise as in the previous section

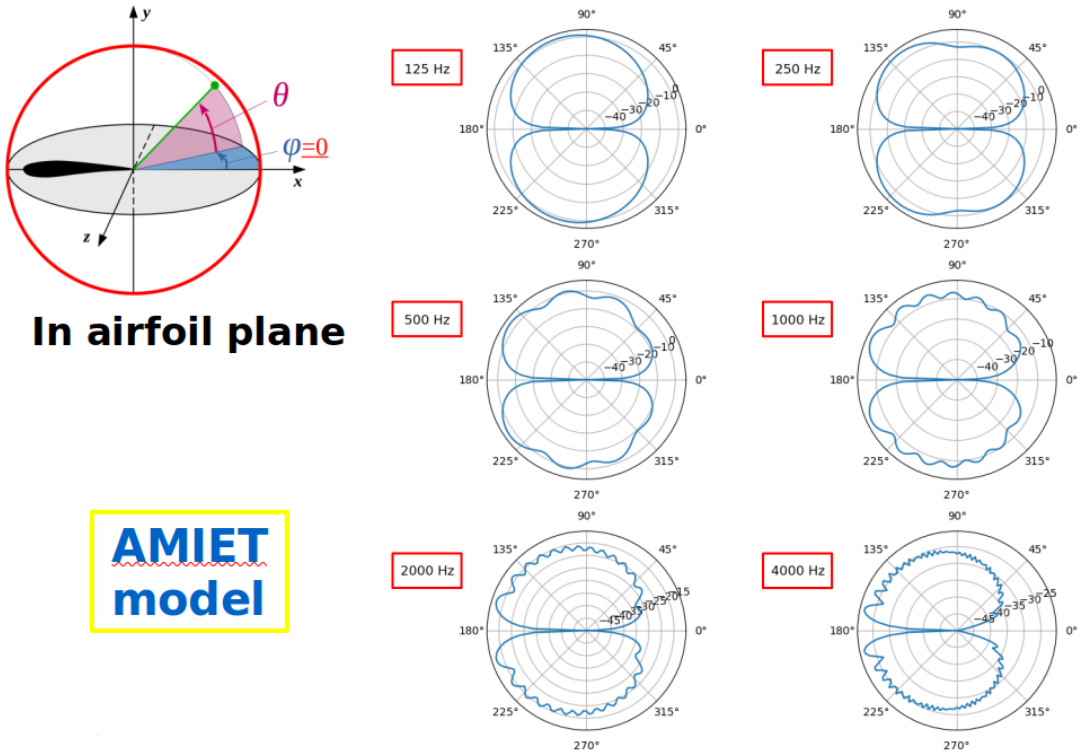

Figure 3: Airfoil section TE noise directivity of Amiet model in the airfoil plane (the observer locations are illustrated by the sketch on the upper left of the figure by the red line).

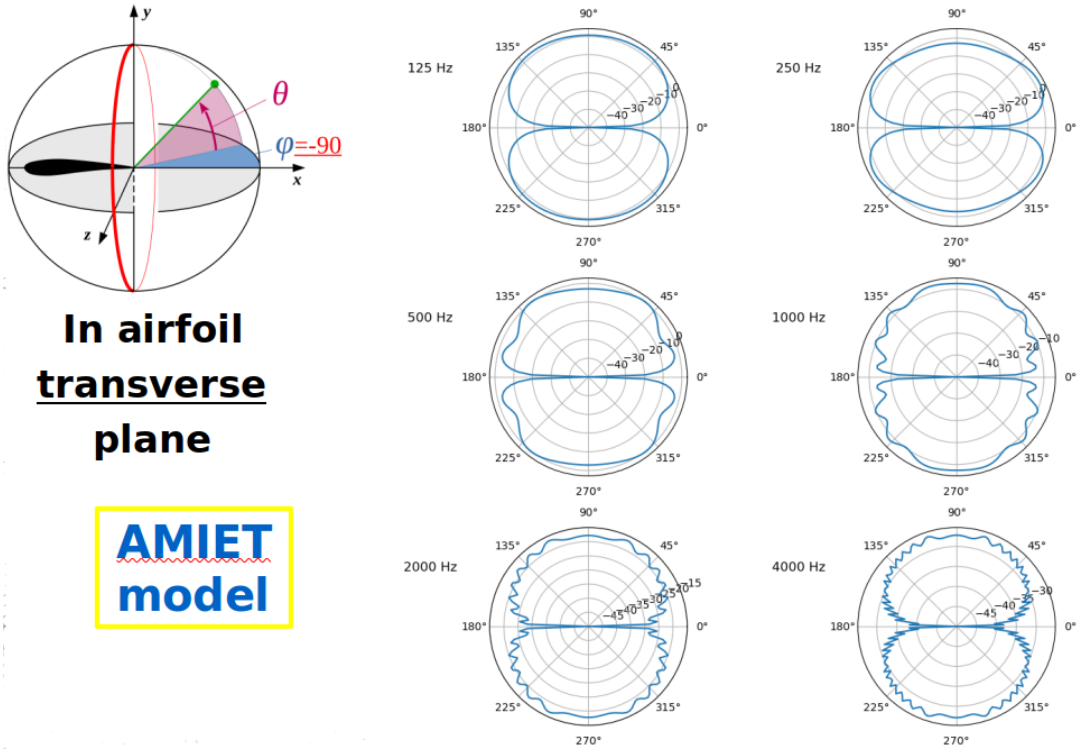

Figure 4: Airfoil section TE noise directivity of Amiet model in the airfoil transverse plane (the observer locations are illustrated by the sketch on the upper left of the figure by the red line).

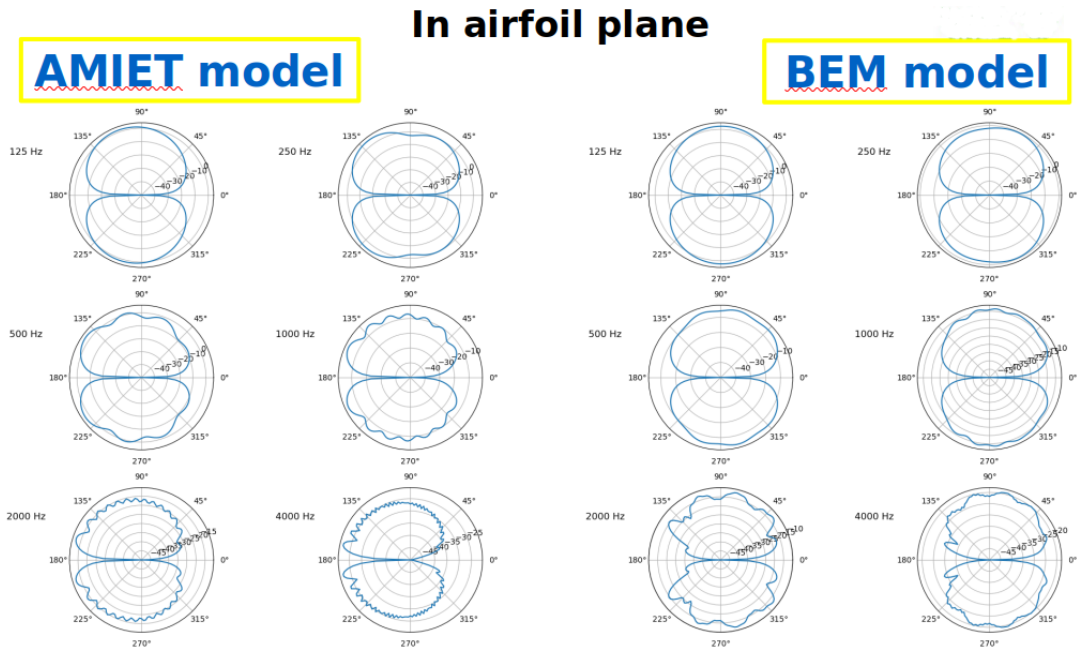

Figure 5: Airfoil section TE noise directivity of Amiet model and BEM model in the airfoil plane.

2.1.4 Effect of airfoil shape and trailing edge bluntness on noise

In this section, the influence of the airfoil shape (more precisely its thickness) on trailing edge noise is investigated. It must be reminded here that Amiet TE noise model does assume a flat plate as a approximation of the airfoil geometrical shape, while the BEM can account for the real airfoil geometry.

The TE noise levels are evaluated for a flat plate using the Amiet model and the BEM model. If using the BEM model, the airfoil can also be modelled as a plate with a given thickness, with its real geometry either with a sharp or a blunt trailing edge. The different TE noise predictions at a point located above the TE are displayed in Fig. 6.

It appears the BEM method for a flat airfoil is missing some of the acoustic energy compared to the Amiet models, and other geometries. It is not clear at this stage what is producing this effect.

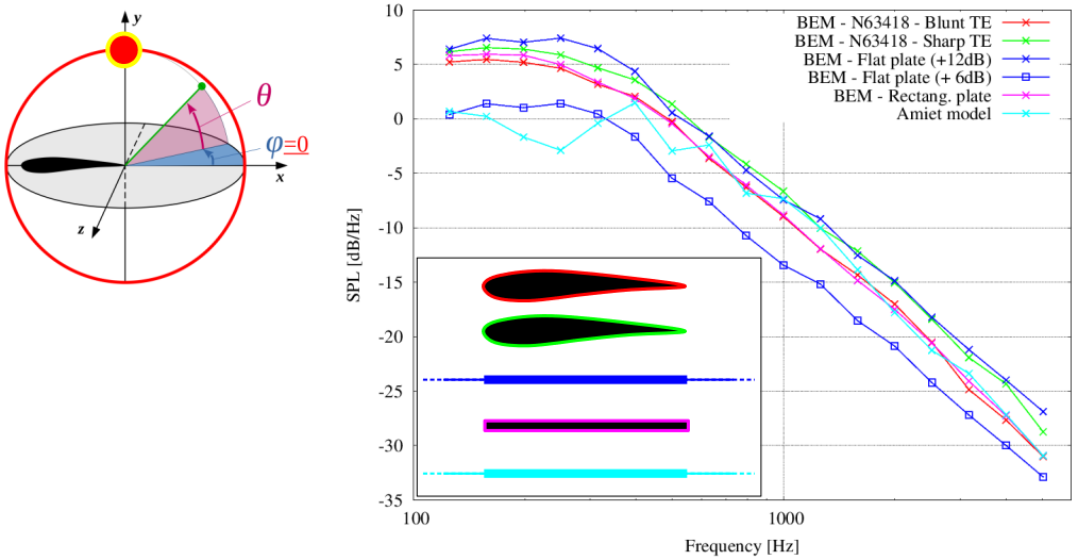

Figure 6: Influence of airfoi shape and TE bluntness on TE noise perdictions using Amiet TE noise model and BEM (Noise is evaluated at a point directly above the TE as indicated in the sketch at the upper left of the figure).

The effect of the TE bluntness is investigated further in terms of noise directivity patterns. In Fig. 7, the TE noise directivity in the airfoil plane is compared, using the BEM, for a sharp and blunt TE. It is observed that the effects are small and only detectable at higher frequencies.

Finally, the relative thickness of the airfoil itself and its impact on TE noise directivity is investigated in Fig. 8. Once again, the effects are small and only detectable at higher frequencies.

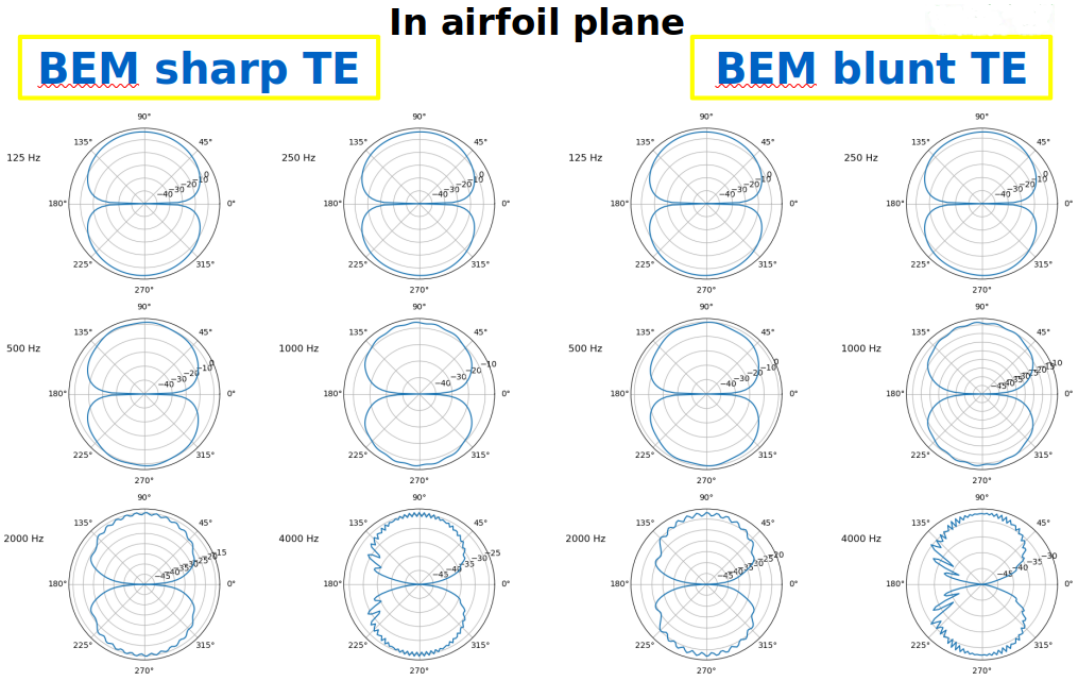

Figure 7: Influence of TE bluntness on TE noise perdictions using BEM (sharp versus blunt TE).

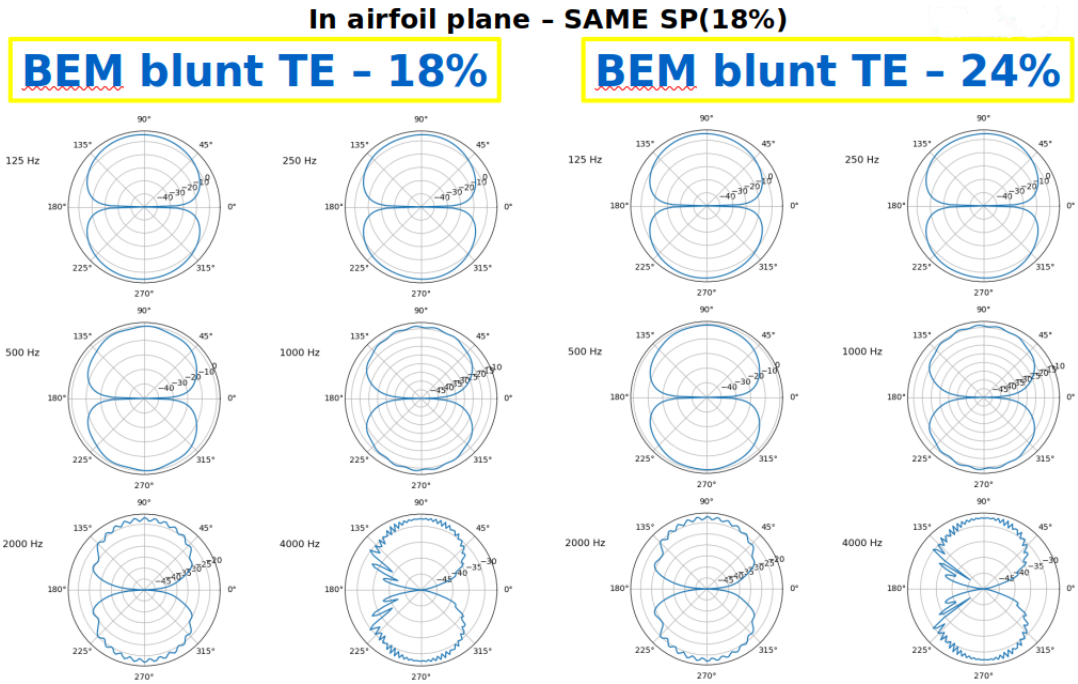

Figure 8: Influence of TE bluntness on TE noise perdictions using BEM (18% and 24% bluntness).

2.2 Comparisons with Wind Turbine Noise measurements

2.2.1 DANAERO NM80 turbine

The final report for this activity takes the form of a conference publication presented at the WTN 2023 conference. In this publication, Task 39 participants wind turbine noise prediction frameworks are confronted with actual field noise measurement of the NM80 turbine (see previous section). These data were kindly provided by Vestas, and could be published under the conditions that noise levels were anonymized. The resulting article can be found later in this report (see Section 6)

2.2.2 MEXICO turbine

An additional benchmark of wind turbine noise prediction codes has been considered as part of WP2. The so-called Mexico rotor, which has been extensively used as part of the earlier IEA Wind Task 29 MexNext (Aerodynamics), is considered. It is a smaller rotor equipped with extensive instrumentation. This 3-bladed wind turbine of 4.5 m diameter is placed in the 9.5 m×9.5 m open section of the Large Low-speed Facility (LLF) of DNW in the Netherlands (see Fig. 9).

An acoustic array was positioned between nozzle exit and the model, below the jet (depicted in red in Fig. 9). As can be observed the array could not be placed directly upstream of the model, but was positioned slightly sideways due to the restricted space available between the nozzle (depicted in orange) and external balance (depicted in blue). The 4 m×4 m phased array consisted of 140 electret microphones (circular arrangement) sampled at a frequency of 51.2 kHz over a period of up to 60 s for each data point.

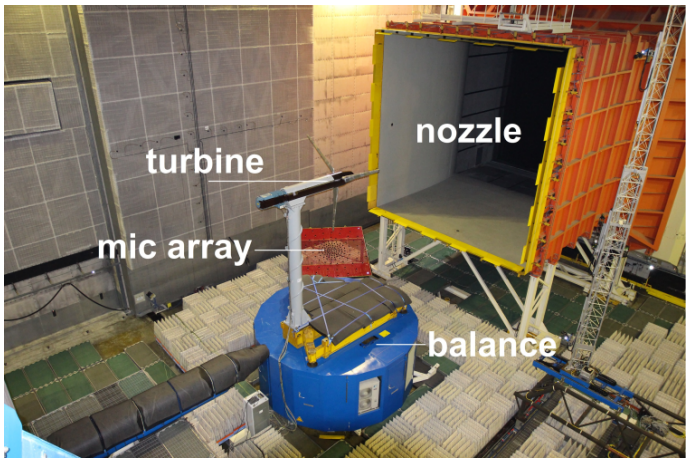

Figure 9: LLF open jet wind tunnel facility at DNW.

Comparisons with the measured noise data include two wind turbine noise prediction frameworks:

- The SILENT code developed by ECN (now TNO) institute in The Netherlands.
- The HAWC2-Noise code developed by DTU.

In order to verify that the aerodynamic calculations are correct (as these are a prerequisite for the aeroacoustic calculation to make sense), the normal and tangential forces exerted on the blades are displayed as a function of radius along the span in Fig. 10. It is observed that there is a good agreement between the DTU calculations and measurements for the two lowest wind speed, but this deteriorates at larger angles of attack, in particular toward the root, due to massive separation of the flow.

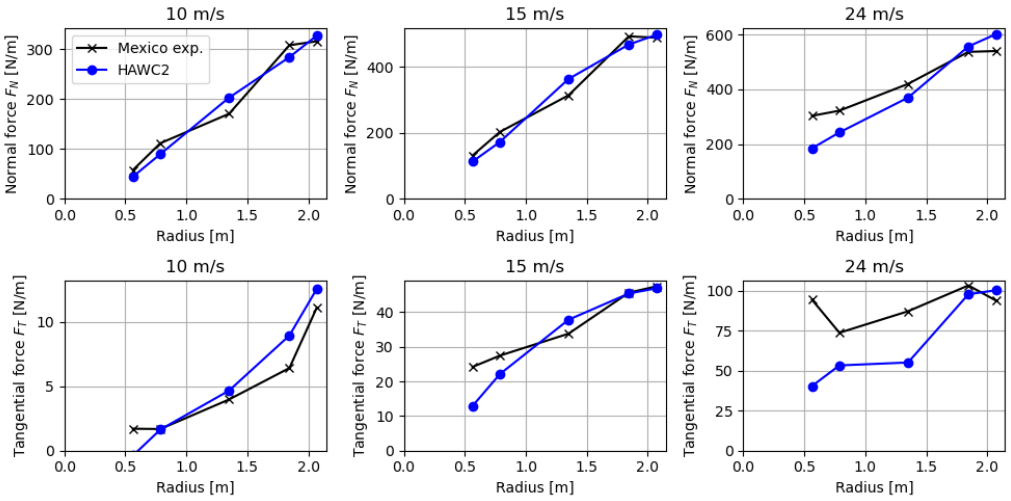

Figure 10: Comparison of measured and predicted aerodynamic forces along the chord.

The main results of this exercise are displayed in Figs. 11 and 12. The difference between the two figures stems from the CFD calculations done as a pre-processor for the DTU TE noise model. In the first figure, the CFD calculations are done for a fully turbulent boundary layer, while in the second one the natural transition model by Drela is used with a factor $N_{\text{crit}} = 9$. It is observed that the agreement is fair in the high-frequency range at lower wind speed in both cases. In contrast, there are large discrepancies at lower frequencies (say below 5 KHz) if using the natural transition model. This indicates that transition on the blade does indeed occur early along the chord in the experiment (probably the blade is tripped in this case). However, for larger wind speeds, the flow becomes detached on most of the blade span (as illustrated above) and the comparisons between measurement and model deteriorate.

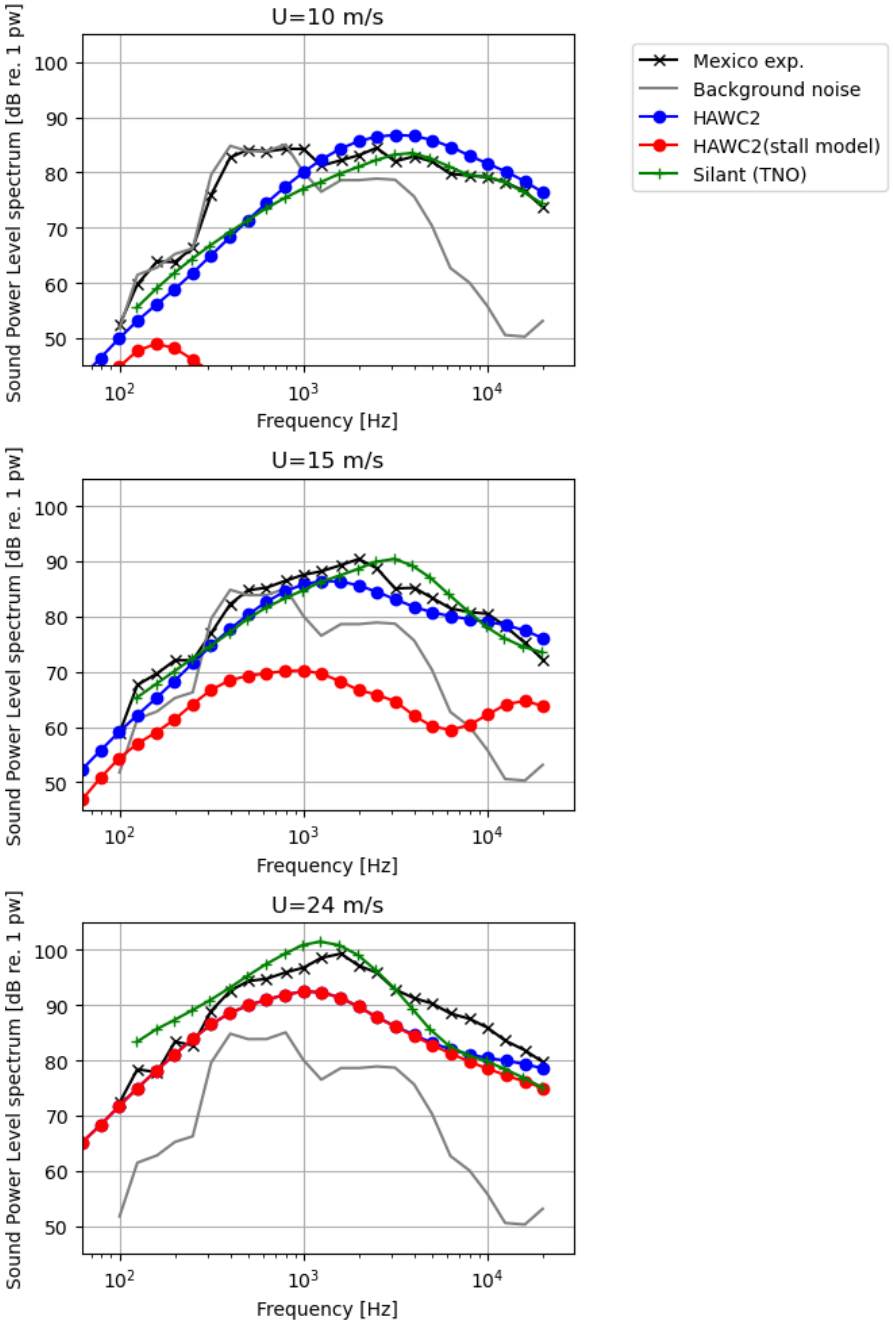

Figure 11: Comparison of measured noise and prediction code results for the Mexico rotor (Fully turbulent boundary layer for TE noise model).

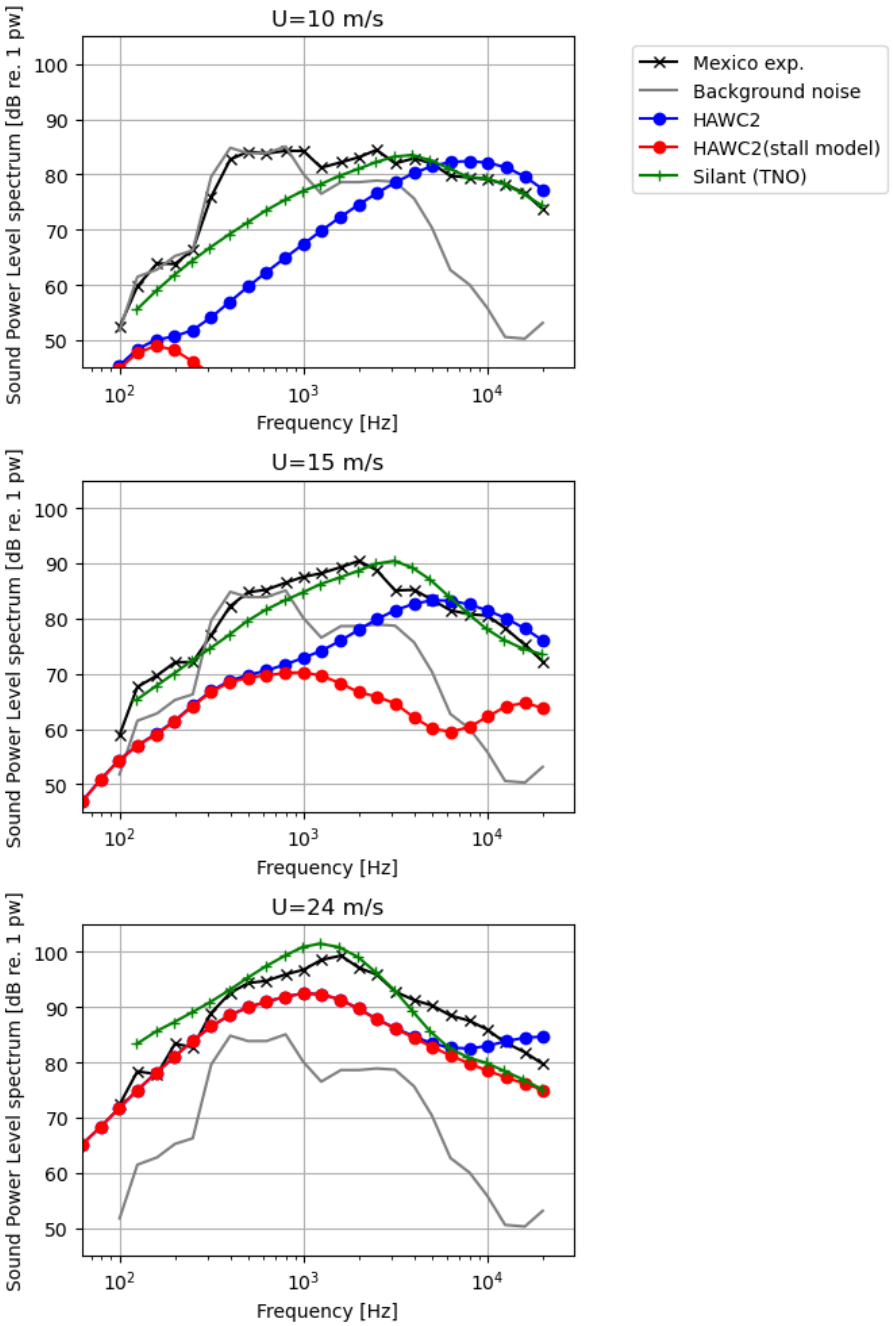

Figure 12: Comparison of measured noise and prediction code results for the Mexico rotor (Natural transition with $N_{\text{crit}} = 9$ of turbulent boundary layer for TE noise model).

3 Serration benchmark

This part of the Task 39 activities is dedicated to the investigation of trailing edge serration, and associated noise reduction at airfoil level. It focuses on a series of wind tunnel measurement campaigns conducted by various Task 39 participants in their respective wind tunnel facilities. During the first phase of the Task 39, 5 wind tunnel facilities were considered. At the end of the Task 39 period of activity, this was extended to 8 facilities.

Noise measurements on 3 different serration geometries in 5 different wind tunnels have been performed in the first phase of Task 39. In the proposed continuation, the data of these measurements are collected and stored in a common file format. The uncertainty of the wind tunnel measurements as well as systematic differences between the measurements in the different tunnels has been assessed.

Several configurations of the data base are chosen for model validation. They have been published under at the annual AIAA/CEAS aeroacoustics conference. Note that an additional publication by the Task 39 participants summarizing the overall Task 39 WP3 investigations is still pending.

Based on the experience, some guidelines for testing aerofoils in wind tunnels are provided. The guidelines include wind tunnel corrections, a list of relevant parameters for the test matrix and tolerances of the model and serrations.

The results of this collaboration work are provided as Annexes below in the present document. These consists of:

- Annex 3: Benchmarking of wind turbine noise simulation codes. A conference paper was presented and published as proceedings at the AIAA/CEAS Aeroacoustics 2022 Conference (see Section 7).

- Annex 4: Document on best practises for wind tunnel testing. This takes the form of a presentation that summarizes the serration benchmark activities (see Section 8).

4 Tip noise

This part of the work concerns the study of tip noise. Wind tunnel noise measurements of a wind turbine blade tip shape were conducted in the DTU PLC wind tunnel.

The results of this measurement campaign were published at the WTN2023 conference and the conference paper is available in Section 9/Annex 5.

The ultimate goal is to provide a database that can be shared with Task 39 participants, e.g. for model validation.

5 WP2 / Annex 1 - Report on WTN code benchmark

DTU Wind Energy-E-****

IEA Wind TCP - Task 29 T3.7 & Task 39 Wind Turbine Noise Code Benchmark - Preliminary Results

Franck Bertagnolio and Andreas Fischer (DTU)
Ferdinand Seel, Thorsten Lutz
and Cordula Hornung (IAG)
Koen Boorsma, Gerard Schepers
and Miguel Restrepo Botero (TNO)
Christina Appel and Michaela Herr (DLR)
Carlo Sucameli (TUM)
Pietro Bortolotti (NREL)
Wouter van der Velden and Damiano Casalino (3DS)

DTU Wind Energy, Denmark
April 2023

Abstract This document gathers the preliminary results from the benchmark of wind turbine noise codes as delivered so far by DTU Wind Energy (Technical University of Denmark, DK), IAG (University of Stuttgart, DE), TNO (The Netherlands Organisation for Applied Scientific Research, NL), DLR (German Aerospace Center, DE), and NREL (National Renewable Energy Laboratory, USA).

ISBN 978–87–550–****-* (Internet)
ISSN 0106–****

Print: Internal Report, DTU Wind energy · 2023

Contents

1 Introduction *5*

2 Description of the modelling frameworks *5*
2.1 TNO - Silant *5*
2.2 IAG Stuttgart - IAGNoise+ *6*
2.3 TUM - Cp-Max AAM *6*
2.4 DLR - hybrid RANS-based CAA method PIANO/FRPM *7*
2.5 3DS wind turbine multi-fidelity approach *7*
2.5.a BEMT-based low-fidelity methodology *7*
2.5.b LBM/FW-H-based middle-fidelity methodology *7*
2.5.c LBM/FW-H-based high-fidelity methodology *8*

3 Benchmark description *8*

4 Analysis of aerodynamic results *9*
4.1 Sectional aerodynamic results *9*
4.1.a Relative and effective velocities *9*
4.1.b Normal and tangential aerodynamic forces *9*
4.1.c Angle of attack *9*
4.1.d Lift and drag aerodynamic forces *9*
4.2 Boundary layer aerodynamic results *12*
4.2.a Boundary layer thicknesses *12*
4.2.b Pressure distributions around airfoils *14*
4.2.c Profiles across boundary layer *16*

5 Analysis of aeroacoustic spectral results *23*
5.1 Surface pressure fluctuations *23*
5.2 Far-field noise spectra *25*

6 Calculations using different aerodynanic inputs but the same rotor noise model *28*
6.1 Aerodynamic results *28*
6.1.a Boundary layer thicknesses *28*
6.1.b Profiles across boundary layer *29*
6.2 Aeroacoustic results *32*
6.2.a Surface pressure fluctuations *32*
6.2.b Far-fied noise *34*

7 Further comparisons of various trailing-edge noise models *38*
7.1 Boundary layer aerodynamic results *38*
7.2 Aeroacoustic results *38*
7.2.a Surface pressure fluctuations *38*
7.2.b Far-fied noise *41*

8 Temporal and spatial variability of noise *43*
8.1 Integrated noise spectra as a function of time *43*
8.2 Directivity of integrated noise spectra *54*

A Geometry and sign conventions for the benchmark results *58*

1 Introduction

The aim of this report is to compare the results obtained by various wind turbine rotor noise prediction codes. These codes include in all cases the trailing edge (TE) noise contribution from the blades, and in most cases also the turbulent inflow noise contribution.

At the time of writing, the results obtained by the following participants are included in the present report:

- DLR - Institute of Aerodynamics and Flow Technology (German Aerospace Center) using the PIANO CAA code (Note that only the TE noise is modeled). The TE noise calculation is based on a boundary layer turbulence reconstruction techniques from RANS calculation. Turbulent inflow noise is not included in the modeling.
- DTU Wind Energy (Technical University of Denmark) using the HAWC2-Noise code which couples the aeroelastic code HAWC2 using the BEM method with a wind turbine aerodynamic noise prediction module using a TNO-Blake type model for trailing-edge (TE) noise and Amiet's model for turbulent inflow (TI) noise. Note that the most recent DTU TE noise model [13], using Howe's formulation for the TE noise scattering part, is used for the comparisons with the other participants' results. Nevertheless, further comparisons are conducted involving Amiet's formulation for TE scattering, as well as an older version of the TNO model [3].
- Institute for Aerodynamic and Gas Dynamics (University of Stuttgart, Germany) using the aerodynamic 3D CFD code Flower (using $k-\omega$ SST turbulence model) and a TNO-Blake type TE noise models and Paterson and Amiet's model [26] with Moriarty's thickness correction [24] for the TI noise.
- TNO - Wind Energy Technology (The Netherlands Organisation for Applied Scientific Research) using a BEM aerodynamic code and the BPM noise model for TE noise as well as Amiet for TI noise.

Three particular test cases from the overall benchmark are considered: Test Cases 1.1, 1.2 and 1.3. Test Cases 1.1 and 1.3 are fully axi-symmetric configurations of the wind turbine rotor and inflow with two different rotational speeds: 12.3 rpm and 16.1 rpm. The Test Case 1.2 is identical to 1.1, but the the flexibility of the blades is taken into account in this case. A fourth Test Case 1.4 is also included in the original benchmark description. The latter includes inflow wind shear, but the analysis of this case will be considered at a later time.

2 Description of the modelling frameworks

In this section, the different models and numerical frameworks used by the different participants are reviewed.

2.1 TNO - Silant

The aeroacoustic calculation of TNO is divided into three programs: Blademode [5], RFOIL [19] and SILANT[23].

BladeMode is an in-house software developed by TNO (then ECN Wind Energy) for calculating the aero-elastic stability of blades. In this case it is used to calculate the quasi steady aerodynamic state of the rotor using BEM theory, taking into account torsional and bending deformations. The resulting sectional angle of attack and Reynolds number distribution along the blade span are then used to as input to the SILANT model.

This program includes the noise calculation from turbulent trailing edge noise and tip noise based on the model of Brooks, Pope and Marcolini [6] and inflow noise using the model of Amiet [1] and Lowson [20].

However for the turbulent trailing edge noise model, input is also needed of the boundary layer displacement thickness at the trailing edge of the airfoil sections along the blade. The RFOIL 2D panel code (with interacting boundary layer method) has been used to generate a database of this variable for each airfoil as a function of chord Reynolds number and angle of attack, which is fed to the SILANT code as a look-up table.

The resulting sectional noise source strengths are acoustically summed to result in the overall rotor source levels and 1/3-Octave band spectra. In addition to calculating noise sources, SILANT can also calculate propagation effects after specifying receiver location, taking into account directivity, refraction, spreading, Doppler and absorption effects of each individual sectional source receiver combination. As such it can also provide an estimate for the noise level fluctuations or 'swish' observed in the vicinity of the turbine.

2.2 IAG Stuttgart - IAGNoise+

The Institute of Aerodynamics and Gas Dynamics (University of Stuttgart, Germany) uses the IAGNoise+ noise prediction code. This semi-empirical model computes the generated trailing edge noise (TEN) based on 3D flow solutions from computational fluid dynamics (CFD) simulations. In this work, Reynolds-averaged Navier Stokes (RANS) simulations using a k-ω SST turbulence model were run with the flow solver FLOWer.

IAGNoise+ employs a TNO-Blake type model for the computation of TE noise [4]. Compared to a classical TNO-type model, the current implementation [17] includes the part of the wall pressure fluctuation source term that is associated with turbulence-turbulence interaction and usually neglected in the basic model. This inclusion allows for more accurate predictions at higher angles of attack, where slight to moderate flow separation occurs. Additionally, the anisotropy factor was adjusted to also include adverse pressure gradient effects. The IAGNoise+ prediction tool also offers a way to calculate inflow noise, based on the model proposed by Paterson and Amiet [26] with Moriarty's thickness correction [24].

2.3 TUM - Cp-Max AAM

This framework is the one described in [29]. It is based on the in-house developed aeroservoelastic wind turbine solver Cp-Lambda, which implements a BEM formulation and provides the aerodynamic inputs necessary for the aeroacoustic calculations.

Several aeroacoustic models are implemented within this framework. For the purpose of the present paper, trailing edge noise results are provided for two different models (the BPM model [6] and a version of the TNO model described in [29]). For both models, 2D boundary layer characteristics are obtained through XFoil. TI noise spectra are provided for two different formulations of the Amiet model. The first formulation is the full implementation of [25], while the second

one corresponds to the approximations of the Amiet model for high and low frequencies. An additional low-frequency correction is included as shown in [21].

2.4 DLR - hybrid RANS-based CAA method PIANO/FRPM

An automatized 2D process chain for TBL-TEN [27, 12] is used to provide an acoustic prediction for trailing edge noise of 2D profiles. Originally developed to assist low-noise airfoil design optimization, this method has been validated in detail within the BANC framework [14, 15]. The process chain operates via bash scripting the input parameters (like airfoil geometry, Reynolds number, angle of attack, chord length and process parameters, e.g. number of iterations, simulated real time and post processing options). For the RANS simulations the DLR CFD Code TAU, and for the acoustic prediction the DLR CAA code PIANO with the stochastic sound source model FRPM [11] (Fast **R**andom **P**article **M**esh method), are applied.

In a second step the results from process chain are combined with DLR's TAP (**T**urbine **A**coustic **P**rediction) tool to extrapolate and summarize the data for a complete rotor [2]. Ongoing work includes the successive extension of TAP by additional semi-empirical source models for flow separation and TI noise. TI noise predictions applied herein are based on Hornung *et al* [16].

2.5 3DS wind turbine multi-fidelity approach

Wind turbine aerodynamic and acoustic calculations have been carried using the multi-fidelity framework *Opty∂B*-WTNOISE [8]. Three approaches have been used, one being based on a BEMT rotor aerodynamic calculation, and the other two relying on LBM-VLES scale-resolved transient flow simulations.

2.5.a BEMT-based low-fidelity methodology

The conventional BEMT tool *Opty∂B*-BEMT with uniform inflow and Prandtl tip-losses correction is employed [7]. The required blade sectional forces are computed using the boundary layer model by Drela & Giles [10, 9] implemented in the BEMT tool. Post-stall lift and drag coefficients are computed using Viterna & Corrigan approach [30]. The radial distribution of boundary layer data extracted at 97.5% of the chord on the suction side and 95% on the pressure side are used to compute the wall pressure spectrum via a semi-empirical formulation. On the suction side, a model is used, obtained by blending Schlinker's [28] model at low frequency with the Kamruzzaman's [18] one at high frequency, and by recalibrating the overall energy to the Schlinker's model value. On the pressure side, the Schlinker's model is used.

2.5.b LBM/FW-H-based middle-fidelity methodology

PowerFLOW 2.5D simulations are performed by means of a fully automatic workflow fed with sectional coordinate profiles generated by *Opty∂B*-PFROTOR, and values of Mach number and angle of attack computed by *Opty∂B*-BEMT [8]. Simulations are carried out using a coarse-to-fine strategy to speed-up the mean-flow settling at coarse-mesh level before sampling the transient flow data for the acoustic calculations at a fine-mesh level. The span of the extruded section is fixed at 0.1 m and a zig-zag trip of height equal to 1 finest voxel size is automatically created and located at prescribed user location. If the precursor BEMT calculation is performed in free-transition conditions, the estimated natural transition locations at the corresponding radial location can be used as input for the trip

location. It is worth clarifying that PowerFLOW has inherent capabilities to treat boundary-layer transition at wall-model level, and also in relation to the switching mechanism from a Reynolds-average to a scale-resolving turbulence modelling. However, the usage of a thin non-intrusive physical trip allows to significantly reduce the mesh resolution compared to what needed for an inherent scale-resolving activation. For every radial strip selected by the user from the available blade segmentation, the PowerFLOW simulation generates a transient wall pressure file which is used by the frequency-domain FW-H solver *Opty∂B*-FWHFREQ executed by *Opty∂B*-WTNOISE. Full-blade noise spectra are recovered by *Opty∂B*-WTNOISE via an incoherent summation of sectional noise spectra, scaled by the ratio between the physical spanwise extension of the blade strip and the 2.5D simulated span.

2.5.c LBM/FW-H-based high-fidelity methodology

PowerFLOW 3D simulations are performed by means of a fully automatic workflow used for multicopter eVTOL, rotorcraft, fan and wind turbine applications [8]. A series of simulations are carried out with mesh refinement in different blade strips where the turbulent scales are trigged by a trip. Similarly to the 2.5D approach, the full turbine noise levels are recovered by incoherent summation of the individual strip contributions.

3 Benchmark description

The reader is referred to the document entitled "Wind Turbine Noise Code Benchmark (Phase I) - Definition of three rounds of calculations on DANAERO experiment – Aerodynamics & acoustics comparisons" that was worked out by and circulated among the participants during the planning phase of the present benchmark.

4 Analysis of aerodynamic results

In this section, the aerodynamics of the wind turbine is investigated. Two types of physical quantities are considered:

- Sectional aerodynamic data including inflow and relative velocity, angle of attack, aerodynamic forces, pressure distribution
- Profiles of boundary layer aerodynanic data near the trailing edge including velocity, turbulence kinetic energy, turbulence dissipation and turbulence integral length scale across the boundary layer

4.1 Sectional aerodynamic results

4.1.a Relative and effective velocities

The relative velocity and the effective velocity (the latter being the sum of the relative velocity and the induction velocity) are displayed as a function of radius in Fig. 1.

Note that the results obtained wigh the HAWC2 code during the aerodynamic benchmark in Task 29 (red curve) is also displayed in the figures. It is reported here only to ensure that the present HAWC2-noise calculations are consistent with these earlier calculations. It does not mean that this is an accurate and/or validated result. The same remark holds for the results displayed hereafter in this section.

It can be seen that there is a very good agreement between the three codes and that the effect of the induction velocity is small.

4.1.b Normal and tangential aerodynamic forces

The normalized normal and tangential aerodynamic forces, denoted C_N and C_T, respectively, are reported in Fig. 2 as a function of radius.

For Test Case 1.1, there is a relative good agreement between the codes for both quantities. For Test Case 1.3, the IAG results appears to diverge from DTU/TNO results as far as C_N is concerned, but there is also slight discrepancies between all models for C_T. The flexibility (Test Case 1.2) has virtually no influence of the forces.

4.1.c Angle of attack

The angle of attack as a function of radius is displayed in Fig. 3.

For Test Case 1.1, there is a relative good agreement between the codes with differences less than 0.2^o. These discrepancies increases up to 0.5^o toward the tip for Test Case 1.3. The blade flexibility in Test Case 1.2 appears to have a larger impact on DTU results that it is the case for those from TNO.

4.1.d Lift and drag aerodynamic forces

The normalized lift and drag aerodynamic forces, denoted C_L and C_D, respectively, are reported in Fig. 4.

For Test Case 1.1, all models predict similar C_L values, but TNO model predicts increasing C_D values toward the root, while DTU/IAG predicts more or less constant values. The latter is also observed in Test Cases 1.2 and 1.3. For Test Case 1.3, the IAG model predicts lower C_L along the blade which is in accordance with conclusions for the C_N values above.

These normalized forces appear not to be significantly influenced by the flexibility of the blades.

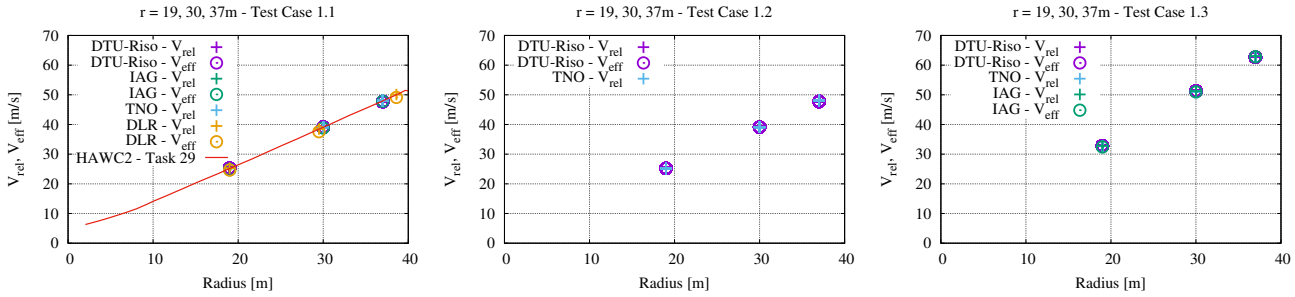

Figure 1. Relative and effective velocities as a function of radius.

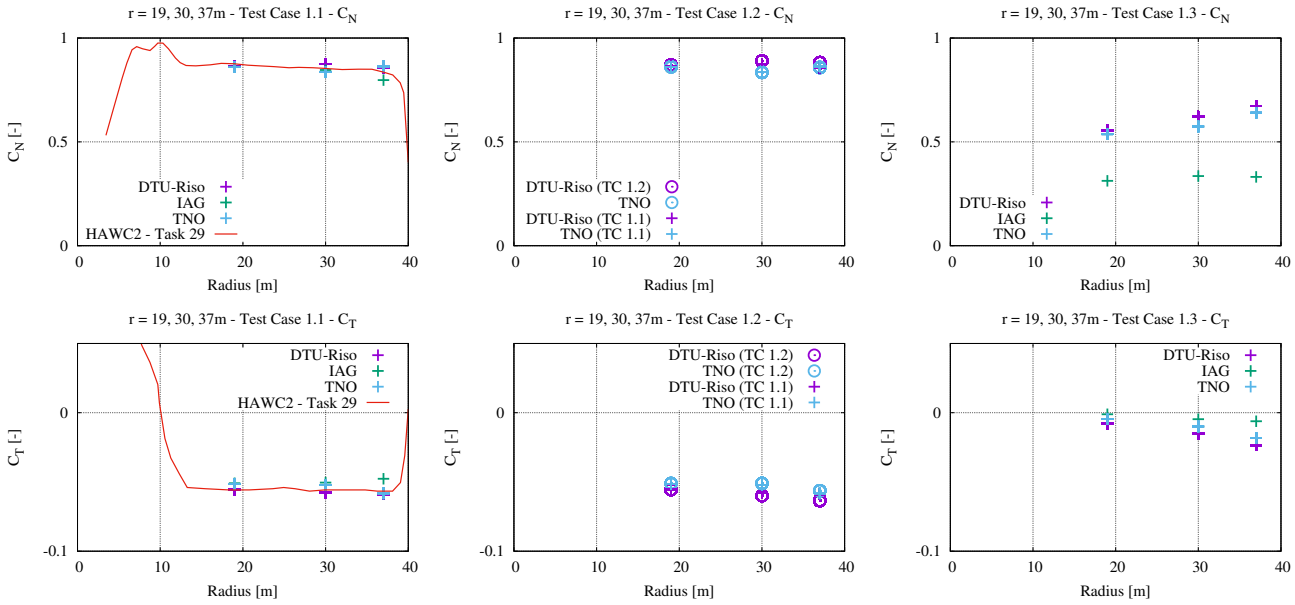

Figure 2. Normal and tangential aerodynamic forces as a function of radius.

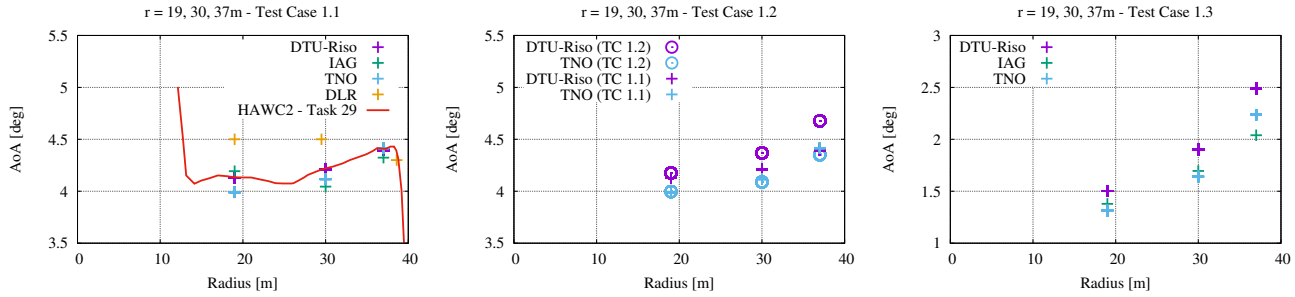

Figure 3. Angle of attack as a function of radius.

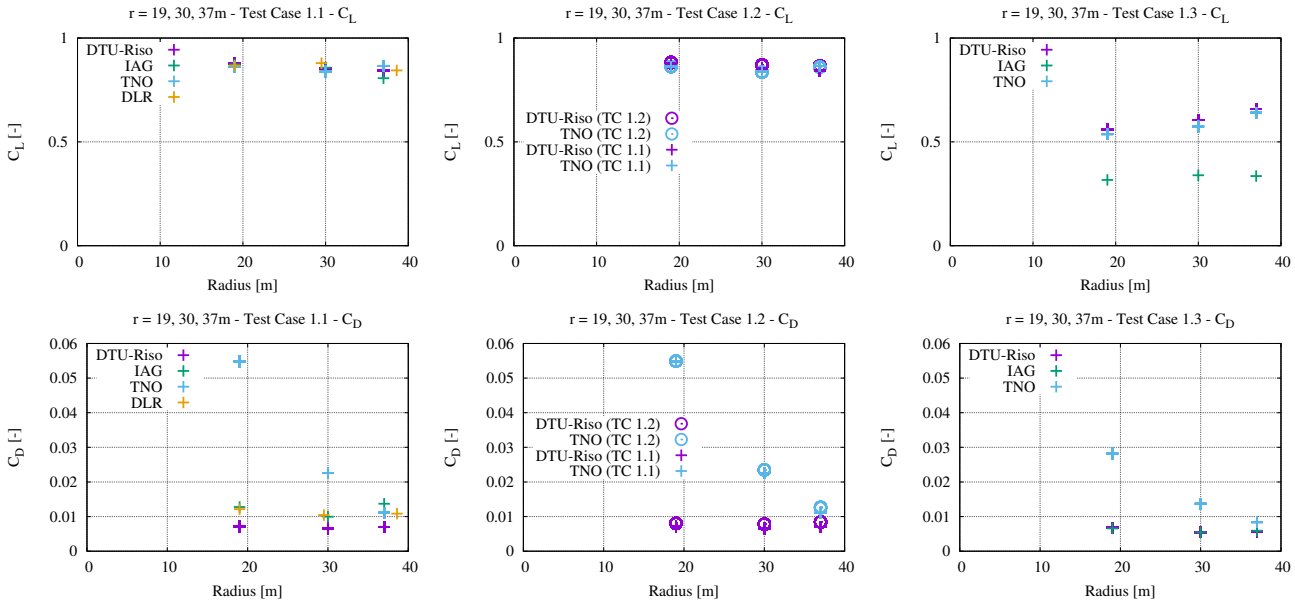

Figure 4. Lift and drag forces as a function of radius.

4.2 Boundary layer aerodynamic results

4.2.a Boundary layer thicknesses

The boundary layer thickness δ, displacement thickness δ^* and momentum thickness Θ are displayed as a function of radius in Figs. 5 and 6 for the suction and pressure sides, respectively.

The boundary layer thicknesses differ largely for the DTU/IAG results. The latter conclusion is attributed to the difficulty of evaluating this quantity numerically (e.g. from a CFD calculation). Note here that IAG is using a criterion based on the turbulent kinetic energy k_T, while DTU is using an iterative algorithm based on 99% of the free-field velocity and the slope of the boundary layer velocity profile. It is expected that these discrepancies should not have a real impact on the noise emission results, unless the boundary layer thickness is specifically used in the noise model.

There is good agreement between the codes for the displacement and momentum thicknesses at the section near the tip of the blade. However, the results from the different models differ increasingly toward the root of the blade.

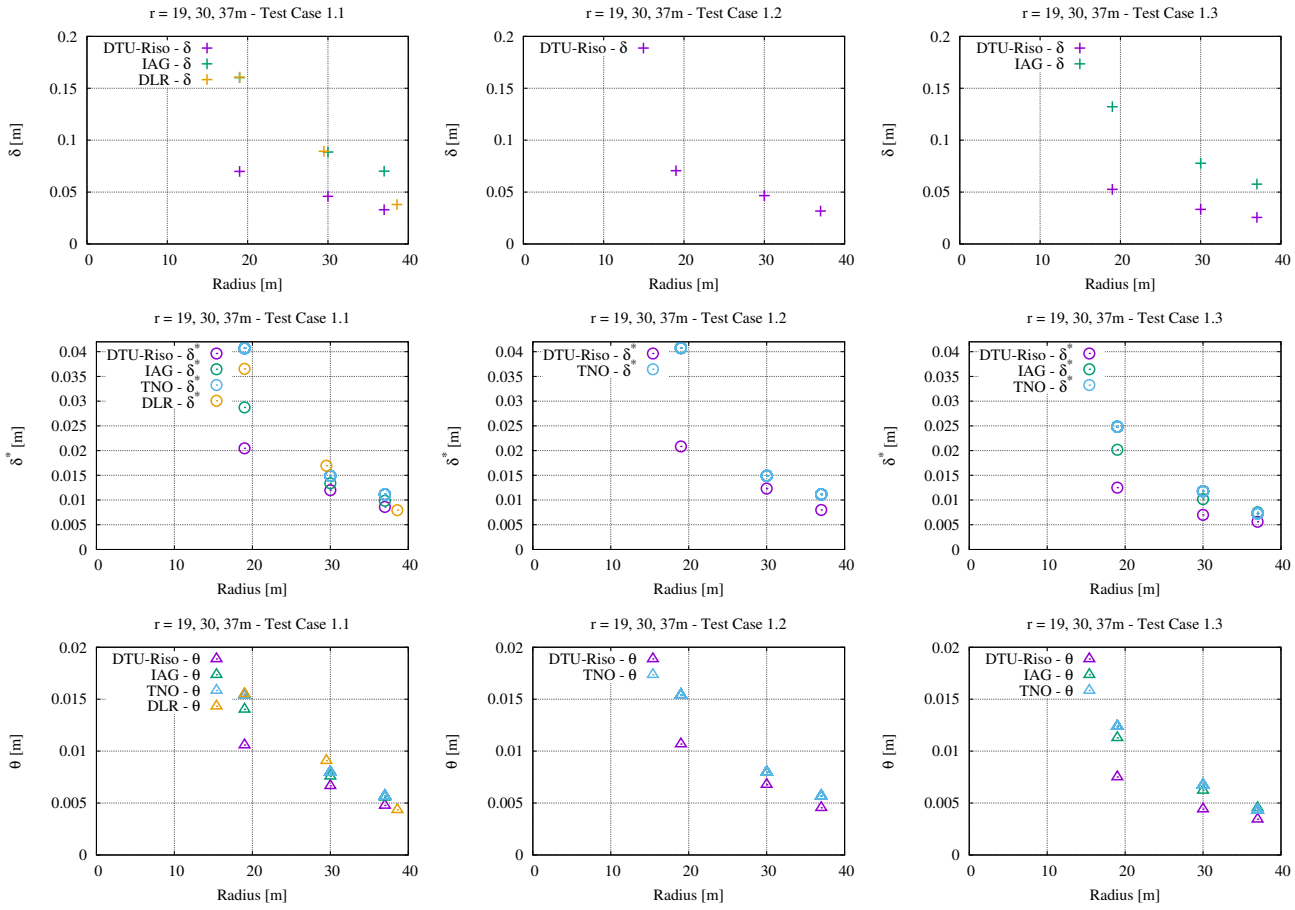

Figure 5. Boundary layer, displacement and momentum thicknesses as a function of radius on the suction side at $x/C = 93\%$.

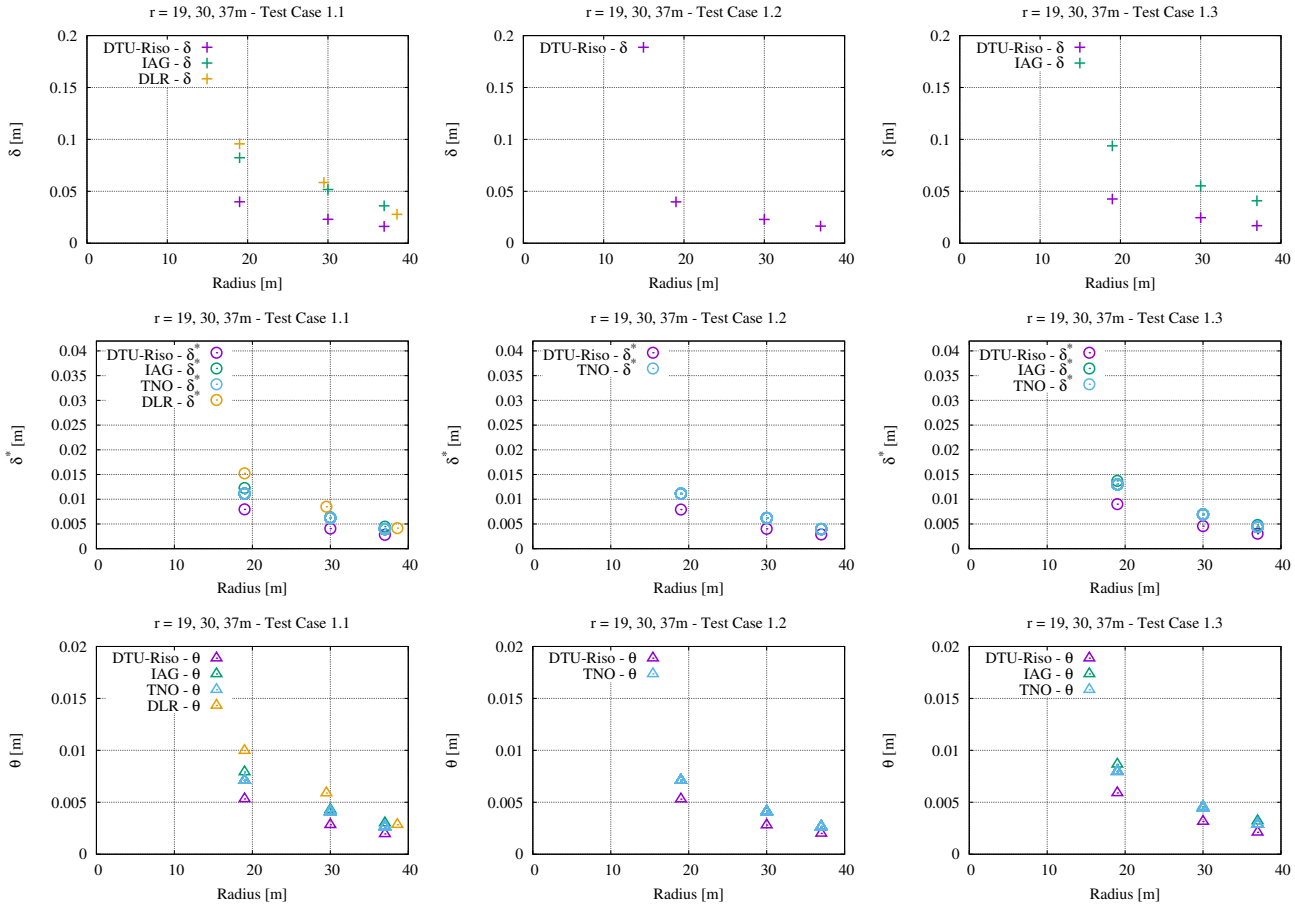

Figure 6. Boundary layer, displacement and momentum thicknesses as a function of radius on the pressure side at $x/C = 91\%$.

4.2.b Pressure distributions around airfoils

The surface pressure coefficient C_p around the airfoil at the 3 considered blade section: 19 m, 30 m and 37 m, respectively are plotted in Fig. 7, only for the Test Case 1.1. The plots are zoomed-in around the trailing edge region in Fig. 8

A very close agreement between DTU and DLR results is observed on the suction side and near the trailing edge, although it gets worse on the pressure side. The discrepancies are slightly larger for the IAG results. Overall, when looking at the entire airfoils' chord, the agreement is acceptable.

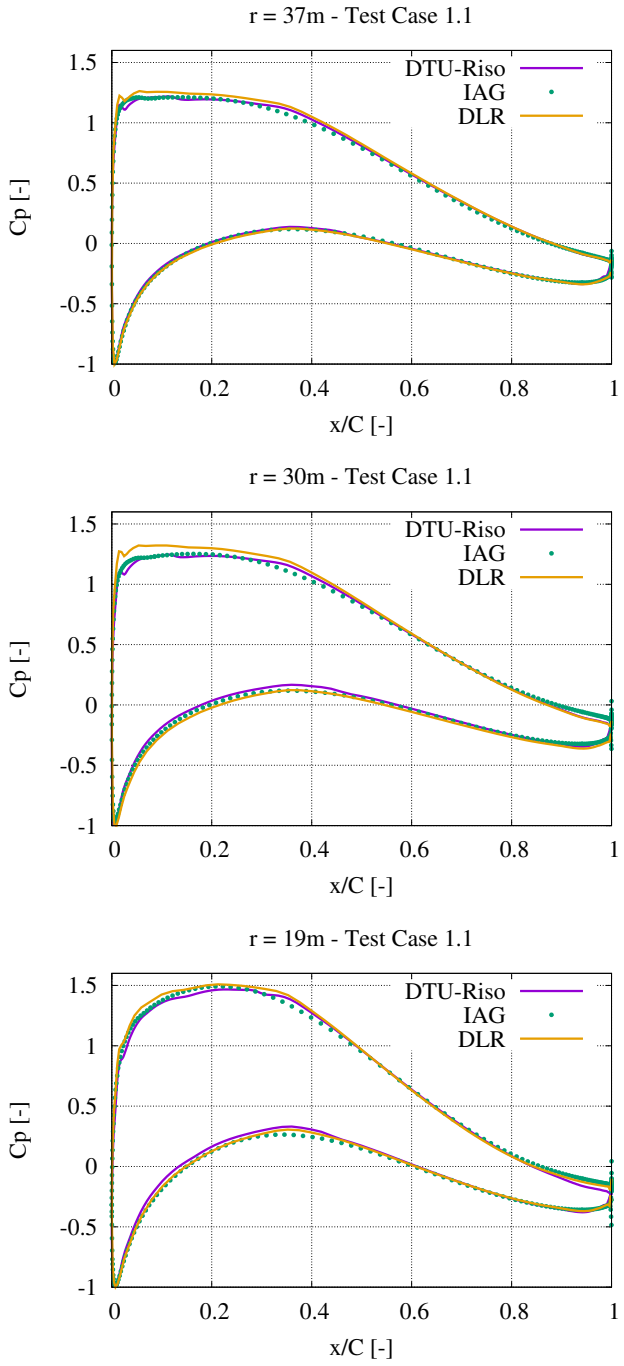

Figure 7. Surface pressure coefficient around airfoil blade sections at the spanwise radii $r = 19$, 30 and 37 m.

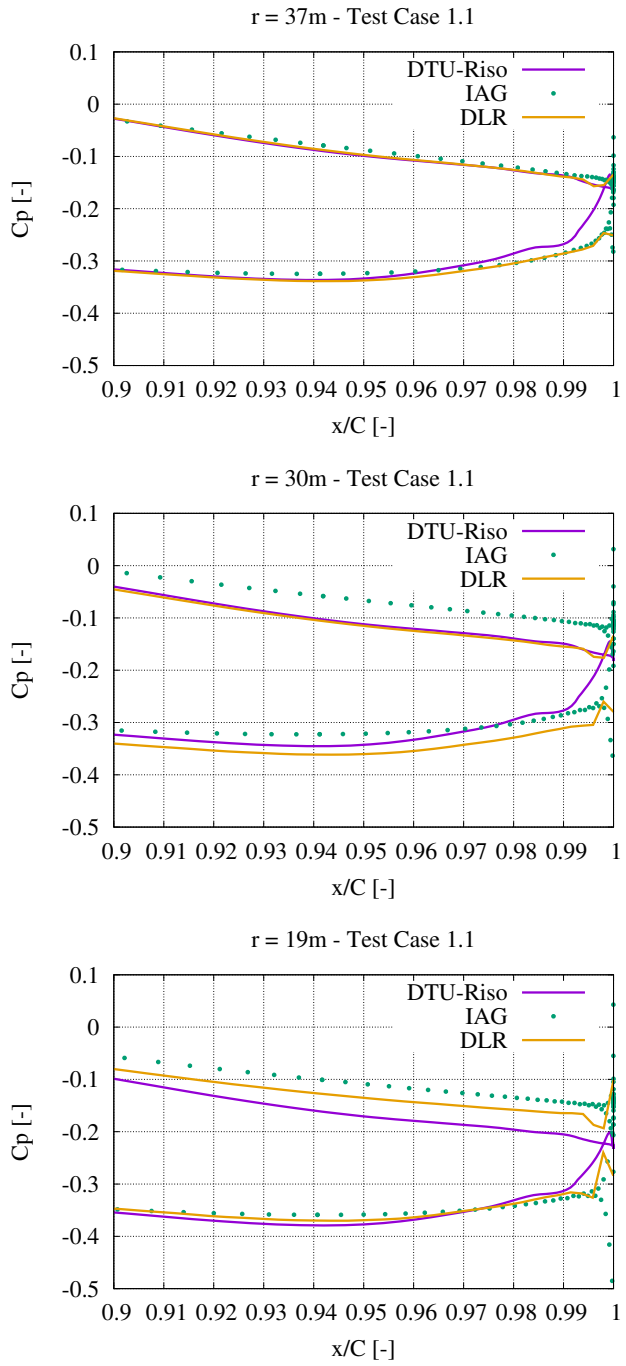

Figure 8. Surface pressure coefficient around airfoil blade sections at the spanwise radii $r = 19$, 30 and 37 m - Zoom of the trailing edge area.

4.2.c Profiles across boundary layer

The flow velocity, turbulent kinetic energy (TKE), turbulent dissipation and turbulence integrale length scale across the boundary layer are displayed at the blade sections at 19, 30 and 37 m along the span on the suction side in Figs. 9, 11 and 13, respectively, and on the pressure side in Figs. 10, 12 and 14, respectively. The chord position relative to the entire chord C where these profiles are extracted $x/C = 93.3$ and 91% for the suction and pressure sides, respectively.

The velocity profiles are in relative good agreement as well as the TKE, although some larger discrepancies are observed for Test Case 1.3. This may be related to the above-mentioned discrepancies of the angle of attack for this case.

The turbulent dissipation are similar in the outer region of the boundary layer, but the IAG code shows a higher peak of dissipation near the wall. It is probably specific to the boundary layer turbulence model used in their code. Note here that the dissipation ϵ is obtained from the ω value from the $k{-}\omega$ SST in both IAG and DTU codes using the following formula:

$$\varepsilon = 0.09\ \omega\, k_{\mathrm{T}}$$

In addition, there is no correction on the above value for the noise calculations.

The turbulence integral length scales differ also in the inner region of the boundary layer, but the agreement is relatively good. This may have a moderate impact on the noise emission. Note that the integral length scale is defined (for CFD calculations) by the following formula:

$$L_{22} = 0.3875\, k_{\mathrm{T}}^{3/2}/\varepsilon \quad \text{and} \quad L_{22} = 0.7468\, L_{\mathrm{int}}$$

according to Lutz *et al* [22], with $\Lambda = L_{int}$ in the plots (to be confirmed???).

As expected, the flexibility of the blades has a relatively little impact on the boundary layer quantities, although measurable for the turbulent kinetic energy (and thus for the integral length scale) as observed for the DTU results for Test Case 1.2.

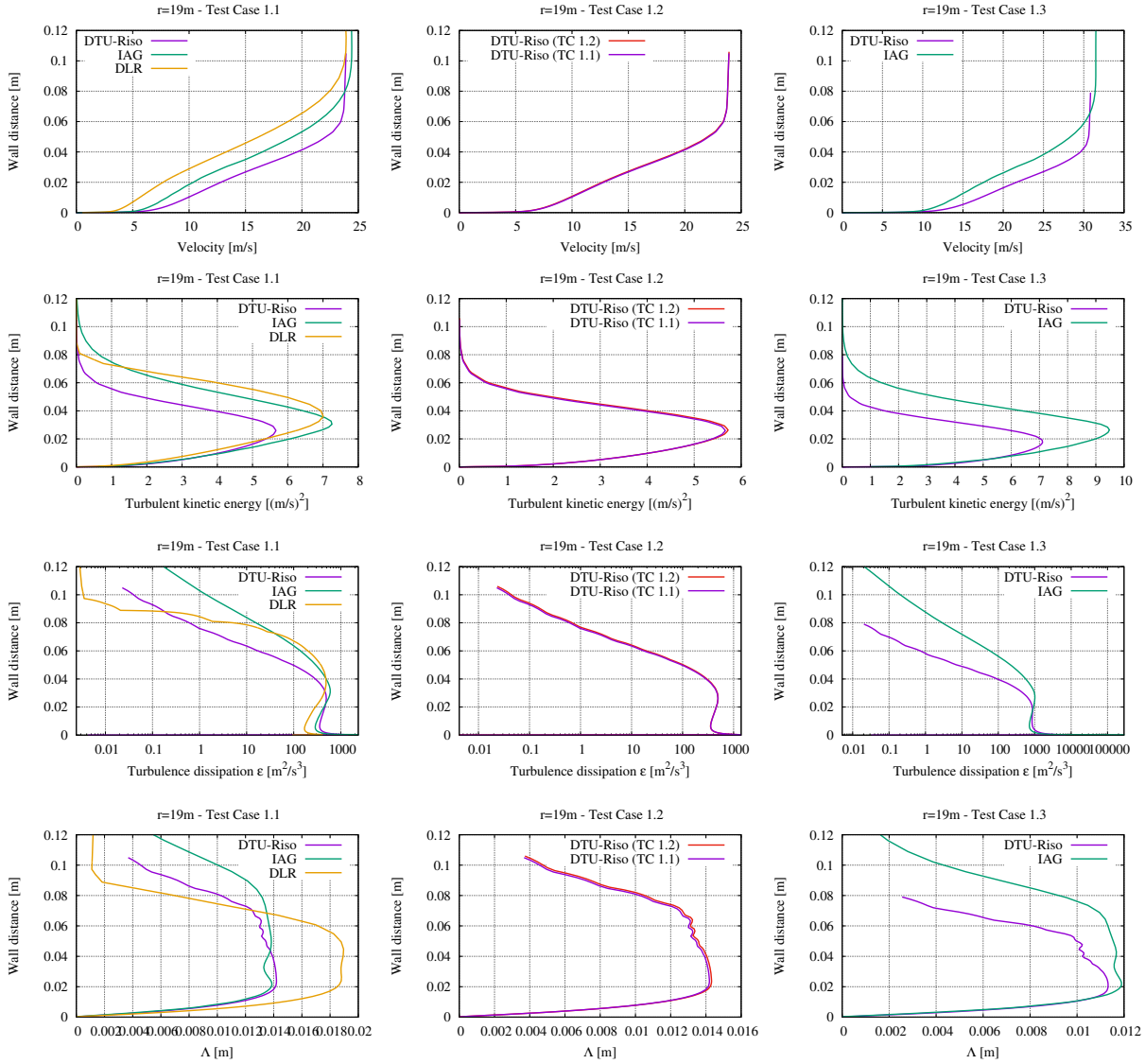

Figure 9. Boundary layer profiles of velocity, TKE, dissipation and integral length scale on the suction side at $x/C = 93\%$ and at the spanwise radius $r = 19\,m$.

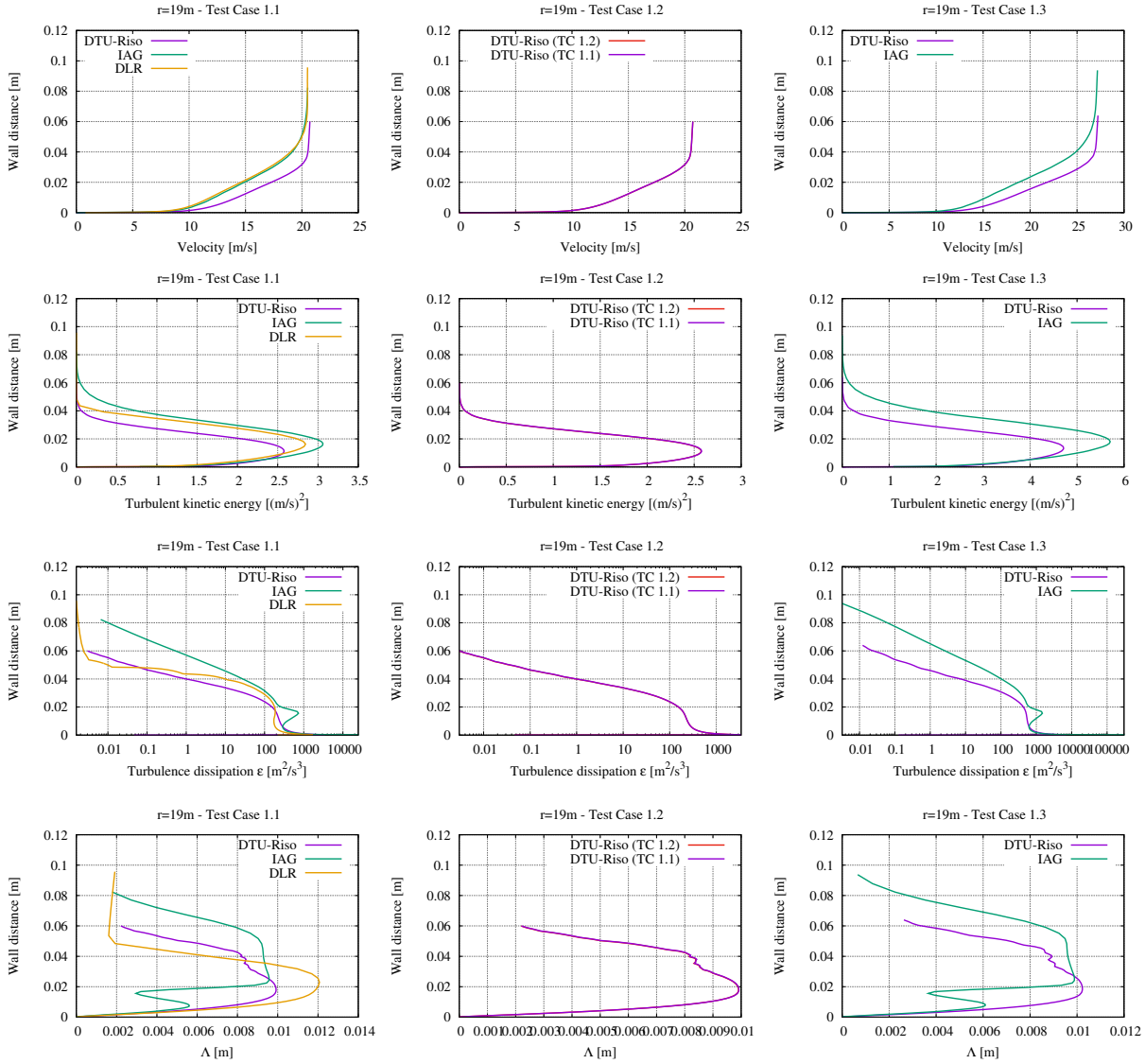

Figure 10. Boundary layer profiles of velocity, TKE, dissipation and integral length scale on the pressure side at $x/C = 91\%$ and at the spanwise radius $r = 19\,m$.

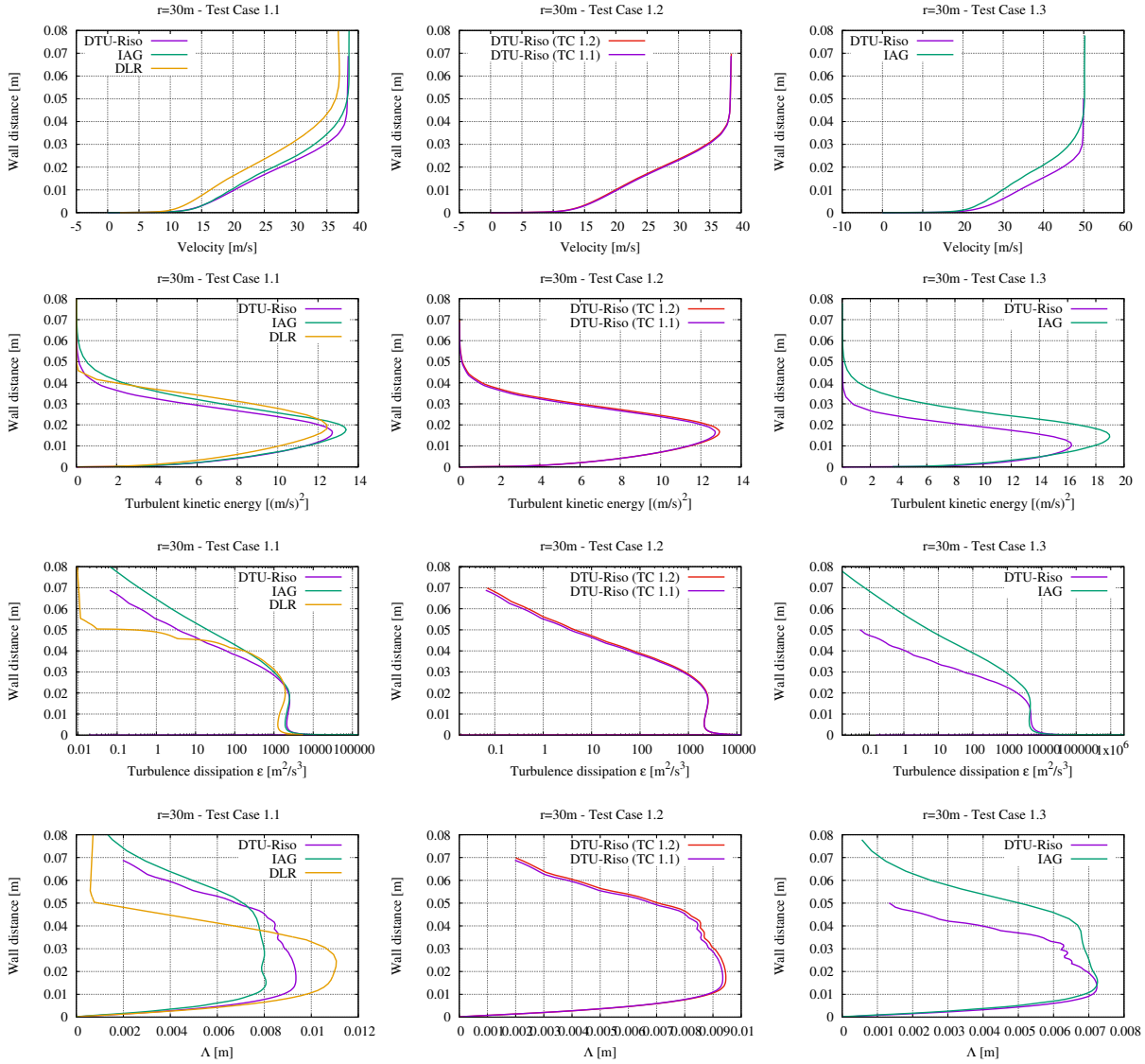

Figure 11. Boundary layer profiles of velocity, TKE, dissipation and integral length scale on the suction side at $x/C = 93\%$ and at the spanwise radius $r = 30\,m$.

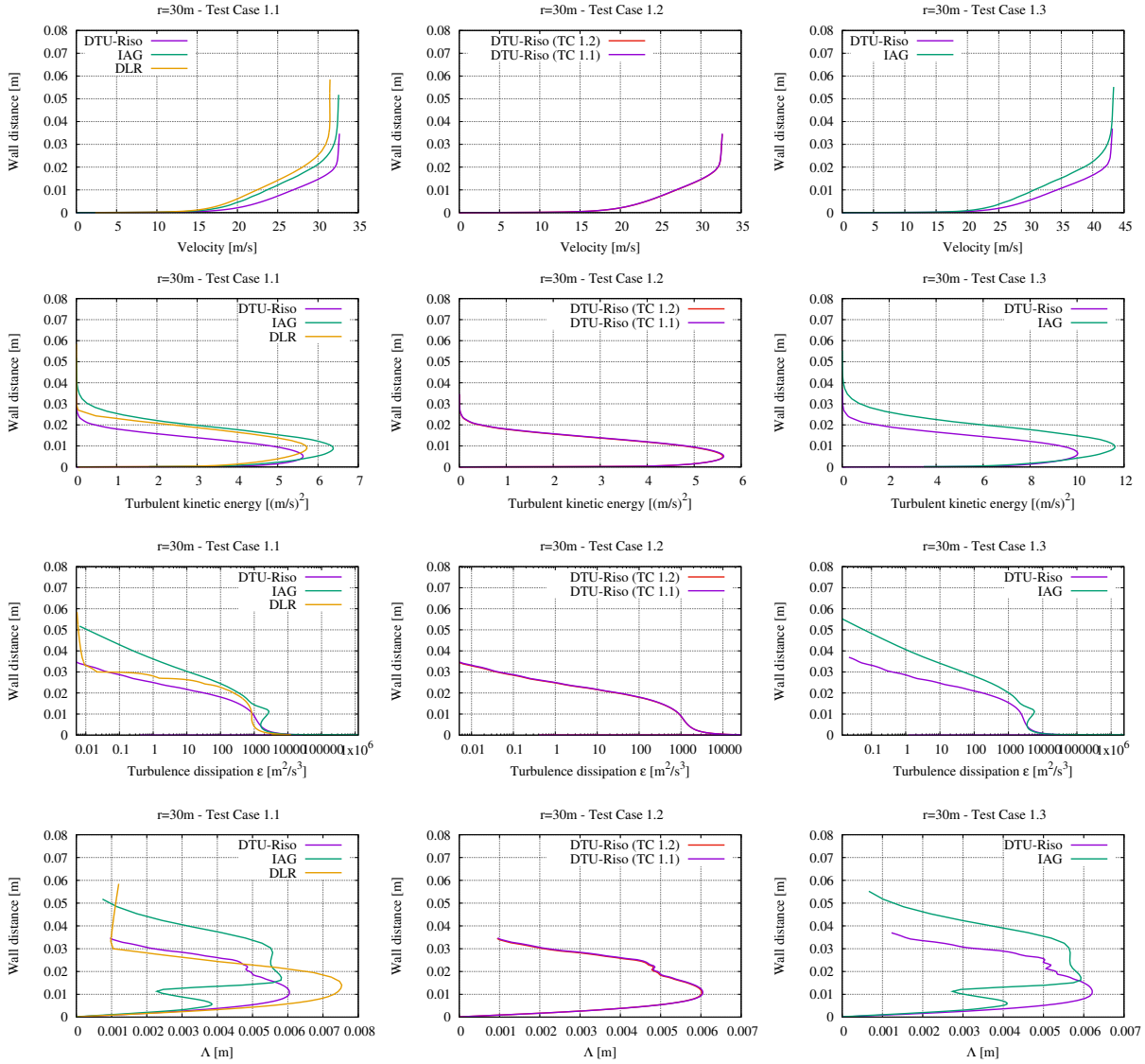

Figure 12. Boundary layer profiles of velocity, TKE, dissipation and integral length scale on the pressure side at $x/C = 91\%$ and at the spanwise radius $r = 30\,m$.

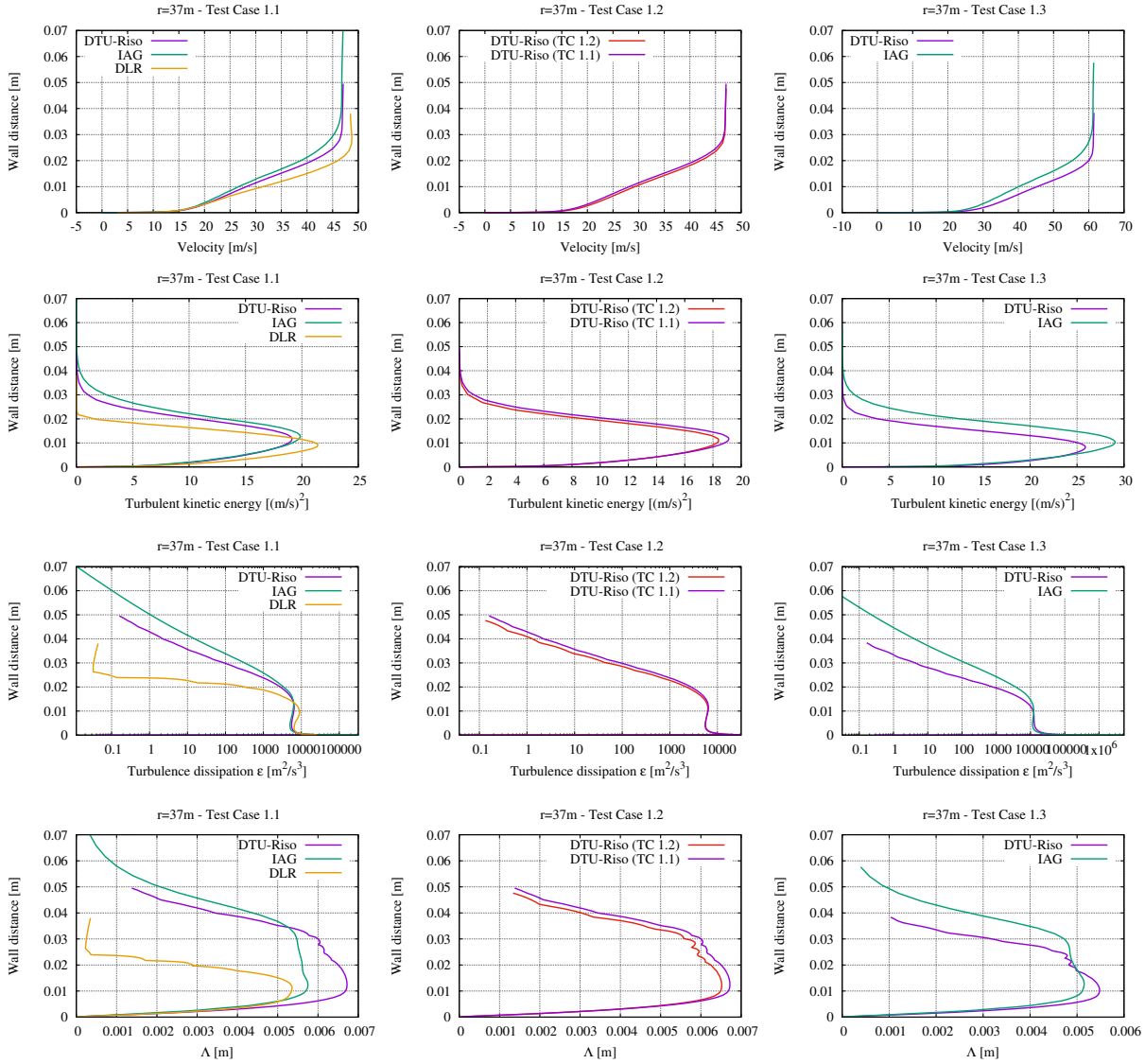

Figure 13. Boundary layer profiles of velocity, TKE, dissipation and integral length scale on the suction side at $x/C = 93\%$ and at the spanwise radius $r = 37\ m$.

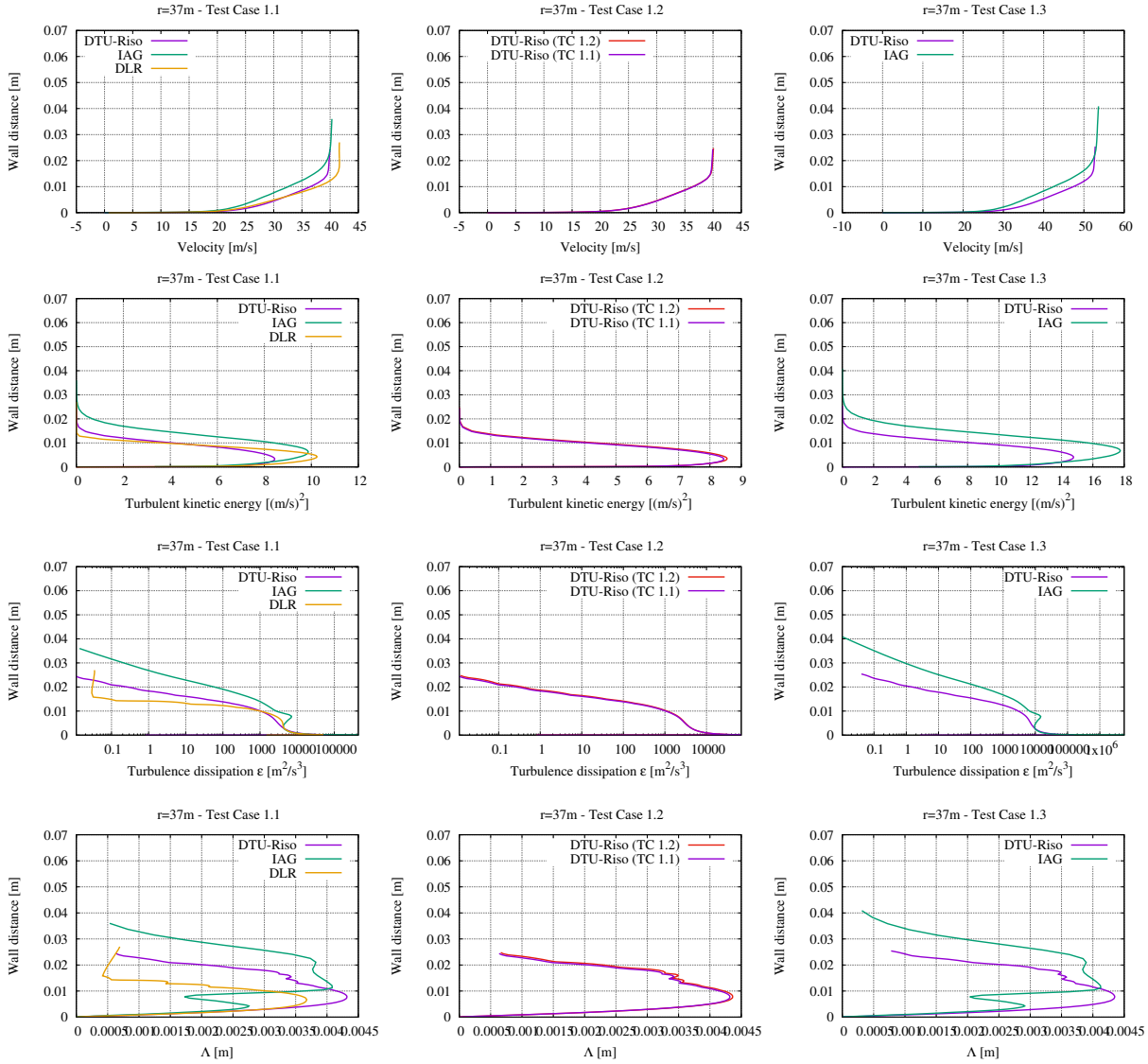

Figure 14. Boundary layer profiles of velocity, TKE, dissipation and integral length scale on the pressure side at $x/C = 91\%$ and at the spanwise radius $r = 37\ m$.

5 Analysis of aeroacoustic spectral results

In this section, quantities directly related to the wind turbine noise emission are investigated. These are:

- The surface pressure fluctuations near the trailing edge for trailing edge noise, but possibly also near the leading edge if one is interested in turbulent inflow noise, and if the considered model provides such quantity in both cases
- The far-field noise at several locations in the surrounding of the turbine

5.1 Surface pressure fluctuations

Note that TNO is using the BPM model for trailing edge noise and the surface pressure spectra are not provided by this model.

The surface pressure spectra are plotted again only for the outer blade section $r = 37\,\mathrm{m}$ and at the chord position $x/C = 93.3\%$ and 91%, for the suction and pressure sides, respectively, in Figs. 15, 16 and 17 for the sections at 19, 30 and 37 m along the span, respectively.

The results differ quite importantly, in particular in the high-frequency range (say above 2000 Hz) where the roll-off of the spectra as a function of frequency are quite different.

Nevertheless, on the suction side and below 1000 Hz, the two codes are in slightly better agreement, but the comparisons are far from satisfactory.

The reason for these large discrepancies should be clarified (e.g. with additional results from a third participant to start with).

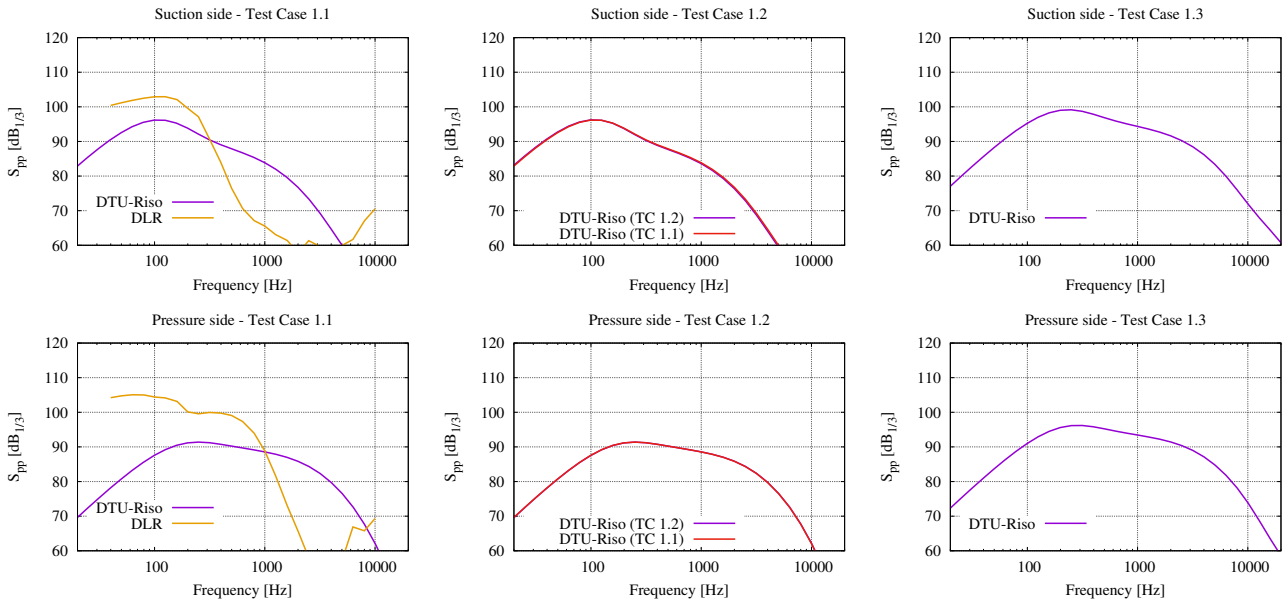

Figure 15. Surface pressure spectra at $r = 19\,m$ and $x/C = 93.3\%$ (top) and 91% (bottom) on the suction and pressure sides, respectively.

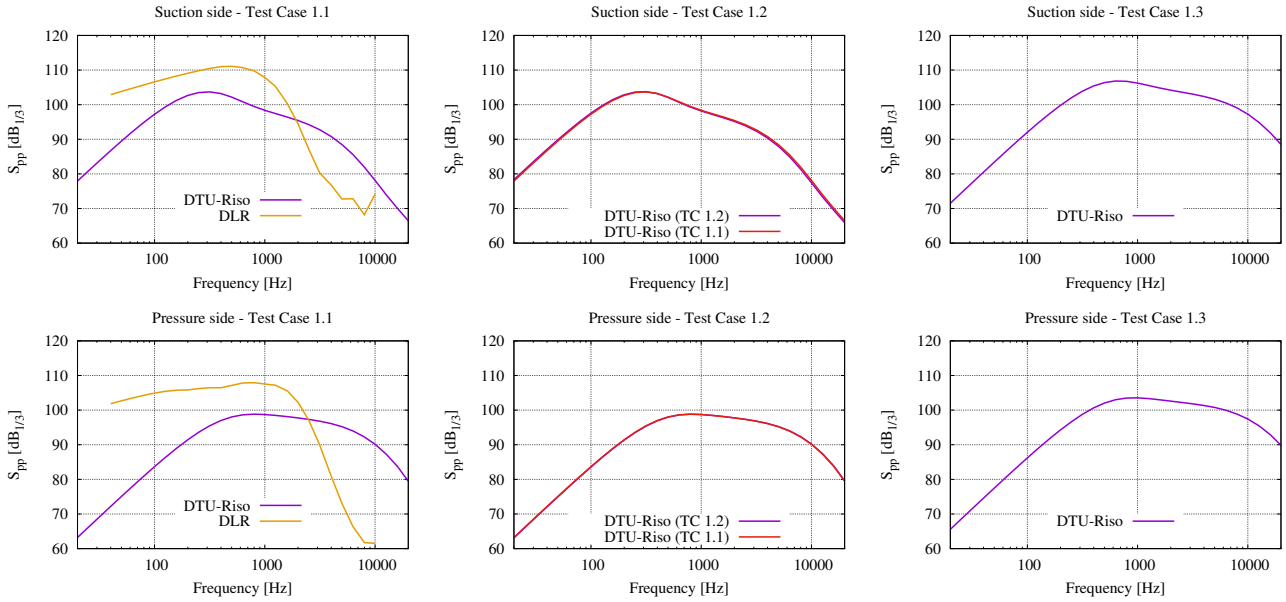

Figure 16. Surface pressure spectra at $r = 30\,m$ and $x/C = 93.3\%$ (top) and 91% (bottom) on the suction and pressure sides, respectively.

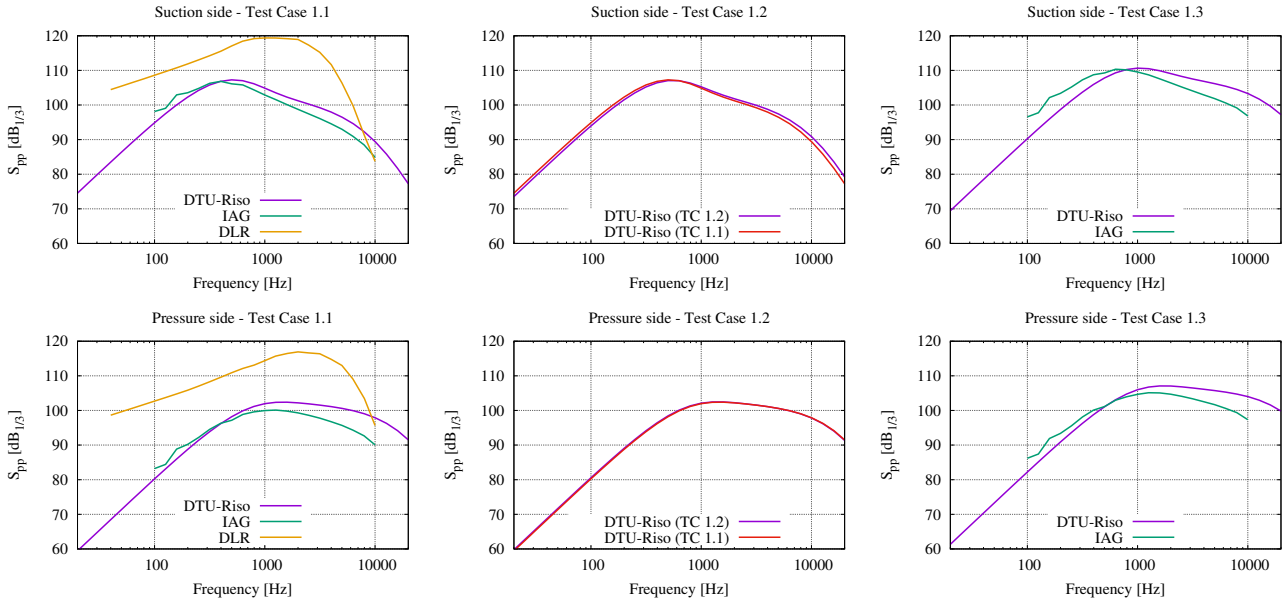

Figure 17. Surface pressure spectra at $r = 37\,m$ and $x/C = 93.3\%$ (top) and 91% (bottom) on the suction and pressure sides, respectively.

5.2 Far-field noise spectra

The overall far-field noise spectra computed at two locations:

- Downwind of the turbine at hub height (denoted as 'down-hub')
- Downwind of the turbine on the ground (denoted as 'down')

are displayed in Fig. 18.

The discrepancies observed earlier for the surface pressure spectra manifest themselves again here in the form of different spectral roll-off slopes.

In order to better distinguish the contributions of the two noise sources, i.e. turbulent inflow noise and trailing edge noise, in the above spectra, these contributions are displayed separately in Fig. 19.

It can be seen that the individual contributions still differ quite a lot.

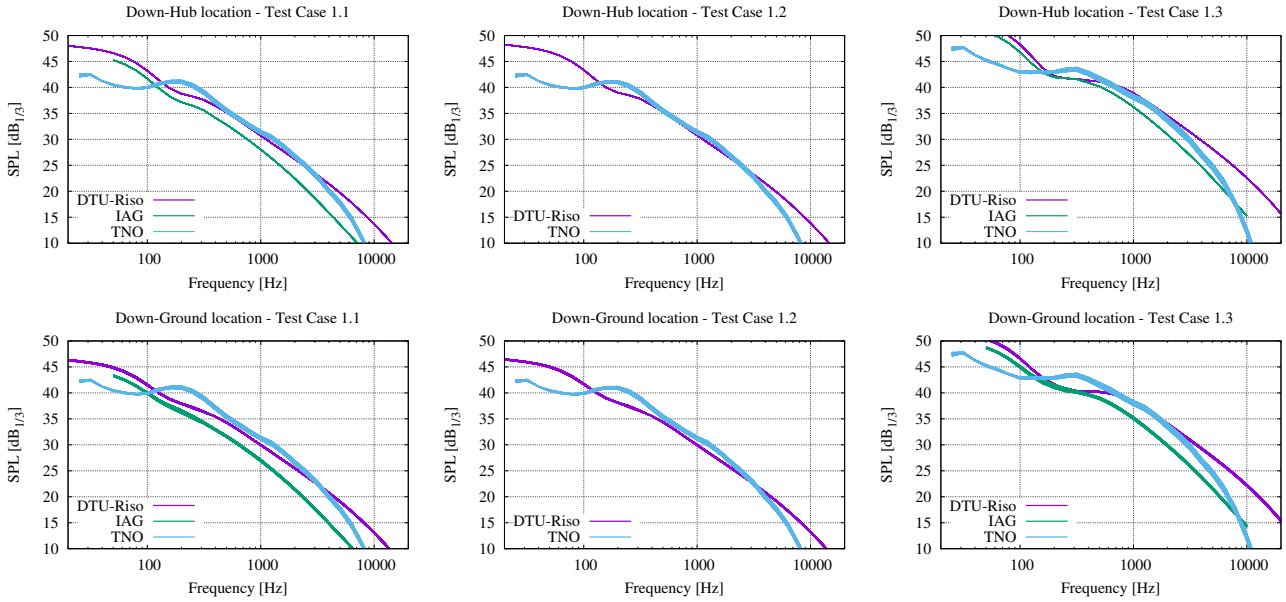

Figure 18. Sound pressure level spectra at 'down-hub' and 'down' positions.

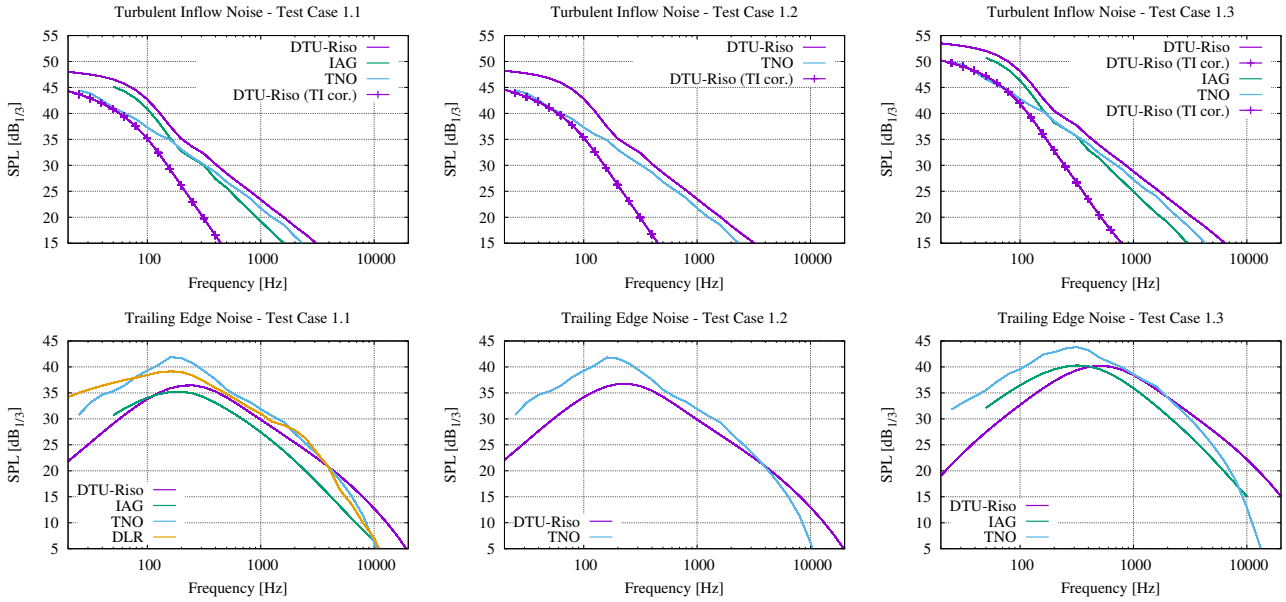

Figure 19. Sound pressure level spectra at 'down-hub' position for turbulent inflow and trailing edge noise.

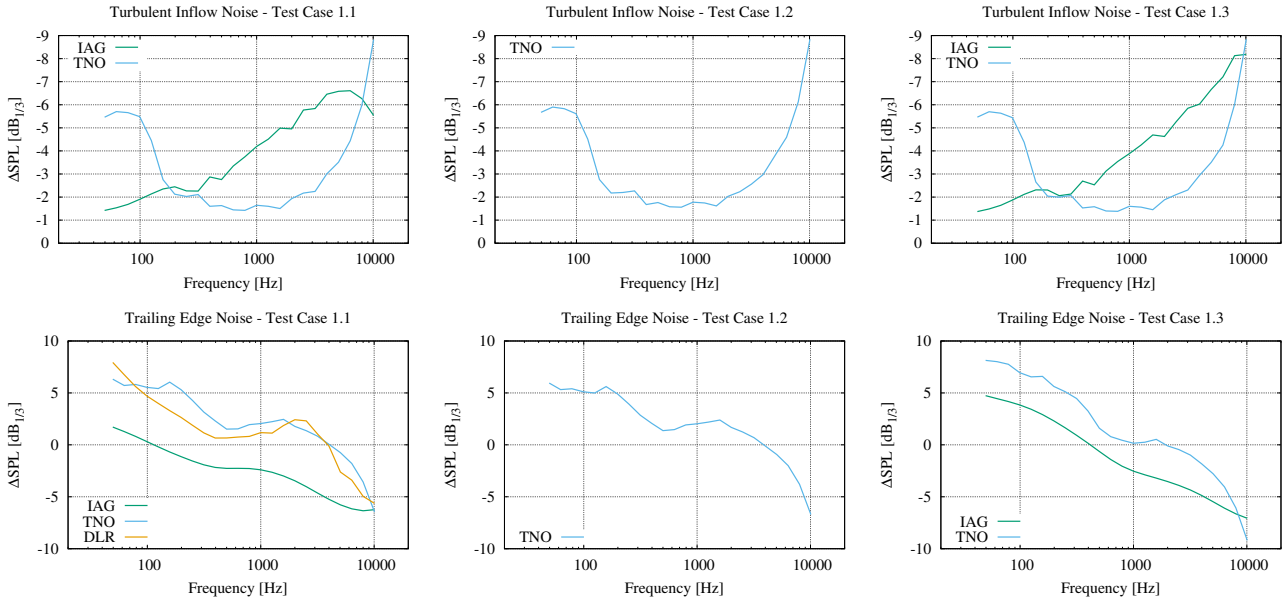

Figure 20. Differences of sound pressure level spectra at 'down-hub' position for turbulent inflow and trailing edge noise for the various models relatively to DTU model (see Fig. 19).

6 Calculations using different aerodynanic inputs but the same rotor noise model

In this section, some aerodynamic flow data at multiple sections along the blade are collected from DLR and IAG. These are used as input for the single aeroacoustic model from DTU for the wind turbine rotor. The aim is to evaluate to which extent the differences in the aerodynamic data are responsible for the discrepancies in noise results observed in the previous analysis of wind turbine noise codes comparisons. Note that TNO results are not included in the present analysis as the so-called BPM model is used in their TE noise modeling approach. The BPM model is based on Xfoil calculations. Thus, the boundary layer profiles (e.g. for the turbulent kinetic energy or its dissipation rate) from RANS calculations used as input in DTU's model are not available in this case.

6.1 Aerodynamic results

6.1.a Boundary layer thicknesses

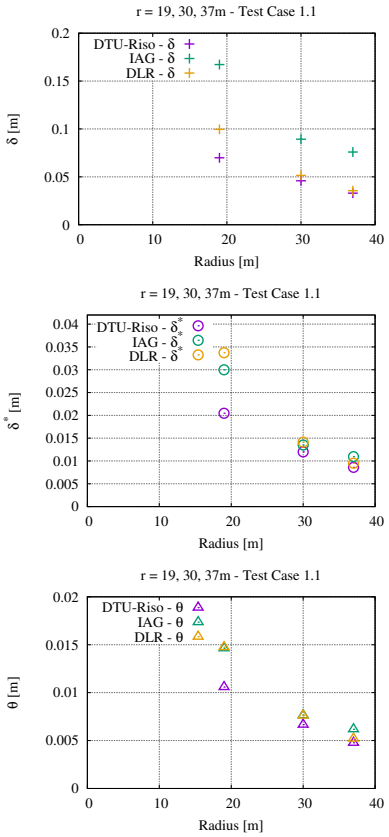

Figure 21. Boundary layer, displacement and momentum thicknesses as a function of radius on the suction side at x/C = 93% (see Fig. 5).

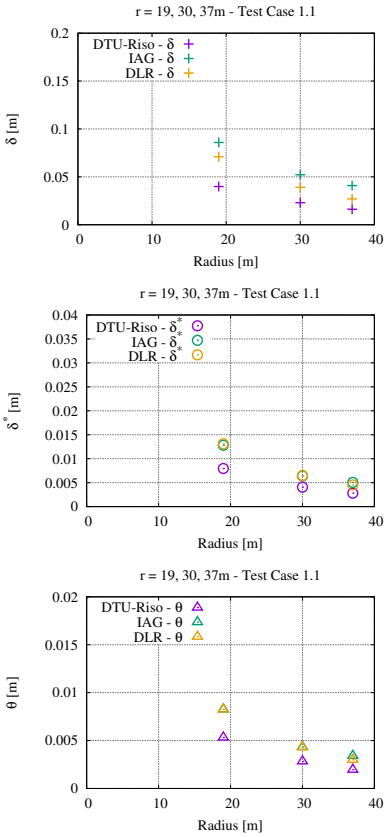

Figure 22. Boundary layer, displacement and momentum thicknesses as a function of radius on the pressure side at x/C = 91%. (see Fig. 6).

6.1.b Profiles across boundary layer

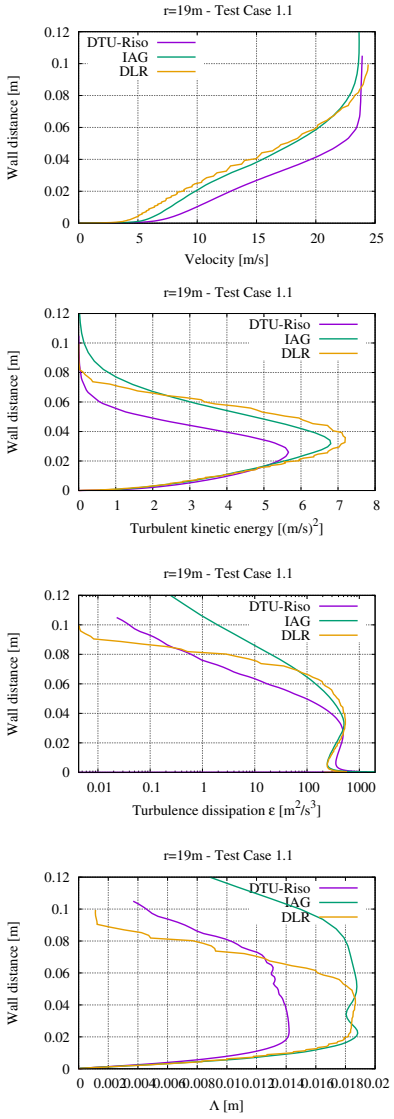

Figure 23. Boundary layer profiles of velocity, TKE, dissipation and integral length scale on the suction side at $x/C = 93\%$ and at the spanwise radius $r = 19\,m$ (see Fig. 9).

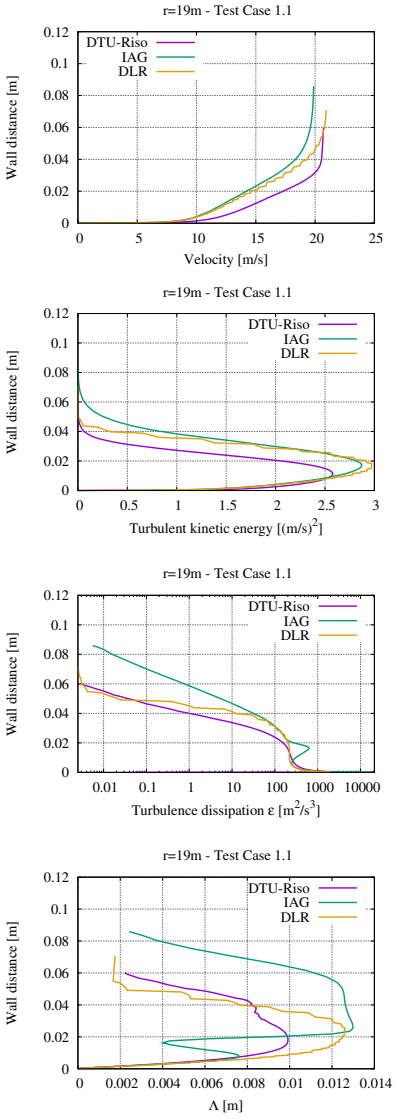

Figure 24. Boundary layer profiles of velocity, TKE, dissipation and integral length scale on the pressure side at $x/C = 91\%$ and at the spanwise radius $r = 19\,m$ (see Fig. 10).

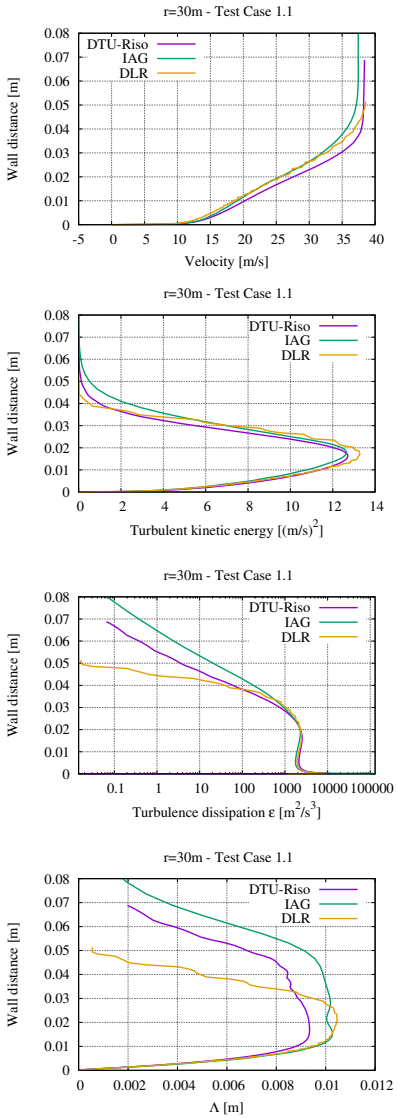

Figure 25. Boundary layer profiles of velocity, TKE, dissipation and integral length scale on the suction side at $x/C = 93\%$ and at the spanwise radius $r = 30\,m$ (see Fig. 11).

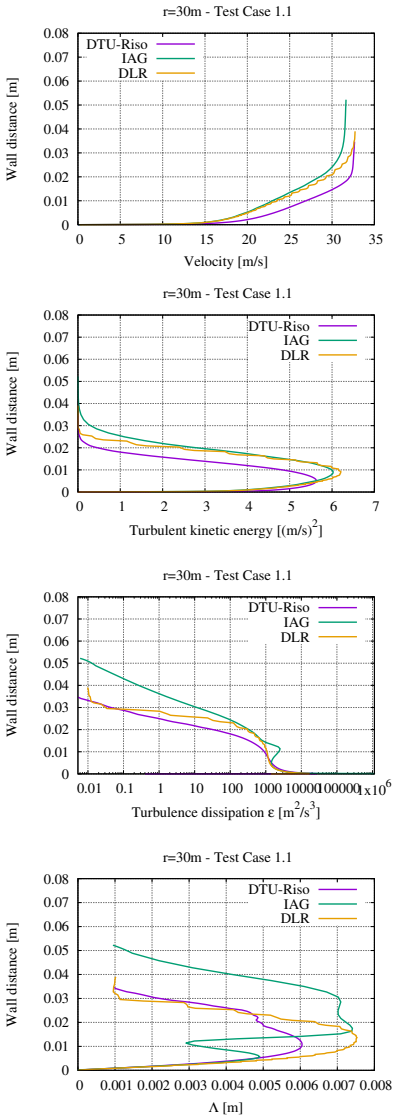

Figure 26. Boundary layer profiles of velocity, TKE, dissipation and integral length scale on the pressure side at $x/C = 91\%$ and at the spanwise radius $r = 30\,m$ (see Fig. 12).

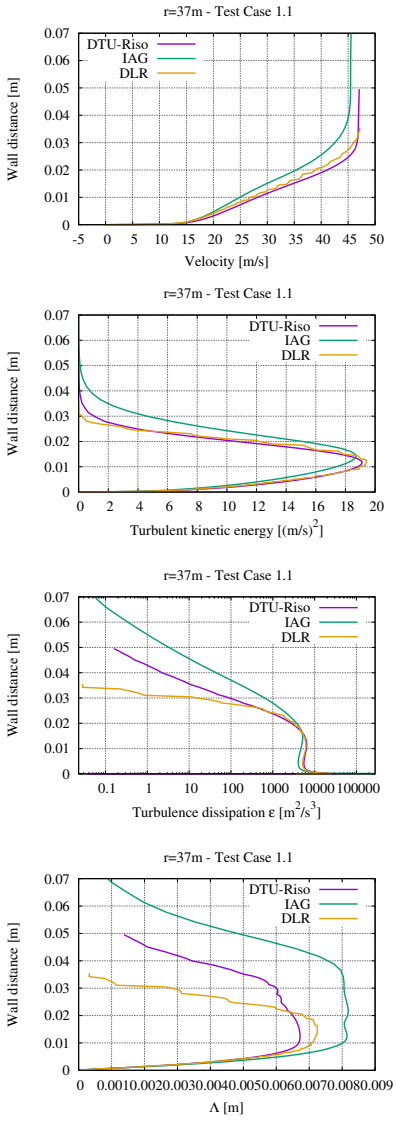

Figure 27. Boundary layer profiles of velocity, TKE, dissipation and integral length scale on the suction side at $x/C = 93\%$ and at the spanwise radius $r = 37m$ (see Fig. 13).

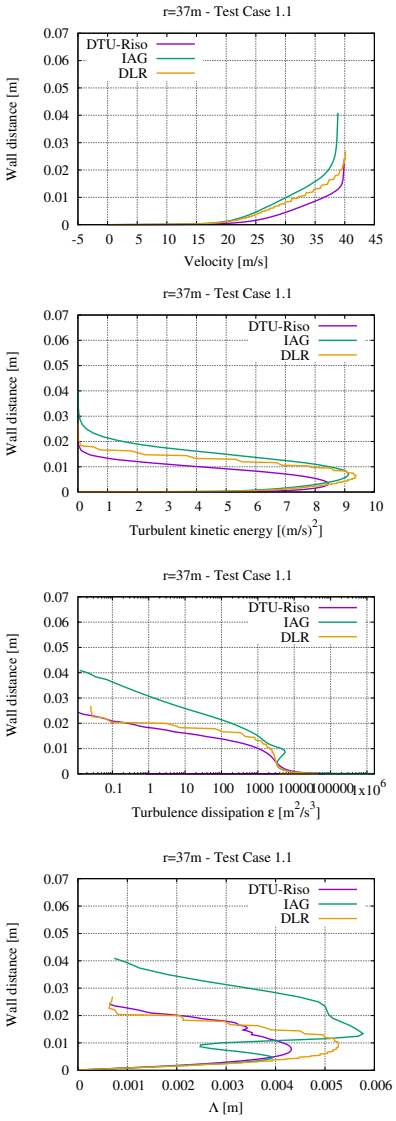

Figure 28. Boundary layer profiles of velocity, TKE, dissipation and integral length scale on the pressure side at $x/C = 91\%$ and at the spanwise radius $r = 37m$ (see Fig. 14).

6.2 Aeroacoustic results

6.2.a Surface pressure fluctuations

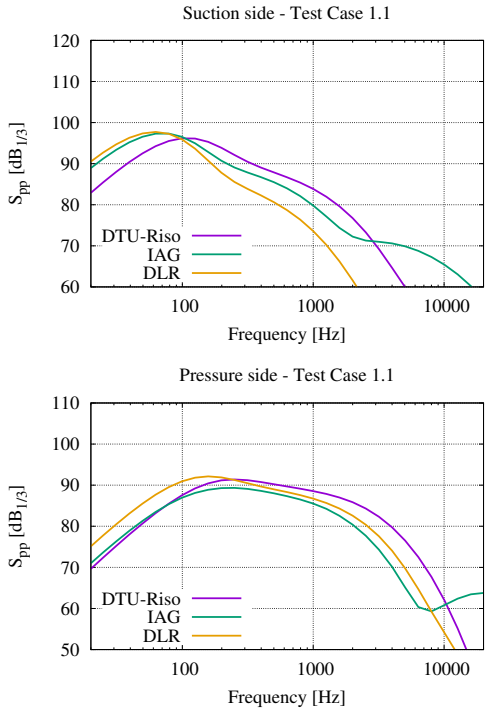

Figure 29. Surface pressure spectra at r = 19 m and x/C = 93.3% (top) and 91% (bottom) on the suction and pressure sides, respectively (see Fig. 15).

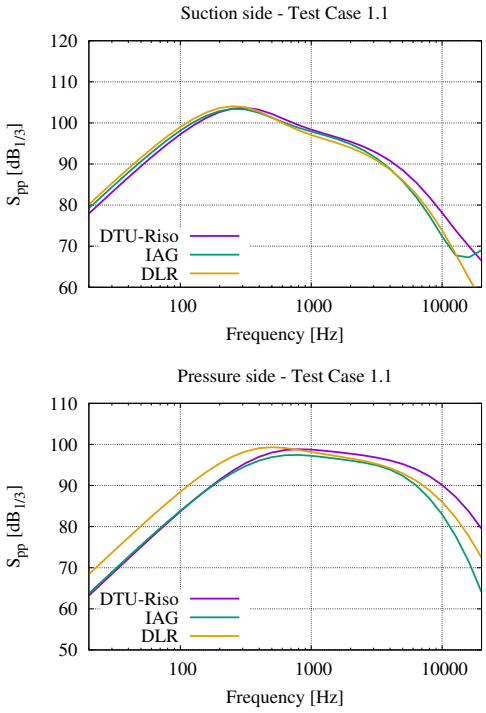

Figure 30. Surface pressure spectra at r = 30 m and x/C = 93.3% (top) and 91% (bottom) on the suction and pressure sides, respectively (see Fig. 16).

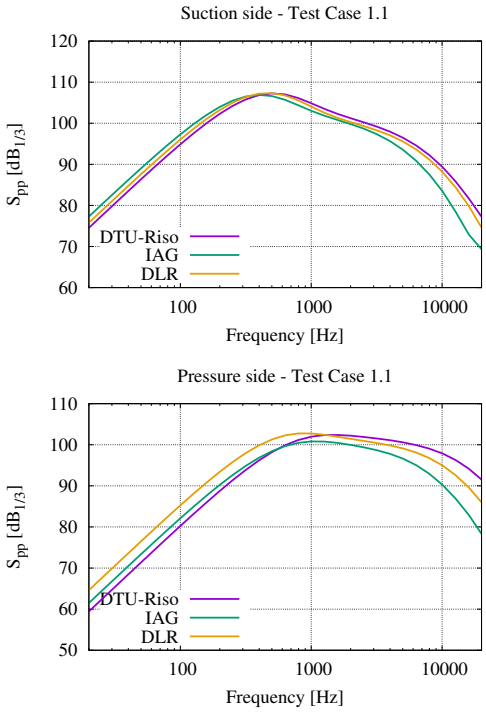

Figure 31. Surface pressure spectra at r = 37 m and x/C = 93.3% (top) and 91% (bottom) on the suction and pressure sides, respectively (see Fig. 17).

6.2.b Far-fied noise

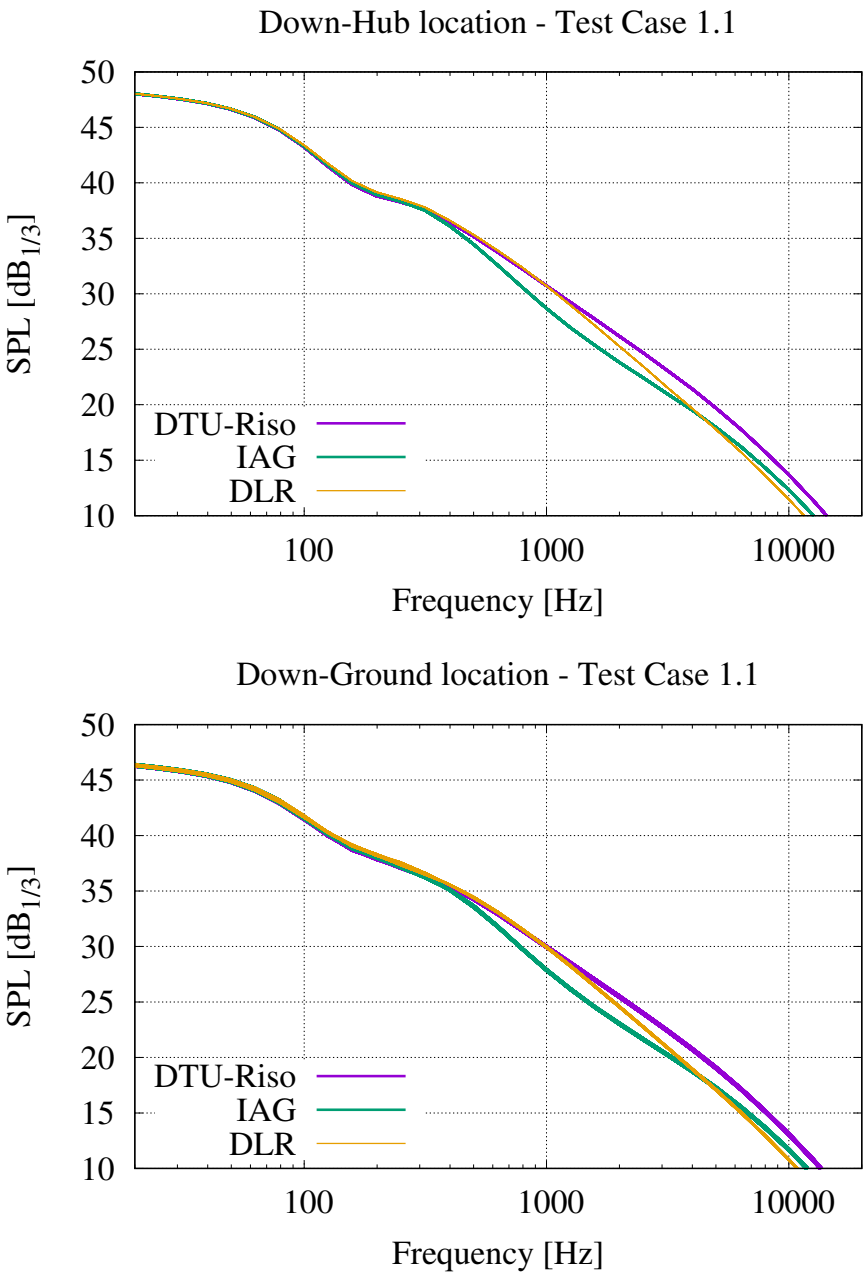

Figure 32. Sound pressure level spectra at 'down-hub' positions (see Fig. 18).

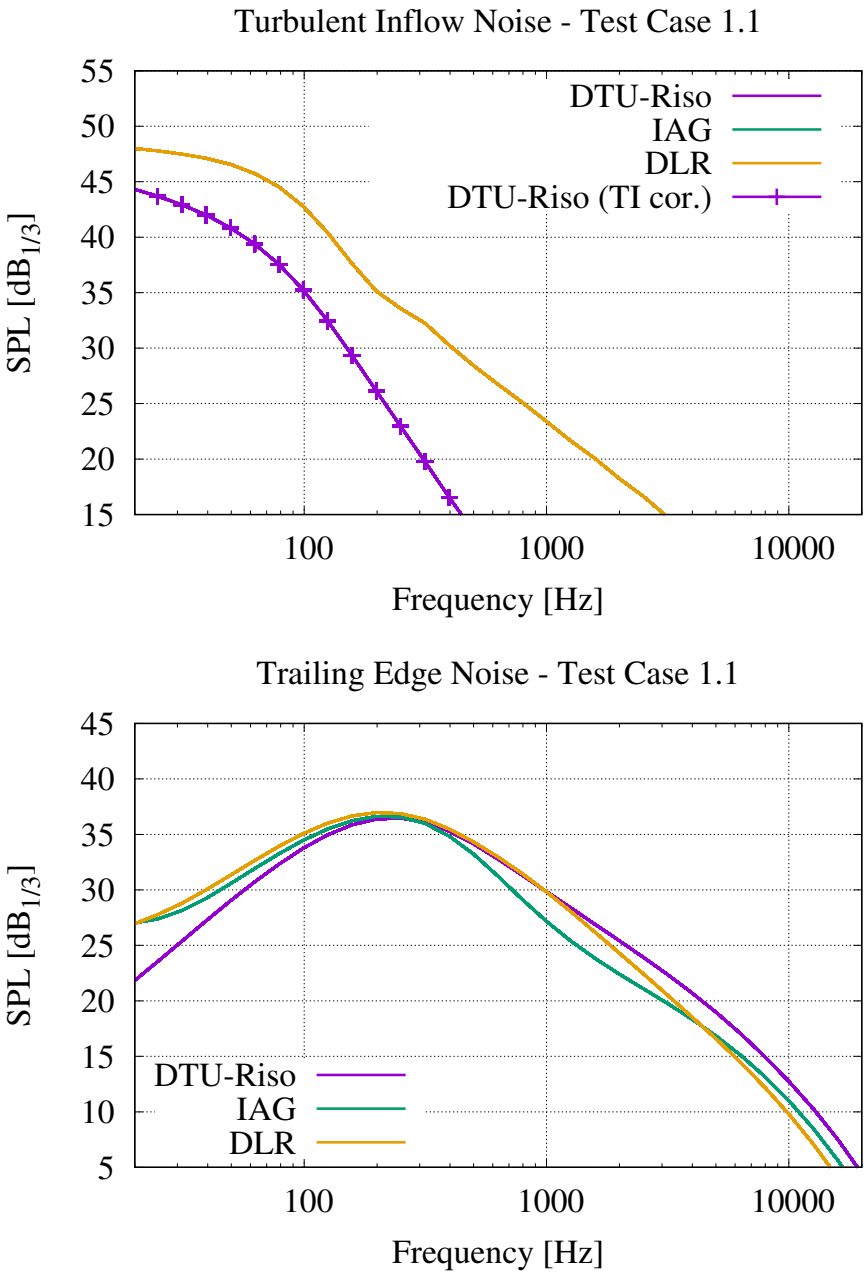

Figure 33. Sound pressure level spectra at 'down-hub' position for turbulent inflow and trailing edge noise (see Fig. 19).

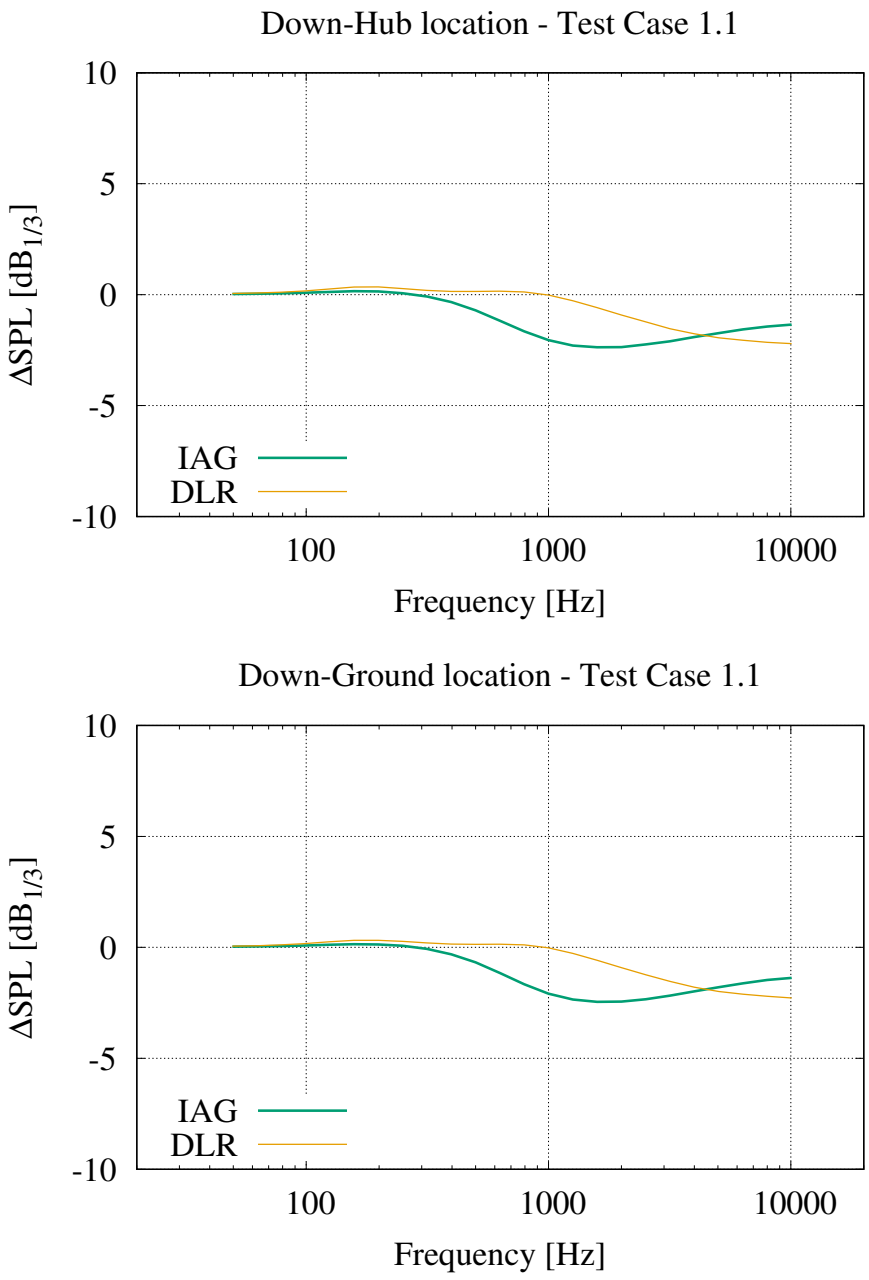

Figure 34. Differences of sound pressure level spectra at 'down-hub' positions for the various models relatively to DTU model (see Fig. 32).

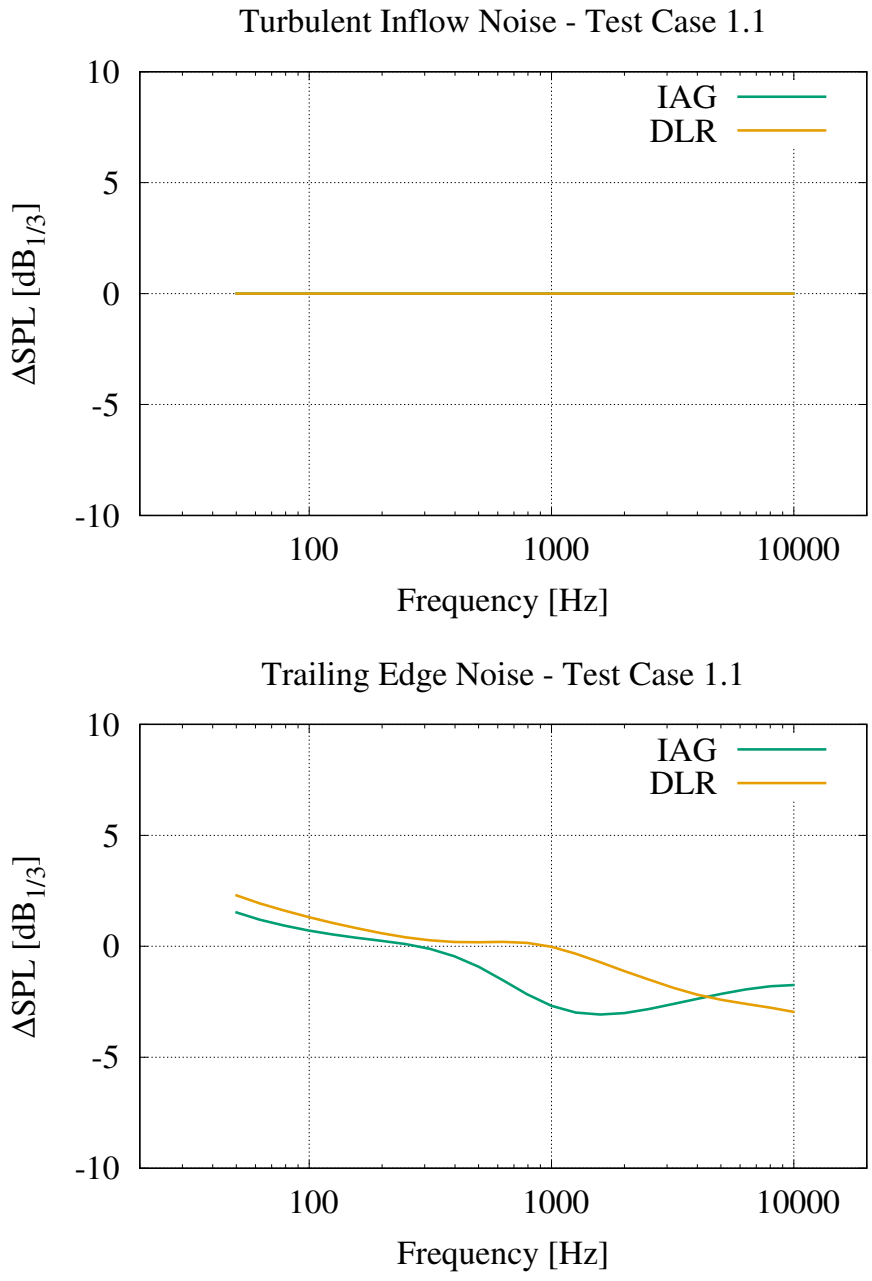

Figure 35. Differences of sound pressure level spectra at 'down-hub' position for turbulent inflow and trailing edge noise for the various models relatively to DTU model (see Fig. 33).

7 Further comparisons of various trailing-edge noise models

This section aims at comparing further available models for the TE noise. In addition to the models considered in Section 5, an additional older TE noise model available at DTU is also included here [3], and is denoted as '(F)' in the figures below. The more recent DTU TE noise model [13] used in the main comparison previously is denoted as '(A)'. Furthermore, two different implementations of each DTU model (for the noise scattering part) are included: one considering the Brooks & Hodgson implementation of Howe's trailing edge model for TE noise scattering (assuming an asymptotic directivity funtion), the other being the Amiet TE formulation (for which directivity effects are implictly included in this formulation).

In addition, new calculations from NREL are also now included in the comparisons for the noise spectra. Aerodynamic comparisons should be provided later on, but the comparisons conducted in Task 29 can be used as reference.

7.1 Boundary layer aerodynamic results

The aerodynamic quantities are independent of the acoustic models. Thus, the reader is referred to earlier comparisons in Section 4 that still apply here.

However, the TE noise model (F) does also include as inputs: 1) the gradient of the surface pressure distribution along the chord near the trailing edge, 2) the skin friction coefficient at the same location which is used to non-dimensionalize the above pressure gradient. It is then informative to display these quantities extracted from the data provided by the participants. The two quantities are plotted as a function of the airfoil thickness along the blade span, both on suction and pressure sides and both at $x/C = 92\%$ and at $x/C = 97.5\%$, in Fig. 36.

A general good agreement between the different aerodynamic models is observed, but some quantitative discrepancies also emerge.

7.2 Aeroacoustic results

7.2.a Surface pressure fluctuations

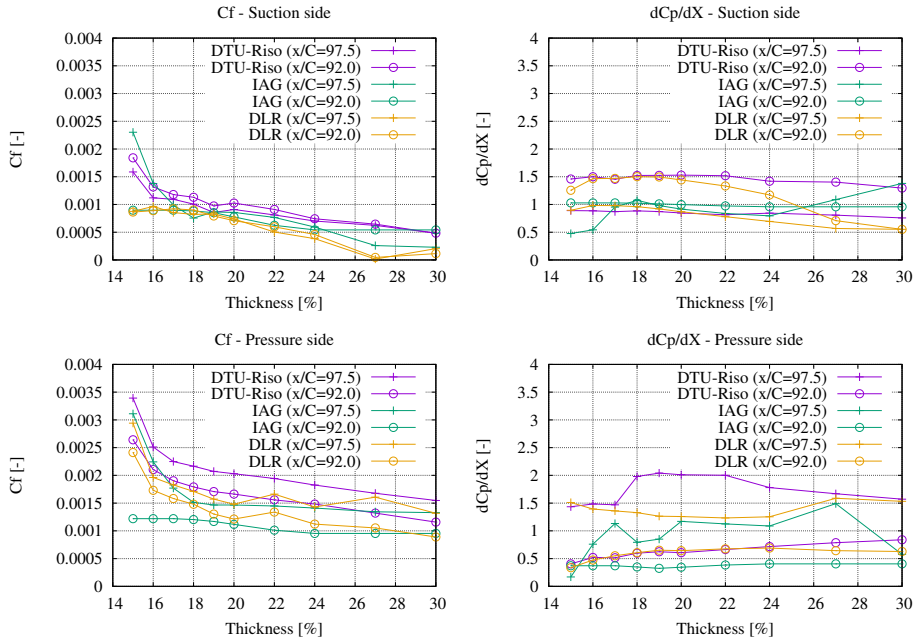

Figure 36. Friction coefficient and surface pressure gradient at x/C = 92% and 97.5% on the suction and pressure sides for varying airfoil thicknesses along the blade span.

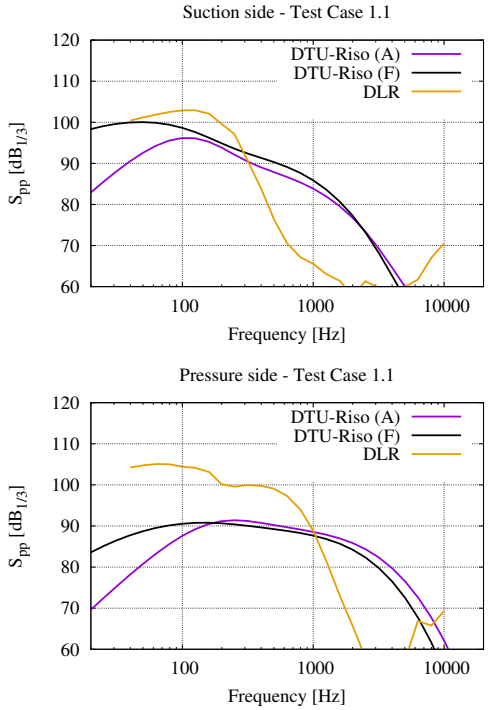

Figure 37. Surface pressure spectra at r = 19 m and x/C = 93.3% (top) and 91% (bottom) on the suction and pressure sides, respectively (see Fig. 15).

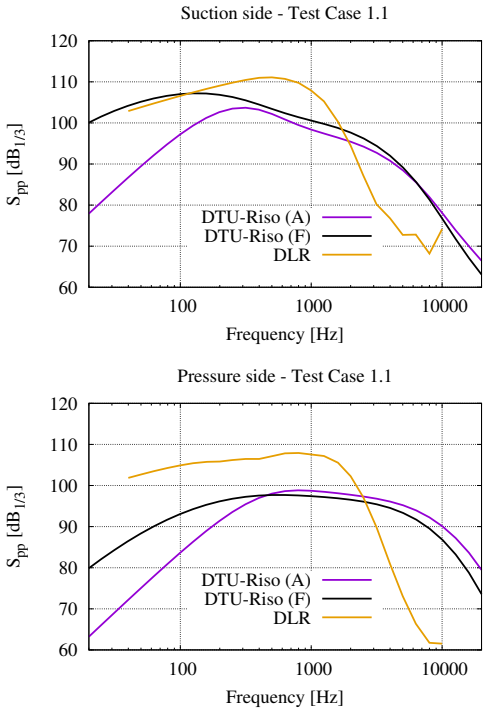

Figure 38. Surface pressure spectra at r = 30 m and x/C = 93.3% (top) and 91% (bottom) on the suction and pressure sides, respectively (see Fig. 16).

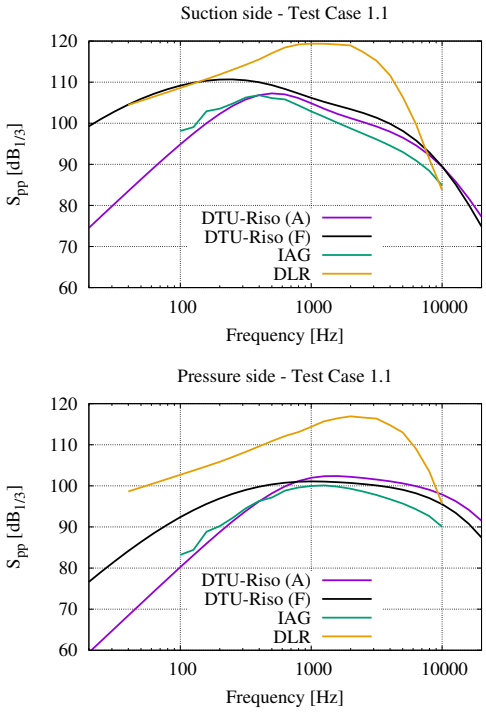

Figure 39. Surface pressure spectra at r = 37 m and x/C = 93.3% (top) and 91% (bottom) on the suction and pressure sides, respectively (see Fig. 17).

7.2.b Far-fied noise

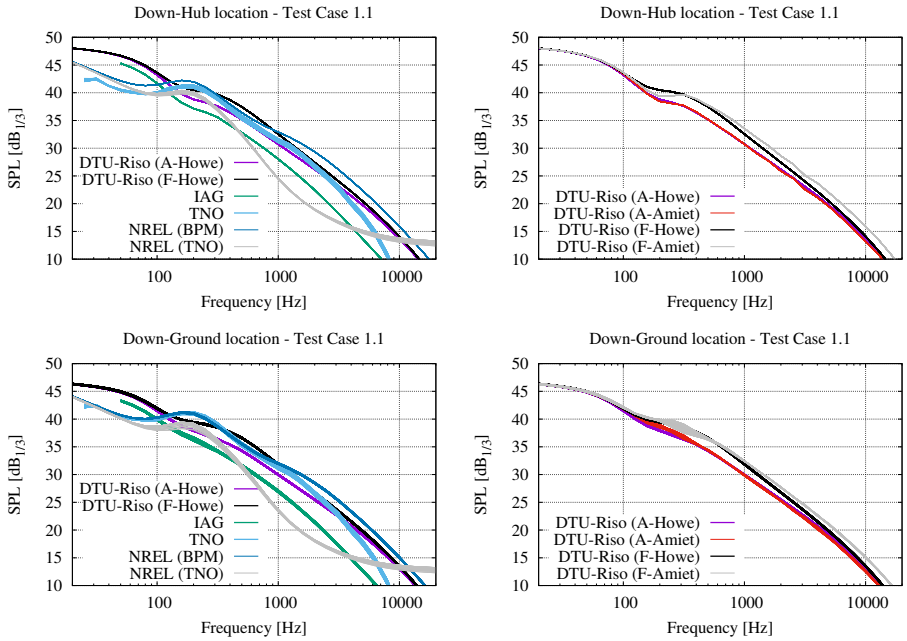

Figure 40. Sound pressure level spectra at 'down-hub' positions (see Fig. 18).

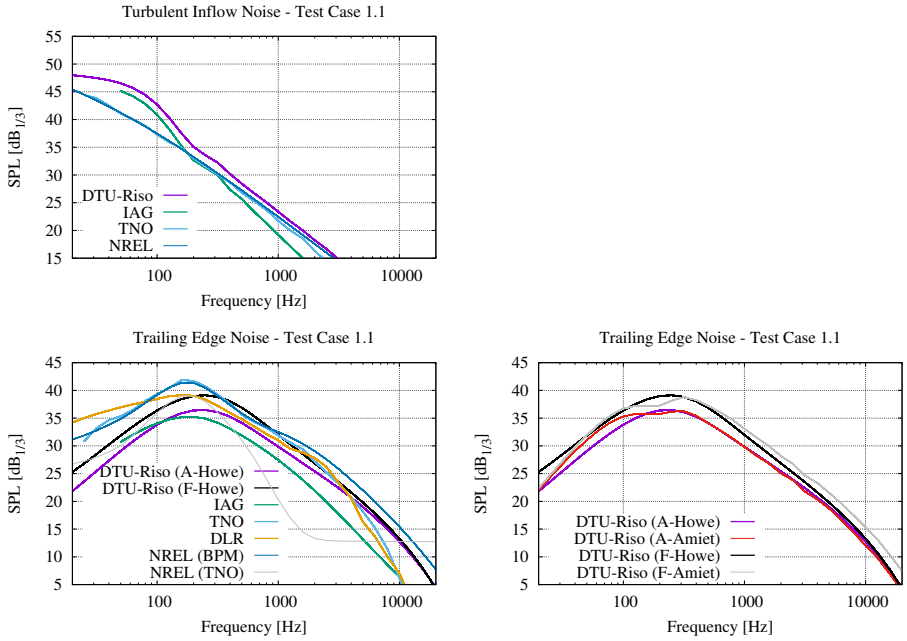

Figure 41. Sound pressure level spectra at 'down-hub' position for trailing edge noise (see Fig. 19).

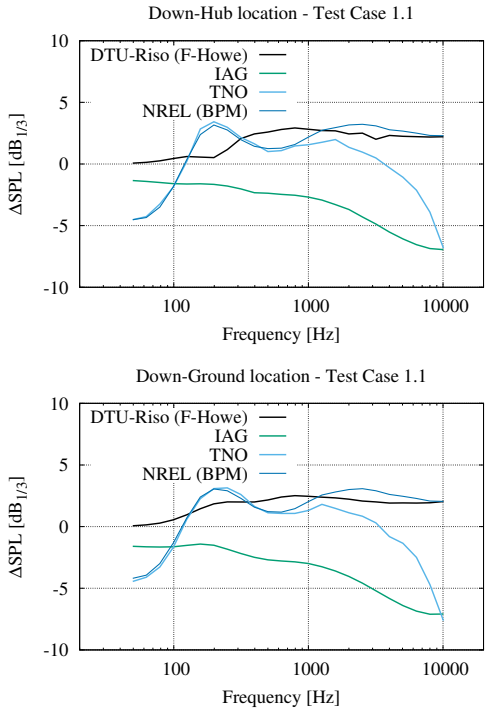

Figure 42. Differences of sound pressure level spectra at 'down-hub' positions for the various models relatively to DTU model (see Fig. 40).

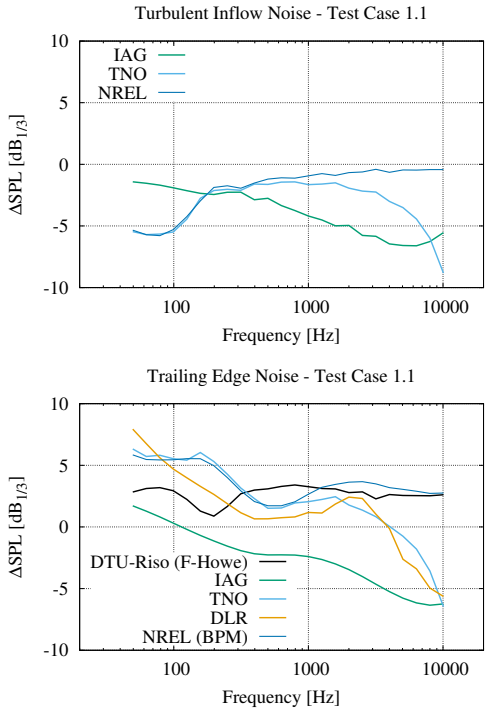

Figure 43. Differences of sound pressure level spectra at 'down-hub' position for trailing edge noise for the various models relatively to DTU model (see Fig. 41).

8 Temporal and spatial variability of noise

8.1 Integrated noise spectra as a function of time

The time-series of frequency-integrated far-field noise spectra L_{ac} computed at the same two locations defined above as a function of the azimuth of one of the blades are displayed in Fig. 44 (with close-up view in Fig. 45 by adapting the plotting ranges along the L_{ac}-axis).

In the case of the 'down-hub' position, it can be seen that all curves remain constant in time (i.e. as a function of azimuth) as it is expected for a fully axi-symmetric configuration for an observer at this position. For the 'down' position, the symmetry breaking is illustrated by the periodic variation of the noise immission level for an observer at this location, with a periodicity of 3P because of the presence of 3 blades. However, it is noted that the DTU/TNO/NREL codes are not exactly in phase, while IAG is nearly out of phase with the other codes. The probable cause for these discrepancies is either a difference in the azimuth angle definition (but this has been investigated, although an error somewhere in the processing of the data is still possible), or an error in the calculation of the directivity pattern (e.g. leading to incorrect angles of the blade relative relatively to the receiver position).

However, in the latter plots, both turbulent inflow and trailing edge noise model results are included, making it difficult to distinguish their individual contributions, which is conducted below.

The time-series of the frequency-integrated spectra, for the turbulent inflow and the trailing edge noise models separately, are displayed in Fig. 46 at the 'down' (or P7) position (with close-up view in Fig. 47). In this case, it is observed that the turbulent inflow noise levels are not in phase for all models, which is also the case for the trailing edge noise levels. Integrated A-weighted spectra at this position are displayed in Figs. 48-49.

The same plots as above, for the turbulent inflow and the trailing edge noise models separately, with or without A-weighing, are now plotted at the position 'P4' in Figs. 50, 51, 52 and 53.

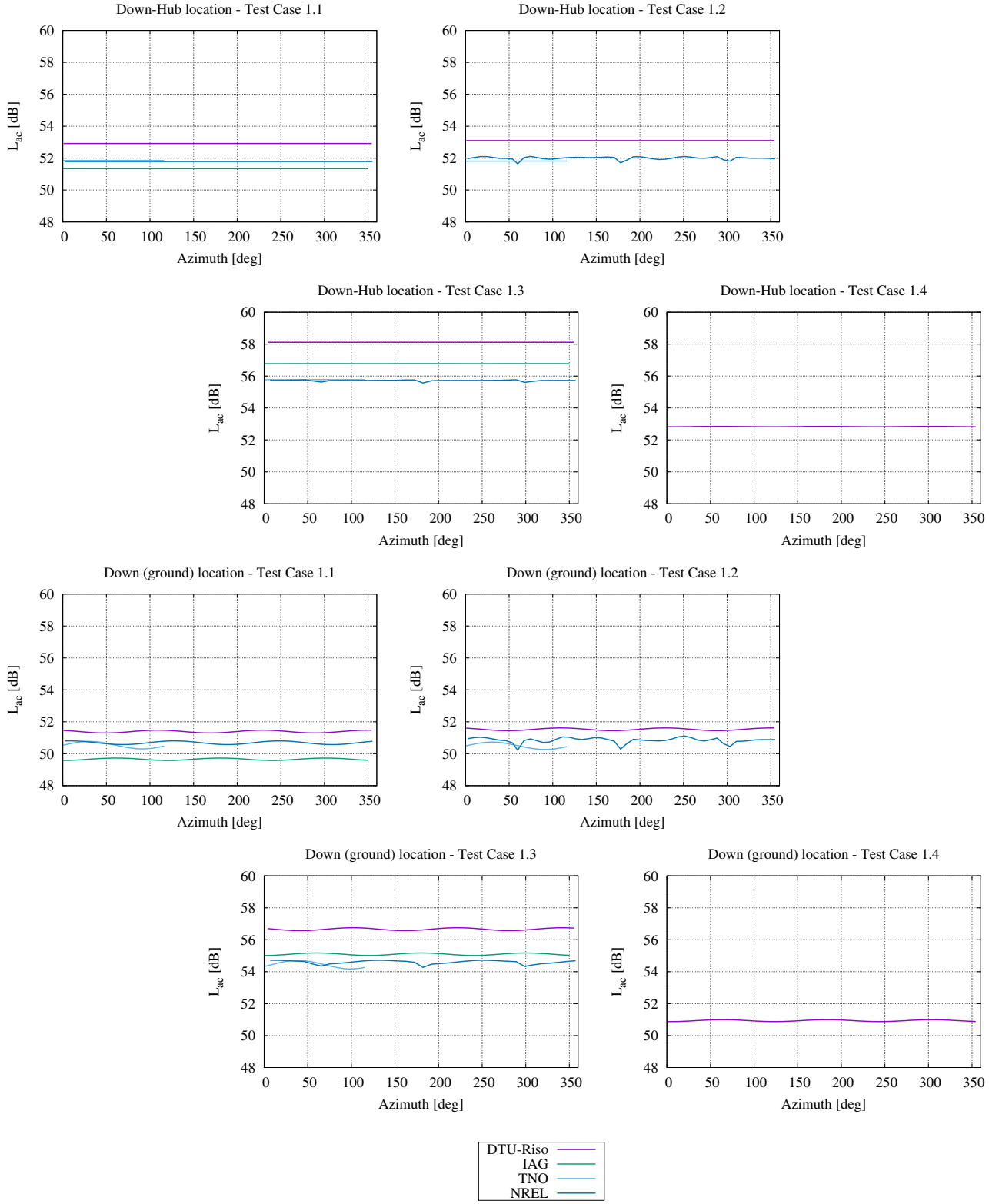

Figure 44. Integrated noise spectra at 'down-hub' and 'down' positions as a function of azimuth rotor position.

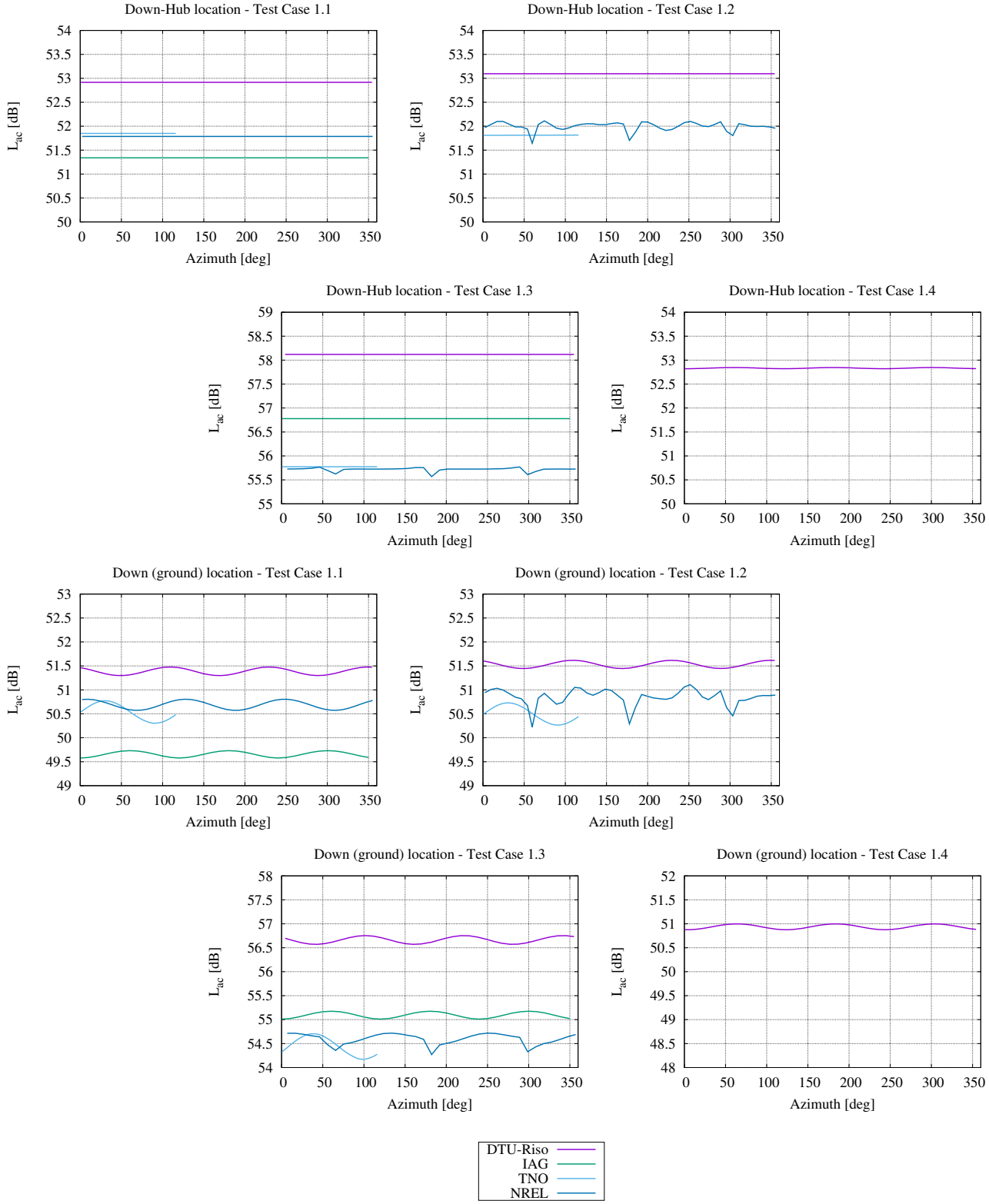

Figure 45. Same as Fig. 44 - Zoomed-in.

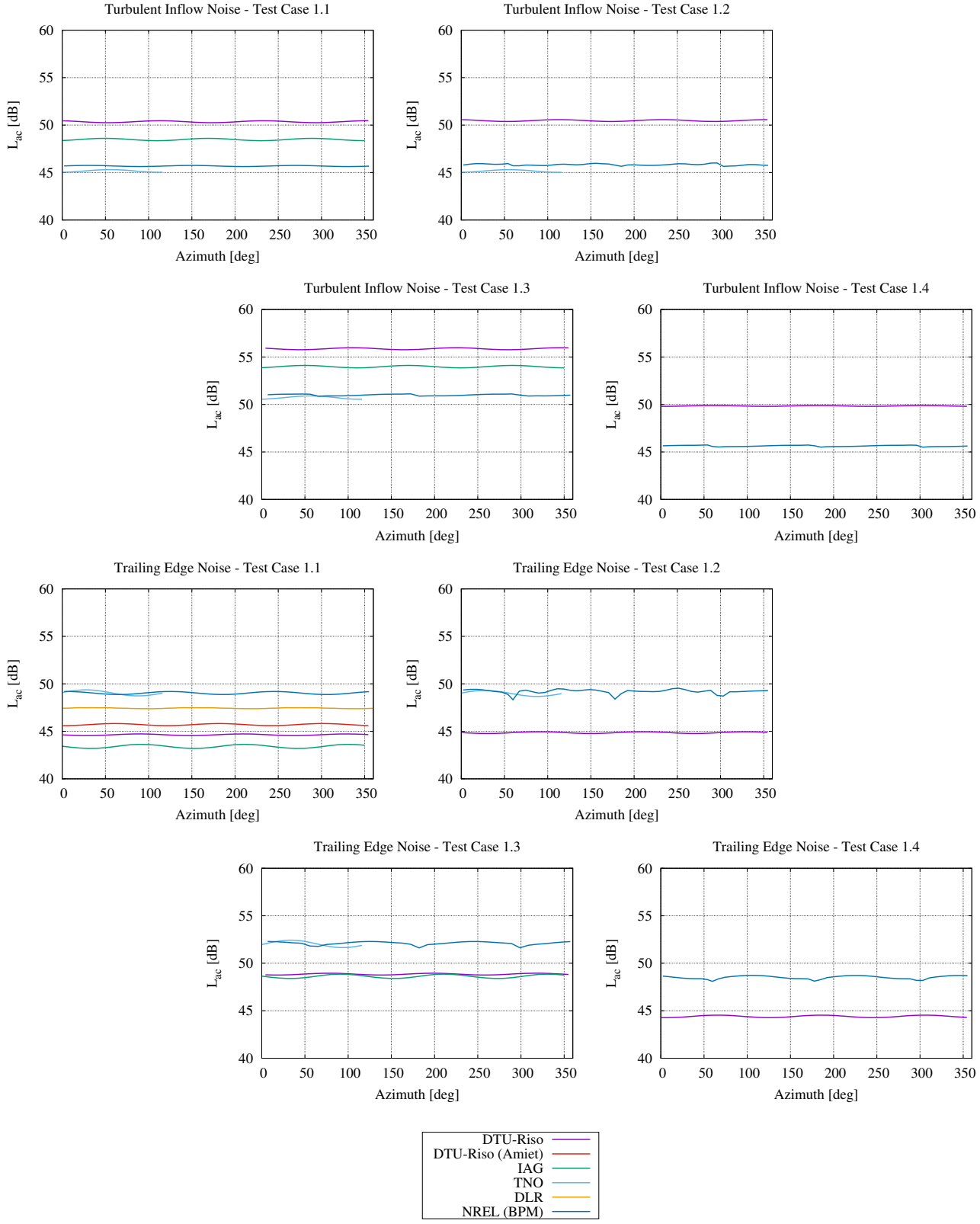

Figure 46. Integrated noise spectra at 'down' position for turbulent inflow and trailing edge noise as a function of azimuth rotor position.

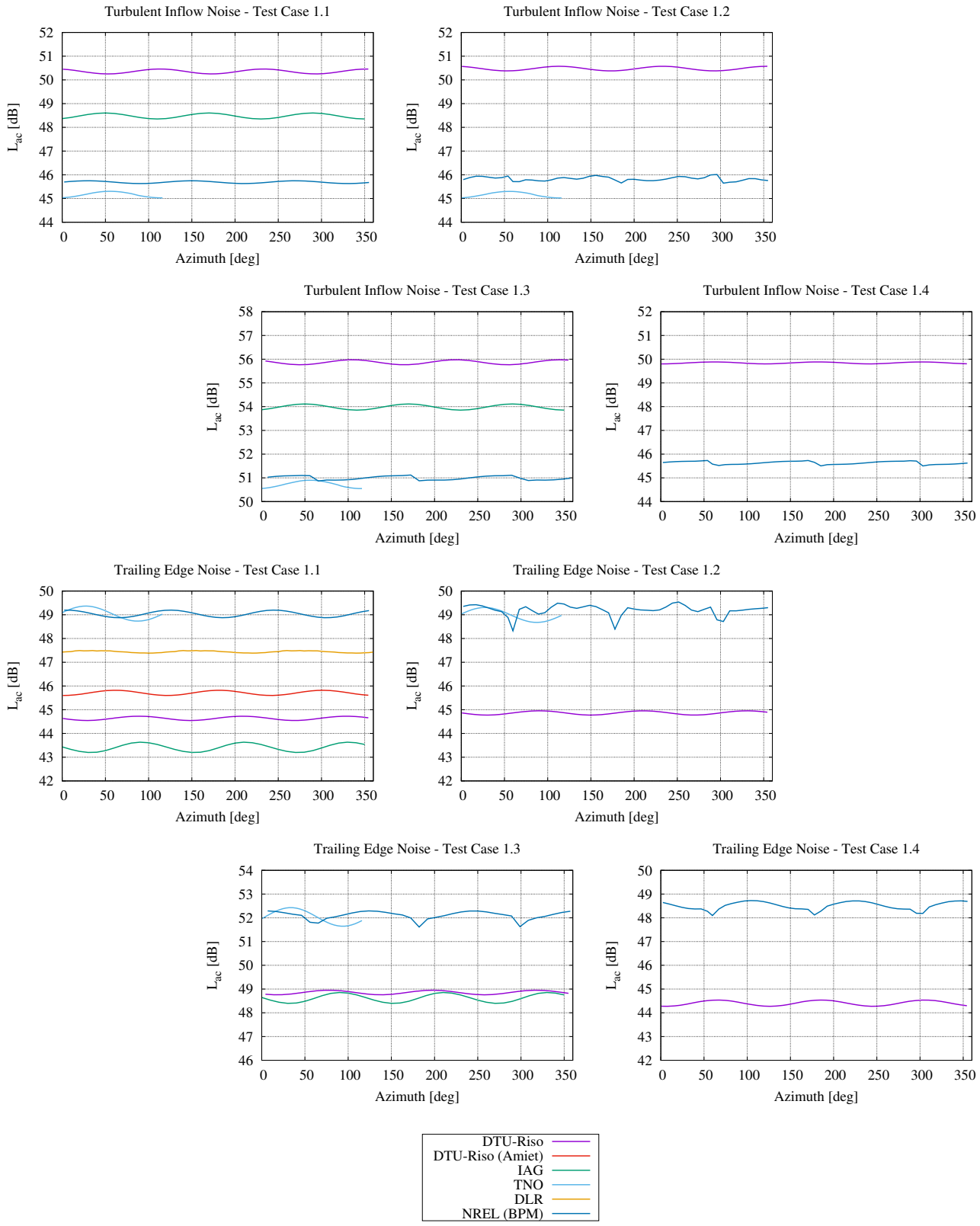

Figure 47. Same as Fig. 46 - Zoomed-in.

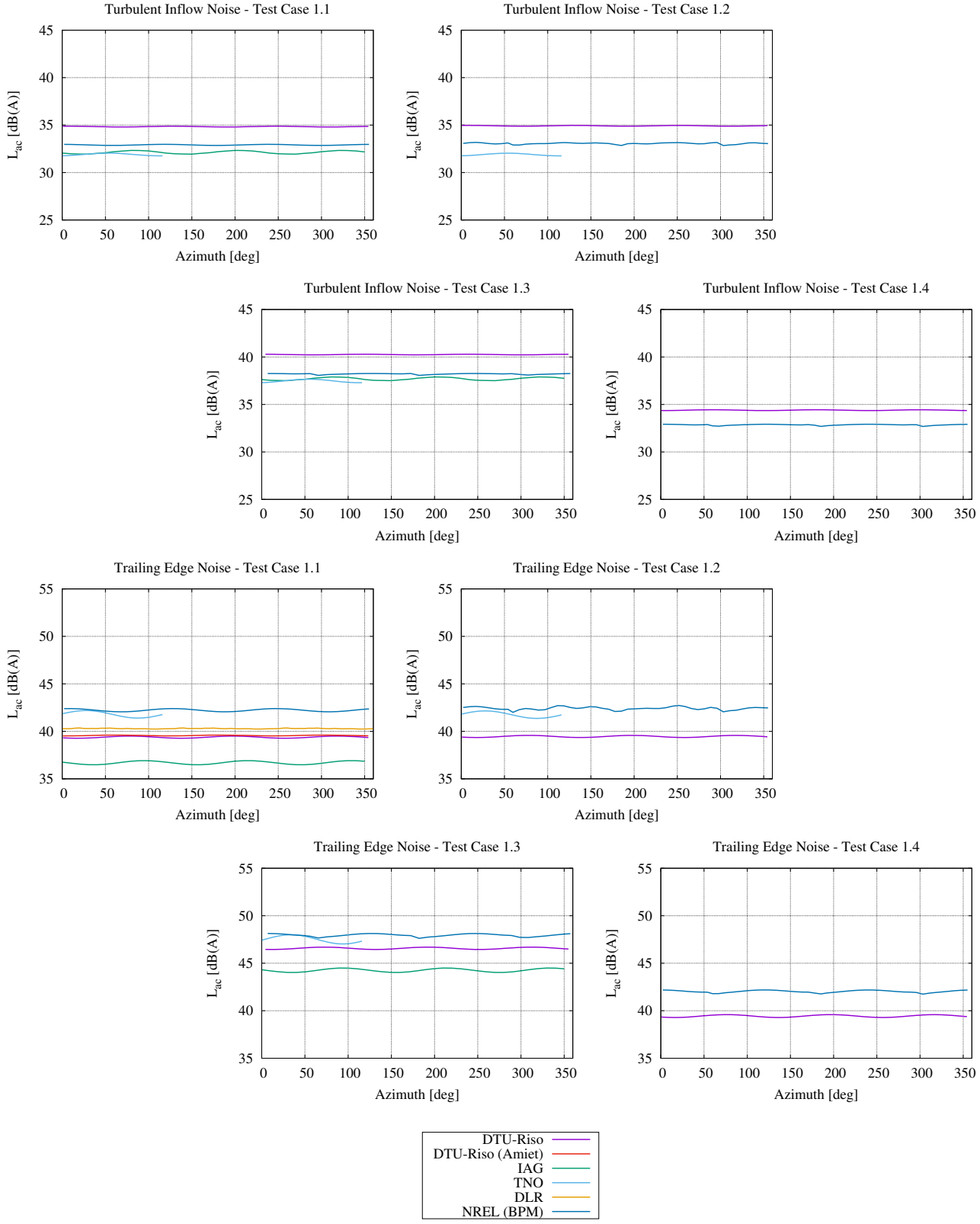

Figure 48. Integrated A-weighted noise spectra at 'down' position for turbulent inflow and trailing edge noise as a function of azimuth rotor position.

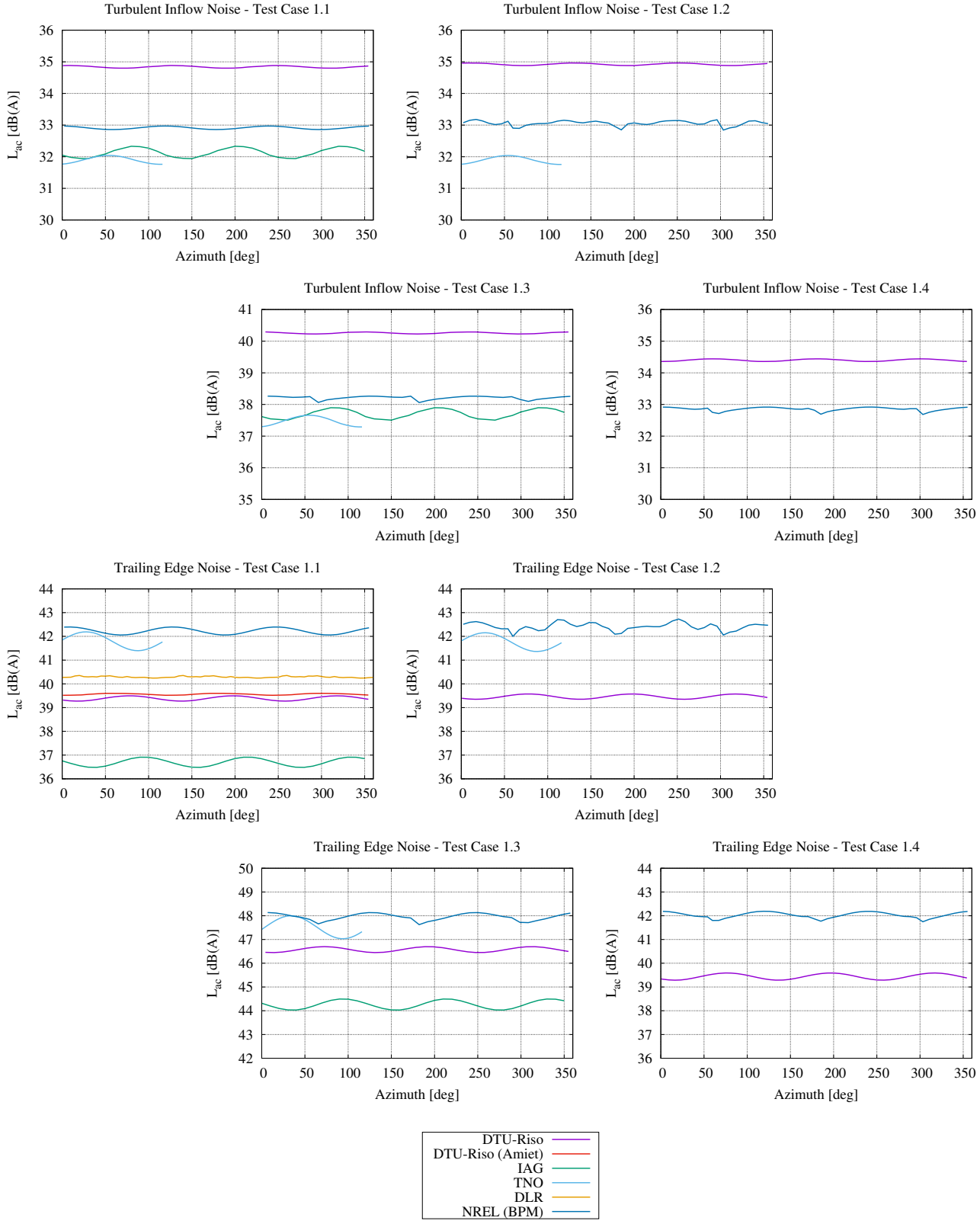

Figure 49. Same as Fig. 48 - Zoomed-in.

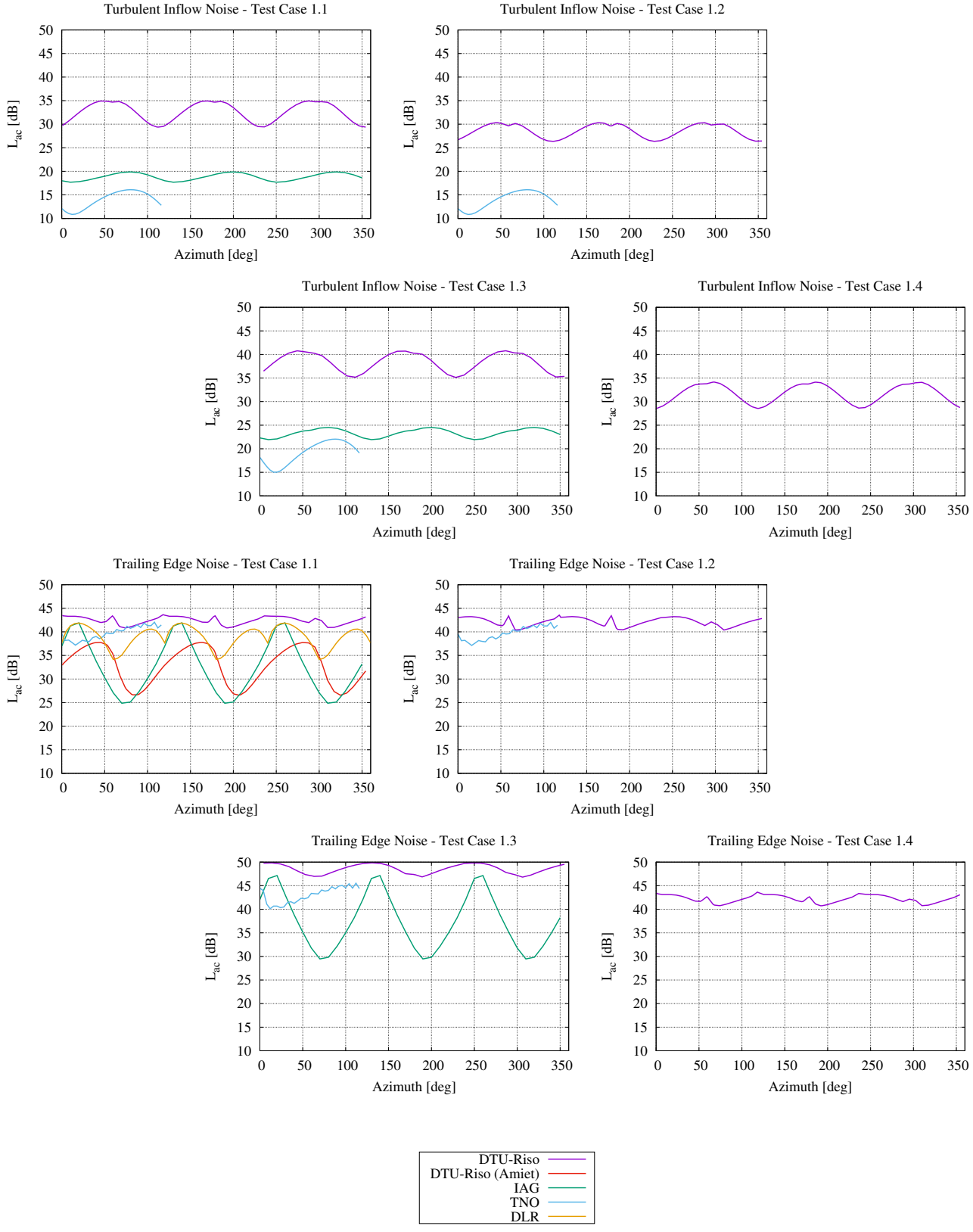

Figure 50. Integrated noise spectra at P4 position for turbulent inflow and trailing edge noise as a function of azimuth rotor position.

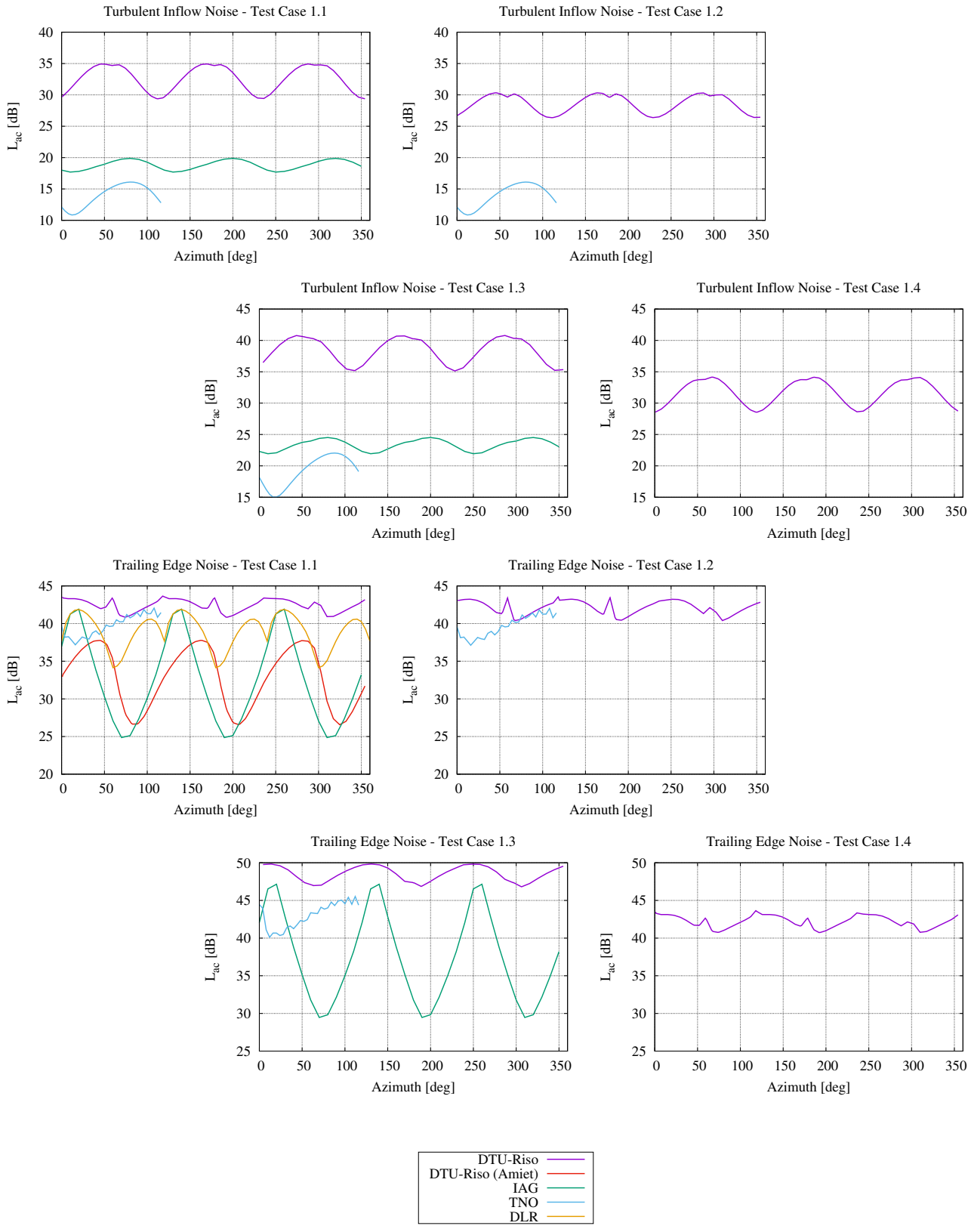

Figure 51. Same as Fig. 50 - Zoomed-in.

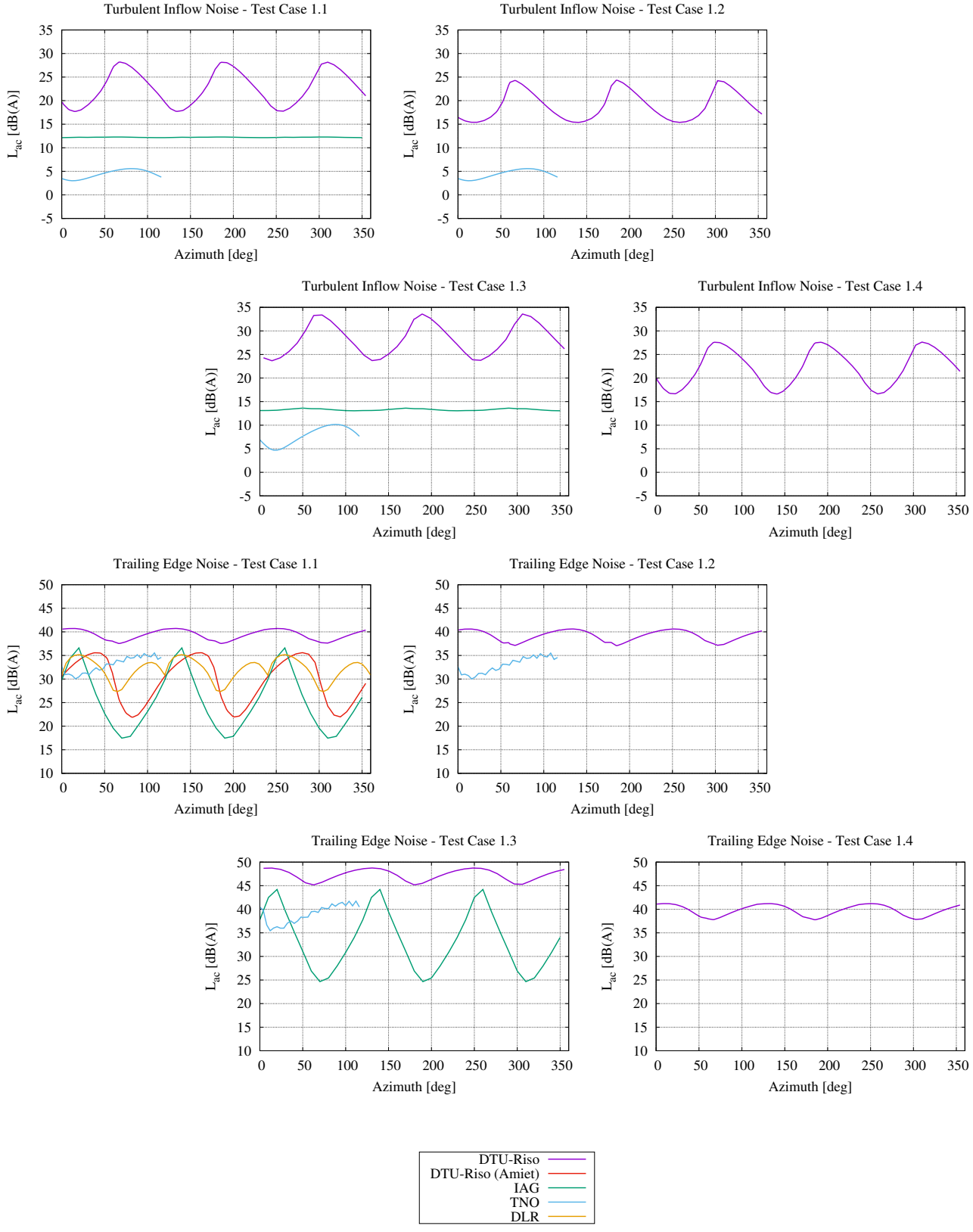

Figure 52. Integrated A-weighted noise spectra at P4 position for turbulent inflow and trailing edge noise as a function of azimuth rotor position.

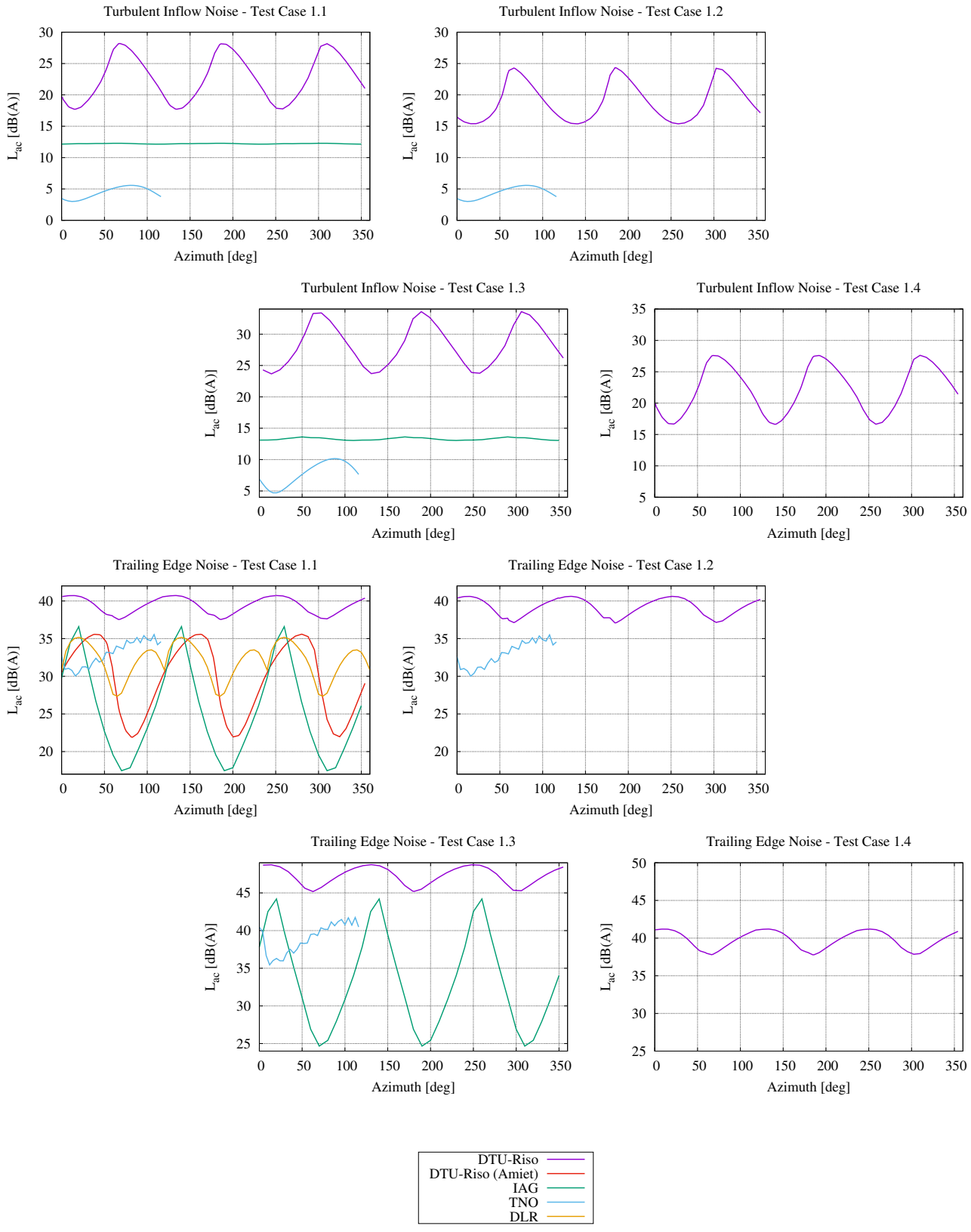

Figure 53. Same as Fig. 52 - Zoomed-in.

8.2 Directivity of integrated noise spectra

The frequency-integrated and time-averated far-field noise spectra L_{ac} are now plotted as a function of the azimuthal position around the turbine in Fig. 54. Note that 0^o is upwind of the turbine, 90^o is to the right of the turbine looking from down from the sky onto the turbine, and so forth.

Fig. 55 displays the same results as above, but for the A-weighted spectra.

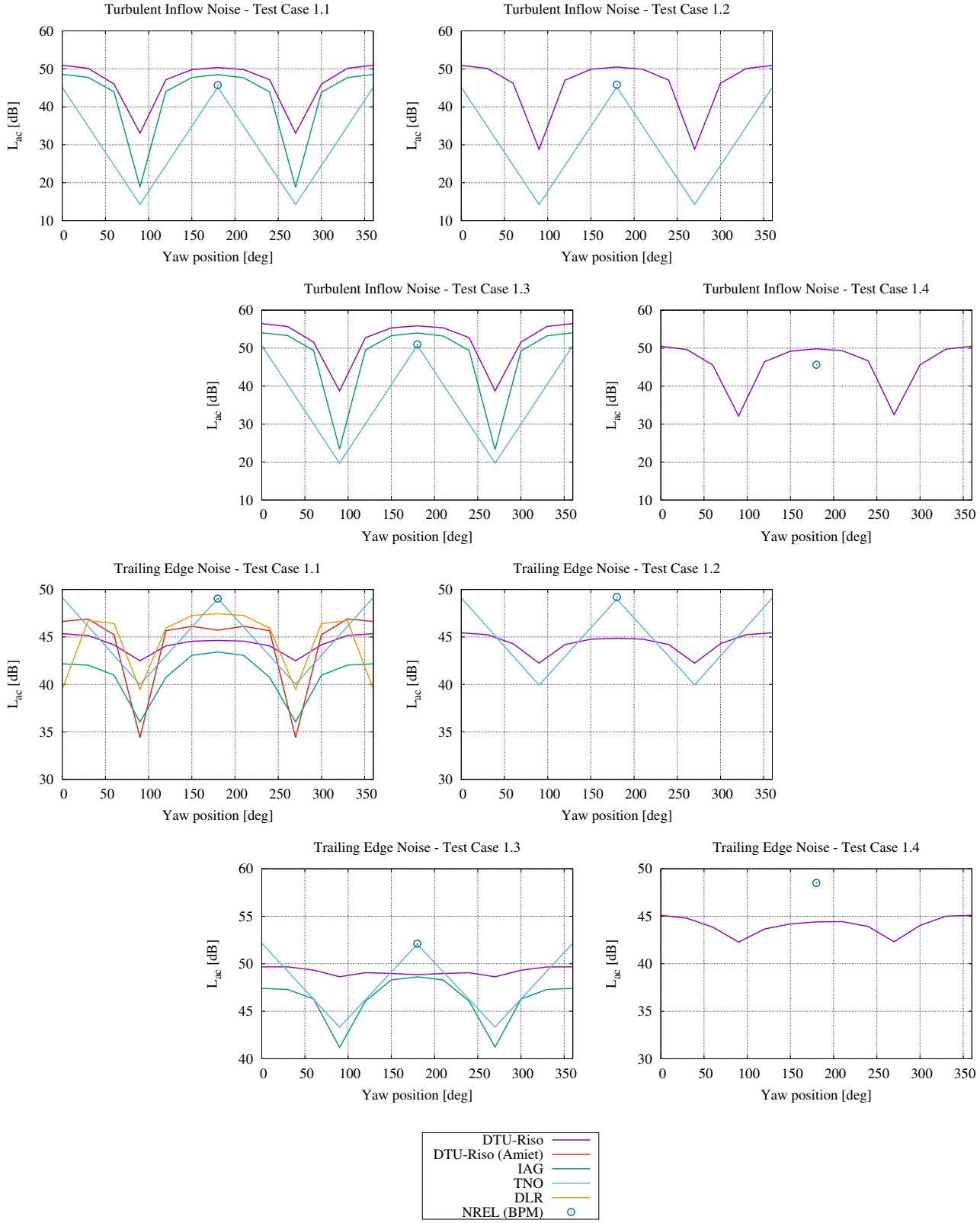

Figure 54. Integrated noise spectra directivity around the wind turbine rotor for turbulent inflow and trailing edge noise as a function of azimuthal position around the turbine on the ground.

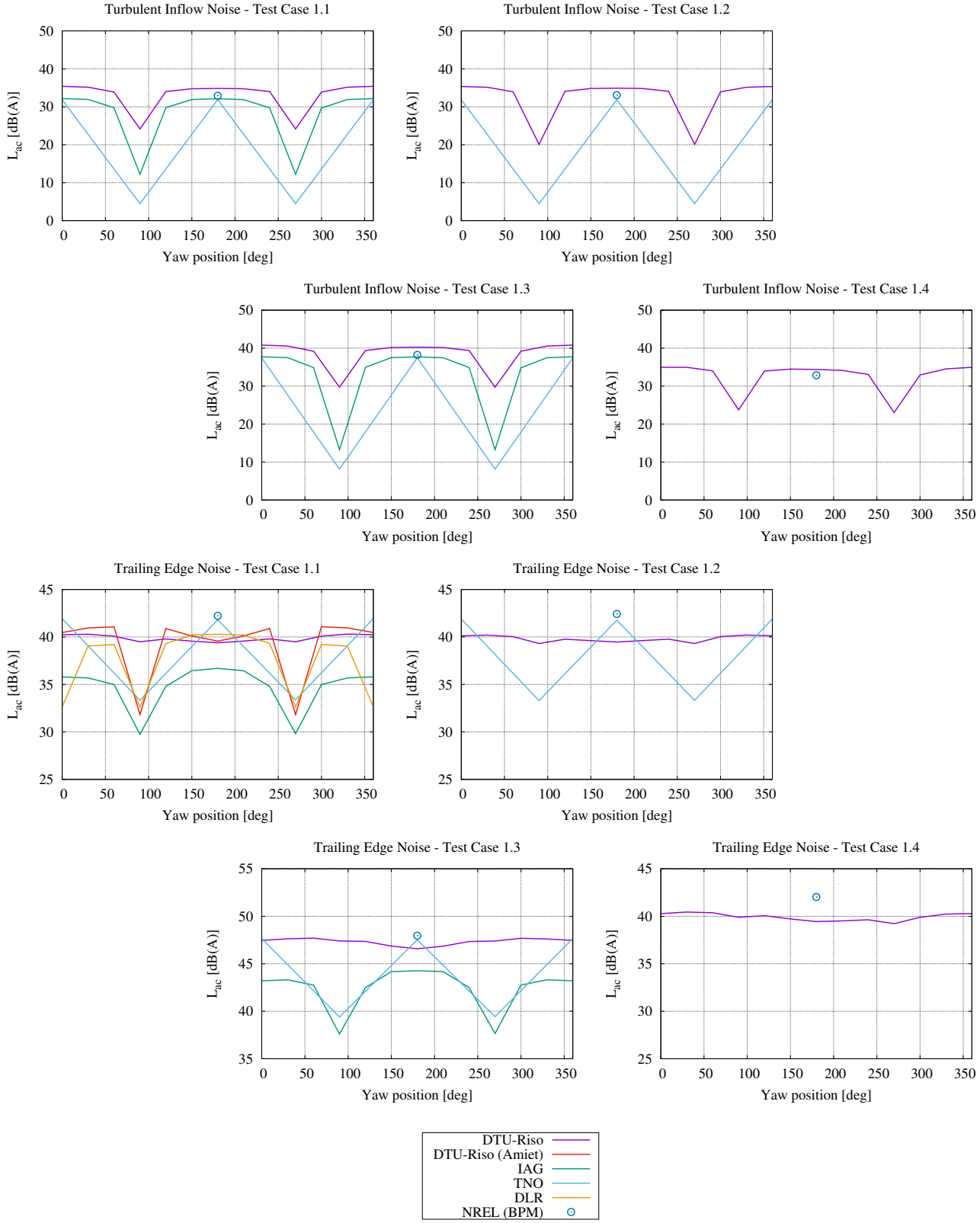

Figure 55. Integrated A-weighted noise spectra directivity around the wind turbine rotor for turbulent inflow and trailing edge noise as a function of azimuthal position around the turbine on the ground.

APPENDICES

A Geometry and sign conventions for the benchmark results

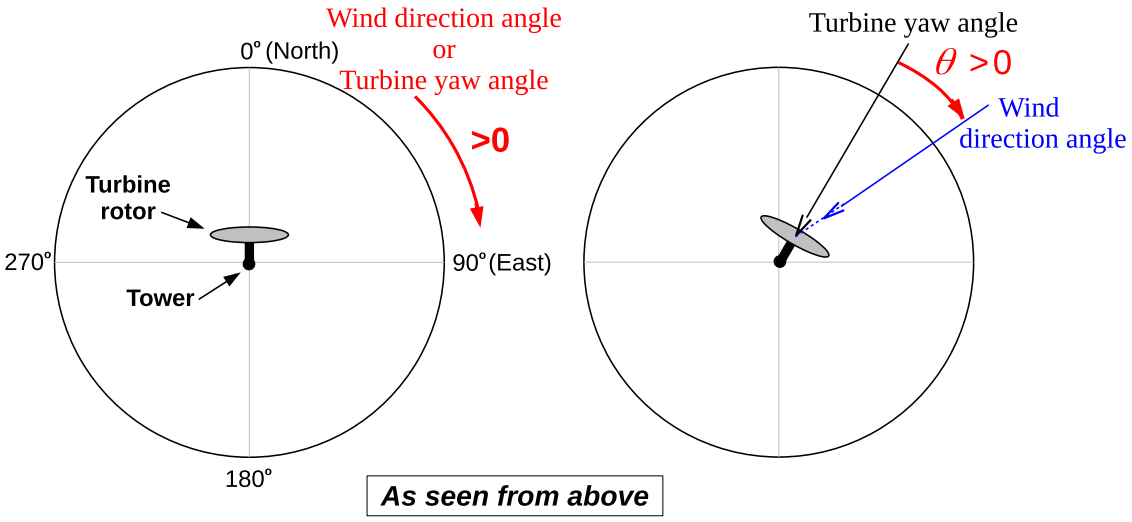

Figure 56. Yaw angle convention.

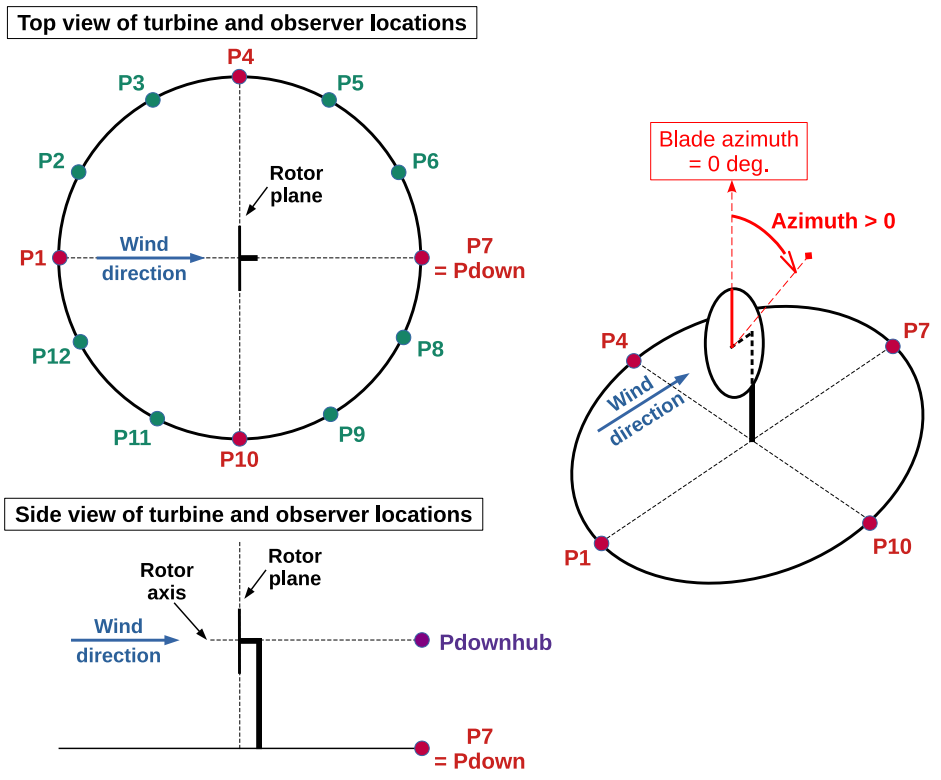

Figure 57. Observer locations and blade azimuth angle convention.

References

[1] R. K. Amiet, *Acoustic Radiation from an Airfoil in a Turbulent Stream*, J. Sound Vib. **41** (1975), no. 4, 407–420.

[2] C. Appel, B. Faßmann, and S. Lin, *CAA-basierte Schallvorhersage für Windkraftanlagen*, DAGA 2020 (Conference) (Hannover, Germany), Deutsche Gesellschaft für Akustik e.V., March 2020.

[3] F. Bertagnolio, A. Fischer, and W. J. Zhu, *Tuning of Turbulent Boundary Layer Anisotropy for Improved Surface Pressure and Trailing-Edge Noise Modeling*, Journal of Sound and Vibration **333** (2014), no. 3, 991–1010.

[4] W. K. Blake, *Mechanics of Flow-Induced Sound and Vibration, Vol.I and II*, vol. in Applied Mathematics and Mechanics, Frenkiel, F.N. and Temple, G. (eds.), Academic Press, 1986.

[5] K. Boorsma and J.G. Schepers, *Enhanced wind turbine noise prediction tool SILANT*, Presented at the Fourth International Meeting on Wind Turbine Noise (Rome (Italy)), AIAA Paper 2010-645, April 2011.

[6] T. F. Brooks, S. D. Pope, and M. A. Marcolini, *Airfoil Self-Noise and Prediction*, NASA Reference Publication 1218, Retrieved from: https://ntrs.nasa.gov/archive/nasa/casi.ntrs.nasa.gov/19890016302.pdf, NASA Langley Research Center, Hampton (VA), July 1989, (Accessed: 2020-04-08).

[7] D. Casalino, E. Grande, G. Romani, D. Ragni, and F. Avallone, *Definition of a benchmark for low reynolds number propeller aeroacoustics*, Aerospace Science and Technology **113** (2021).

[8] D. Casalino, W. Van der Velden, and G. Romani, *A framework for multi-fidelity wind-turbine aeroacoustic simulations*, 28th AIAA/CEAS Aeroacoustics Conference, June 2022, Southampton, UK, 2022.

[9] M. Drela, *Xfoil: An analysis and design system for low reynolds number airfoils. in: Mueller t.j. (eds) low reynolds number aerodynamics. lecture notes in engineering, vol 54*, Springer, Berlin, Heidelberg, 1989.

[10] M. Drela and M.B̃. Giles, *Viscous-inviscid analysis of transonic and low reynolds number airfoils*, AIAA Journal **25** (1987), no. 10, 1347–1355.

[11] R. Ewert, *RPM - the fast Random Particle-Mesh method to realize unsteady turbulent sound sources and velocity fields for CAA applications*, 13^{th} AIAA/CEAS Aeroacoustics Conference (Rome, Italy), Conf. Proceedings, 2018, AIAA 2007-3506.

[12] B. Faßmann, N. Reiche, R. Ewert, M. Herr, and J. Delfs, *Evaluation of Wind Turbine Noise based on Numerical Simulation Methods*, 18^{th} AIAA/CEAS Aeroacoustics Conf. (Proc.) (Atlanta, Georgia), 2018, AIAA 2018-3924.

[13] A. Fischer, F. Bertagnolio, and H. Aa. Madsen, *Improvement of TNO type trailing edge noise models*, European Journal of Mechanics B - Fluids **61** (2017), 255–262.

[14] M. Herr, R. Ewert, C. Rautmann, M. Kamruzzaman, D. Bekiropoulos, A. Iob, R. Arina, P. Batten, S. Chakravarthy, and F. Bertagnolio, *Broadband Trailing-Edge Noise Predictions - Overview of BANC-III Results*, 21^{th} AIAA/CEAS Aeroacoustics Conf. (Proc.) (Dallas (TX)), AIAA Paper 2015-2847, June 21-26 2015.

[15] M. Herr, M. Kamruzzaman, and C. Bahr, *BANC-IV-1: TBL-Trailing-edge noise*, Fourth Workshop on Benchmark Problems for Airframe Noise Computations (BANC-IV) (Lyon, France), 22^{nd} AIAA-CEAS Aeroacoustics Conference (Workshop), June 2016.

[16] C. Hornung, C. Scheit, N. Noffke, and M. Kamruzzamann, *Turbulence Inflow Noise Prediction of Wind Turbine Rotors: The physically correct Representations of the Simplified Amiet and Lowson Model*, 9th International Conference on Wind Turbine Noise (Remote from Europe), Conference Proceedings, May 2021.

[17] Cordula Hornung, Thorsten Lutz, and Ewald Krämer, *A model to include turbulence-turbulence interaction in the prediction of trailing edge far field noise for high angles of attack or slightly separated flow*, Renewable Energy **136** (2019), 945–954.

[18] M. Kamruzzaman, D. Bekiropoulos, T. Lutz, W. Würz, and E. Krämer, *A semi-empirical surface pressure spectrum model for airfoil trailing- edge noise prediction*, International Journal of Aeroacoustics **14** (2015), no. 5-6, 833–882.

[19] C. Lindenburg, *Bladmode, program for rotor blade mode analysis*, Tech. Rep. ECN-C-02-050-r2, ECN, The Netherlands, 2002.

[20] M. V. Lowson, *Assessment and prediction of wind turbine noise*, ETSU W/13/00284/REP, UK, 1993.

[21] M. V. Lowson and J. B. Ollerhead, *A Theoretical Study of Helicopter Rotor Noise*, J. Sound Vib. **9** (1969), no. 2, 197–222.

[22] T. Lutz, A. Herrig, W. Würz, M. Kamruzzaman, and E. Krämer, *Design and Wind-Tunnel Verification of Low-Noise Airfoils for Wind Turbines*, AIAA Journal **45** (2007), no. 4, 779–785.

[23] B. Montgomerie, A. Brand, J. Bosschers, and R. van Rooij, *Three-dimensional effects in stall*, Tech. Rep. ECN-C-96-079, ECN, The Netherlands, 1997.

[24] P. Moriarty, G. Guidati, and P. Migliore, *Prediction of Turbulent Inflow and Trailing-Edge Noise for Wind Turbines*, Proc. of the 11^{th} AIAA/CEAS Aeroacoustics Conf. (Monterey, CA), AIAA Paper 2005-2881, 2005.

[25] R. W. Paterson and R. K. Amiet, *Acoustic Radiation and Surface Pressure Characteristics of an Airfoil Due to Incident Turbulence*, 3^{rd} AIAA Aero-Acoustics Conference (Palo Alto, CA), Conf. Proceedings, July 1976.

[26] ———, *Noise and Surface Pressure Response of an Airfoil to Incident Turbulence*, Journal of Aircraft **14** (1977), no. 8, 729–736.

[27] C. Rautmann, *Numerical Simulation Concept for Low-Noise Wind Turbine Rotors*, DLR Forschungsbericht FB-2017-35, DLR (Institute for Aerodynamics and Flow Technology), Brauschweig, Germany, 2017, Dissertation.

[28] R. H. Schlinker and R. K. Amiet, *Helicopter rotor trailing edge noise.Technical Report 1*, NASA Contractor Report 3470, Retrieved from: https://ntrs.nasa.gov/archive/nasa/casi.ntrs.nasa.gov/19820003986.pdf, NASA Langley Research Center, 1981, (Accessed: 2020-04-08).

[29] C. R. Sucameli, P. Bortolotti, A. Croce, and C. L. Bottasso, *Comparison of some wind turbine noise emission models coupled to BEM aerodynamics*, Journal of Physics: Conference Series **1037** (2018), 022038.

[30] L. A. Viterna and R. D. Corrigan, *Fixed pitch rotor performance of large horizontal axis wind turbines*, NASA N83 19233 (1981).

6 WP2 / Annex 2 - Conference proceedings on comparisons between wind turbine noise code prediction models and measurement data

INCEEUROPE

10th International Conference
on
Wind Turbine Noise
Dublin – 21st to 23rd June 2023

Wind turbine noise code benchmark: A comparison and verification exercise

Franck Bertagnolio¶, Andreas Fischer
DTU Wind and Energy Systems, Roskilde, Denmark

Christina Appel, Michaela Herr
DLR, Institut für Aerodynamik und Strömungstechnik, Braunschweig, Germany

Ferdinand Seel, Thorsten Lutz
Institut für Aerodynamik und Gasdynamik, Universität Stuttgart, Stuttgart, Germany

Koen Boorsma, Gerard Schepers, Miguel Restrepo Botero
Wind Energy, TNO Energy Transition, Petten, The Netherlands

Damiano Casalino, Wouter van der Velden
Dassault Systèmes Deutschland GmbH, Stuttgart, Germany

Carlo R. Sucameli
Lehrstuhl für Windenergie, Technische Universität München, München, Germany

Pietro Bortolotti
National Wind Technology Center, National Renewable Energy Laboratory, Golden, CO, USA

Summary

In a number of institutions and companies, researchers and engineers are developing numerical models and frameworks that are used to predict the aerodynamic noise emissions from wind turbine rotors. The simulation codes range from empirically tuned engineering models to high-fidelity computational ones. Their common feature is the fact that they all specifically model the main aerodynamic noise mechanisms occurring at the rotating blades (namely, the turbulent boundary layer): trailing-edge and turbulent inflow noise. Nevertheless, different modelling techniques and implementations may generate different results, even when assessed on the same rotor design and operating conditions, which raises the question of the actual fidelity and reliability of these

¶Corresponding author: frba@dtu.dk

models. Trailing-edge noise is put at the forefront of the present study, as it is recognized to be the main source of audible noise from modern wind turbines.

The present benchmark aims at comparing the results from different modelling approaches and drawing some conclusions from these comparisons. This effort, denoted as Wind Turbine Noise Code benchmark, was initiated in 2019 as a joint activity between the IEA Wind Task 39 (Quiet Wind Turbine Technology) and Task 29 (Detailed Aerodynamics of Wind Turbines, now Task 47).

In addition to the investigation of the noise emissions themselves, the rotor aerodynamic characteristics are investigated, as they are the source of the noise generation mechanisms discussed herein.

A number of test cases are defined, and the aerodynamic and aeroacoustic predictions from the various models are compared. A fair agreement between the aerodynamic predictions is observed. There exist some discrepancies between the different noise prediction methods, but it is difficult to conclude if one methodology is better than another in order to design a wind turbine with noise as a constraint.

1. Introduction

It is a well-accepted fact that trailing-edge (TE) noise is the prominent source of aerodynamic broadband noise from wind turbines in the audible range [35]. Therefore, it is important for the wind industry to assess and subsequently mitigate (e.g. using serration) this particular source of noise in order to reduce the environmental impact of wind turbines and wind farms. Aerodynamic noise sources also include turbulent inflow (TI) noise, which is normally more dominant at lower frequencies than TE noise (at least for modern multimegawatt wind turbines), but it can also be audible.

The present work aims at comparing various simulation methods for predicting and quantifying these two main aerodynamic noise sources from wind turbines. Note that other noise sources such as mechanical/tonal noise, low-frequency tower-blade interaction, tip noise, etc., are not considered in the present study, although these can have a significant impact on the acoustic footprint of a wind turbine. In addition, atmospheric propagation effects (such as reflection, refraction, diffraction, and air absorption) are also neglected, despite their potential impact on the perceived noise at dwellings.

This work is conducted as part of the IEA Wind Technology Collaboration Programme. Various institutions from participating countries have contributed to the present comparisons by using their own simulation framework that can model wind turbine aerodynamic noise emissions. The goal is to compare the different methodologies and analyze the consistency (or the lack thereof) of the results when simulating the same rotor in the same operating conditions.

In the following, the context and objectives of the present study are discussed. The various modelling strategies that are used for the comparisons are reviewed. The first part of the study concentrates on the comparisons of the aerodynamic quantities that are essential for the prediction of wind turbine aerodynamically generated noise. Then, the actual noise predictions are considered, focusing on the relationship between the aerodynamic and acoustic results. The study is concluded with comparisons of some of the model results with actual field noise measurement data from a wind turbine.

2. Context and objectives

TE and TI noise are the respective results of the interaction of the airfoil boundary layer (BL) and atmospheric turbulence with the blades. A variety of numerical methods have been derived to model these phenomena, ranging from relatively simple empirical formulae to high-end computationally expensive simulation codes. In a long-term effort, various models for TE noise were investigated at the airfoil level in a series of comparison rounds as part of the Benchmark Problems for Airframe Noise Computation (BANC) [20, 21]. The present study attempts to compare a number of these models when considering a full wind turbine rotor, identify some potential pitfalls in this context, and possibly improve the use and prediction results of these methods in the future. For example, higher-fidelity models could be used to tune or improve lower-fidelity ones, which are more suited to the constraint of a rapid turnaround time typical of industrial design.

The first objective is to make sure that the underlying aerodynamic simulations of the rotor flow are sufficiently close to each other, so that the impact on noise predictions related to possible discrepancies in the aerodynamic input data is minimized. Therefore, the first part of the study concentrates on rotor aerodynamic characteristics.

The second objective is to compare acoustic results. An analysis is conducted in an attempt to identify 1) the reasons for discrepancies between similar methodologies if/when such discrepancies are observed and 2) trends between different modelling approaches, e.g. empirical vs. high-fidelity models.

3. Computational methods

The various computational frameworks used in the present article are described in this section. A rough categorization of the different methodologies is introduced here.

The *first* step in the prediction of aerodynamic noise from a turbine usually consists of calculating the aerodynamic flow field around the turbine's rotor. Two main methodologies can be applied here:

- The most popular engineering method for predicting a wind turbine rotor flow aerodynamic is the blade element momentum (BEM) method, originally derived by Glauert [18], which is based on mass and momentum conservation principles.
- The second option is to numerically solve the associated conservation equations (here, Navier-Stokes or Euler) using computational fluid dynamics (CFD). This is usually much more computationally expensive.

The *second* step consists of defining the TE noise modelling approach. Note that the prediction of this noise source from wind turbines requires detailed boundary layer characteristics along the blades, which are normally not provided by BEM methods.

Three approaches are generally adopted:

- *Empirical modelling:* in all cases, this amounts to using the well-known Brooks Pope Marcolini (BPM) model [10]. Note that this model can include various aerodynamic noise sources (e.g. tip noise, blunt TE noise), but only TE noise is considered here. The model is based on theoretical work for the scaling of TE noise and empirical fitting using a series of experiments on the NACA0012, during which aerodynamic and acoustic properties were measured.

- *Semi-empirical modelling:* the models are extensions of the original model named TNO * developed by Parchen [36]. The TNO TE noise model and its revised versions are a combination of Kraichnan theory for BL turbulence, including various assumptions for characterizing the turbulence, and a scattering model for the TE noise prediction using either Howe or Amiet theory. A flow solver (CFD or Xfoil) is typically used for determining the aerodynamic and turbulent flow inputs to the overall model. These methodologies will be denoted as semi-empirical or TNO-type models in the following.
- *High-fidelity modelling:* the models are based on high-performance computing for solving the main rotor flow field and the acoustic field, either jointly or separately.

In addition, each of the above methods uses a flow solver to compute the aerodynamics around the blades, which are in most cases used as inputs for the above noise models (except when the aerodynamic and acoustic calculations are coupled, e.g. for the Lattice-Boltzmann Method).

Furthermore, as far as TI noise modelling is concerned, the frameworks used by the participants of the present comparison exercise are all implementations of the Amiet TI model [1, 37]. Two main versions can be distinguished here. The first one is the complete model implementation that involves the computation of the unsteady lift from a flat plate. The second is based on its asymptotic approximation for higher frequencies. Note that a simpler version using Lowson's method can also be used for TI noise modelling [30]. Nevertheless, more elaborate modelling methods are available for predicting TI noise from wind turbines [26].

The various numerical frameworks from the different participating institutions are summarized below. For further details about these frameworks, the reader is referred to the IEA Wind Technology Collaboration Programme website and the report specifically related to the present work [4].

3.1. TNO - SILANT

The aeroacoustic calculation of TNO is divided into three programs: Blademode [7], RFOIL [28], and SILANT[33].

BladeMode is an in-house aeroelastic blade stability software using the BEM theory. It is used in a quasi-steady configuration for the present application. The resulting sectional angle of attack and Reynolds number distribution along the blade span are then used as input to the SILANT model. This program includes the noise calculation from turbulent TE noise and tip noise based on the BPM model [10] and TI noise using the model of Amiet [1] and Lowson [29]. The RFOIL2D panel code with interacting BL is used to provide the boundary layer displacement thickness at the TE of the airfoil sections along the blade. The data are stored as a look-up table for the SILANT model.

The resulting sectional noise source strengths are acoustically summed over the blades and rotor. In addition to calculating noise sources, SILANT can also include Doppler effects (and additional effects related to atmospheric propagation which are ignored in the present work).

3.2. NREL - OpenFAST

OpenFAST is a popular multi-physics solver developed and released by the National Renewable Energy Laboratory. OpenFAST integrates an aeroacoustic model that is described in Bortolotti et al. [8]. The model implements a conventional turbulent inflow model from Amiet [1], with the optional

*Note that the designation of the so-called TNO TE noise model originates from the institute where its conceptor worked at the time. It is the same TNO institute at which two of the authors of the present article are working. In order to avoid confusion, it must be made clear that these two authors use a different TE noise model in their computational framework, but that both models will be referred to as TNO in the figure captions.

correction defined by Moriarty et al. [34]. The model also implements the noise sources defined by Brooks et al. [10]. The models implemented in OpenFAST were subjected to a validation study operating a GE 1.5 MW wind turbine. The results are discussed in Bortolotti et al. [9] and Hamilton et al. [19].

3.3. TUM - Cp-Max AAM

This framework is the one described in [41]. It is based on the in-house-developed aeroservoelastic wind turbine solver Cp-Lambda, which implements a BEM formulation and provides the aerodynamic inputs necessary for the aeroacoustic calculations.

Several aeroacoustic models are implemented within this framework. For the purpose of the present paper, TE noise results are provided for two different models (the BPM model [10] and a version of the TNO model described in [41]). For both models, 2D boundary layer characteristics are obtained through XFoil. TI noise spectra are provided for two different formulations of the Amiet model. The first formulation is the full implementation of [37], while the second one corresponds to the approximations of the Amiet model for high and low frequencies. An additional low-frequency correction is included, as shown in [30].

3.4. IAG Stuttgart - IAGNoise+

The Institute of Aerodynamics and Gas Dynamics (University of Stuttgart, Germany) uses the IAGNoise+ noise prediction code. This semi-empirical model computes the generated TE noise based on 3D flow solutions from CFD simulations. In this work, Reynolds-averaged Navier Stokes (RANS) simulations using a k-ω SST turbulence model were run with the flow solver FLOWer.

IAGNoise+ employs a TNO-Blake-type model for the computation of TE noise [5]. Compared to a classical TNO-type model, the current implementation [22] includes the part of the wall pressure fluctuation source term that is associated with turbulence-turbulence interaction and usually neglected in the basic model. This inclusion allows for more accurate predictions at higher angles of attack, where slight to moderate flow separation occurs. Additionally, the anisotropy factor was adjusted to also include adverse pressure gradient effects. The IAGNoise+ prediction tool also offers a way to calculate inflow noise, based on the model proposed by Paterson and Amiet [38] with Moriarty's thickness correction [34].

3.5. DTU - HAWC2-Noise

This framework uses the HAWC2 code [27] as a basis. It is a time-domain multibody aeroelastic code used for the study and design of wind turbines. The blade element momentum theory by Glauert [18] is applied in order to calculate the aerodynamic loading [32].

The aerodynamic data are used as inputs to an acoustic module that can account for TI noise using the Amiet model [1], and TE noise using a version of the TNO model [17] for which scattering is accounted for using the Amiet model [2]. Both noise model formulations are in the spectral domain. Therefore, it is assumed that that the acoustic emissions are quasi-stationary (at each time step of the aeroelastic solver), and spectrograms can be obtained for each of the noise sources. The detailed aerodynamic characteristics of the turbulent BL, which are used as input to the TE noise model, are computed as a preprocessing step with the 2D RANS solver EllipSys2D at each discrete section along the blades.

3.6. 3DS wind turbine multi-fidelity approach

Wind turbine aerodynamic and acoustic calculations have been performed using the multi-fidelity framework *Opty∂B*-WTNOISE® [12, 42]. Three approaches have been used: one is based on a blade element momentum theory (BEMT) rotor aerodynamic calculation, and the other two rely on lattice Boltzmann method very large eddy simulation (LBM-VLES) scale-resolved transient flow simulations.

3.6.1. BEM-based methodology

The BEMT tool uses BEM theory with uniform inflow and tip-loss correction [11], and a viscous panel method available in *Opty∂B*-BEMT is used for defining the boundary layer flow on the blades [13, 14]. Wall pressure spectra are computed with semi-empirical formulations. On the suction side, a model is used, obtained by blending Schlinker's [40] model at low frequency with Kamruzzaman's [25] model at high frequency, and by recalibrating the overall energy to the Schlinker model value. On the pressure side, the Schlinker model is used. The Schlinker and Amiet model is used for TI noise [1].

3.6.2. 2.5D LBM/FW-H-based methodology

PowerFLOW® 2.5D simulations are performed by means of a fully automatic workflow fed with sectional coordinate profiles generated by *Opty∂B*-PFROTOR, and values of Mach number and angle of attack computed by *Opty∂B*-BEMT [12].

Simulations are carried out on extruded blade sections of fixed span of 0.1 m. For every radial strip selected by the user from the available blade segmentation, the PowerFLOW simulation generates a transient wall pressure file which is used by the frequency-domain FW-H solver *Opty∂B*-FWHFREQ executed by *Opty∂B*-WTNOISE. Full-blade noise spectra are recovered by *Opty∂B*-WTNOISE via an incoherent summation of sectional noise spectra, scaled by the ratio of the physical spanwise extension of the blade strip and the 2.5D simulated span.

3.6.3. 3D LBM/FW-H-based methodology

PowerFLOW 3D simulations are performed by means of a fully automatic workflow used for multicopter eVTOL, rotorcraft, fan, and wind turbine applications [12]. A series of simulations are carried out with mesh refinement in different blade strips where the turbulent scales are trigged by a trip. Similar to the 2.5D approach, the full turbine noise levels are recovered by incoherent summation of the individual strip contributions.

3.7. DLR - hybrid RANS-based CAA method PIANO/FRPM

An automatized 2D process chain for turbulent boundary layer trailing edge noise (TBL-TEN) [16, 39] is used to provide an acoustic prediction for trailing-edge noise of 2D profiles. Originally developed to assist low-noise airfoil design optimization, this method has been validated in detail within the BANC framework [20, 21]. The process chain operates via bash scripting the input parameters (like airfoil geometry, Reynolds number, angle of attack, chord length and process parameters, e.g. number of iterations, simulated real time and post processing options). The CFD code TAU, which is developed at the German Aerospace Center (DLR), is applied for the RANS simulations, and the DLR computational aeroacousics (CAA) code PIANO with the stochastic sound source model FRPM [15] (**F**ast **R**andom **P**article **M**esh method) is applied for the acoustic prediction.

In a second step, the results from the process chain are combined with DLR's TAP (**T**urbine **A**coustic **P**rediction) tool to extrapolate and summarize the data for a complete rotor [3]. Ongoing work includes the successive extension of TAP by additional semi-empirical source models for flow separation and TI noise. TI noise predictions applied herein are based on Hornung et al. [23].

4. Test case definitions and physical inputs

All the calculations presented in this article are based on the 2.3 MW wind turbine NM80. The use of the NM80 turbine geometry has been granted to the participants of Task 39 for the present study. This turbine was initially investigated as part of the DANAERO project [31]. It was further used as a reference turbine for the aerodynamic benchmark that was conducted as part of IEA Wind Task 29 (now Task 47) [6]. Some details of the turbine geometry can be found in the latter publications. Four test cases were defined for the present study, although only one of them will be considered in the present article. The main operational conditions of interest are the following:

- Test Case 1.1: Axisymmetric configuration (i.e. no rotor tilt), rigid structure, a wind speed of 6.1 m/s, turbulence intensity of 8.96%, and a rotor speed of 12.3 rpm. Additional information such as atmospheric conditions, blade pitch, etc., are also specified.

For the rotor noise calculations, a number of observer positions are defined. Twelve positions are defined on the ground around the turbine, equally distributed on a circle with a radius equal to the maximum height of the turbine (i.e. tower height plus half-rotor diameter), as depicted in Fig. 1. In addition, a single point is located at the same distance but on the rotor axis in the downstream direction. Note that in all noise calculations, atmospheric propagation effects and ground reflections are discarded, but the geometrical spreading is accounted for.

In addition, results from a noise measurement campaign conducted on a megawatt-size turbine will be considered.

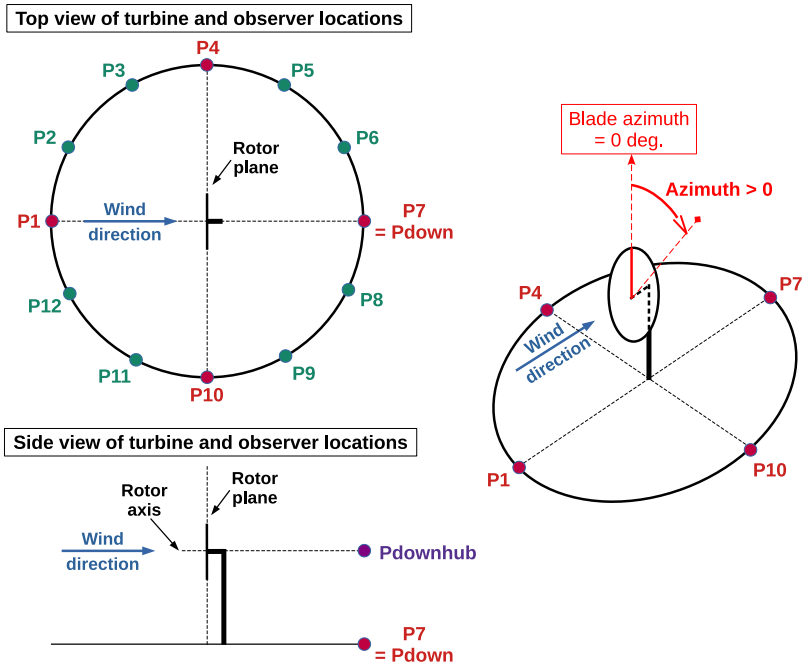

Fig. 1 Sketch of the observer locations around the turbine for the noise calculation results.

5. Comparison of aerodynamic results

As mentioned earlier, the aeroacoustic emissions of a wind turbine are highly dependent on the atmospheric inflow and resulting flow on the blades, which is computed using BEM theory or CFD in this work. Therefore, the first step for comparing numerical frameworks is comparing the aerodynamic data along the blades. Three spanwise locations along the blades were chosen for the comparisons: $r = 19$ m, 30 m and 37 m from the root of the blade.

Note that since both TI and TE noise are scaling with the Mach number (to a specific power depending on the mechanism), it is well-known that toward the blade tip, as the effective velocity becomes higher, the aerodynamic noise emissions increase. Consequently, this study focuses on BL characteristics on the outer part of the blades.

5.1. Incoming flow

The relative and effective (i.e. including rotor induction) inflow velocities, angles of attack, and lift and drag coefficients at the three spanwise locations are displayed in Fig. 2. The agreement between the inflow velocities is nearly perfect, which is consistent with the imposed rotor speed of the test case. Some discrepancies are observed between the calculated angles of attack, but these remain relatively small, within less than 1 deg, and these appear to become even smaller toward the tip of the blade. The lift coefficients present very small discrepancies as well, but the drag coefficients do depart more significantly.

Overall, all methods deliver similar results in terms of the aerodynamic loading on the turbine.

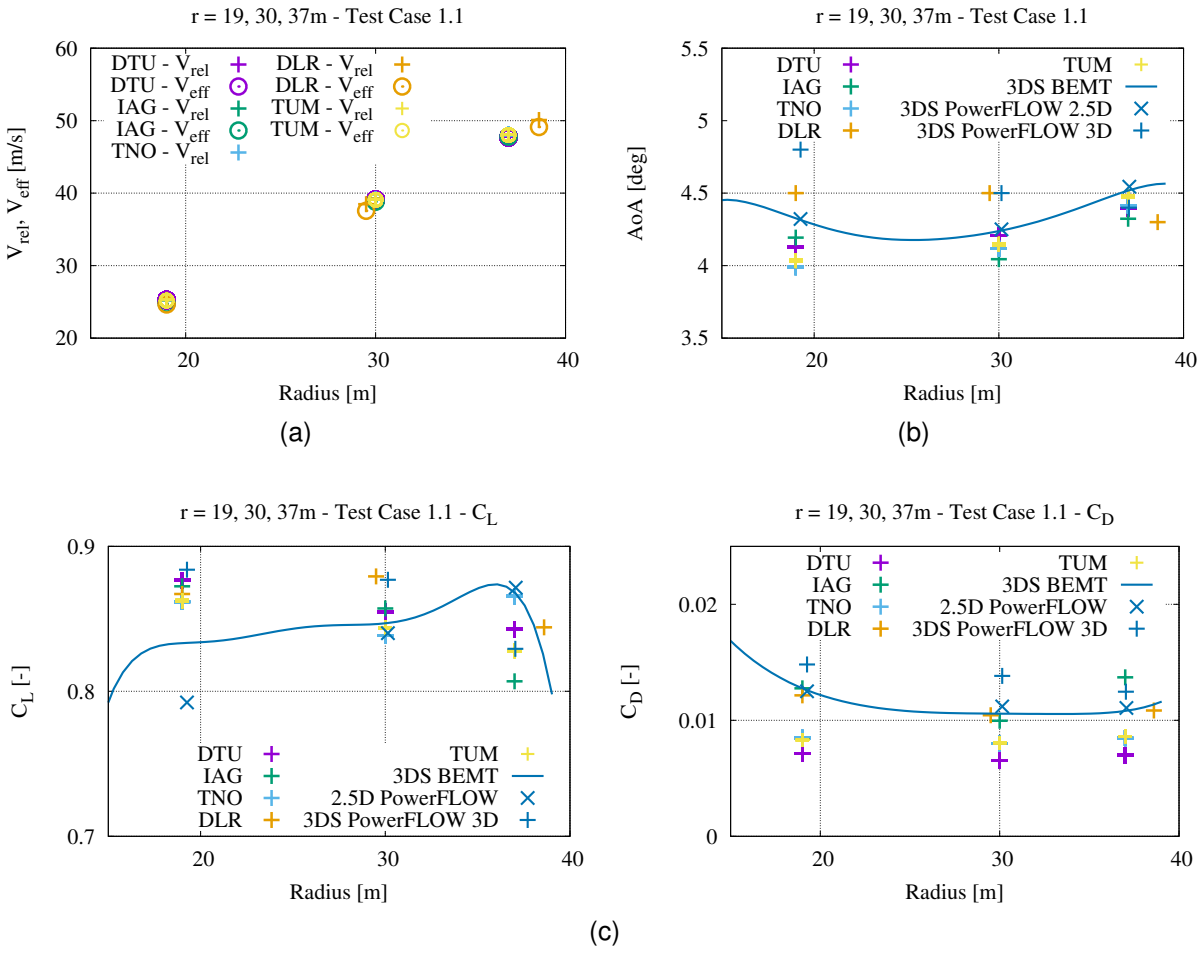

Fig. 2 Aerodynamic quantities of the incoming flow along the blade span: (a) relative and effective inflow velocity, (b) angle of attack, and (c) lift and drag coefficients.

5.2. Boundary layer thicknesses and profiles near the TE

It is well-known that the turbulent BL characteristics near the TE have a large impact on the TE noise emissions. These characteristics are investigated in the present section.

The BL thickness δ, BL displacement thickness δ^*, and BL momentum thickness θ are displayed in Fig. 3 for the suction and pressure sides. It can be observed that there is relatively good agreement between all methods, and that the discrepancies appear to be getting smaller toward the tip of the airfoil, which should contribute to a better convergence of the aerodynamic noise model results in the following sections.

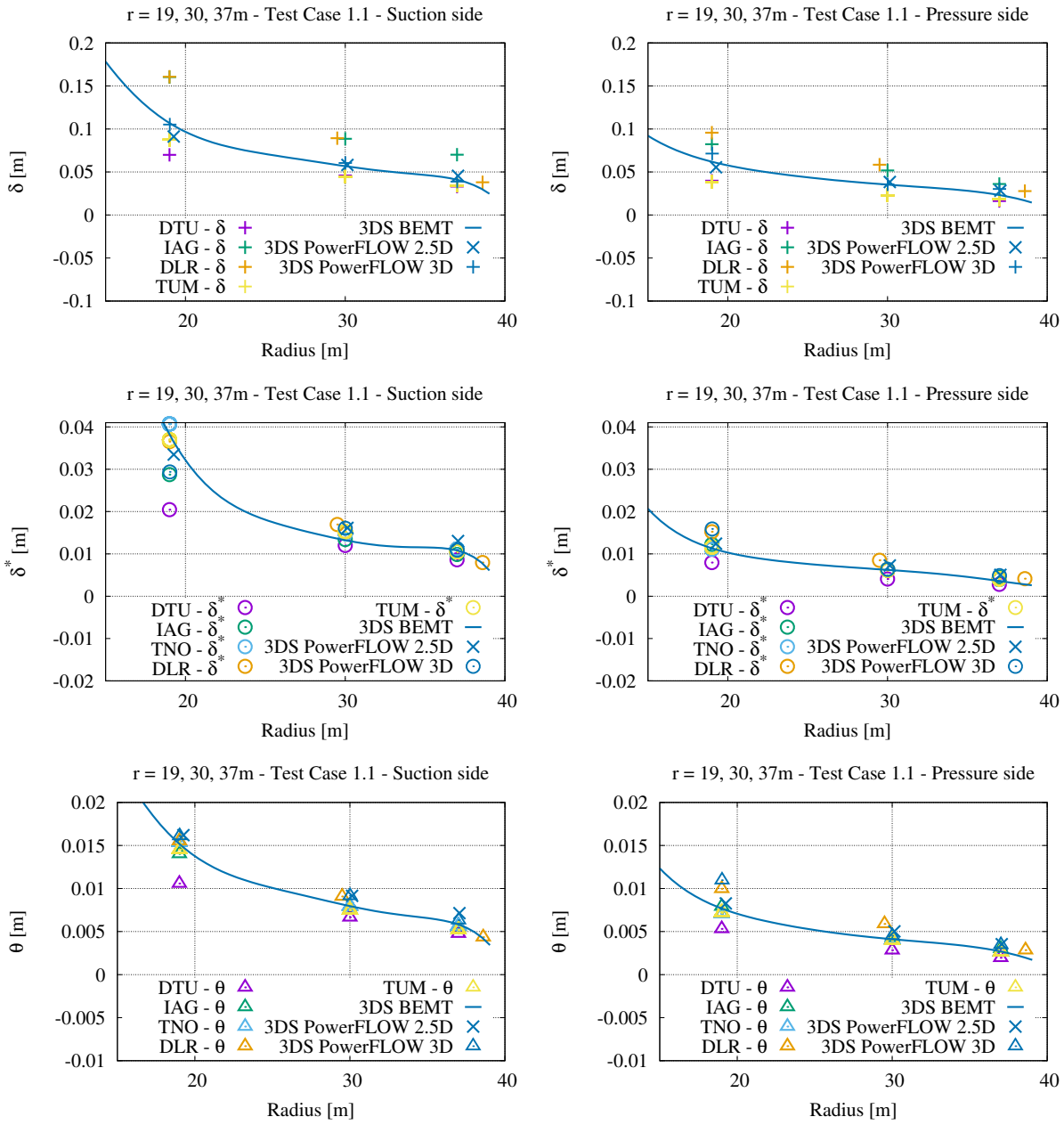

Fig. 3 Boundary layer thickness (top), displacement thickness (middle), and momentum thickness (bottom) along the blade span on the *suction* side of the airfoil at $x/C = 93\%$ (left) and *pressure* side at $x/C = 91\%$ (right).

The boundary layer profiles for BL velocity, turbulent kinetic energy, turbulence dissipation rate, and

integral length scales, which are again important parameters influencing TE noise, are displayed in Fig. 4 for the suction and pressure sides at the outer spanwise section $r = 37$ m. Note that results from only a few methods are displayed here, as these quantities do not need to be explicitly calculated in some of the present numerical frameworks in order to compute TE noise.

There are noticeable discrepancies in the turbulent quantities. Note here that DLR and the Technical University of Denmark (DTU) use 2D CFD calculations to obtain the BL profiles at various sections along the span, whereas the University of Stuttgart Institute for Aerodynamic and Gas Dynamics (IAG) conducts a full 3D CFD simulation of the entire blade. This may affect the resulting computed BL profiles.

The impact of these turbulent BL quantities on the surface pressure spectra at the same location (see Section 5.3), and TE noise at the rotor level (see Section 6), is investigated in the following.

5.3. Surface pressure spectra near TE

The surface pressure spectra on the suction side at $x/C = 93\%$ and pressure side at $x/C = 91\%$ (i.e. relatively close to the TE) are displayed in Fig. 5. Since these spectra are characteristics of the turbulent flow in the vicinity of the TE, it is expected that they will have a large impact on the TE noise emission.

There is relatively good agreement between DTU, IAG, and the 3DS BEMT results above the peak frequency around 400–500 Hz on the suction side. The 3DS PowerFLOW results show higher spectral levels across the whole frequency range with slightly smaller slope above the peak frequency. It is noteworthy that all methods exhibit peak frequencies close to each other.

However, the discrepancies are larger on the pressure side. Nevertheless, all methods exhibit higher peak frequencies, which could be expected from the smaller BL thicknesses (see Fig. 3) and lower integral length scales (see Fig. 4). The spectra appear flatter above peak frequency for most methods. In addition, the spectral levels, e.g. at peak frequencies, are also lower in agreement with the observed lower turbulent kinetic energy levels on the pressure side (see Fig. 4).

When comparing high-fidelity model results to those that use the semi-empirical TNO model (or its variants) in Fig. 6, it is observed that the high-fidelity results (here, only PowerFLOW 2.5D and 3D) indicate a larger energy content in the low-frequency range, but also at high frequencies for the suction side. The semi-empirical methods also appear to converge on the suction side at higher frequencies.

The main takeaway from the present section is a lack of variety of methodologies for evaluating the surface pressure, which prevents the drawing of firmer conclusions. It is restricted here to three semi-empirical modelling approaches, with the LBM approach being the only one characterized by high modeling fidelity. Since surface pressure is the direct link between the boundary layer turbulent quantities and the noise emission, this is probably key to a better understanding of the discrepancies between the different noise models at the rotor level.

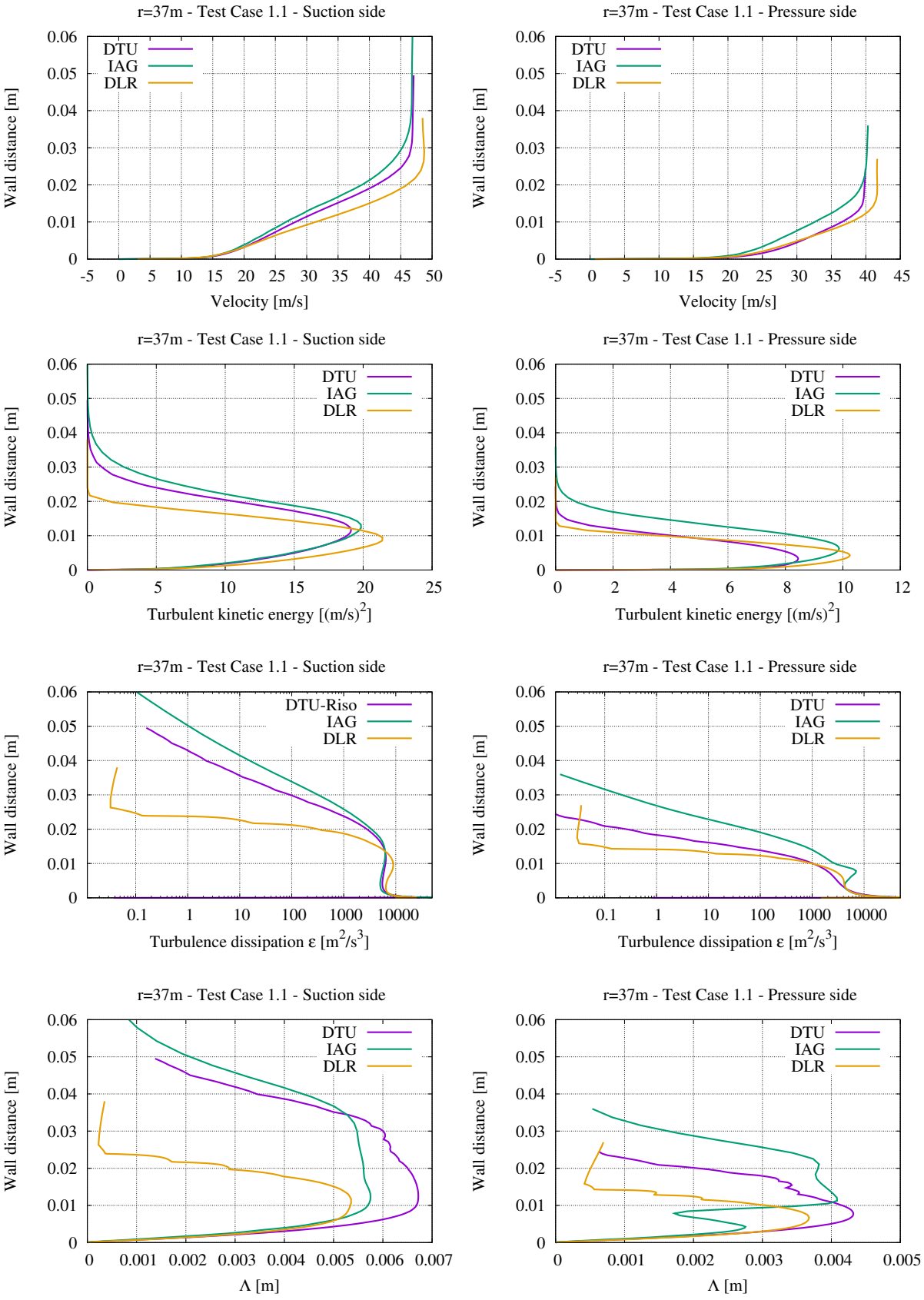

Fig. 4 Boundary layer profiles of: velocity (top row), turbulent kinetic energy (second row), turbulence dissipation rate (third row), and integral length scale (bottom row) at the blade span $r = 37$ m on the suction side of the airfoil at $x/C = 93\%$ (left) and pressure side at $x/C = 91\%$ (right).

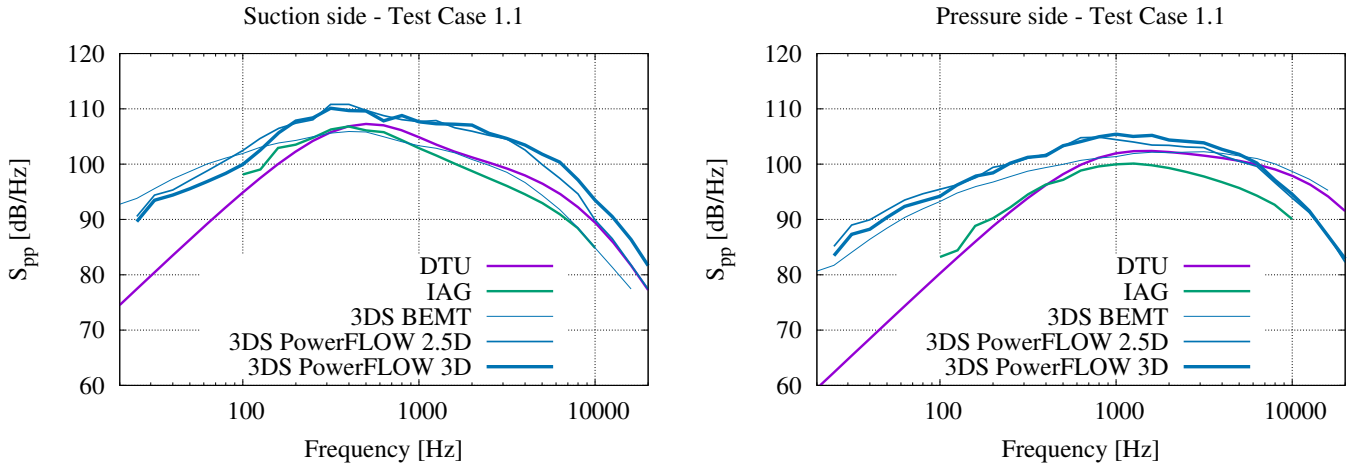

Fig. 5 Surface pressure spectra on the suction side at $x/C = 93\%$ (left) and on the pressure side at $x/C = 91\%$ (right) at the blade span $r = 37$ m.

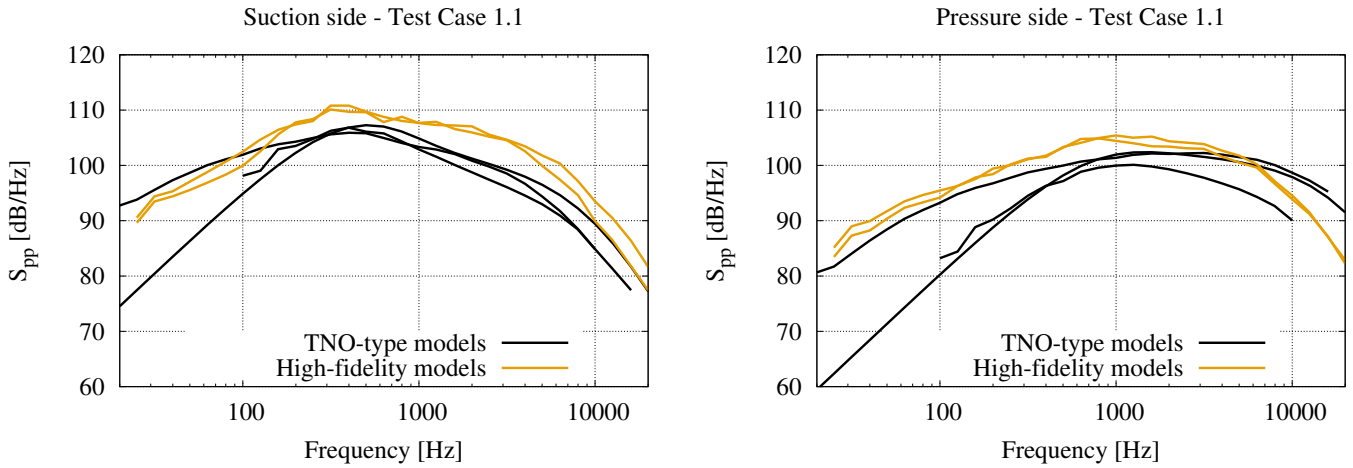

Fig. 6 Surface pressure spectra on the suction side at $x/C = 93\%$ (left) and on the pressure side at $x/C = 91\%$ (right) at the blade span $r = 37$ m.

6. Comparison of acoustic results

In this section, the aerodynamic noise emission of the full rotor is discussed.

6.1. Test case 1.1

The individual contributions from the TI and TE noise at the ground location downstream of the turbine are displayed in Fig. 7.

There is good agreement in the TI noise predictions in the high-frequency range, for $f \gtrsim 200$ Hz. This is to be expected for two separate reasons: first, all implementations are essentially similar, since they are based on the same Amiet model. Second, the model is built for a flat plate at no incidence. It follows that the actual blade shape or its angle of attack distribution does not influence the output of TI models and is mainly influenced by the velocity distribution along the blades, which is essentially identical for all the frameworks considered.

Below 200 Hz, two groups of prediction methods emerge: one predicts a continuous spectral slope toward lower frequencies while the other exhibits a higher energy bump in this frequency range. From Fig. 8, it is clear that the difference lies in the implementation of the full Amiet TI model, or its high-frequency asymptotic approximation, as discussed in Section 3. In addition, there is a larger spread of the results for the full Amiet models, which is attributed to the various implementations by the different participants. This highlights the dependency of rotor noise on the specific airfoil noise models, and this would probably require further investigations at the airfoil level.

Regarding TE noise, the spread of the model results is larger than for TI noise, as expected. The spectral slopes of the different models in the high-frequency range appear in good agreement, although an energetic spread with an amplitude slightly lower than 10 dB exists at any given high frequency. Looking toward the spectral peak, the peak frequency is in relative good agreement for all methods, with a spread amplitude of approximately 200 to 300 Hz. However, there is an even larger spread in the peak spectrum values. It is noteworthy that the high-fidelity methods, which exhibited larger energy levels for the wall-pressure spectra (see Section 5.3), now predict lower noise levels.

Looking at TE noise in Fig. 8, a number of features emerge that distinguish between high-fidelity, semi-empirical (TNO-type) and empirical (BPM) models, as discussed in Section 3. High-fidelity models predict lower spectral energy in the high-frequency range (beyond peak frequency), although a more noticeable energy bump at higher frequencies (above 1000 Hz) emerges. The latter is probably caused by the pressure-side TE noise contribution, since bluntness noise is not included in these models. This spectral bump is not clearly visible in the other modelling approaches, if it is indeed caused by the pressure-side TE noise contribution, even though it is a part of them. The trends for the different high-fidelity models are different for the low-frequency range. The empirical models consistently predict higher energy levels in the high-frequency range. The semi-empirical models lie somewhere in between for most of the spectral range, with some of them predicting lower energy for the pressure-side spectral bump at very high frequency.

The above comparisons, in particular for TE noise, indicate that there is a need to simplify the comparisons in order to trace back the origin of the observed discrepancies at the rotor level. It could be implemented by coming back to a simpler configuration with a rotating airfoil section of limited span [4], or even to a static 2D airfoil [20, 21] for which comparisons with wind tunnel data are possible.

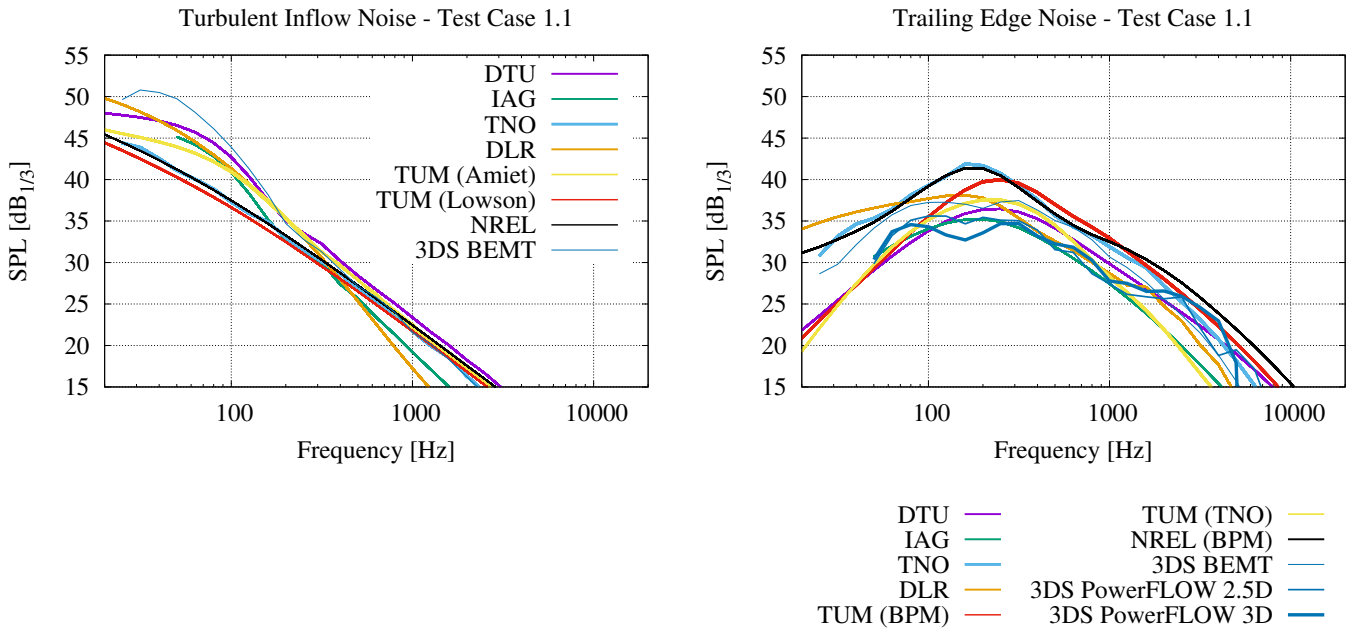

Fig. 7 TI noise (left) and TE noise (right) spectra at a location downstream of the rotor on the ground.

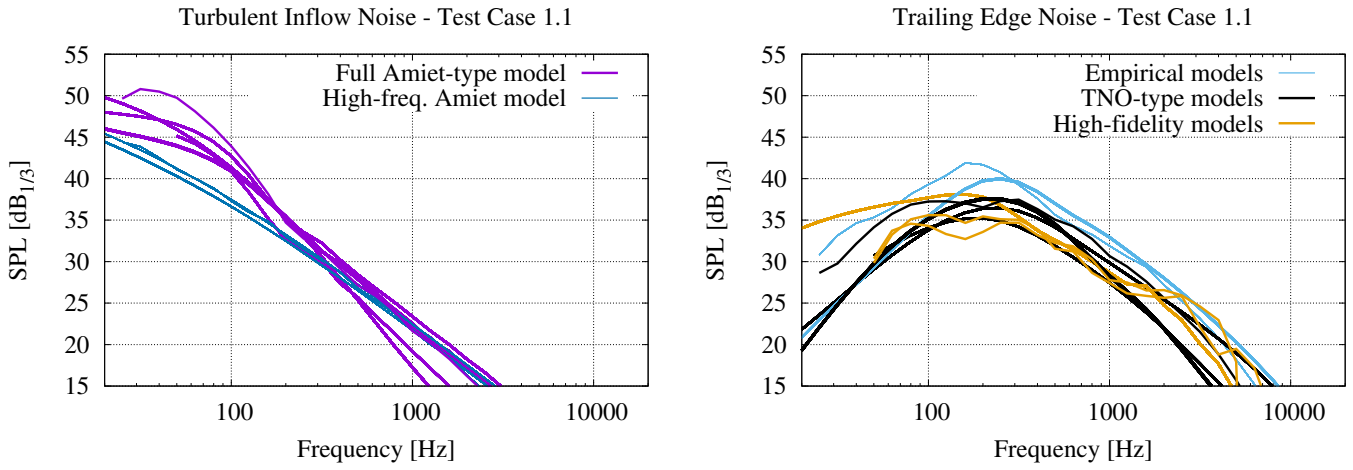

Fig. 8 TI noise (left) and TE noise (right) spectra at a location downstream of the rotor on the ground.

6.2. Wind turbine noise model directivity pattern

Test-case 1.1 is also used to investigate the directivity pattern around the wind turbine on the ground. As mentioned earlier, the noise spectra are predicted at various locations distributed around the turbine. These spectra are A-weighted and integrated across frequency and displayed in Fig. 9.

All models predict a reduction of noise in the plane of the rotor, although with various amplitudes relative to the upstream and downstream directions. This is an expected result given the more dipole-like behavior of TI noise, explaining the sharper deficit observed in the figure for this specific noise mechanism. The cardioid directivity pattern for TE noise, at airfoil level, similarly leads to a rotor plane noise deficit, which appears less pronounced.

Furthermore, the directivity pattern appears symmetric with respect to the rotor plane. Common sense would suggest that the perceived noise is higher downstream of the rotor, but it must be reminded that atmospheric effects are not included here.

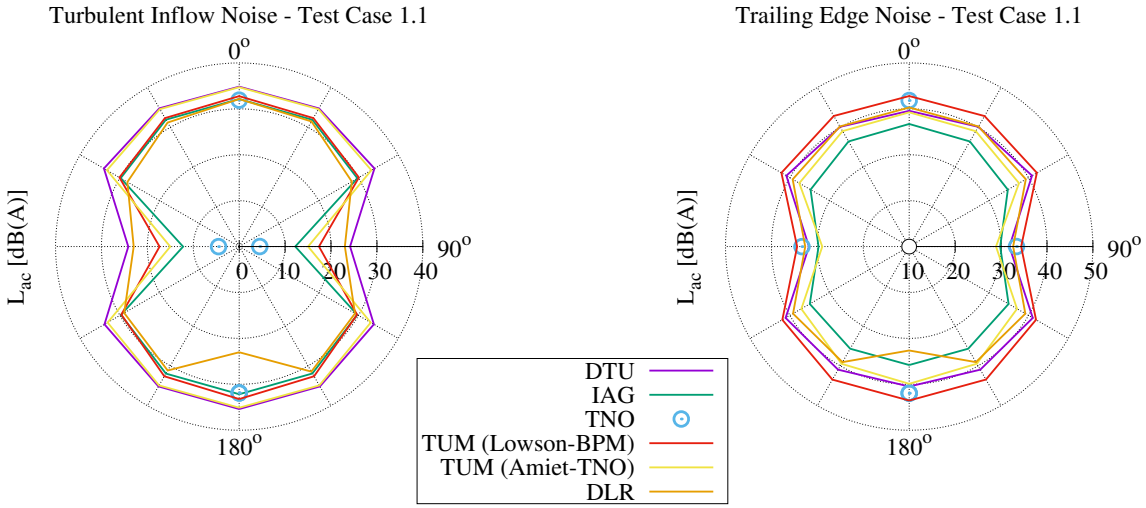

Fig. 9 A-weighted integrated spectra of TI noise (left) and TE noise (right) around the turbine on the ground.

6.3. Comparison with noise field measurements

The measurement of wind turbine noise for site assessment is often conducted according to the IEC 61400-11 standard [24]. The NM80 turbine that has been considered in the present work has been acoustically assessed using that standard. In the present section, the model results are compared to these field noise measurements.

The measured noise spectrum at a wind speed of 8 m/s is compared with six different models in Fig. 10. Note that the TI contribution for the DLR results is an extrapolation of lower wind speed data, and that it might slightly underestimate the actual noise level in the frequency range 100–400 Hz, but the results are unaffected above peak frequency at 500 Hz.

A higher energy spectral bump is observed in the measurements in the frequencies ranging from 100 to 300 Hz. It is attributed to mechanical noise, as a spectral tone at the center frequency of 137 Hz has been clearly identified during the same measurement campaign. This is compatible with the observed local energy peaks maxima located at the 1/3 octave band center frequencies: 125 Hz for the fundamental tone and 250 Hz and 500 Hz for the harmonics. Therefore, the models

that do not account for mechanical noise are underpredicting the measurement data in this frequency range. Elsewhere there is a good agreement between models and measurements, which stay nearly within the ±2 dB uncertainty margin of the measurements, except at very low and very high frequencies. As expected from the results observed in the previous section, the Lowson-TNO approach underpredicts the noise levels in the low-frequency range corresponding to the TI noise contribution, and overpredicts in the high-frequency range where TE noise dominates.

The acoustic power curves of the A-weighted integrated spectra as a function of wind speed are displayed in Fig. 11. The model results remain again within ±2 dB of the measured noise levels, except at the wind speed of 6 m/s. Unfortunately, the measured spectrum is not available at this wind speed. The reason for this discrepancy remains unknown. It was checked that the design rotational speed and blade pitch at this wind speed did match the design electrical power output in the HAWC2 model. Therefore, it can only be surmised that the turbine controller is more aggressive/optimal than the design parameters available for the present comparisons, and that rotational speed is increased at this particular wind speed in reality to maximize the power output.

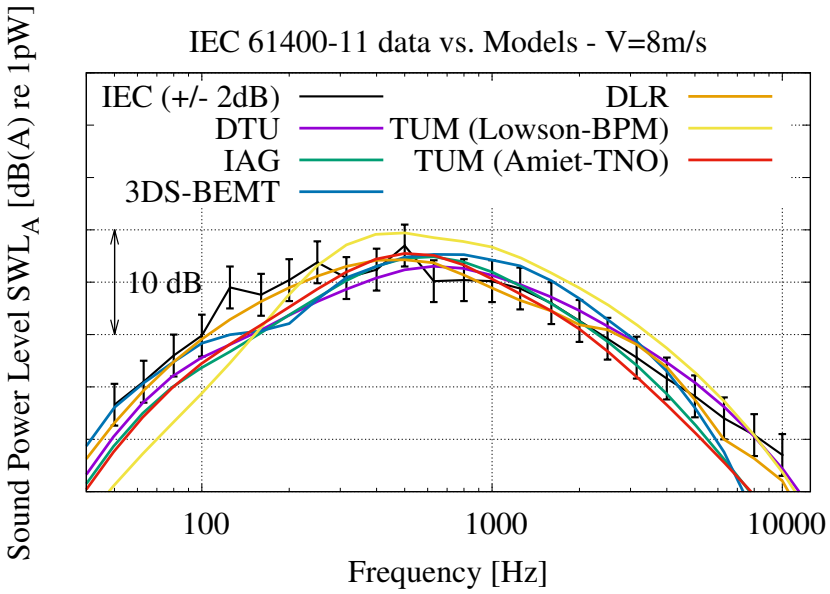

Fig. 10 A-weighted sound power spectrum of the measured noise using IEC 61400-11 standard measurement procedure versus model results for a wind speed of 8 m/s.

7. Conclusions

The comparisons presented in this paper highlight a number of discrepancies when evaluating wind turbine rotor noise with various methodologies based on airfoil TI and TE noise modelling.

It is observed that the use of a single identical model for TI noise (Amiet model) and its different implementations may yield significantly different noise predictions at the rotor level. Nevertheless, this model appears to be the main engineering approach for modelling this phenomenon, although higher-fidelity models exist.

Regarding the prediction of TE noise and the analysis conducted in the present work, a bottleneck is identified. It resides in connecting the aerodynamic quantities, in particular the turbulent

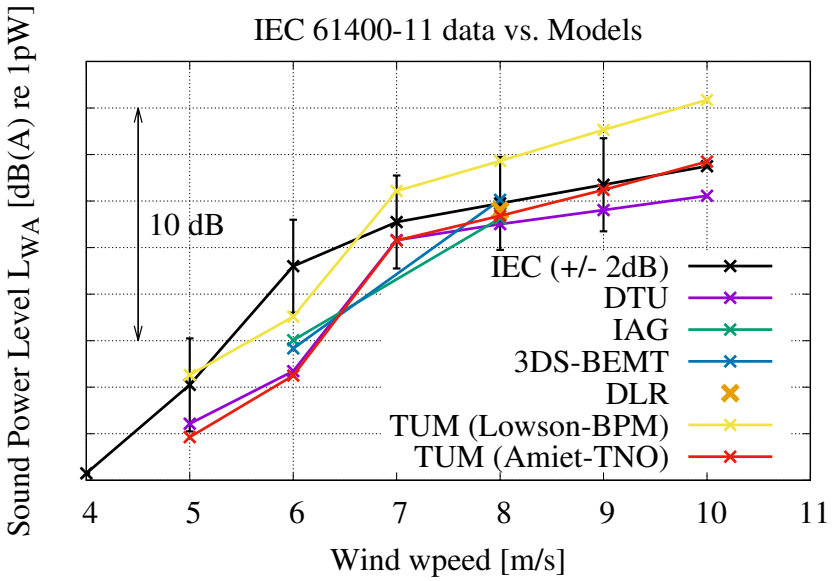

Fig. 11 Integrated A-weighted sound power as a function of wind speed using IEC 61300-11 standard measurement procedure versus model results.

boundary layer, to the rotor noise emission through the surface pressure. Indeed, the surface pressure models have not been thoroughly investigated, mainly because of a lack of available results. The use of simpler configurations is therefore suggested, e.g. limited spanwise section, or even 2D section in standstill, in order to identify the origin of these discrepancies.

A largely expected result from the present study is the presence of a noise level deficit in the rotor plane. This feature has been observed earlier in the field as well as in numerical predictions. The present contribution tends to confirm that there is a sharper deficit originating from TI noise, which would suggest that it is even more pronounced at lower frequencies.

Note that wind turbine designers in the industry, while mostly resorting to empirical models in the design loops for reducing turnover time, have access to a considerable amount of experimental data which can be used to tune and improve their modelling frameworks. The present study indicates that introducing semi-empirical models, which aim at accounting for more physical processes in the prediction tools, still suffer from relatively large discrepancies between each other when predicting rotor noise emissions. Therefore, it can be surmised that tuning or improving these models is still required. High-fidelity model results appear to somehow converge for TE noise within the high-frequency range, still with some discrepancies. Note, however, that only two high-fidelity approaches (for TE noise) were considered in the present work. Nevertheless, when comparing different models of varying fidelity with actual wind turbine noise measurements, it appears that all model results stay for the most part within the ± 2 dB uncertainty margin associated with the field measurement.

To conclude, real field conditions are difficult to reproduce within rotor noise models (e.g. blade leading edge erosion or fouling, atmospheric turbulence influencing the BL turbulence and subsequently TE noise, etc.). These are also difficult to identify (when comparing with measurements) and quantify. Therefore, many aspects remain to be considered for developing accurate prediction models for wind turbine rotor noise.

Acknowledgments

The present benchmark is conducted as a sub-task of the IEA Wind TCP research Task 39 (Quiet Wind Turbine Technology), as well as a part of IEA Wind TCP research Task 29 Phase IV (Analysis of Aerodynamic Measurements).

DTU participation was partly supported by the EUDP projects Jr.nr. 64016-0056 and Jr.nr. 134-21022 funded by the Danish Energy Agency (Energistyrelsen), as well as by countries participating to the Task for supporting the Operating Agent duties.

The DanAero projects were funded partly by the Danish Energy Authorities (EFP2007. Journal nr.: 33033-0074 and EUDP 2009-II. Journal nr.: 64009-0258), and partly by eigenfunding from the project partners Vestas, Siemens, LM, Dong Energy and DTU.

Financial support of the German Federal Ministry for Economic Affairs and Climate Action (BMWK) to the operation of Task 39 is also highly acknowledged.

The authors are thankful to Vestas Wind Systems A/S for providing the noise measurements of the NM80 turbine, as well as allowing their anonymized display in the present article.

This work was authored in part by the National Renewable Energy Laboratory, operated by Alliance for Sustainable Energy, LLC, for the U.S. Department of Energy (DOE) under Contract No. DE-AC36-08GO28308. Funding provided by the U.S. Department of Energy Office of Energy Efficiency and Renewable Energy Wind Energy Technologies Office. The views expressed in the article do not necessarily represent the views of the DOE or the U.S. Government. The U.S. Government retains and the publisher, by accepting the article for publication, acknowledges that the U.S. Government retains a nonexclusive, paid-up, irrevocable, worldwide license to publish or reproduce the published form of this work, or allow others to do so, for U.S. Government purposes.

References

[1] Amiet, R. K. (1975). Acoustic Radiation from an Airfoil in a Turbulent Stream. *J. Sound Vib.*, 41(4):407–420.

[2] Amiet, R. K. (1976). Noise due to Turbulent Flow Past a Trailing Edge. *J. Sound Vib.*, 47(3):387–393.

[3] Appel, C., Faßmann, B., and Lin, S. (2020). CAA-basierte Schallvorhersage für Windkraftanlagen. In *DAGA 2020 (Conference)*, Hannover, Germany. Deutsche Gesellschaft für Akustik e.V.

[4] Bertagnolio, F., Fischer, A., Seel, F., Lutz, T., Hornung, C., Boorsma, K., Schepers, G., Botero, M. R., Appel, C., Herr, M., Sucameli, C., Bortolotti, P., v. d. Velden, W., and Casalino, D. (2023). Task 29 T3.7 & Task 39 Wind Turbine Noise Code Benchmark - Preliminary Results. Retrieved from: https://usercontent.one/wp/iea-wind.org/wp-content/uploads/2021/05/report_WTNCBenchmark.pdf, Accessed: 2023-04-29, IEA Wind TCP.

[5] Blake, W. K. (1986). *Mechanics of Flow-Induced Sound and Vibration, Vol.I and II*, volume in Applied Mathematics and Mechanics. Frenkiel, F.N. and Temple, G. (eds.), Academic Press.

[6] Boorsma, K., Schepers, G., Aagard Madsen, H., Pirrung, G., Sørensen, N., Bangga, G., Imiela, M., Grinderslev, C., Meyer Forsting, A., Shen, W. Z., Croce, A., Cacciola, S., Schaffarczyk, A. P., Lobo, B., Blondel, F., Gilbert, P., Boisard, R., Höning, L., Greco, L., Testa, C., Branlard, E., Jonkman, J., and Vijayakumar, G. (2023). Progress in the validation of rotor aerodynamic codes using field data. *Wind Energy Science*, 8(2):211–230.

[7] Boorsma, K. and Schepers, J. (2011). Enhanced wind turbine noise prediction tool SILANT. In *Presented at the Fourth International Meeting on Wind Turbine Noise*, AIAA Paper 2010-645, Rome (Italy).

[8] Bortolotti, P., Branlard, E., Platt, A., Moriarty, P., Sucameli, C., and Bottasso, C. L. (2020). Aeroacoustics Noise Model of OpenFAST. Technical report, NREL, Boulder, USA. Available at: https://www.osti.gov/servlets/purl/1660130.

[9] Bortolotti, P., Guo, Y., Simley, E., Roadman, J., Hamilton, N., Moriartya, P. J., Sucameli, C. R., and Bertagnolio, F. (2021). Validation Efforts of an Open-Source Aeroacoustics Model for Wind Turbines: Preprint. Technical report, NREL, Boulder, USA. Available at: https://www.osti.gov/servlets/purl/1808274.

[10] Brooks, T. F., Pope, S. D., and Marcolini, M. A. (1989). Airfoil Self-Noise and Prediction. NASA Reference Publication 1218, Retrieved from: https://ntrs.nasa.gov/archive/nasa/casi.ntrs.nasa.gov/19890016302.pdf, NASA Langley Research Center, Hampton (VA). (Accessed: 2020-04-08).

[11] Casalino, D., Grande, E., Romani, G., Ragni, D., and Avallone, F. (2021). Definition of a benchmark for low reynolds number propeller aeroacoustics. *Aerospace Science and Technology*, 113.

[12] Casalino, D., Van der Velden, W., and Romani, G. (2022). A framework for multi-fidelity wind-turbine aeroacoustic simulations. In *28th AIAA/CEAS Aeroacoustics Conference, June 2022, Southampton, UK*.

[13] Drela, M. (1989). *XFOIL: An Analysis and Design System for Low Reynolds Number Airfoils. In: Mueller T.J. (eds) Low Reynolds Number Aerodynamics. Lecture Notes in Engineering, vol 54*. Springer, Berlin, Heidelberg.

[14] Drela, M. and Giles, M. B. (1987). Viscous-inviscid analysis of transonic and low reynolds number airfoils. *AIAA Journal*, 25(10):1347–1355.

[15] Ewert, R. (2018). RPM - the fast Random Particle-Mesh method to realize unsteady turbulent sound sources and velocity fields for CAA applications. In 13^{th} *AIAA/CEAS Aeroacoustics Conference*, Conf. Proceedings, Rome, Italy. AIAA 2007-3506.

[16] Faßmann, B., Reiche, N., Ewert, R., Herr, M., and Delfs, J. (2018). Evaluation of Wind Turbine Noise based on Numerical Simulation Methods. In 18^{th} *AIAA/CEAS Aeroacoustics Conf. (Proc.)*, Atlanta, Georgia. AIAA 2018-3924.

[17] Fischer, A., Bertagnolio, F., and Madsen, H. A. (2017). Improvement of TNO type trailing edge noise models. *European Journal of Mechanics B - Fluids*, 61:255–262.

[18] Glauert, H. (1935). *Airplane Propellers*, volume In: Aerodynamic Theory Volume IV (W. F. Durand, Ed.). Springer, Berlin, Heidelberg.

[19] Hamilton, N., Bortolotti, P. E., Jager, D., Guo, Y., Roadman, J. M., and Simley, E. (2021). Aeroacoustic Assessment of Wind Plant Controls. Technical report, NREL, Boulder, USA. Available at: https://www.osti.gov/servlets/purl/1785330.

[20] Herr, M., Ewert, R., Rautmann, C., Kamruzzaman, M., Bekiropoulos, D., Iob, A., Arina, R., Batten, P., Chakravarthy, S., and Bertagnolio, F. (2015). Broadband Trailing-Edge Noise Predictions - Overview of BANC-III Results. In 21^{th} *AIAA/CEAS Aeroacoustics Conf. (Proc.)*, AIAA Paper 2015-2847, Dallas (TX).

[21] Herr, M., Kamruzzaman, M., and Bahr, C. (2016). BANC-IV-1: TBL-Trailing-edge noise. In *Fourth Workshop on Benchmark Problems for Airframe Noise Computations (BANC-IV)*, 22^{nd} AIAA-CEAS Aeroacoustics Conference (Workshop), Lyon, France.

[22] Hornung, C., Lutz, T., and Krämer, E. (2019). A model to include turbulence-turbulence interaction in the prediction of trailing edge far field noise for high angles of attack or slightly separated flow. *Renewable Energy*, 136:945–954.

[23] Hornung, C., Scheit, C., Noffke, N., and Kamruzzamann, M. (2021). Turbulence Inflow Noise Prediction of Wind Turbine Rotors: The physically correct Representations of the Simplified Amiet and Lowson Model. In *WTN 2021*, Remote from Europe.

[24] IEC (2012). International Standard, Wind Turbines - Part 11: Acoustic Noise Measurement Techniques. IEC 61400-11, International Electrotechnical Commission, Geneva (CH). ISBN 978-2-83220-463-4.

[25] Kamruzzaman, M., Bekiropoulos, D., Lutz, T., Würz, W., and Krämer, E. (2015). A semi-empirical surface pressure spectrum model for airfoil trailing- edge noise prediction. *International Journal of Aeroacoustics*, 14(5-6):833–882.

[26] Klein, L., Gude, J., Wenz, F., Lutz, T., and Krämer, E. (2018). Advanced CFD-MBS coupling to Assess Low-Frequency Emissions from Wind Turbines. *Wind Energy Science*, 3:713–728.

[27] Larsen, T. J. and Hansen, A. M. (2007). How 2 HAWC2, The User's Manual. Tech. Rep. RISØ-R-1597(ver.3-1), Risø-DTU, Roskilde, Denmark. Available at `http://www.hawc2.dkdownload/hawc2-manual` (Accessed: 2021-03-11).

[28] Lindenburg, C. (2002). Bladmode, program for rotor blade mode analysis. Tech. Rep. ECN-C-02-050-r2, ECN, The Netherlands.

[29] Lowson, M. V. (1993). Assessment and prediction of wind turbine noise. ETSU W/13/00284/REP, UK.

[30] Lowson, M. V. and Ollerhead, J. B. (1969). A Theoretical Study of Helicopter Rotor Noise. *J. Sound Vib.*, 9(2):197–222.

[31] Madsen, H. A., Bak, C., Paulsen, U. S., Gaunaa, M., Fuglsang, P., Romblad, J., Olesen, N. A., Enevoldsen, P., Laursen, J., and Jensen, L. (2010). The DAN-AERO MW Experiments. In 48^{th} *AIAA Aerospace Sciences Meeting Including The New Horizons Forum and Aerospace Exposition (Proceedings)*, AIAA Paper 2010-645, Orlando (FL).

[32] Madsen, H. A., Larsen, T. J., Pirrung, G. R., Li, A., and Zahle, F. (2020). Implementation of the blade element momentum model on a polar grid and its aeroelastic load impact. *Wind Energy Science*, 5(1):1–27. doi:10.5194/wes-5-1-2020.

[33] Montgomerie, B., Brand, A., Bosschers, J., and van Rooij, R. (1997). Three-dimensional effects in stall. Tech. Rep. ECN-C-96-079, ECN, The Netherlands.

[34] Moriarty, P., Guidati, G., and Migliore, P. (2005). Prediction of Turbulent Inflow and Trailing-Edge Noise for Wind Turbines. In *Proc. of the* 11^{th} *AIAA/CEAS Aeroacoustics Conf.*, AIAA Paper 2005-2881, Monterey, CA.

[35] Oerlemans, S., Sijtsma, P., and López, B. M. (2007). Location and Quantification of Noise on a Wind Turbine. *J. Sound Vib.*, 299(5-6):869–883.

[36] Parchen, R. (1998). Progress report DRAW: A Prediction Scheme for Trailing-Edge Noise Based on Detailed Boundary-Layer Characteristics. TNO Rept. HAG-RPT-980023, TNO Institute of Applied Physics, The Netherlands.

[37] Paterson, R. W. and Amiet, R. K. (1976). Acoustic Radiation and Surface Pressure Characteristics of an Airfoil Due to Incident Turbulence. In 3^{rd} *AIAA Aero-Acoustics Conference*, Conf. Proceedings, Palo Alto, CA.

[38] Paterson, R. W. and Amiet, R. K. (1977). Noise and Surface Pressure Response of an Airfoil to Incident Turbulence. *Journal of Aircraft*, 14(8):729–736.

[39] Rautmann, C. (2017). Numerical Simulation Concept for Low-Noise Wind Turbine Rotors. DLR Forschungsbericht FB-2017-35, DLR (Institute for Aerodynamics and Flow Technology), Brauschweig, Germany. Dissertation.

[40] Schlinker, R. H. and Amiet, R. K. (1981). Helicopter rotor trailing edge noise.Technical Report 1. NASA Contractor Report 3470, Retrieved from: https://ntrs.nasa.gov/archive/nasa/casi.ntrs.nasa.gov/19820003986.pdf, NASA Langley Research Center. (Accessed: 2020-04-08).

[41] Sucameli, C. R., Bortolotti, P., Croce, A., and Bottasso, C. L. (2018). Comparison of some wind turbine noise emission models coupled to BEM aerodynamics. *Journal of Physics: Conference Series*, 1037:022038.

[42] van der Velden, W. C., Casalino, D., and Romani, G. (2023). Full-Scale Serrated Wind Turbine Trailing Edge Noise Certification Analysis Based on the Lattice-Boltzmann Method. In *AIAA SCITECH 2023 Forum (Proceedings)*, AIAA 2023-0970, National Harbor (MD).

7 WP2 / Annex 3 - Conference proceedings on comparisons of serration noise measurements in various facilities

Benchmarking of the NACA 63_3-018 Trailing-Edge Noise in a Broad Reynolds Number Range as Part of the IEA Task 39

Guillem Vergés i Plaza*
Technical University of Denmark, Frederiksborgvej 399, 4000, Roskilde, Denmark
Flow Physics and Technology Department, Delft University of Technology, 2629 HS Delft, The Netherlands

Andreas Fischer†, Oliver Lylloff‡, Christian Bak§, Anders S. Olsen¶, Franck Bertagnolio‖
Technical University of Denmark, Frederiksborgvej 399, 4000, Roskilde, Denmark

Salil Luesutthiviboon**, Tercio Lima Pereira††, Daniele Ragni‡‡, Francesco Avallone§§
Flow Physics and Technology Department, Delft University of Technology, 2629 HS Delft, The Netherlands

Alexandre Suryadi¶¶, Michaela Herr***
German Aerospace Center (DLR), Lilienthalplatz 7, 38108 Braunschweig, Germany

An experimental aero-acoustic characterisation of the NACA 63_3-018 airfoil is presented in this study, featuring trailing-edge noise emissions with and without serrations. Measurements have been carried out for a chord-based Reynolds number range between 0.18×10^6 and 4.8×10^6. Two airfoil models with different chord lengths have been tested in five different wind tunnels. The goal is to compare the measurements in different facilities, quantify the uncertainties, and establish a validation database that can serve as a benchmark for computational studies. The tests have been performed with clean and forced-transition boundary layers for a variety of angles of attack. The effect on the spectral slope and peak levels is evaluated. Scaling laws have been applied to compare different test conditions. The quality and nature of the collapse, as well as the applicability limits of the scaling, are examined. Different serration geometries have been tested at different flap angles. The noise reduction dependence on the aerodynamic loading is discussed. This work is based on an initiative of Task 39 "Quiet Wind Turbine Technology" of the Technology Collaboration Programme (TCP) of the International Energy Agency (IEA).

Nomenclature

α_{eff}	=	effective angle of attack (deg)
α_{geo}	=	geometrical angle of attack (deg)
b	=	span width (m)
c	=	chord length (m)
C_d	=	drag coefficient (-)
C_l	=	lift coefficient (-)
C_p	=	pressure coefficient (-)
δ^*	=	displacement thickness, subscript may indicate pressure side ($_{PS}$) or suction side ($_{SS}$) (m)

*MSc Student, European Wind Energy Master - Rotor Design - Aerodynamics, E-mail: guillem.verges@gmail.com
†Senior Researcher, Department of Wind and Energy Systems, E–mail: asfi@dtu.dk
‡Postdoc, Department of Wind and Energy Systems, E–mail: ollyl@dtu.dk
§Professor, Department of Wind and Energy Systems, E–mail: chba@dtu.dk
¶Senior Development Engineer, Department of Wind and Energy Systems, E–mail: sols@dtu.dk
‖Senior Researcher, Department of Wind and Energy Systems, E–mail: frba@dtu.dk
**PhD Candidate, Section Aircraft Noise Climate Effect, E–mail: s.luesutthiviboon@tudelft.nl
††PhD Candidate, Section Wind Energy, E–mail: l.t.limapereira@tudelft.nl
‡‡Associate Professor, Section Wind Energy, E–mail: d.ragni@tudelft.nl
§§Assistant Professor, Section Wind Energy, E–mail: f.avallone@tudelft.nl
¶¶Research Engineer, Dept. of Wind Energy, Institute of Aerodynamics and Flow Technology, E-mail: alexandre.suryadi@dlr.de,
***Head of Wind Energy Department, Institute of Aerodynamics and Flow Technology, E-mail: michaela.herr@dlr.de

f	=	frequency (Hz)
t_{TE}	=	trailing-edge thickness (m)
M_U	=	wind tunnel free-stream velocity based Mach number (-)
$OSPL_{1/n}$	=	overall sound pressure level calculated from 1/n octave band spectrum (dB)
PSD	=	far-field noise power spectral density (dB/Hz)
r	=	distance between the observer and the sound source (m)
Re_c	=	chord-based Reynolds number (-)
$SPL_{1/n}$	=	1/n octave band sound pressure level (dB)
$SPL_{1/n,scaled}$	=	scaled 1/n octave band sound pressure level (dB)
$\Delta SPL_{1/n}$	=	noise reduction based on 1/n octave band sound pressure level (dB)
St_ℓ	=	Strouhal number based on characteristic length ℓ (-)
U	=	wind tunnel free-stream velocity (m/s)
X, Y, Z	=	chordwise, vertical, and spanwise coordinates from the TE (Fig. 1) (m)

I. Introduction

Trailing-edge (TE) noise arises from the interaction of the turbulent boundary layer, and the pressure fluctuations that it generates in the surface, with the trailing edge [1, 2]. It has been identified as a primary noise source for wind turbines [3]. It is thus of industrial interest to predict and mitigate its impact, an example of this is the Task 39 of the International Energy Agency Wind Technology Collaboration Programme (IEA Wind TCP Task 39). Its goal is to accelerate the development and deployment of quiet wind turbine technology by providing supporting research database as the foundation for establishing international standards and governmental regulations. The task addresses the engineering questions of wind turbine noise generation, reduction, and propagation, and the socio-psychological questions of the wind turbine noise impact to health, well-being and consent and other non-noise factors. An interdisciplinary work group is also established to disseminate the interaction between engineering and socio-psychological sciences.

The goal of this collaborative paper is to create a high quality and comparable database of trailing-edge noise from both straight and serrated TEs. A very related effort in the same direction is the Benchmark problems for Airframe Noise Computations (BANC) workshop (category I, TE noise), a series of workshops which aim to cross-check available measurement data with different computation methods [4–6]. The experimental data-sets available so far were composed of a symmetric NACA 0012, a cambered DU96–W180, and a NACA 64-618 airfoils without serrations in a Re_c range from 1×10^6 to 1.5×10^6. This Reynolds range, however, is lower than the one that modern wind turbines work at. It is also desirable to characterise the error bars and understand the uncertainty in the measurements carried out with different models and in different facilities. Additionally, serrations have become largely used to reduce the trailing-edge noise of wind turbines [7], and experimental data is required to validate new noise models (e.g. [8]). Therefore, it is of high interest to include serrations into the data-base.

These gaps were partially tackled in the study of Ferret Gasch et al. [9] where two Siemens-Gamesa cambered airfoils were tested to a maximum Re_c of 3.7×10^6. These results were used to blindly test the accuracy of different noise prediction codes. The recommendations of such study insisted again in the need of carrying out uncertainty quantification of the measurements and improve the validation database specially at moderate to high Reynolds numbers.

The leading aero-acoustic facilities in Europe have carried out cross-facility aero-acoustic tests of a NACA 63_3-018 airfoil as the first collaborative step to establish the database as well as to quantify the uncertainty. This airfoil has been selected because its symmetry helps to accurately determine the zero angle of attack, but when placed at different α the resulting pressure distributions are similar to those commonly found in wind turbines (e.g. [10]). In order to cover the largest Re_c possible, two models have been built: a large one (subsequently called *HRM*: High Reynolds number Model), with 0.9 m chord, and a small one (*LRM*: Low Reynolds number Model) with a chord of 0.2 m. The HRM has been tested in the Poul La Cour Tunnel (PLCT) at the Denmark Technical University (DTU), and the LRM has been studied in both the A-Tunnel at TU Delft, and the Acoustic Wind Tunnel Braunschweig (AWB) in the German Aerospace Center (DLR). The aerodynamics of the HRM have also been measured in the low-speed Wind-Tunnel Braunschweig (NWB) of the German-Dutch Wind Tunnels Foundation (DNW) and in the Low-Turbulence Tunnel (LTT) of TU Delft.

This paper presents preliminary comparisons of test results from the aforementioned facilities. This paper is structured as follows. A description of the model and serration geometries is given in Section II, followed by a summary of the facilities set-up in Section III. The aerodynamic results are then analysed in Section IV, succeeded by the study of the acoustic results with straight trailing edge in Section V. Finally, the effect of the serrations is discussed in Section VI.

II. Model Description

Two NACA 63_3-018 airfoils (Fig. 1) were built for this study, namely the Low Reynolds number Model (LRM) and the High Reynolds number Model (HRM). They have a chord length of 0.2 m and 0.9 m respectively. The base span width is 0.4 m for the LRM and 1.816 m for the HRM, and modular extensions were also built to adapt the models to the specific heights of the wind tunnel test sections. The LRM span width was 0.4 m when tested in the A-Tunnel, and 0.8 m in the AWB. For the HRM, these values were 1.25 m in the LTT, 2 m in the PLCT (DTU), and 2.8 m in the NWB. The HRM was made of sheet metal skins over rib and stringer structures. The LRM was manufactured as an assembly of three solid modular aluminium structures. More details about the models may be found in [11, 12]. The trailing edge thickness is $t_{TE} = 7.5c \times 10^{-4}$ for both models.

The HRM is equipped with 192 surface pressure tabs. They are organised in 7 rows in order to characterise the flow three-dimensionality. The main row, in the middle of the model, has higher density with 96 tabs. They have an offset in the spanwise direction to minimise interferences. In the LTT, since the base span of the model could not fit completely in the test section, this mid row was not fully centered. It was located around $1c$ (0.9 m) from the bottom wall instead. The LRM has 28 pressure tabs in the middle of the span with an spanwise angle of 15 deg.

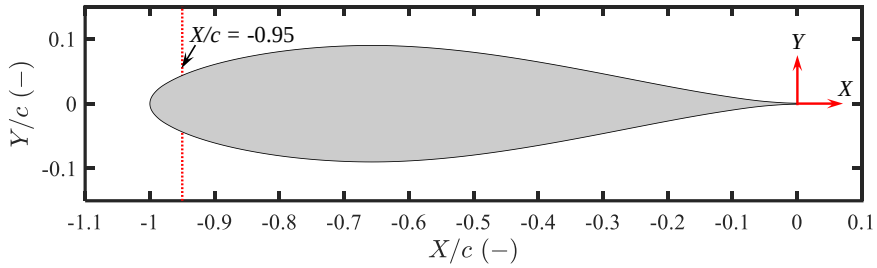

Fig. 1 NACA 63_3-018 airfoil with tripping location and axis orientations.

The measurements have been carried out with both clean and tripped boundary layer. The forced transitions helps with the comparability of the results, and supports the reproducibility of the measurements. For the tripped boundary layer case, zig-zag strips have been employed at $X = -0.95c$ on both sides of the airfoil. For the LRM a thickness of 0.5 mm, a width of 6 mm, and an angle of 70 deg. have been used. For the HRM these values are 0.4 mm, 12 mm, and 60 deg. respectively. The HRM tripping was applied with a base tape of 0.06 mm thickness (Fig. 7).

Different trailing-edge serrations have been tested. Two geometries have been selected: sawtooth and iron serrations, illustrated in Fig. 2. The geometries are taken from a numerical investigation of Avallone et al. [13], which compared the iron serrations to the conventional sawtooth ones, and found increased noise reduction in the former. This was attributed to decreased scatter in the serration roots. The serrations' wavelength is $0.05c$, and the peak amplitude is $0.1c$. Both types have been installed parallel to the chord ($\varphi = 0$ deg), and the sawtooth serrations have also been tested at $\varphi = 8$ deg for the LRM and $\varphi = 4$ deg for the HRM. Details about the installation procedure may be found in the work of Luesutthiviboon et al. [11]. There is significant uncertainty in the flap angle of the serrations. This has been measured in the serrations tested by DTU, where important deviations from the nominal values were detected. The iron and sawtooth serrations which should have been placed at $\varphi = 0$ deg were measured to be at 4.16 deg and 4.43 deg respectively. Moreover, spanwise differences up to 3.8 deg were also found. For the flapped case at nominal $\varphi = 4$ deg. the real value (spanwise averaged) was 9.39 deg.

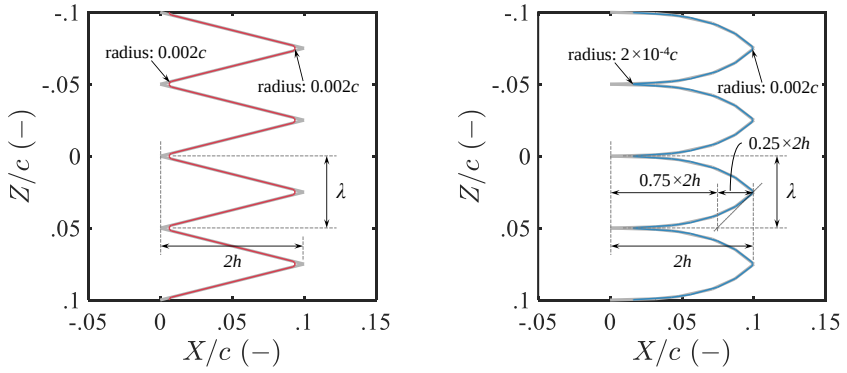

(a) Sawtooth serrations **(b) Iron serrations**

Fig. 2 Drawings of the trailing-edge serrations used on the airfoil. In gray, the geometry used in the study of Avallone et al. [13].

III. Facilities Description

A. The PLCT at DTU

The Poul La Cour Wind Tunnel is a closed loop return wind tunnel (Fig. 3). The airline is 66 m long and 27 m wide (furthest separated points of the airline tube, but neglecting the wind tunnel buildings). The air volume inside the airline is about 3875 m^3. The whole airline is built in concrete because of acoustic considerations. The fan of the wind tunnel is driven by a 2.4 MW engine and has a diameter of 4.7 m. The fan was limited to 400 RPM or an engine power output of 1.8 MW, because the tunnel loss estimate proved to be too conservative. The fan can generate an air flow of up to 630 m^3/s at 400 RPM when a test object is placed in the tunnel.

The settling chamber has a cross section of 6 x 9 m and is equipped with a honeycomb and 3 mesh grids to rectify the flow and reduce turbulence before entering the test section. The mesh grid goes from a coarse to a fine mesh size. The grid size of the finest mesh is 0.2 mm. The flow is accelerated through a nozzle with a contraction ratio of 9:1 before entering the test section. The test section has a cross section of 2×3 m and is 9 m long. The top speed is 105 m/s and the turbulence intensity is below 0.1 %.

Measurements can be carried in a traditional hard-wall configuration [14] to focus on the aerodynamics, or in the acoustic configuration that is based on the new Kevlar wall technology [15]. The noise is measured by a phased array with 84 microphones of the type B&K type 4985 1/4". It is placed in the anechoic chamber with a distance of 1.2 m from the Kevlar wall, and it is centered above the trailing edge of the aerofoil and its mid-span. The microphone data was acquired with a B&K LAN-XI type 3053 system at a sample rate of 16384 Hz. The measurements have been post-processed using the deconvolution algorithm *CLEAN based on spatial coherence*, CLEAN-SC [16]. More information about the set-up and the post-processing may be found in O. Lylloff's PhD [17].

B. The A-Tunnel at TU Delft

At Delft University of Technology, the small NACA 63_3-018 was tested in the A-Tunnel, an open-jet anechoic vertical wind tunnel. Full description of the facilities and results to be further discussed in this paper have been presented in a publication of Luesutthiviboon et al. [11]. In the A-tunnel, a semi-open test section is placed in a room treated by acoustically absorbent foam wedges. Acoustic characterization of the A-Tunnel anechoic chamber including further extensive details can be found in a publication of Merino-Martinez et al. [18]. To achieve different free-stream velocity ranges, the test section can be placed on different outlet nozzles having different contraction ratios. Two different nozzles have been used for the measurements, one with a cross-section of 400×700 mm ($2c \times 3.5c$), which will be referred as *Large* or *TUD-A-L*, and one with a cross-section of 400×250 mm ($2c \times 1.25c$), which will be called *Small* or *TUD-A-S*. The Small nozzle allowed for a higher Re_c range, but its relatively smaller jet width limited the measurements to $\alpha = 0$ deg. A photograph of the TUD-A-L case in the A-Tunnel is shown in Fig. 4a. The full measurement envelope is presented in Fig. 13.

This paper presents both aerodynamic and acoustic data from the A-Tunnel. Static pressure distributions were

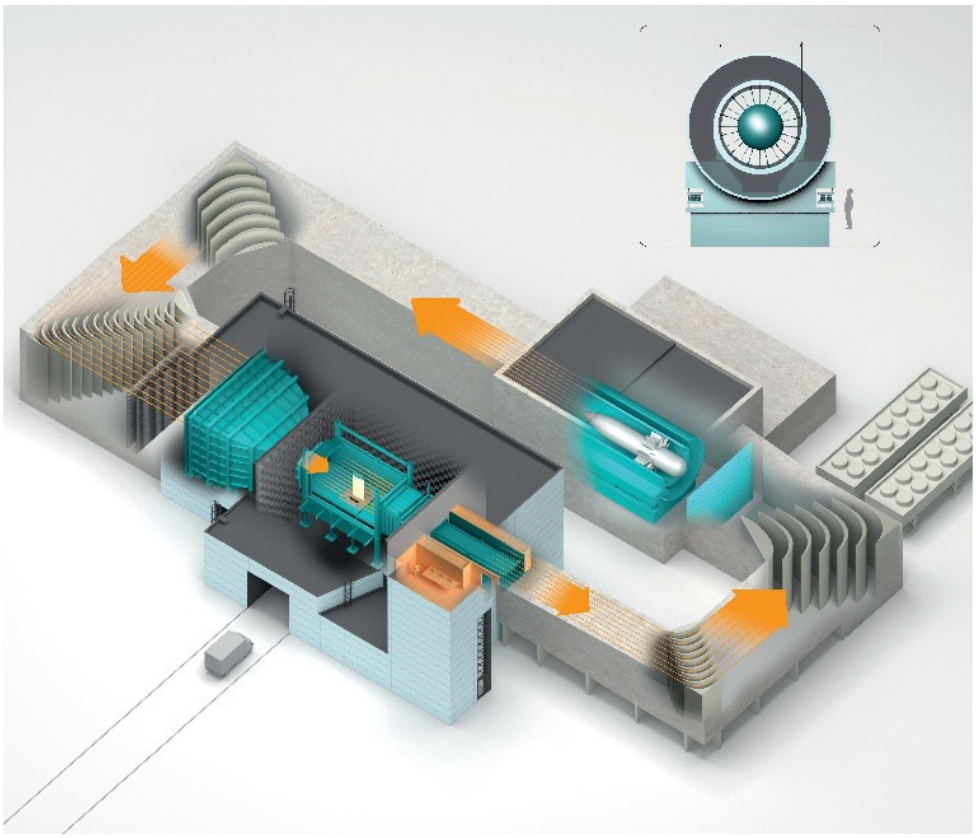

Fig. 3 The Poul La Cour Wind Tunnel.

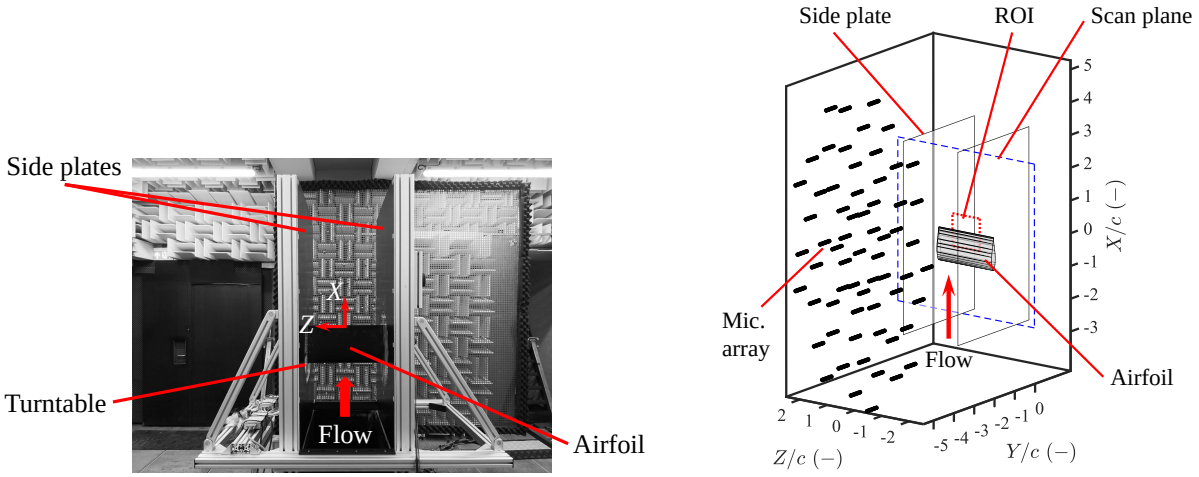

(a) **(b)**

Fig. 4 (a) The small NACA 63_3-018 airfoil in the A-Tunnel and (b) Schematic of the microphone array in the A-tunnel.

collected via Honeywell TruStability HSCDRRN025MDAA3 differential pressure transducers with a ±2.5 kPa range and ±6 Pa accuracy. Subsequently, the lift coefficients are calculated by a method described in Section IV.A.

The Hot-Wire Anemometry (HWA) Technique was employed to extract the boundary-layer velocity profiles at $X/c = -0.02$, i.e. close to the TE. Specifications of the HWA system can be found in the publication of Luesutthiviboon et al. [11].

The acoustic data was recorded using an array of 64 microphones and post-processed using conventional frequency-domain beamforming (CBF) [19]. The acoustic maps were then integrated using the Source Power Integration (SPI) technique. A schematic of the microphone array and the Region Of Integration (ROI) is shown in Fig. 4b. For more details about post-processing technique, the paper from Merino-Martinez [18] may be consulted.

C. The LTT at TU Delft

The large NACA 63_3-018 model was tested in the Low-Turbulence Tunnel (LTT) at TU Delft. The aforementioned publication of Luesutthiviboon et al. [11] also contains full details of the LTT facility, including aero-acoustic results.

The LTT is a closed-circuit wind tunnel originally designed for aerodynamic tests. The LTT has a contraction ratio of 17.8 and a turbulence intensity range between 0.015% and 0.07% for free-stream flow speeds between 20 and 70 m/s. The airfoil was installed in a specially-made test section, in which the wall panels are 'acoustically treated' by Kevlar-covered Melamine wedges.

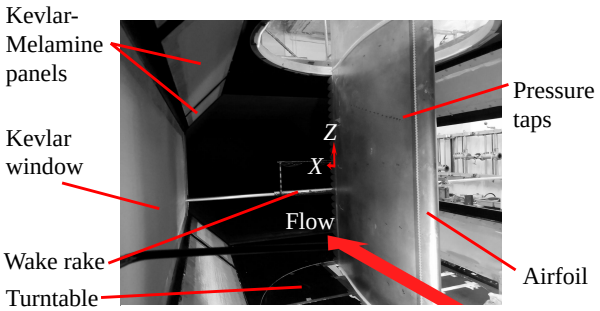

Fig. 5 The large NACA 63_3-018 airfoil in the LTT.

This paper only presents aerodynamic test results from the LTT, namely, the lift curves, and the boundary layer profiles. To read the static surface pressure data, the 101 pressure taps on the model were connected to a DTC pressure system with 6 ESP–HD scanners. The aerodynamic corrections for the LTT hard-wall test section can be found in the works of Timmer and Garner et al. [20, 21]. It has been confirmed by Luesutthiviboon et al. [11] that the pressure distribution and lift obtained in the acoustically test section do not deviate from that obtained in the hard-wall configuration. A brief comparison of both set-ups is also presented in this study.

Velocity fields at the TE region of the model were extracted by the Particle Image Velocimetry (PIV) technique. Specifications of the PIV setup can be found in the work of Luesutthiviboon et al. [11]. The edge of the boundary layer was defined where the spanwise vorticity is constant. Subsequently, the boundary layer integral parameters were extracted.

D. The AWB at DLR

The Acoustic Wind Tunnel Braunschweig (AWB) is an anechoic open-jet, closed-circuit wind tunnel operated by the German Aerospace Center (DLR - *Deutsches Zentrum für Luft- und Raumfahrt*), Braunschweig. The test section is treated with acoustic linings to reduce sound reflection in the test section. The nozzle cross-section is 0.8 m in width and 1.2 m in height, and the maximum wind speed at the nozzle is 65 m/s with a turbulence intensity of 0.3% [22]. The wind tunnel model is installed along the width of the nozzle via two side extensions of the nozzle (see Fig. 6). Two far field sound measurement systems were used extensively in the measurement campaign.

The directional microphone with a 1.4 m outer diameter elliptic reflector is placed along a motorized traversing system below and facing the model's pressure side. At the near-focal point of the elliptical reflector is a Brüel&Kjær 4136 1/4" microphone, which records the reflected noise. The distance between the microphone to the sound source (geometrically represented by the model's trailing edge) is approximately 1.15 m. Because the directional mirror's insensitivity to the distance to the sound source, its height with respect to the wind tunnel center line was not adjusted [23]. Assuming line sources, the noise was measured along a straight line cutting through the mid-span of the model.

Prior to the actual measurement, a scan along the streamwise axis was performed with the directional microphone to identify the leading-edge and trailing-edge noise distribution. Furthermore, because sound is convected with the free-stream and refracted by the wind tunnel's shear layer, the measured distribution is further downstream than the position of the model. The shifted position is predominantly dependent on the freestream velocity. The result of the scan shows that each noise source has a distinct distribution, so trailing-edge noise measurement can be done within a narrow range around the shifted position of the trailing edge. From this narrow range, a maximum level was selected to represent the far field sound pressure level. The range of the baseline measurement was from -30 mm to 30 mm with 5 mm increments from the shifted trailing edge. Whereas, for the serrated trailing edge measurement from -30 mm to 60 mm with the same increments from the shifted baseline trailing edge. Noise was measured for 20 s at a rate of 65 kHz, and a high-pass filter with a cut-off frequency of 500 Hz was applied in the data acquisition. The measured time series was converted in the frequency domain using the method of averaged periodogram with 50% overlap and Hanning window. The narrowband spectral resolution was 16 Hz. The background noise, the direction microphone system response function (assuming line source distributions) were corrected according to the method of Schlinker [24]. More details on the procedure can be found in Herr [25].

The microphone array consists of 96 *LinearX* 1/2" microphones arranged within a 1 m diameter circle. It was installed above the wind tunnel model facing the suction side. Noise was measured for 30 s at a sampling rate of 100 kHz. A high-pass filter with a cut-off frequency of 500 Hz was also applied in the data acquisition of the microphone array. The measurements were processed using CLEAN-SC [16] with removal of the diagonal component of the cross-spectral power matrix and Amiet's 2D shear layer correction. The spectra were calculated using the method of averaged periodogram with 0% overlap and rectangular windows. The narrowband spectral resolution was 24.4 Hz and the level is adjusted to a reference observer at a distance of 1 m from the sound source. In order to separate the trailing-edge noise from other noise sources, the post-processing was done for a localised area around the trailing edge with a span width of 0.4 m and a chord length of 0.16 m, and the sound pressure level is considered only for sound sources identified within this area.

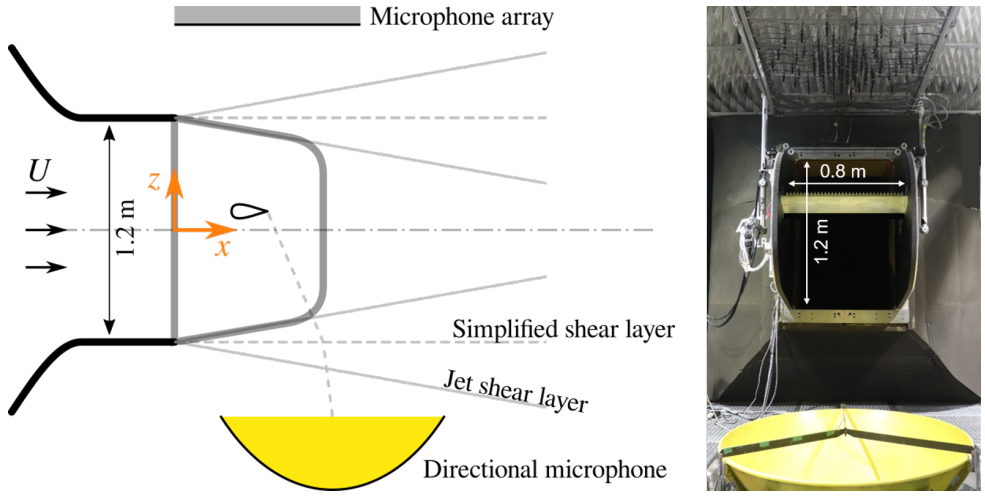

Fig. 6 AWB test set-up.

E. The NWB at Braunschweig

Aerodynamic measurements were performed in the closed test section of the Low-Speed Wind-Tunnel Braunschweig (NWB - *Niedergeschwindigkeitswindkanal Braunschweig*) of the German-Dutch Wind-Tunnels Foundation (DNW - *Deutsch-Niederländische Windkanäle*), see Fig. 7. The NWB is a closed-circuit low-speed wind tunnel that can be operated in a closed or open anechoic test section environment [26]. Its closed test section provides a cross-sectional area of 3.25 m × 2.8 m and a length of 8 m. Dedicated model extensions were built to extend the original HRM span to 2.8 m. Aerodynamic coefficients were derived from integration of the pressure distribution at midspan, cf. Section II. An additional wake rake with 135 total pressure probes (of 2.5 mm distance) and 7 static pressure probes was used on a high-resolution traversing system for drag measurements. Lift and drag polars were corrected for wall interference

according to the standard procedure by Garner et al. [21], thereby neglecting compressibility effects. Arrays of 10 G.R.A.S. 48LA 1/4" surface microphones in different layouts were also applied on the HRM in the closed test section. Necessary data corrections to account for the signal averaging over the sensing area of the microphones are currently being developed and validated pior to data release. Accordingly, the current paper is limited to the presentation of first aerodynamic test data. The results from a follow-up acoustic campaign in the NWB acoustic plenum (i.e. open-jet anechoic test environment) are not yet fully post-processed and will be subject of future work in this ongoing cooperation.

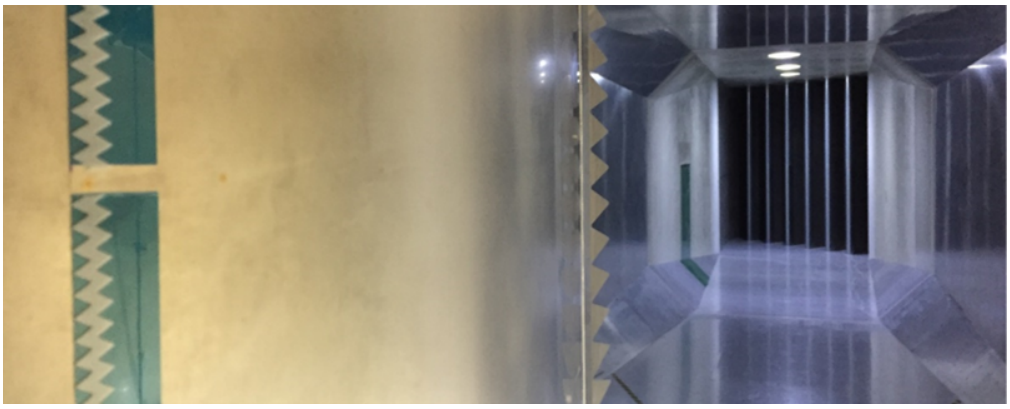

Fig. 7 NWB test set-up with tripping detail.

F. Facility summary

Table 1 provides an overview of the main characteristics of the wind tunnels used for this study. Note that the LTT and the NWB also have an aero-acoustic configuration (Kevlar panels and open-jet respectively), but aero-acoustic results from these facilities have not been used in this work.

Facility	**DTU**	**A-Tunnel** *Small/Large*	**LTT**	**AWB**	**NWB** *Closed*
Max. flow speed [m/s]	105	Small: 75 Large: 35	120	65	90
Test section [m]	3×2	S: 0.25×0.4 L: 0.7×0.4	1.8×1.25	1.2×0.8	3.25×2.8
Max. TI [%]	0.1	0.15	0.07	0.3	Long.: 0.06 Transv.: 0.15
Re_c measured ($\times 10^6$) [-]	1 - 4	S: 0.38 - 1 L: 0.18 - 0.46	1 - 3	0.38 - 0.77	1.9 - 4.8
Acoustic set-up	Kevlar walls	Open-jet	-	Open-jet	-
Aerodynamic set-up	Kevlar/Hard walls	Hard walls	Kevlar/Hard walls	Open-jet	Hard walls
Acoustic data	Mic. array, (CBF, Clean-SC)	Mic. array, (CBF)	-	Mic. array (Clean-SC) + Elliptic mirror	-
Boundary layer profiles	HWA	HWA	PIV	-	-
Airfoil model tested (span $\times$ chord [m])	HRM (2×0.9)	LRM (0.4×0.2)	HRM (1.25×0.9)	LRM (0.8×0.2)	HRM (2.8×0.9)
Model aspect ratio	2.22	2.00	1.39	4.00	3.11
Plot label	DTU	TUD-A-S TUD-A-L	TUD-LTT	AWB-MA AWB-EM	NWB
Plot colour	Green	Yellow Blue	Purple	Dark red Light red	Black

Table 1 Summary of the main characteristics and data retrieved from each facility.

IV. Aerodynamic Comparison

A brief aerodynamic comparison is given in this section. The lift and drag coefficients are presented in Subsection IV.A, where a comparison between tests with hard and Kevlar walls is also shown. The serrations effect on the lift curves is studied in Subsection IV.B, and finally the displacement thickness near the trailing edge is shown in Subsection IV.C.

A. Polar Curves

The lift coefficient measurements are presented in Fig. 8 for every facility, for both the clean and the tripped conditions. The C_l is obtained from the surface integral of the pressure coefficients C_p, measured by means of the surface pressure tabs described in Section II. Different wind tunnel corrections have been applied for each facility. For the A-Tunnel and the AWB measurements, which use open jet configuration, the effective angle of attack had to be corrected for distortions of the jet by the airfoil loading. A constant relation $\alpha_{eff} = K\alpha_{geo}$ was assumed, and the correction factor K was found by comparing the measured pressure distributions to XFOIL predictions [27]. The K values calculated from XFOIL were similar than the ones obtained from Brooks et al. analytical formula [28]. For the NWB, the LTT, and the DTU measurements with hard walls, the standard wind tunnel corrections according to Garner et al. have been applied [21]. DTU's Paul La Cour Tunnel measurements taken with Kevlar walls have been corrected using the methodology explained in Devenport et al. [15, 29], which is based on potential flow methods that take into account the wall presence including the flow transpiration through the Kevlar membranes. Details of this correction and a validation with Virginia Techical Unveristy can be found in the study of Fischer et al. [12]. The different nature of these corrections is represented in the polar plots, since using XFOIL for the corrections leads to the results matching a pre-defined set of polars. The measures corrected with XFOIL are shown with empty markers, whereas the other

methods are plotted with filled markers.

In the LTT and the DTU campaigns, the aerodynamic coefficient have been measured with both hard walls and Kevlar walls. A comparison of such measurements is given in Fig. 10. In the rest of figures, the measurements taken with Kevlar walls have been used.

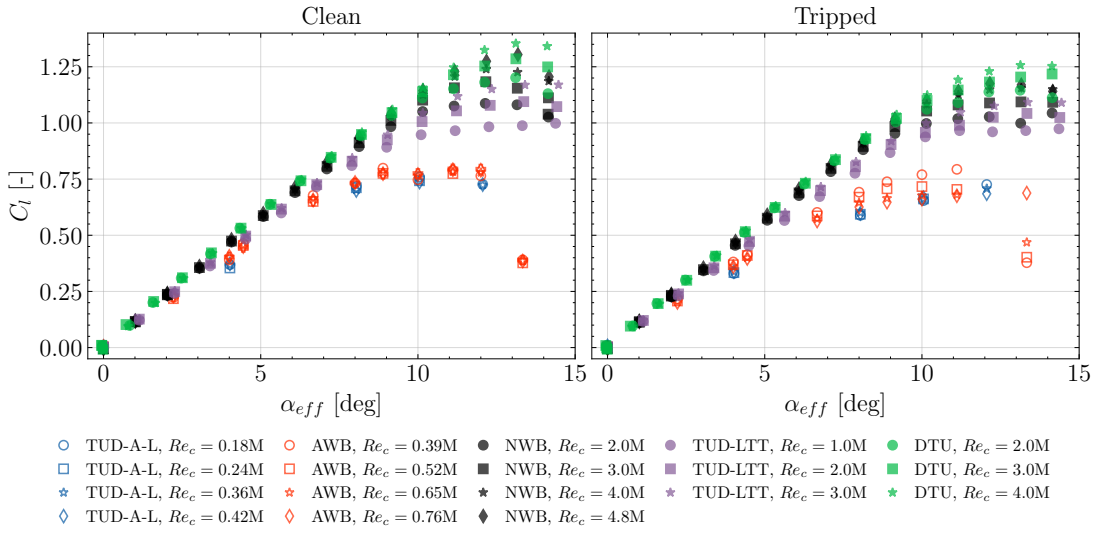

Fig. 8 Lift coefficient measured in the different facilities for a variety of Re_c numbers. Empty markers represent the measures corrected using XFOIL, and full markers indicate other correction methods.

The Reynolds number effect is clearly visible in Fig. 8. The measurements at the A-Tunnel and the AWB, at significantly lower Re_c than the other ones, show a reduced $C_{l,max}$ and an earlier onset of separation. There is a good agreement between both facilities with a slight difference in the slope in the linear region, which could be caused by the different aspect ratio in the tests (2 in the A-Tunnel, 4 in the AWB). A higher aspect ratio can lead to a increase in the lift coefficient slope [30]. The trend with Re_c in the stall region observed for the AWB measurements with tripped conditions appear to be the opposite as expected. The free transition point, as calculated with XFOIL, coincides with the position of the tripping device on the suction side. This possible interference is suspected as the source of such trend, but it has not been investigated further. A laminar separation bubble is observed for both the A-Tunnel and the AWB clean measurements, but it does not appear at higher Re_c. In the tripped case, the measured C_p are very similar and aligned with the XFOIL predictions. The C_p distributions are not shown here for conciseness. For the HRM results, a good agreement is observed specially between DTU and NWB, the former showing a slightly higher $C_{l,max}$ for the equivalent Re_c. This higher $C_{l,max}$ may be influenced by the use of Kevlar walls, as visible in Fig. 10. The LTT data has a lower slope which again could be attributed to a reduced aspect ratio and the pressure tabs not being in the middle of the test section. The different inflow turbulence of the tunnels could also play a role. Higher $C_{l,max}$ are measured in the clean cases, and the separation behaviour appears to be sensible to Re_c than in the tripped counterpart (except for the AWB as discussed above).

The drag coefficient results are shown in Fig. 9. All the data has been obtained from the momentum deficit in the wake using wake-rake measurements, as described in Section 7.2.3. of Russo [31]. As Re_c increases, C_d decreases, as seen very clearly by the difference between the models. In addition, larger drag values are observed in the tripped case compared to the clean measurements.

Fig. 10 compares the measurements in the LTT and the PLCT (DTU) for Kevlar and hard walls. The LTT data shows a very good agreement between both configurations at positive α_{eff}. However, a mismatch is observed at negative stall. The cause is an asymmetry in the test set-up with Kevlar walls. One side of the test section (facing suction side at $\alpha > 0$) was a Kevlar-Melamine panel with a solid back plate for noise absorption, whereas the opposite side was composed of a single Kevlar panel to allow for the acoustic measurements. Further details and consequences of the asymmetric permeability are explained in the study of Luesutthiviboon et al. [11]. DTU results also agree well, with the hard walls leading to a slightly lower $C_{l,max}$. The hard wall measurements were carried out with tripping at 5% in the suction side and 10% in the pressure side, unlike the Kevlar case, which was tested at symmetric 5% tripping. However,

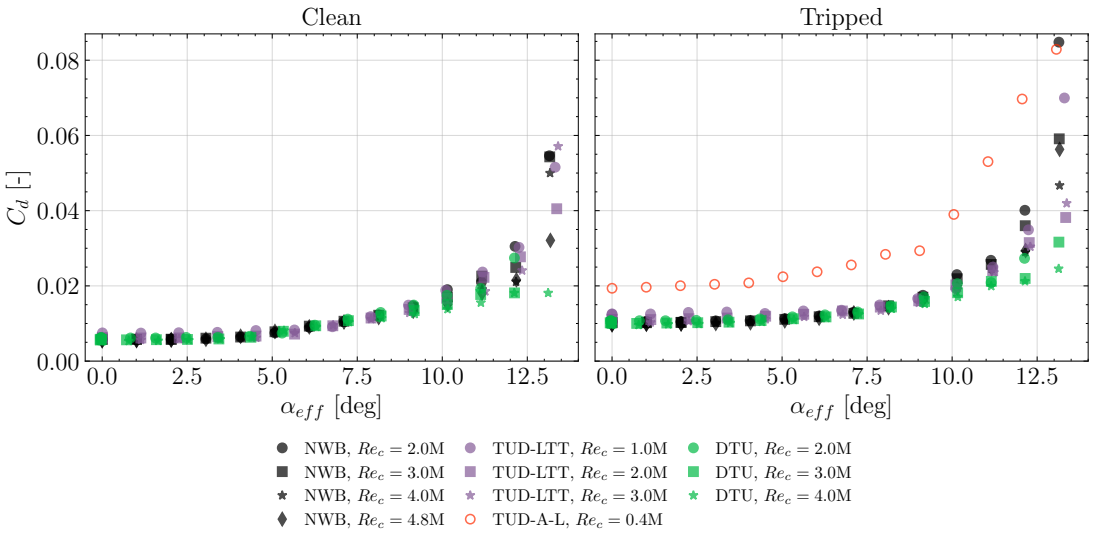

Fig. 9 Drag coefficient measured in the different facilities for a variety of Re_c numbers. Empty markers represent the measures corrected using XFOIL, and full markers indicate other correction methods.

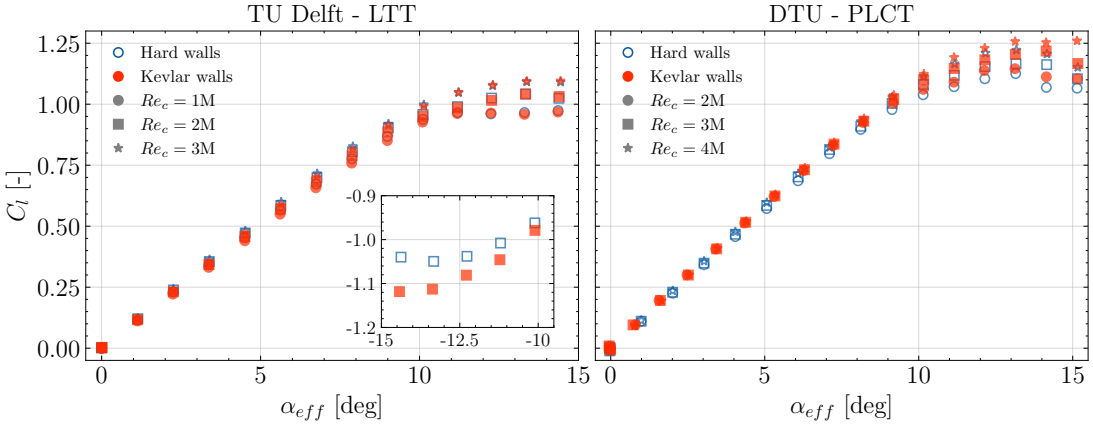

Fig. 10 Comparison of the lift coefficient curves measured in Kevlar and hard wall configurations at the Poul La Cour Tunnel (DTU) and the Low Turbulence Tunnel (LTT). The boundary layer was tripped in all the cases. Inner axis in the LTT plot shows negative stall behaviour.

it is considered that the trends appearing in the plot are the consequence of the different walls and not the tripping, since the same trends are found in the clean case.

B. Polar Curves - Serrations Effect

The serrations effect on the lift coefficient is presented in Fig. 11. The lift coefficient difference is calculated as $\Delta C_l = C_l - C_{l,ref.}$, where $C_{l,ref.}$ corresponds to the equivalent α_{eff} with straight trailing edge. Hence, positive ΔC_l values indicate increase in the lift coefficient when serrations are in place. The serrations installation in the HRM blocked the pressure tabs closest to the trailing-edge on both sides of the airfoil. Therefore, the results are not as accurate as in the baseline case, and are biased with respect to it. The general trends are still captured. Both geometries show positive ΔC_l because C_l has been calculated with the same reference chord but the serrations feature extended surface area. Higher ΔC_l is observed for iron serrations compared to the sawtooth ones, which is also attributed to a comparably larger surface area. The iron case also shows a higher sensibility with α_{eff}. Due to uncertainties in the installations the serration flap angles were higher than nominal in the DTU-PLCT tests ($\sim$ 4 deg.). It explains why the difference in ΔC_l

is larger than in the other tunnels. It is interesting to note that the same trends are also found in this case, but with an offset in ΔC_l.

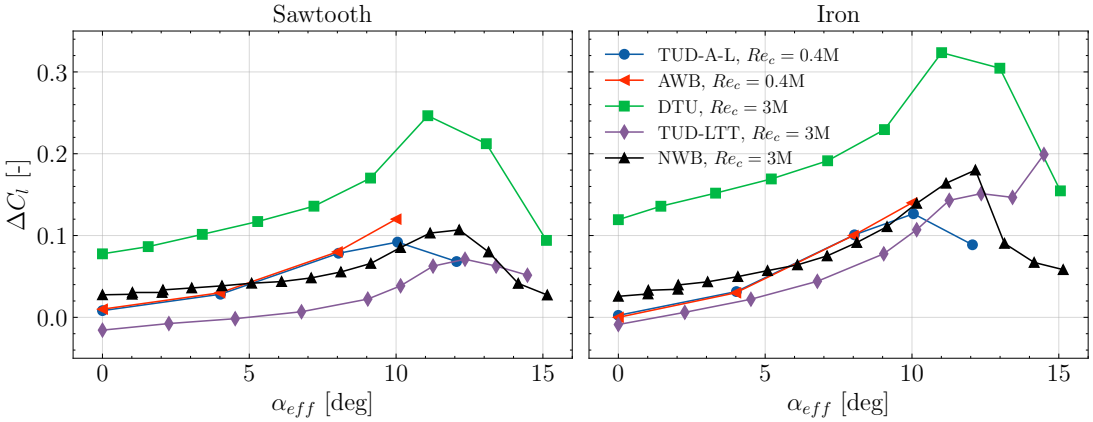

Fig. 11 Increase of lift coefficient with iron and sawtooth serrations measured at the different facilities. It was measured that DTU serrations were flapped 4 deg. instead of the nominal $\varphi = 0$ deg.

C. Displacement Thickness near the Trailing-Edge

The boundary-layer velocity profiles in the vicinity of the trailing edge were measured. HWA was used in the PLCT (DTU) and in the A-Tunnel (TU Delft), and PIV was employed in the LTT (TU Delft). The HWA measurements were performed at $X/c = -0.02$. Once the velocity profiles were obtained, the boundary-layer parameters were extracted. The location of the boundary-layer thickness and the edge velocity were determined by the region were the velocity fluctuations became constant, and fitting of the logarithmic layer was employed [32]. The work of Luesutthiviboon et al. [11] describes in detail the results obtained at TU Delft.

The boundary-layer displacement thickness (δ^*) is of special interest. It will be the parameter chosen to represent the turbulence length scale when scaling the acoustic results in Section V.D, following the classic scaling of Brooks et al. [33]. The measurements are presented in Fig. 12 for $\alpha_{eff} = 0$ deg and straight trailing edge. The lines show the XFOIL predictions obtained with 250 panels and $N_{crit} = 9$. This amplification factor has been chosen after comparing the C_p predictions with the measurements. Dashed lines represent the predictions for the LRM, and solid lines the HRM ones (to account for the different Re_c/M_U relation). Great accordance with XFOIL is observed in the HRM measures. The discrepancies are larger in the LRM, likely a result of a lower measurement resolution near the wall due to a very thin boundary layer. XFOIL captures well the general trends in terms of Re_c and tripping effect. It will be used to calculate δ^* for the scaling of the acoustic results given the lack of data for the rest of test conditions.

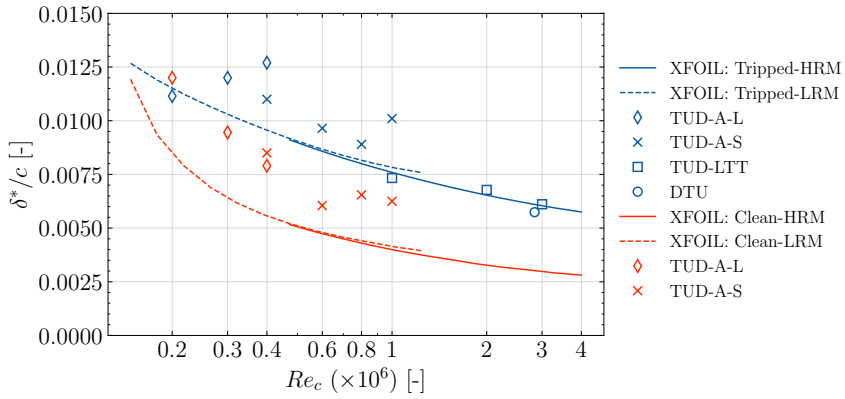

Fig. 12 Displacement thickness measured in the different facilities as a function of Re_c. Blue lines and markers correspond to the tripped boundary-layer conditions, whereas the clean cases are indicated with red.

V. Acoustic Comparison with Straight Trailing Edge

The far-field acoustic measurements with straight trailing-edge are compared in this Section. A summary of the data is firstly given in Fig. 13. The effect of the Reynolds number and the tripping is presented in Subsection V.A, the impact of the angle of attack is assessed in Subsection V.B, and the differences between facilities and measurement techniques are checked in Subsection V.C. Finally, the measurements are scaled together to the same conditions in Subsection V.D, and the collapse is studied. A reference pressure of 20 μPa is used to express the acoustic data with the Sound Pressure Level (SPL).

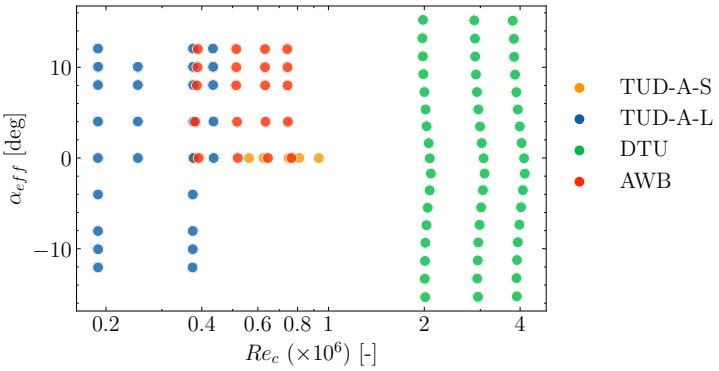

Fig. 13 Summary of the acoustic data for the baseline configuration with tripped boundary layer.

The broad Re_c range measured is shown in Fig. 13. The measurements carried out in the AWB and the A-Tunnel used the LRM, whereas the HRM was tested in the PLCT (DTU). In the lower Re_c range there are several overlapping points which allow for direct comparison between facilities. The geometrical angles of attack in the AWB and the A-Tunnel have been chosen such that their effective angle of attack are equivalent.

A. Effect of the Reynolds Number and the Tripping of the Boundary Layer

Fig. 14 presents the measured SPL in 1/3 octave bands in every facility for the straight trailing edge. Different Re_c numbers are presented together, and the tripped and clean cases are compared. All the results are normalised to a span width and an observer distance of 1m.

The forced transition effect is visible in all the facilities. The turbulent boundary layer arising from the tripping leads to a thicker δ^* than its clean counterpart, as shown in the HWA and PIV measurements presented in Fig. 12. This creates a noise increase in all the cases presented, which is found to be more important at low frequencies, and larger for increasing Re_c. The two lowest Re_c measured (0.19×10^6 and 0.25×10^6) are not following this pattern, and show larger $SPL_{1/3}$ for the clean case. The displacement thickness measurements shown in Fig. 12 indicate that δ^* may be

higher for the clean case at the lowest Reynolds numbers.

DTU measurements (Fig. 14b) and AWB measurements carried out with the elliptic mirror (Fig. 14d) show a high-frequency peak. The location of the peaks scales to very similar trailing-edge thickness based Strouhal numbers $St_{t_{TE}} = f t_{TE}/U$. This suggests that the cause of the peaks is trailing-edge bluntness noise [33]. The same phenomena would be also visible in the A-Tunnel and the array measurements in the AWB if the high frequency limit was larger. In the AWB case, the peaks are more clearly visible in the clean case. It could be explained by a major distortion of the vortex shedding from the turbulent boundary layer developed in the tripped case.

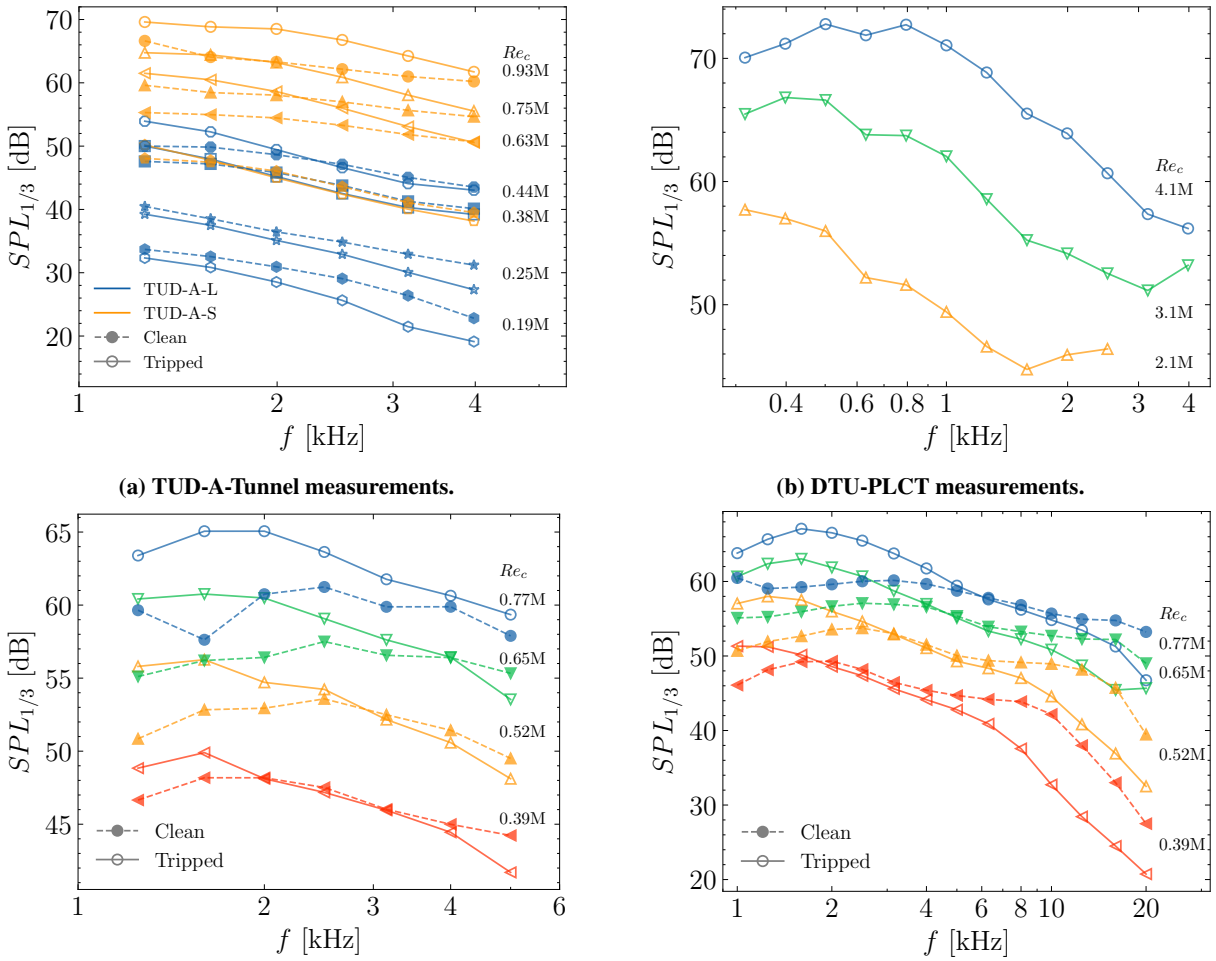

(a) TUD-A-Tunnel measurements.

(b) DTU-PLCT measurements.

(c) DLR-AWB measurements with microphone-array.

(d) DLR-AWB measurements with elliptic-mirror.

Fig. 14 Effect of the Reynolds number and the tripping in the trailing-edge noise measurements of the different facilities. Solid lines with empty markers represent the tripped conditions, and dashed lines with full markers indicate the clean equivalent.

B. Effect of the Angle of Attack

The acoustic polars, presented in Figs. 15 and 16, give a general overview of the angle of attack effect on the trailing-edge noise. The Overall Sound Pressure Level ($OSPL$) has been calculated from the 1/12 octave band spectrum, adding the bands between 1.2 kHz and 5 kHz. This range has been chosen since it contains the common f values for the LRM. These $OSPL$ values should only be analysed comparatively between the different cases to check that the trends are the same, but they do not represent the total $OSPL$ since the peak location of the spectrum is likely located at lower frequencies, specially for non-zero α_{eff}. To allow for similarity between different conditions, the $OSPL$ has

been scaled according to the classical law [33]:

$$OSPL_{scaled} = OSPL - 50\log_{10}(M_U/M_{ref}) - 10\log_{10}(\delta^*_{SS}/\delta^*_{ref}) - 10\log_{10}(b/b_{ref}) - 20\log_{10}(r_{ref}/r) \quad (1)$$

Where M_U is the Mach number based on the free-stream velocity, δ^*_{SS} is the boundary-layer thickness at the suction side, b is the span of the trailing edge, and r is the observer distance. The subscript $_{ref}$ indicates the reference quantities of the scaling, which are chosen as $M_{ref} = 0.13$, $\delta^*_{ref} = 0.008$ m, $b_{ref} = 1$ m, and $r_{ref} = 1$ m.

Fig. 15 compares the trends found in the LRM measures. A good alignment between facilities is observed. For the tripped conditions, the $OSPL$ decreases with α_{eff} and increases with Re_c. The effect of the angle of attack is attributed to the change introduced in the spectral shape: the level increases at low f and decreases at high f, and hence the frequency range selection for the $OSPL$ calculation determines the tendency. The change in the spectral shapes is further discussed in Fig. 17. The trend with Re_c could be explained similarly. The takeaway here is that it is consistent between facilities and with the qualitative expectations. The $OSPL$ at $Re_c \approx 0.4 \times 10^6$, the overlapping point for both facilities, agree within 2 dB. For the clean cases, the same trend with the angle of attack is observed except at $\alpha_{eff} = 8$ and 10 deg. In these cases, the presence of tones from laminar boundary layer instability noise lead to a $OSPL$ increase. These tones may be seen in Fig. 19, where the noise power spectral density is presented. There is also a good agreement in the Re_c at which this phenomena is observed.

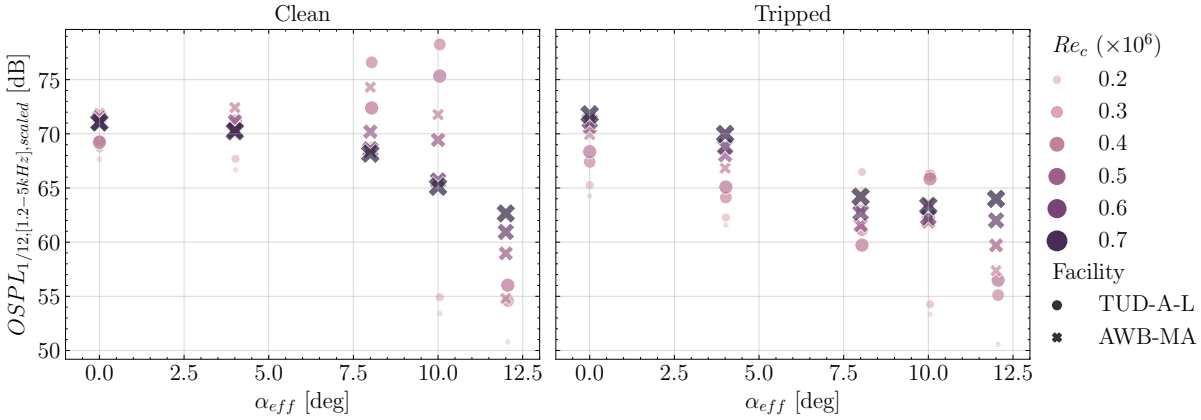

Fig. 15 Acoustic polars of the Low Reynolds number Model measured at A-Tunnel and the AWB for the baseline configuration and both tripped and clean boundary layer.

In Fig. 16 the acoustic polars measured at DTU for the tripped case are shown. The same trends with respect to the angle of attack and the Reynolds number are observed. In this case, the frequency range in the $OSPL$ calculations is 0.4 kHz to 5 kHz, since the Clean-SC post-processing allowed for a better resolution in the low frequency range. A Strouhal-based definition of the integration bounds would have allowed for direct comparison between the LRM and the HRM results. However, due to large Re_c range of the measurements, there is not enough overlapping part of the spectrum in the St space.

Fig. 17 shows the angle of attack effect on the spectra. Different α_{eff} are plotted together for the same Re_c for each facility. Both clean and tripped cases are presented. In the DTU measurements (Fig. 17b) a noise increase at lower frequencies is observed, accompanied by a noise reduction at higher frequencies. This is accredited to a thicker boundary layer developed in the suction side. In the other facilities only the noise reduction at high frequencies is observed due to the lack of low frequency data. From the AWB elliptic mirror data (Fig. 17d) the very high frequency results can also be studied. At $f > 8$–10 kHz, the levels increase again with the angle of attack. This could be attributed to higher energy content in the thinner pressure side boundary layer at these frequencies. The clean cases show the presence of tones at $\alpha_{eff} = 4$ and 8 deg, more clearly visible in the PSD plot shown in Fig. 19.

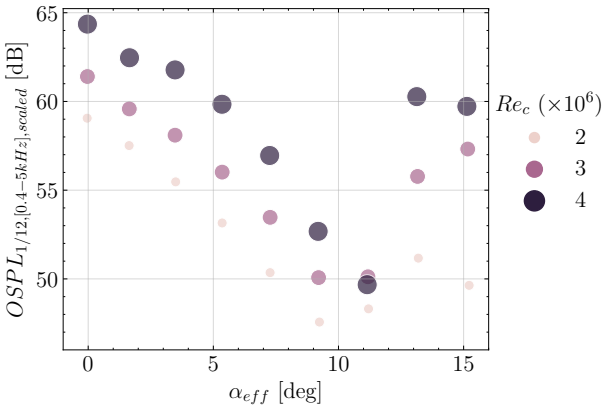

Fig. 16 Acoustic polars of the High Reynolds number Model measured at DTU-PLCT for the baseline configuration and tripped boundary layer.

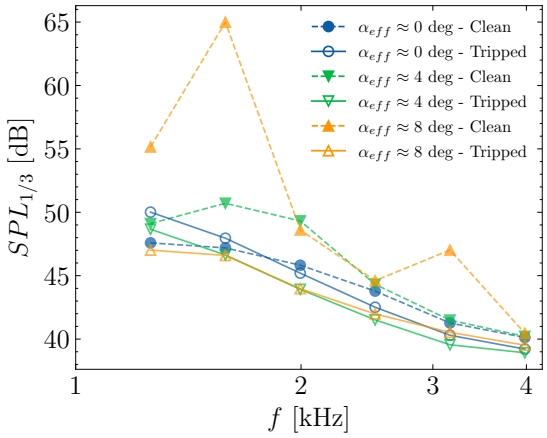

(a) TUD-A-Tunnel measurements at $Re \approx 0.38 \times 10^6$.

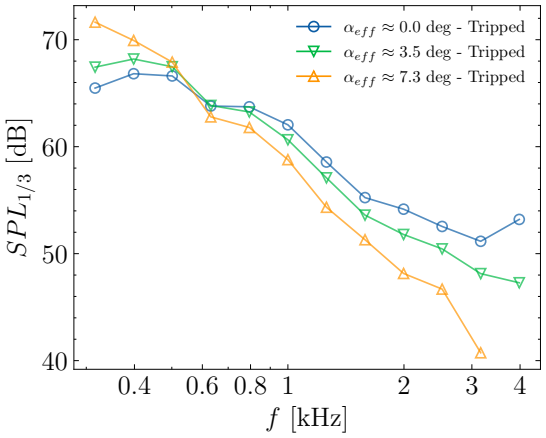

(b) DTU-PLCT measurements at $Re \approx 3 \times 10^6$.

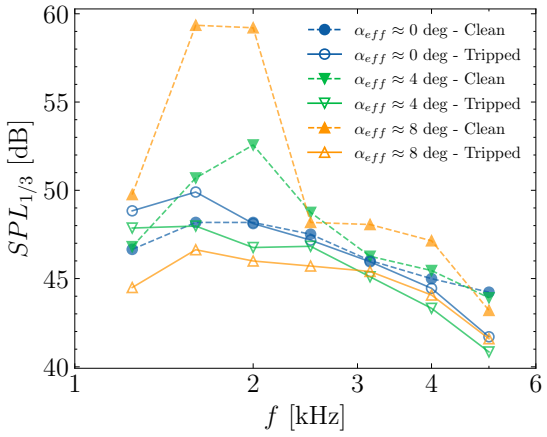

(c) DLR-AWB measurements with microphone-array at $Re \approx 0.39 \times 10^6$.

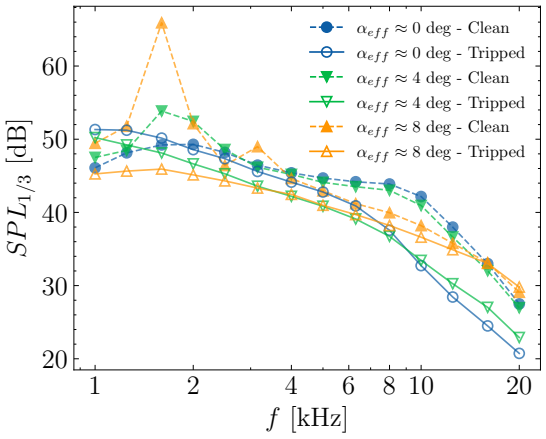

(d) DLR-AWB measurements with elliptic-mirror at $Re \approx 0.39 \times 10^6$.

Fig. 17 Effect of the angle of attack and the tripping in the trailing-edge noise measurements of the different facilities. Solid lines with empty markers represent the tripped conditions, and dashed lines with full markers indicate the clean equivalent.

C. Effect of the Facility and the Measurement Technique

The overlapping measurement point at $Re_c \approx 0.38 \times 10^6$ between the A-Tunnel and the AWB is now studied. The acoustic data is presented using the power spectral density.

In Fig. 18, the case at $\alpha_{eff} = 0$ deg shows a very good agreement between the two nozzles of the A-Tunnel. This allows both set-ups to be interpreted together in a continuous way. The two measurement techniques used in the AWB also collapse very well. Such results strengthen the consistency of the data. The peak levels of both facilities are virtually equal, but a mismatch in the spectral slope leads to deviations up to 6 dB at higher frequencies. There is still a difference in the post-processing used in each facility. It would be interesting to study the possible scatter introduced by using different beamforming algorithms, and establish a common post-processing method. Differences in the shear layer correction can also lead to a deviations in the spectral slope.

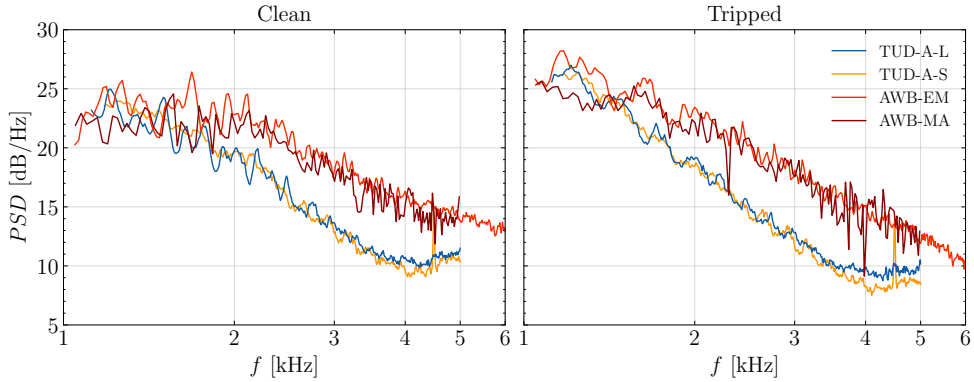

Fig. 18 Far-field noise power spectral density measured at the A-Tunnel and the AWB at 30 m/s for the baseline configuration with tripped boundary layer and $\alpha_{eff} = 0$ deg.

At $\alpha_{eff} = 8$ deg (Fig. 19), the presence of the laminar boundary-layer feedback-loop tones is clearly visible in the clean case. The small mismatch in the peaks location between the AWB and the A-Tunnel may correspond to deviations in the dynamic pressure or more likely to different development of the boundary layer attributed to the distinct aspect ratio, as observed previously in the small discrepancies in the polar curves (Fig. 8). Minor differences are also now observed between the elliptic mirror and the microphone array data from the AWB. The likely reason is the different directivities measured with each system, since the equipment are located at either side of the airfoil as depicted in Fig. 6. The elliptic mirror data will be taken for the subsequent comparisons. It does not only have a broader f range, but it is also consistent with the other facilities, which have the measurement system facing the pressure side of the airfoil when the model is pitched towards positive angles of attack.

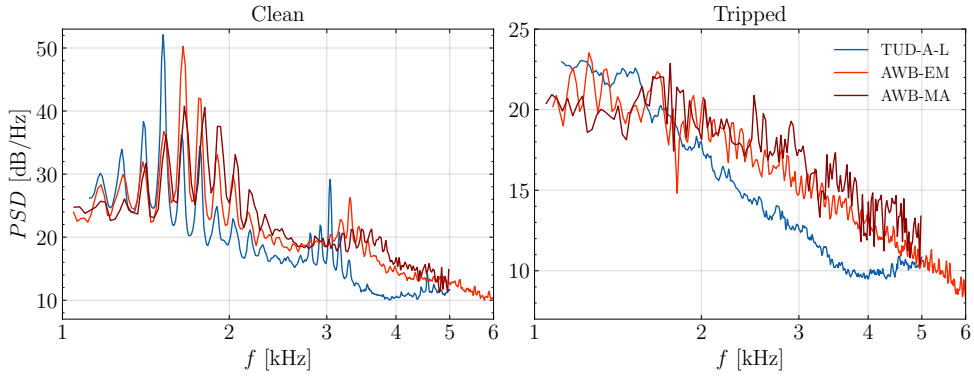

Fig. 19 Far-field noise power spectral density measured at the A-Tunnel and the AWB at 30 m/s for the baseline configuration with tripped boundary layer and $\alpha_{eff} \approx 8$ deg.

D. Scaling Study

This section studies the collapse of the scaling of the measurements performed at different Reynolds and Mach numbers. The classic scaling law has been applied [33]:

$$SPL_{scaled} = SPL - 50\log_{10}(M_U/M_{ref}) - 10\log_{10}(\delta^*_{SS}/\delta^*_{ref}) - 10\log_{10}(b/b_{ref}) - 20\log_{10}(r_{ref}/r) \quad (2)$$

Although this form of scaling is not expected to provide a perfect collapse in all the frequency range [34], it is the most widely used form, and it provides a useful first approach to compare and study the data. Only the forced transition cases are compared here, since the test conditions are more equivalent across the different facilities and the uncertainty is reduced. To have an estimate of the peak location of the measurements, the range of expected peaks $St_{\delta^*_{SS}}$ according to BPM [33] are plotted together with the measurements. Although the model was developed using a different airfoil and measurement techniques, it is depicted here as a rough reference to know where the peak frequency may lie.

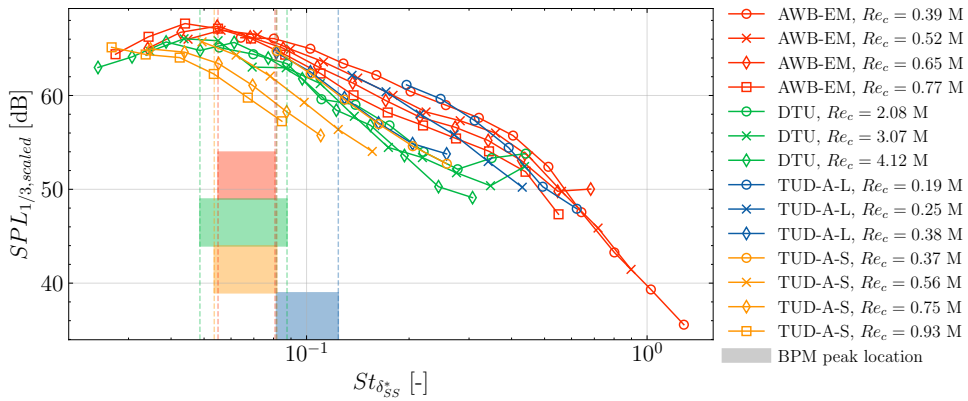

Fig. 20 Scaling of the measurements at different facilities for the tripped boundary layer case at $\alpha_{eff} = 0$ deg. The peak location predicted by the BPM model is also presented with vertical lines. Each colour covers the measurement range from the respective facility.

The scaled spectra at $\alpha_{eff} = 0$ deg. is presented in Fig. 20. According to the BPM predictions, the peak St_{δ^*} lies within the measured range. Good agreement in the peak locations and levels is observed between AWB and DTU despite deviations in the spectral slope. A trend with the Reynolds number is also observed: the curves shift to lower St_{δ^*} as Re_c increases. It is aligned with the BPM measurements, which estimated the peak St_{δ^*} as $St_{\delta^*} = 0.02M^{-0.6}$. This is particularly pronounced for the TUD results, which cover a much more extended peak Strouhal range than the corresponding BPM predictions. The mismatch between AWB and TUD, which encompass the same M_U and Re_c range, is not clear and should be investigated further. The effect of the different post-processing is suspected and should be assessed.

Fig. 21 shows the scaled spectrum at α_{eff} between 3 deg and 4 deg. The peak values agree well within 1.5 dB. As $St_{\delta^*_{SS}}$ increases, however, the collapse worsens and the scatter grows up to 10 dB. In that region, the same trend as the $\alpha_{eff} = 0$ deg is observed: within each facility, the lower the Re_c the higher the scaled SPL. This is specially visible for the two lower Re_c (0.19 and 0.25 million) measured in the A-Tunnel. The different Re_c may change the nature of the flow field and the behaviour of the boundary layer, which decreases the scaling collapse. This effect is found to be more important at the lower Re_c numbers. The large Re_c measurements performed at DTU escape this trend and show a more stable collapse.

The cases at α_{eff} between 7 deg and 8 deg are plotted in Fig. 22. The scatter between the DTU and the AWB results at low frequencies is larger in the preceding cases. Looking back at the lift curves (Fig. 8) it is observed how the loading difference is already important at this polar region. Different noise results are also expected in such a case. The better agreement between the A-Tunnel and the AWB, which polar curves are more alike, also supports this argument. The cases at $Re_c = 0.19 \times 10^6$ and 0.25×10^6 in the A-Tunnel are not shown in this plot, since the tripping effect was jeopardised by the location of the stagnation point, and laminar boundary-layer instability tones appeared.

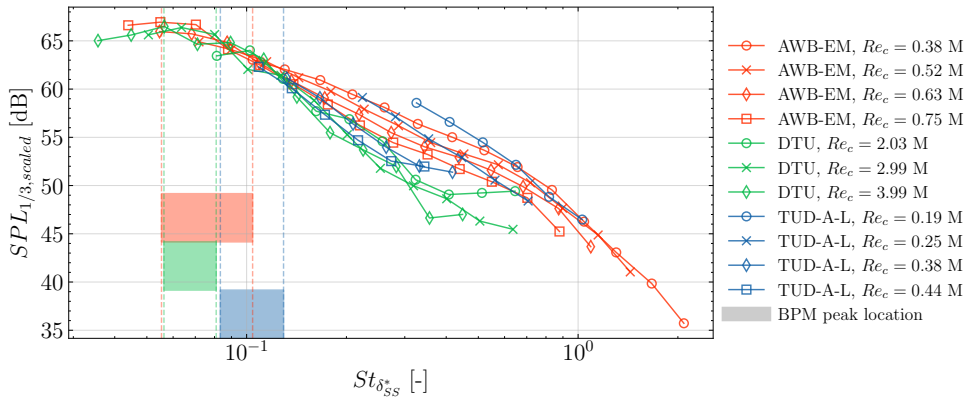

Fig. 21 Scaling of the measurements at different facilities for the tripped boundary layer case at $\alpha_{eff} \approx$ 3–4 deg. The peak location predicted by the BPM model is also presented with vertical lines. Each colour covers the measurement range from the respective facility.

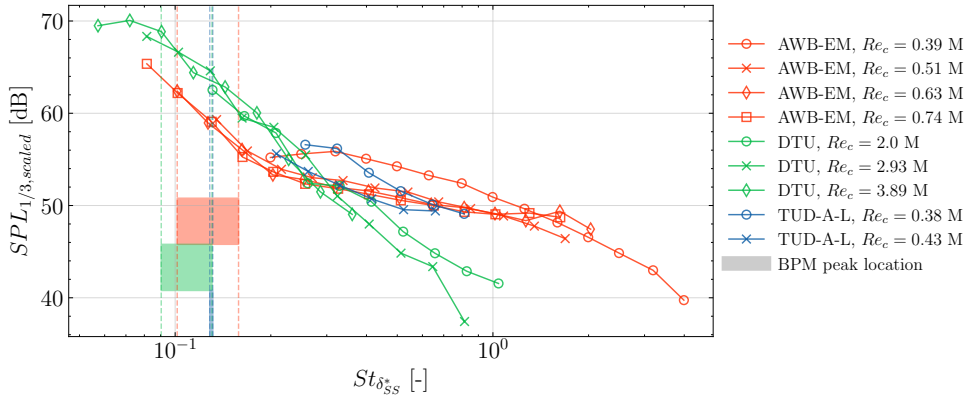

Fig. 22 Scaling of the measurements at different facilities for the tripped boundary layer case at $\alpha_{eff} \approx 7 - 8$ deg. The peak location predicted by the BPM model is also presented with vertical lines. Each colour covers the measurement range from the respective facility.

VI. Noise Reduction Comparison with Different Serrations

The effect of the noise reduction devices is studied in this Section. The noise reduction is calculated as $\Delta SPL_{1/3} = SPL_{1/3} - SPL_{1/3,\,\text{ref.}}$, where the reference Sound Pressure Level $SPL_{1/3,\,\text{ref.}}$ corresponds to the equivalent case with straight trailing edge at the same α_{eff} and Re_c. Therefore, negative $\Delta SPL_{1/3}$ indicate noise reduction. For this section, the DTU results have been post-processed with conventional frequency-domain beamforming instead of Clean-SC. The latter had convergence issues at low frequencies for the serrated cases, where the signal-to-noise ratio is lower. The CBF results show increased levels with respect to the Clean-SC equivalent [17], but this is acceptable in this section since the focus is on $\Delta SPL_{1/3}$.

$\Delta SPL_{1/3}$ is presented against $St_{\delta^*_{SS}}$ in Fig. 23 for the iron and sawtooth serrations without nominal flap angle. Only the tripped boundary layer cases are considered here. There is a fair scaling with $St_{\delta^*_{SS}}$, which supports previous results that showed that the noise reduction maximum depends on U [35, 36]. Two regions of noise reduction are identified for both serrations in the LRM results (AWB and TUD-A) The second noise reduction peak is similar to the results of P. Zhou et al. [37], which were also measured at similar Re_c number as the LRM. The HRM measurements (DTU) show two noise reduction regions in the sawtooth case, but only one in the iron case. The reason for the difference needs to be further investigated with additional measurements at high Reynolds number. At this point we cannot rule out that the noise reduction mechanisms behave differently at high Reynolds numbers. [37] found that this second peak was highly dependant on the serration flexibility and the flow alignment. The serration deformation was dependant not only on the stiffness and flow speed but also on the aerodynamic loading, which is directly related to the serration geometry. The

aerodynamic forces on the flap are much higher for the HRM compared to the LRM. Hence, it is possible that the flaps were subject to small scale vibrations due to the flexibility. Small scale vibrations could counteract the noise benefits in the high frequency range. Additionally, the iron shaped serrations have a larger surface area but the same thickness as the sawtooth serrations. Hence, the ratio of the aerodynamic forces to the flap stiffness is less favourable for the iron shaped serrations than the sawtooth serrations. The uncertainty in the serration flap angle could also play a role in the mismatch. In the first noise reduction peak, the iron serrations lead to a noise decrease up to 7.5-8 dB, whereas reductions up to 5 dB are seen for the sawtooth serrations. This is aligned with the computational studies by Avallone et al. [13].

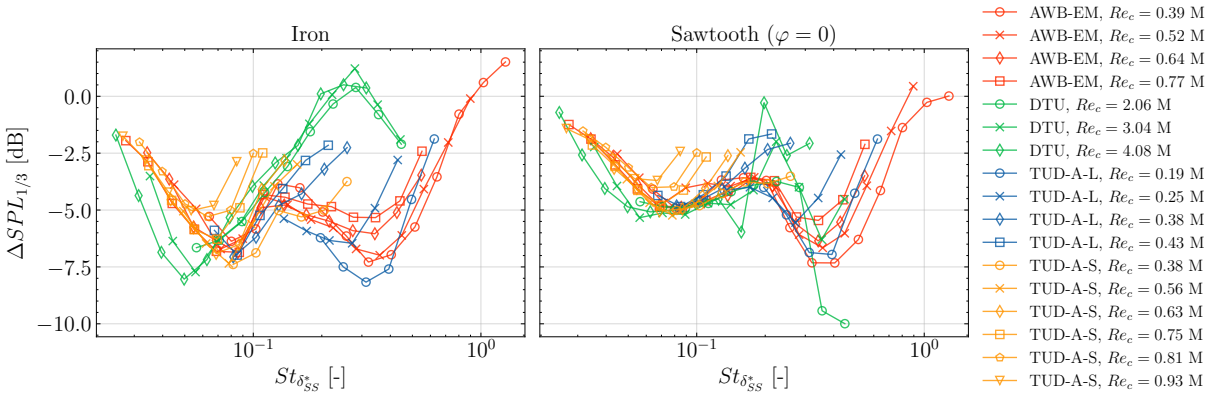

Fig. 23 Scaling of the $\Delta SPL_{1/3}$ with iron and sawtooth serrations with the displacement thickness based Strouhal number at $\alpha_{eff} = 0$ deg.

The cases with flapped serrations are shown in Fig. 24. Two noise reduction region are also identified here. The noise reduction maximum ($\sim$ 4 dB), however, is lower than in the preceding cases. This may be explained with appearing counter-rotating streamwise-oriented vortices in the serration edges when the airfoil is loaded [38, 39], since the airfoil is actually cambered when tested with flapped serrations.

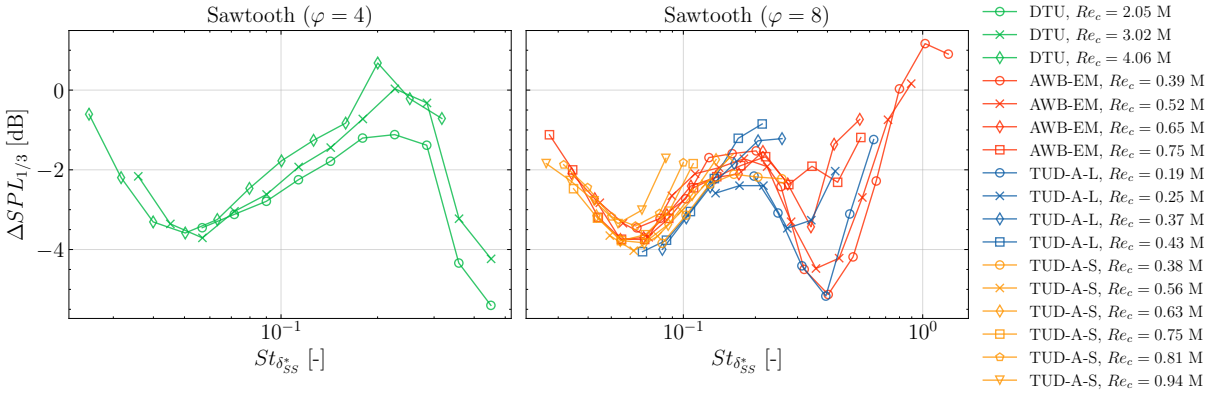

Fig. 24 Scaling of the $\Delta SPL_{1/3}$ with flapped sawtooth serrations with the displacement thickness based Strouhal number at $\alpha_{eff} = 0$ deg.

The effect of the angle of attack is summarised in Fig. 25. The $\Delta OSPL$ has been calculated for frequencies between 1200 and 5000 Hz for the LRM ($Re_c \approx 0.38 \times 10^6$), and between 400 and 3000 Hz for the HRM ($Re_c \approx 3 \times 10^6$). These values are arbitrarily chosen to have the best possible representation of the low frequencies, which drive the $OSPL$. Ideally, the same f or St range would have been chosen, but the present case is limited by the low SNR in the LRM results at low frequencies. Comparison between the models should be then analysed with care due to this difference. The noise reduction is presented for both the clean and the tripped cases. For the clean conditions, it is interesting to note the additional noise reduction measured at $\alpha_{eff} = 4$ and 8 deg. This noise decrease comes from the removal of the

laminar boundary-layer instability noise. It follows the study of [40], and it is attributed to bypass transition near the trailing edge that prevents separation, and removes the amplifier of the Tollmien-Schlichting waves.

For the tripped conditions, it is observed in the spectra (omitted for conciseness) that the angle of attack initially leads to a level increase at intermediate and high frequencies. This effect propagates to lower frequencies too when α_{eff} increases further, and it affects all the spectrum when stall is reached. This may be attributed again to the increasing airfoil loading, with the same reasoning explained previously for the flapped serrations. In Fig. 25 the Re_c effect is also observed. The earlier departure of the LRM cases from the attached polar region leads to noise increases at lower α_{eff} than in the HRM results. The larger slope observed for the iron serrations shows again a higher sensibility to the aerodynamic loading due to the increased surface area, as seen previously in the lift coefficient measurements (Fig. 11).

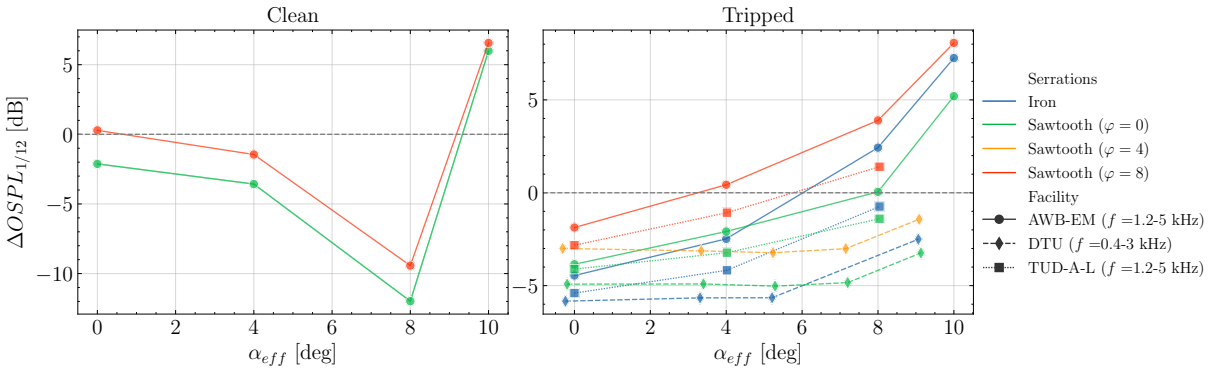

Fig. 25 Overall Sound Pressure Level as a function of the angle of attack and the serration type. LRM data (AWB-EM and TUD-A-L) measured at $Re_c \approx 0.38 \times 10^6$, and HRM data (DTU) at $Re_c \approx 3 \times 10^6$. The frequency range for the calculation of the $OSPL_{1/12}$ is indicated in the facility legend.

VII. Conclusion

The aerodynamic and aero-acoustic characterisation of the NACA 63_3-018 has been presented in this paper. Two models of this airfoil have been built for such purpose, with chord lengths of 0.2 m and 0.9 m, and they have been measured in 5 different wind tunnels: the A-Tunnel and the LTT at TU Delft, the Poul La Cour Tunnel at DTU, and the AWB and the NWB at DLR. The Re_c of the measures ranges from 0.18×10^6 to 4.8×10^6. Multiple angles of attack have been tested. The models have been studied with tripped and clean boundary layer, and sawtooth and iron serrations have also been installed and measured in both models.

The aerodynamic coefficients have been presented for the clean and tripped configurations for different Re_c. Tripping the boundary layer leads to a decrease of $C_{l,max}$ and a lower Re_c sensitivity in the stall region. Increasing Re_c leads to an increase of $C_{l,max}$ for both the clean and tripped case. This effect is very visible between models. Slight deviations in the lift slope were attributed to different aspect ratios. The effect of using Kevlar or hard walls for the testing has been also assessed. Good agreement between both configurations was observed, except for the negative stall region in the LTT measurements, which is the consequence of asymmetries in the set-up. The effect of the serrations on the lift coefficient has also been studied. A higher ΔC_l was found for the iron serrations due to a larger surface area. However, the measurements with serrations contained significant uncertainties in the flap angle. This was specially important for the DTU case, which showed deviations of 4 deg with respect to the nominal value. The velocity profile in the vicinity of the trailing edge has been also measured. The boundary layer displacement thickness (δ^*) has been calculated and compared to XFOIL predictions, which agreed well in terms of Re_c and tripping trends.

The acoustic results have been firstly discussed for the straight trailing edge configuration. The effect of the tripping on the far-field noise has been assessed. Within the same Re_c measured, it was observed that the forced boundary layer lead to a level increase up to 5 dB in the low frequency part of the spectrum. This was related to the increase of δ^*. Broadband peaks in the high frequency part were found and attributed to trailing-edge bluntness noise. Increasing the angle of attack lead to a rise in the levels in the low frequency part of the spectrum, and a decrease in the high frequency part. This was also associated to the varying thickness of the boundary layer. For the clean configuration, laminar boundary-layer instability tones appeared at non-zero α_{eff}. They were found to be Re_c dependant, and good agreement on the tone presence and location between facilities was observed. An overlapping measurement point was available at

$Re_c \approx 0.38 \times 10^6$ between the A-Tunnel and the AWB. Good agreement at frequencies around 1-2 kHz was found, but differences in the spectral slope lead to a mismatch up to 6 dB at 3-4 kHz. Although the physical model tested was the same, the post-processing of the data was different, and it could have introduced some deviations. A study of the possible scatter introduced in this step is required. The scaling of the acoustic data showed a good agreement on the peak locations and levels, specially between AWB and DTU results. Generally, the curves shifted towards lower St_{δ^*} as Re_c increases. This was particularly pronounced in the TUD measurements, which covered a more extended peak Strouhal range than the AWB equivalent and the BPM predictions. The Re_c effect was particularly visible at $\alpha \approx 7 - 8$. At this angle the lift coefficients were already different due to early separation at low Re_c, and thus the acoustic results were also distinct for the two airfoil models.

The noise reduction effect has been measured and studied for the different serration types. Tones present in the clean measurements were significantly attenuated with the add-ons installed, leading to reductions in the $OSPL$ up to 10 dB. The noise reduction spectrum $\Delta SPL_{1/3}$ scaled fairly well with St_{δ^*}, and good agreement was found between different facilities and Re_c. Two noise reduction peaks were generally observed. The iron serrations were found to provide up to 7.5-8 dB of maximum noise reduction, whereas for the sawtooth serration it was around 5 dB. The overall sound reduction decreased with the flap angle and the angle of attack. This is likely a consequence of the increased aerodynamic loading and the appearance of counter-rotating vortices in the serration edges. The iron serrations were more sensible to α_{eff} changes due to a larger surface that lead to higher loading, as it was observed when comparing the ΔC_l.

Funding Sources

The current work is part of Task 39 "Quiet Wind Turbine Technology", an initiative within the Technology Cooperation Programme (TCP) by the International Energy Agency (IEA). The authors would like to thank the German Federal Ministry for Economic Affairs and Climate Action (BMWK) for supporting the operation of this task.
The authors would like to thank the Danish Energy Agency for funding the participation of the Technical University of Denmark in the IEA Task 39 under the programme "Energiteknologiske Udviklings- og Demonstrationsprogram (EUDP)", Journal number 134-21022.

Acknowledgments

Special thanks are due to Jorge Pereira Gomes for his valuable support during the NWB measurement campaigns. We would like to thank the wind tunnel engineers Jimmy S. Beckerlee and Sigurd B. Ildvedsen for conducting the experiments in the Poul La Cour wind Tunnel at the Technical University of Denmark.

References

[1] Howe, M. S., "A review of the theory of trailing edge noise," *Journal of Sound and Vibration*, Vol. 61, No. 3, 1978, pp. 437–465. https://doi.org/10.1016/0022-460X(78)90391-7.

[2] Lee, S., Ayton, L., Bertagnolio, F., Moreau, S., Chong, T. P., and Joseph, P., "Turbulent boundary layer trailing-edge noise: Theory, computation, experiment, and application," *Progress in Aerospace Sciences*, Vol. 126, 2021, p. 100737. https://doi.org/10.1016/J.PAEROSCI.2021.100737.

[3] Oerlemans, S., Sijtsma, P., and Méndez López, B., "Location and quantification of noise sources on a wind turbine," *Journal of Sound and Vibration*, Vol. 299, No. 4-5, 2007, pp. 869–883. https://doi.org/10.1016/j.jsv.2006.07.032.

[4] Herr, M., Bahr, C., and Kamzurraman, M., "Workshop Category 1: Trailing-Edge Noise. Problem Statement for the AIAA/CEAS Second Workshop on Benchmark Problems for Airframe Noise Computations (BANC-II)," 2012.

[5] Herr, M., and Kamruzzaman, M., "Benchmarking of trailing-edge noise computations - Outcome of the BANC-II workshop," *19th AIAA/CEAS Aeroacoustics Conference*, American Institute of Aeronautics and Astronautics, 2013. https://doi.org/10.2514/6.2013-2123.

[6] Herr, M., Ewert, R., Rautmann, C., Kamruzzaman, M., Bekiropoulos, D., Iob, A., Arina, R., Batten, P., Chakravarthy, S., and Bertagnolio, F., "Broadband trailing-edge noise predictions— overview of BANC-III results," *21st AIAA/CEAS Aeroacoustics Conference*, American Institute of Aeronautics and Astronautics, 2015. https://doi.org/10.2514/6.2015-2847.

[7] Oerlemans, S., and Schepers, J., "Prediction of wind turbine noise and validation against experiment," *International Journal of Aeroacoustics*, Vol. 8, No. 6, 2009, pp. 555–584. https://doi.org/10.1260/147547209789141489.

[8] Fischer, A., Bertagnolio, F., Shen, W. Z., and Madsen, J., "Noise model for serrated trailing edges compared to wind tunnel measurements," *Journal of Physics: Conference Series*, Vol. 753, IOP Publishing, 2016. https://doi.org/10.1088/1742-6596/753/2/022053.

[9] Ferret Gasch, O., Oerlemans, S., Faßmann, B. W., Herr, M., Bertagnolio, F., Fischer, A., Arnold, B., and Lutz, T., "Trailing edge noise prediction of wind turbine airfoils: A benchmark exercise," *25th AIAA/CEAS Aeroacoustics Conference*, American Institute of Aeronautics and Astronautics, 2019. https://doi.org/10.2514/6.2019-2675.

[10] Timmer, W. A., and Rooij, R. P. J. O. M. V., "Summary of the Delft University Wind Turbine Dedicated Airfoils," *41st AIAA Aerospace Sciences Meeting and Exhibit*, American Institute of Aeronautics and Astronautics, 2003. https://doi.org/10.2514/6.2003-352.

[11] Luesutthiviboon, S., Lima Pereira, L. T., Ragni, D., Avallone, F., and Snellen, M., "Aeroacoustic Benchmarking of Trailing-edge Noise from a NACA 63_3–018 Airfoil with Trailing-Edge Serrations," *Under review, AIAA Journal*, 2022.

[12] Fischer, A., Bak, C., Lylloff, O., Olsen, A. S., Mikkelsen, F., Ildvedsen, S. B., Beckerlee, J. S., Kuester, M., and Intaratep, N., "Cross validation of the aerodynamic and acoustic measurements in two Kevlar-walled wind tunnels," *Acccepted for publication in: Journal of Physics: Conference Series*, IOP Publishing, 2022.

[13] Avallone, F., van der Velden, W. C., and Ragni, D., "Benefits of curved serrations on broadband trailing-edge noise reduction," *Journal of Sound and Vibration*, Vol. 400, 2017, pp. 167–177. https://doi.org/10.1016/j.jsv.2017.04.007.

[14] Allen, H. J., and Vinceti, W. G., "Wall interference in a two-dimensional-flow wind tunnel with consideration of the effect of compressibility," Tech. rep., NACA, Ames Aeronautical Laboratory, Moffett Field, California, US, 1944.

[15] Devenport, W. J., Burdisso, R. A., Borgoltz, A., Ravetta, P. A., Barone, M. F., Brown, K. A., and Morton, M. A., "The Kevlar-walled anechoic wind tunnel," *Journal of Sound and Vibration*, Vol. 332, No. 17, 2013, pp. 3971–3991. https://doi.org/10.1016/j.jsv.2013.02.043.

[16] Sijtsma, P., "CLEAN based on spatial source coherence," *International Journal of Aeroacoustics*, Vol. 6, No. 4, 2007, pp. 357–374. https://doi.org/10.1260/147547207783359459.

[17] Lylloff, O., *Aeroacoustic wind tunnel tests*, DTU Wind Energy, PhD Thesis, 2020. https://doi.org/10.11581/dtu:00000102.

[18] Merino-Martínez, R., Rubio Carpio, A., Lima Pereira, L. T., van Herk, S., Avallone, F., Ragni, D., and Kotsonis, M., "Aeroacoustic design and characterization of the 3D-printed, open-jet, anechoic wind tunnel of Delft University of Technology," *Applied Acoustics*, Vol. 170, 2020. https://doi.org/10.1016/j.apacoust.2020.107504.

[19] Johnson, D. H., and Dudgeon, D. E., *Array Signal Processing: Concepts and Techniques*, Prentice Hall, 1993.

[20] Timmer, W., "Two-Dimensional Low-Reynolds Number Wind Tunnel Results for Airfoil NACA 0018," *Wind Engineering*, Vol. 32, No. 6, 2008, pp. 525–537. https://doi.org/10.1260/030952408787548848.

[21] Garner, H. C., Rogers, E. W. E., Acum, W. E. A., and Maskell, E. C., "Subsonic Wind Tunnel Wall Corrections," Tech. rep., AGARD, Paris, 1966.

[22] Pott-Pollenske, M., and Delfs, J., "Enhanced capabilities of the Aeroacoustic Wind Tunnel Braunschweig," *14th AIAA/CEAS Aeroacoustics Conference (29th AIAA Aeroacoustics Conference)*, American Institute of Aeronautics and Astronautics, 2008. https://doi.org/10.2514/6.2008-2910.

[23] Sen, R., "Interpretation of Acoustic Source Maps Made with an Elliptic-Mirror Directional Microphone System," *Aeroacoustics Conference*, 1996.

[24] Schlinker, R., "Airfoil Trailing Edge Noise Measurements with a Directional Microphone," *4th Aeroacoustics Conference*, American Institute of Aeronautics and Astronautics, Atlanta, GA, U.S.A., 1977. https://doi.org/10.2514/6.1977-1269.

[25] Herr, M., "Trailing-Edge Noise—Reduction Concepts and Saling Laws," *Dissertation, DLR Report ISRN DLR-FB-2013-32, ISSN 1434-8454*, 2013.

[26] Bergmann, A., "The Aeroacoustic Wind Tunnel DNW-NWB," *18th AIAA/CEAS Aeroacoustics Conference*, American Institute of Aeronautics and Astronautics, Colorado Springs, Colorado, USA, 2012. https://doi.org/10.2514/6.2012-2173.

[27] Drela, M., "XFOIL: An Analysis and Design System for Low Reynolds Number Airfoils," *Low Reynolds Number Aerodynamics*, edited by T. J. Mueller, Lecture Notes in Engineering, Springer, Berlin, Heidelberg, 1989, pp. 1–12. https://doi.org/10.1007/978-3-642-84010-4.

[28] Brooks, T. F., Marcolini, M. A., and Pope, D. S., "Airfoil trailing edge flow measurements and comparison with theory, incorporating open wind tunnel corrections," *AIAA/NASA 9th Aeroacoustics Conference*, American Institute of Aeronautics and Astronautics, 1984.

[29] Brown, K. A., *Understanding and exploiting wind tunnels with porous flexible walls for aerodynamic measurement*, Virginia Tech, PhD thesis, 2016.

[30] Kiefer, J., Miller, M. A., Hultmark, M., and Hansen, M. O., "Effects of finite aspect ratio on wind turbine airfoil measurements," *Journal of Physics: Conference Series*, Vol. 753, No. 2, 2016. https://doi.org/10.1088/1742-6596/753/2/022040.

[31] Russo, G. P., *Aerodynamic measurements. From phyisical principles to turnkey instrumentation*, Woodhead Publishing, Cambridge, UK, 2011. https://doi.org/10.1533/9780857093688.

[32] Clauser, F. H., "The Turbulent Boundary Layer," *Advances in Applied Mechanics*, Vol. 4, No. C, 1956, pp. 1–51. https://doi.org/10.1016/S0065-2156(08)70370-3.

[33] Brooks, T. F., Pope, D. S., and Marcolini, M. A., "Airfoil Self-Noise and Prediction," Tech. rep., NASA, Hampton, VA, 1989.

[34] Herr, M., Appel, C., Dierke, J., and Ewert, R., "Trailing-Edge Noise Data Quality Assessment for CAA Validation," *16th AIAA/CEAS Aeroacoustics Conference*, American Institute of Aeronautics and Astronautics, 2010. https://doi.org/10.2514/6.2010-3877.

[35] Gruber, M., Joseph, P. F., and Chong, T. P., "On the mechanisms of serrated airfoil trailing edge noise reduction," *17th AIAA/CEAS Aeroacoustics Conference (32nd AIAA Aeroacoustics Conference)*, American Institute of Aeronautics and Astronautics, 2011. https://doi.org/10.2514/6.2011-2781.

[36] Moreau, D. J., and Doolan, C. J., "Noise-reduction mechanism of a flat-plate serrated trailing edge," *AIAA Journal*, Vol. 51, No. 10, 2013, pp. 2513–2522. https://doi.org/10.2514/1.J052436.

[37] Zhou, P., Liu, Q., Zhong, S., Fang, Y., and Zhang, X., "A study of the effect of serration shape and flexibility on trailing edge noise," *Physics of Fluids*, Vol. 32, No. 12, 2020. https://doi.org/10.1063/5.0032774.

[38] Avallone, F., Pröbsting, S., and Ragni, D., "Three-dimensional flow field over a trailing-edge serration and implications on broadband noise," *Physics of Fluids*, Vol. 28, No. 11, 2016. https://doi.org/10.1063/1.4966633.

[39] Arce León, C., Merino-Martínez, R., Ragni, D., Avallone, F., Scarano, F., Pröbsting, S., Snellen, M., Simons, D. G., and Madsen, J., "Effect of trailing edge serration-flow misalignment on airfoil noise emissions," *Journal of Sound and Vibration*, Vol. 405, 2017, pp. 19–33. https://doi.org/10.1016/j.jsv.2017.05.035.

[40] Chong, T. P., and Joseph, P. F., "An experimental study of airfoil instability tonal noise with trailing edge serrations," *Journal of Sound and Vibration*, Vol. 332, No. 24, 2013, pp. 6335–6358. https://doi.org/10.1016/j.jsv.2013.06.033.

8 WP2 / Annex 4 - Presentation of the serration benchmark main results

IEA Task 39 – Quiet Wind Turbines Status of the NACA63018 serration benchmark

Andreas Fischer, Franck Bertagnolio, Oliver Ackermann Lylloff (DTU)
Alexandre Suryadi, Michaela Herr (DLR)
Daniele Ragni, Tercio Lima Pereira, Salil Luesutthiviboon (TU Delft)
Marijn Sanders (University of Twente)
Nanyaporn Intaratep (Virginia Tech)
Roxana Donner, Gert Herold (TU Berlin)

Outline

- Active Partners
- Objectives
- Wind tunnel models and serrations
- Facility overview
- Update low Reynolds number team
- Update high Reynolds number team
- Conclusions

Active Partners

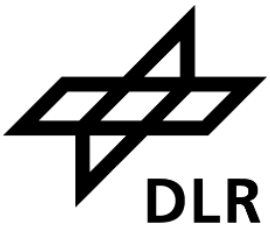

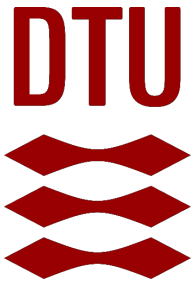

Objectives of the benchmark exercise

- Cross compare acoustic measurements in a wide range of aero-acoustic facilities for a low noise aerofoil configuration
- Align testing and post-processing methods
- Identify reason for the scatter of the data and try to reduce it
- Investigate the scalability of the results for small and large facilities
- Provide a data base for model validation
- Provide uncertainty estimates representative for aero-acoustic testing of low noise aerofoil configurations

Two NACA 63_3-018 aerofoils

Low Reynolds number Model

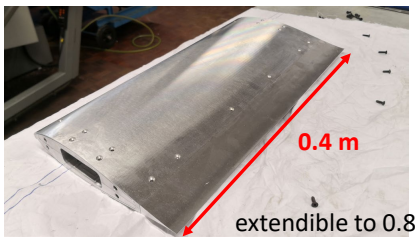

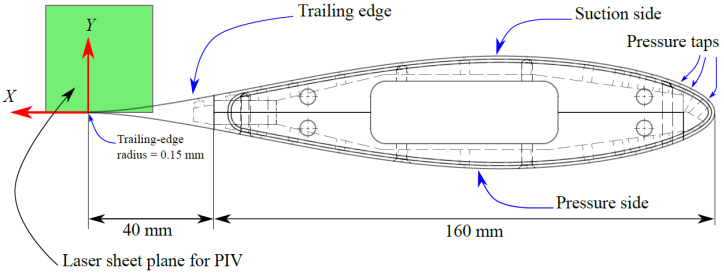

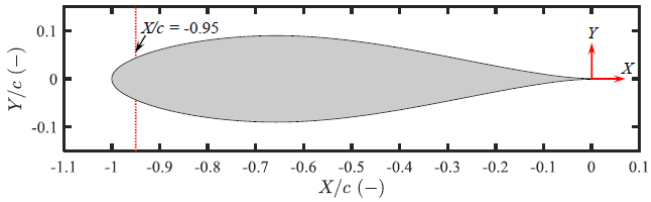

High Reynolds number Model

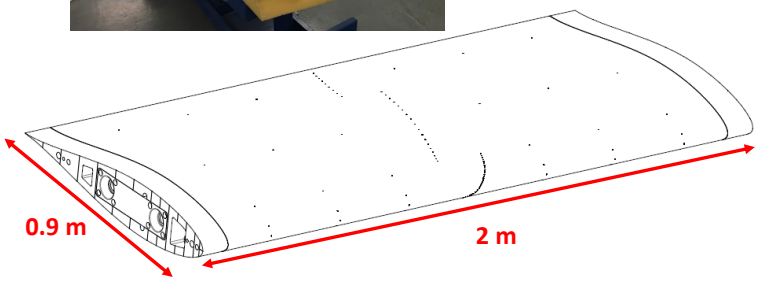

Serration geometries

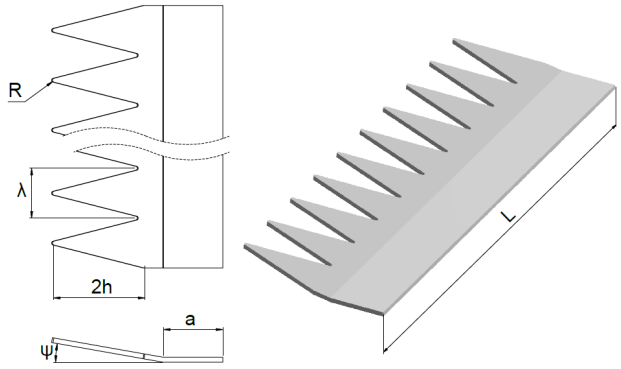

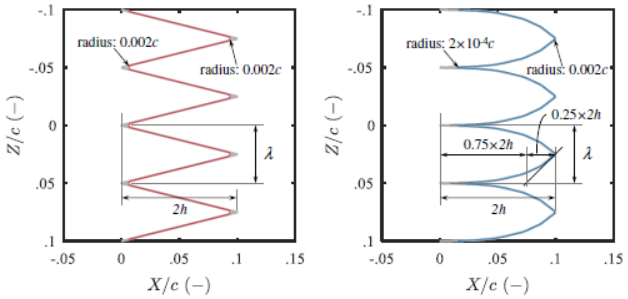

Name	S0	S4	SI
type	Saw-tooth	Saw-tooth	Iron
Height (2h)	0.1 chord	0.1 chord	0.1 chord
Wavelength ()	h	h	h
Flap angle ()	0 deg	4/8 deg	0 deg

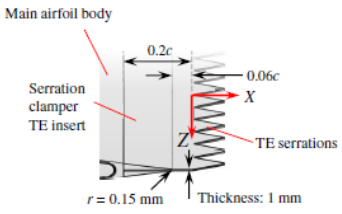

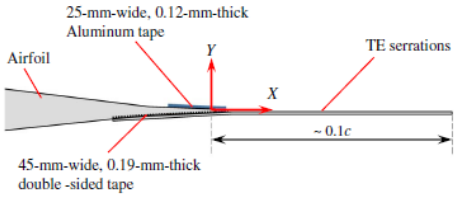

Facility and measurement overview (Update with TU Berlin)

Low Reynolds number Facilities

Facility		Test section						Model			Measurements					
Name	Institution	Hard wall	Kevlar wall (anechoic)	Kevlar wall (integrated)	Open jet	Test section size [HxW] m	Max free stream velocity (m/s)	chord length [m]	span [m]	Serrations	aerofoil pressure ports	wake rake	Surface Microphones	Boundary layer (HW, PIV or BLPR)	Parabolic mirror (far field)	Microphone array (far field)
A-Tunnel (AT)	TUD				X	0.4 x 0.25/0.7	75/35	0.2	0.4	X	X	X		X		X
Aeroacoustic Wind Tunnel Braunschweig (AWB)	DLR				X	1.2 x 0.8	65	0.2		X	X				X	X
Aeroacoustic Wind Tunnel Facility (AF)	Utwente	X	X		X	0.7 x 0.9	60	0.2	0.7		X		X			X
Aeroacoustic Wind Tunnel Berlin	TUB				X	0.33 x 0.4	70	0.2	0.4	X	X					X

High Reynolds number Facilities

Facility		Test section						Model			Measurements					
Name	Institution	Hard wall	Kevlar wall (anechoic)	Kevlar wall (integrated)	Open jet	Test section size [HxW] m	Max free stream velocity (m/s)	chord length [m]	span [m]	Serrations	aerofoil pressure ports	wake rake	Surface Microphones	Boundary layer (HW, PIV or BLPR)	Parabolic mirror (far field)	Microphone array (far field)
Low turbulence Tunnel (LTT)	TUD	X		X		1.25 x 1.8	120	0.9	1.25	X	X	X	X	X		X
Low Speed Wind Tunnel Braunschweig (NWB)	DLR	X			X	2.8 x 3.25	90	0.9	2.8	X	X	X			X	X
Poul la Cour Tunnel (PLCT)	DTU	X	X			2 x 3	110	0.9	2.0	X	X	X		X		X
Virginia Tech Stability Wind Tunnel (VTST)	VT	X	X			1.8 x 1.8	80	0.9	1.8		X					X

Low Reynolds number facilities

Aeroacoustic Wind Tunnel Braunschweig (AWB)

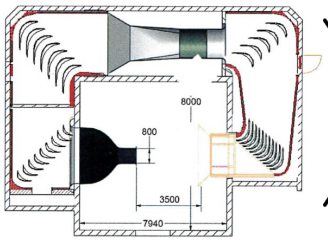

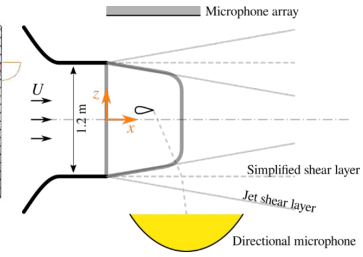

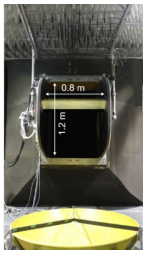

A-Tunnel (AT)

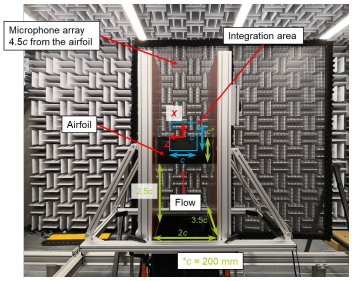

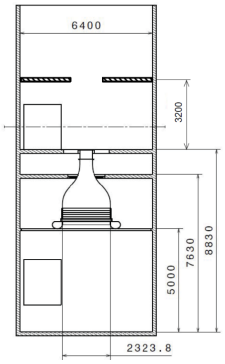

Acoustic Wind Tunnel Facility at Utwente (AF)

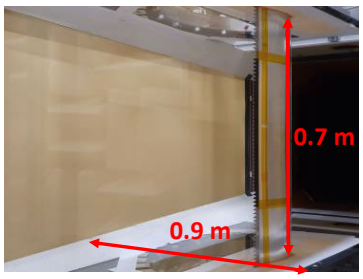

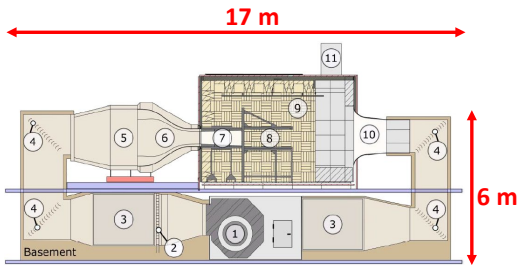

Aeroacoustic Wind Tunnel Berlin

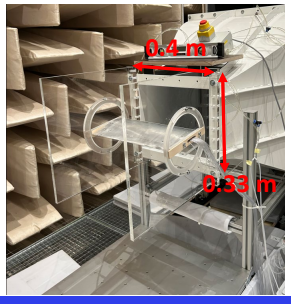

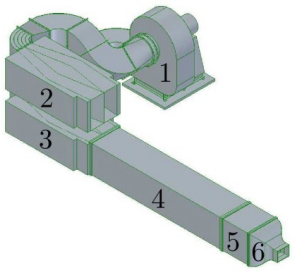

Low Reynolds number team update

- TU Berlin has conducted measurements
- DLR has updated data
- Preliminary comparison is in progress

High Reynolds number facilities

Low Turbulence Tunnel (LTT)

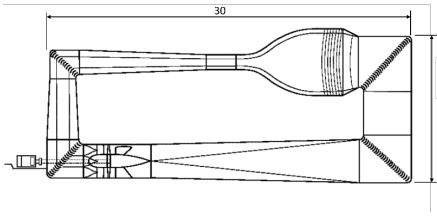

Stability Wind Tunnel (VTST)

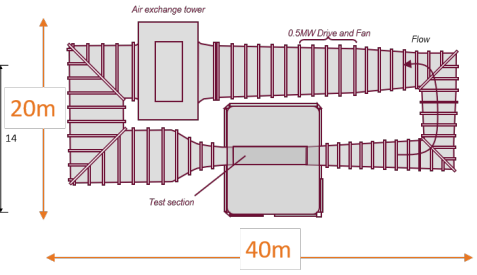

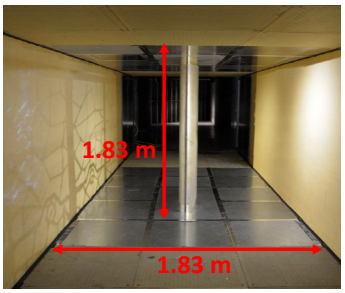

Poul La Cour Wind Tunnel (PLCT)

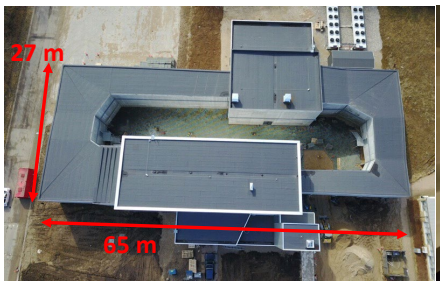

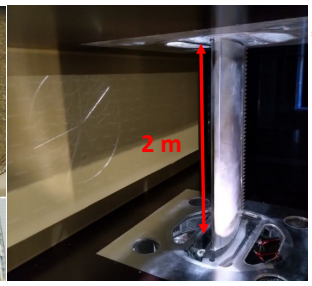

Low Speed Wind Tunnel Braunschweig (NWB)

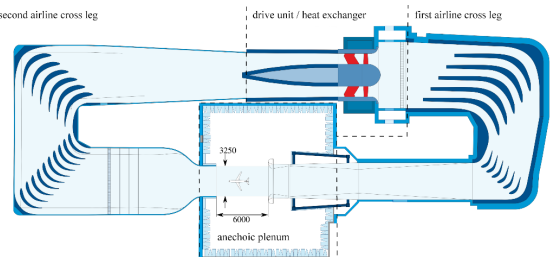

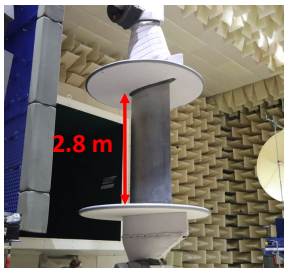

High Reynolds number Team Aerodynamics

VT & PLCT : C_D pressure
LTT & NWB : C_D total

- VT, kevlar, 2M
- VT, kevlar, 3M
- LTT, hardwall, 2M
- LTT, hardwall, 3M
- LTT, kevlar, 2M
- LTT, kevlar, 3M
- NWB, hardwall, 1.96M
- NWB, hardwall, 2.96M
- NWB, anechoic, 1.96M
- NWB, anechoic, 2.96M
- PLCT, kevlar, 2.13M
- PLCT, kevlar, 3.25M

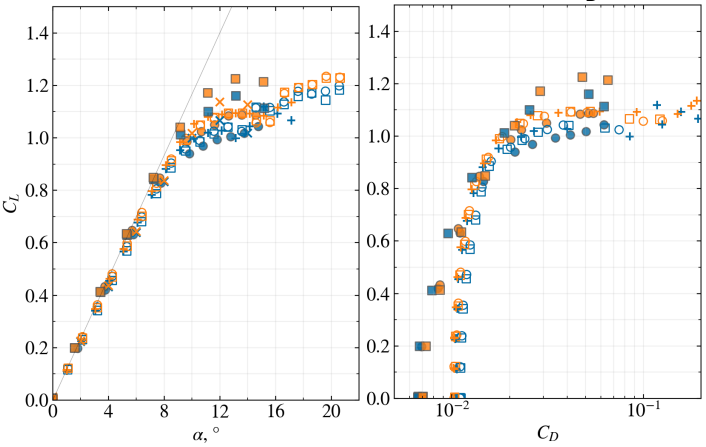

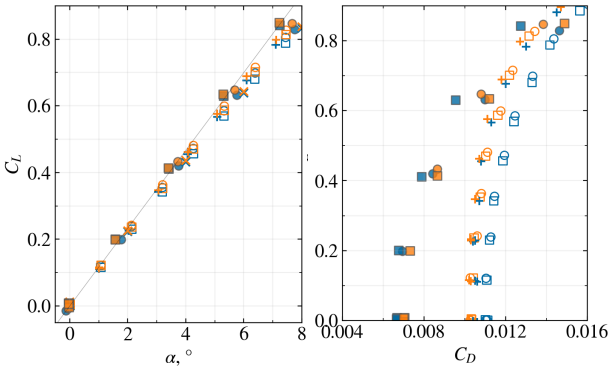

High Reynolds number Team Acoustics

Hardware	Data acq.	Data processing
140 mic array ½" LinearX mics	t = 30 sec fs = 100 kHz Δf = 25Hz	• Conv. Beamforming + CleanSC • 50% overlap, Hanning window • 2d shear layer corr. • Diagonal removal
Elliptical acoustic mirror, ¼" B&Kmic		• Schlinker correction method (1977)

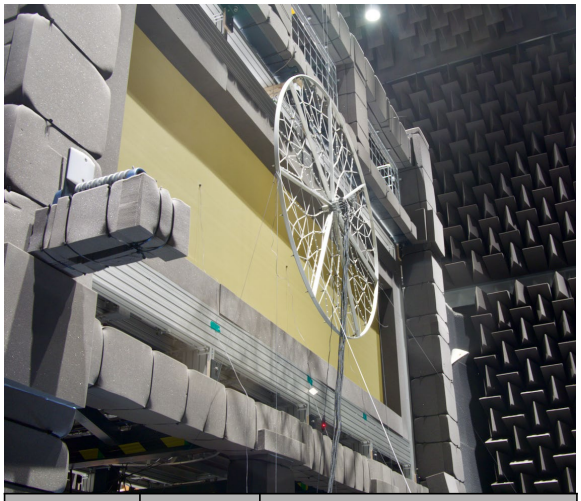

Hardware	Data acq.	Data processing
84 mic array ¼" B&K mics	t = 25 sec fs = 16 kHz Δf = 4Hz	• Conv. Beamforming • 50% overlap, Hanning window • 3d shear layer corr. • Diagonal removal

Hardware	Data acq.	Data processing
251 mic array ¼" GRAS mics	t = 32 sec fs = 51.2 kHz Δf = 6.25Hz	• 126 mics sub-array used • Conv. Beamforming +SiPP • 50% overlap, Hanning window • 3d shear layer corr. • Diagonal removal

Baseline vs Serration, CL=0, Classical Beamforming

NWB / DTU / VT, Trip 5/5

NWB-Array

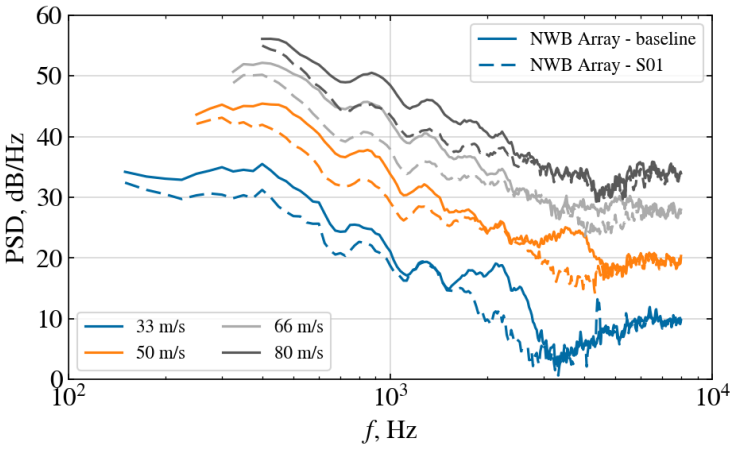

DTU-Array, VT-Array

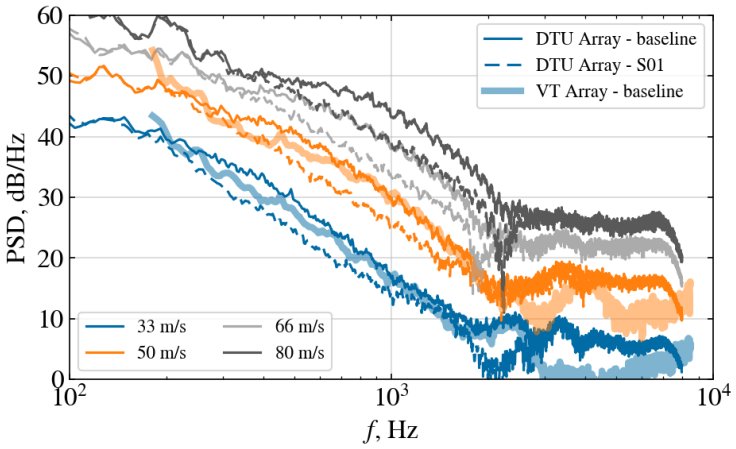

Baseline vs Serration, CL=0, CLEAN-SC

NWB / DTU / VT, Trip 5/5

NWB-Array

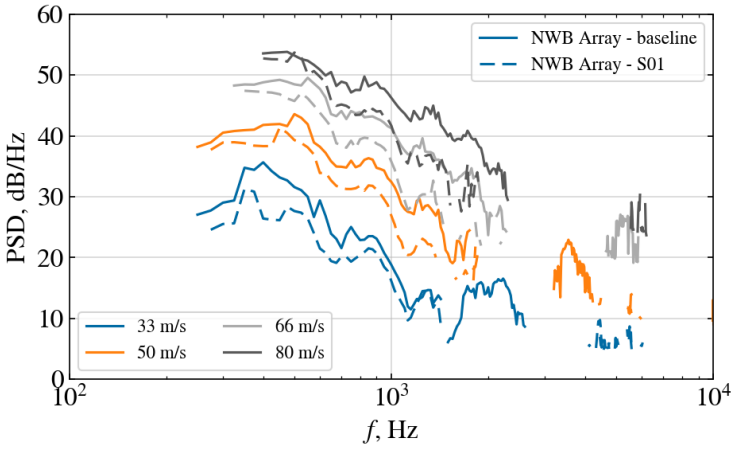

DTU-Array, VT-Array

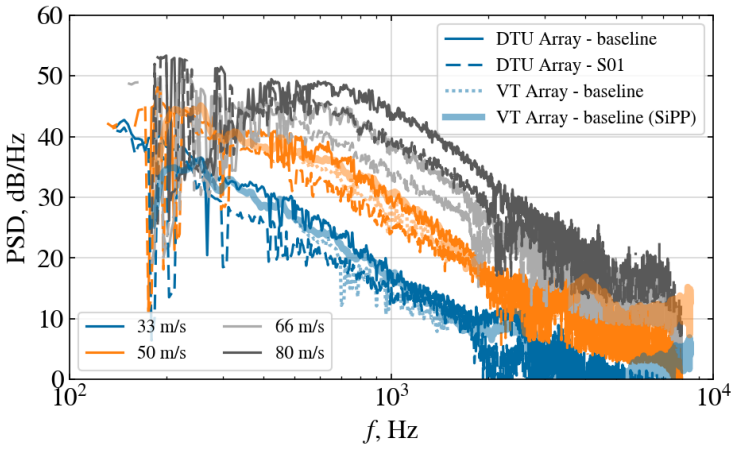

Baseline vs Serration, CL=0.5, Classical Beamforming

NWB / DTU / VT, Trip 5/5

NWB-Array

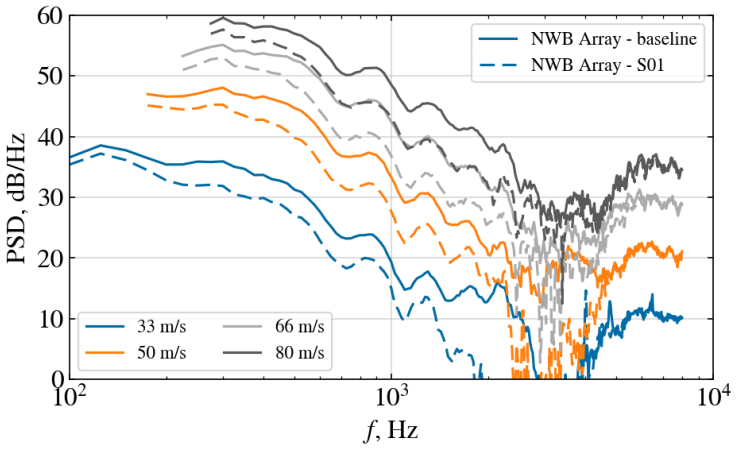

DTU-Array, VT-Array

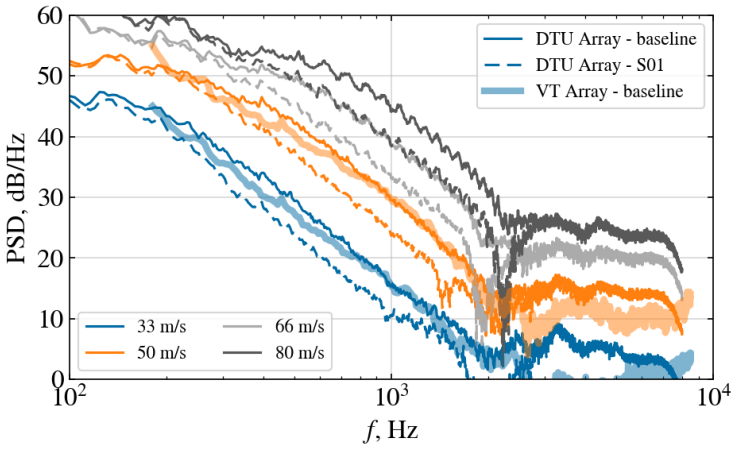

Baseline vs Serration, CL=0.5, CLEAN-SC

NWB / DTU / VT, Trip 5/5

NWB-Array

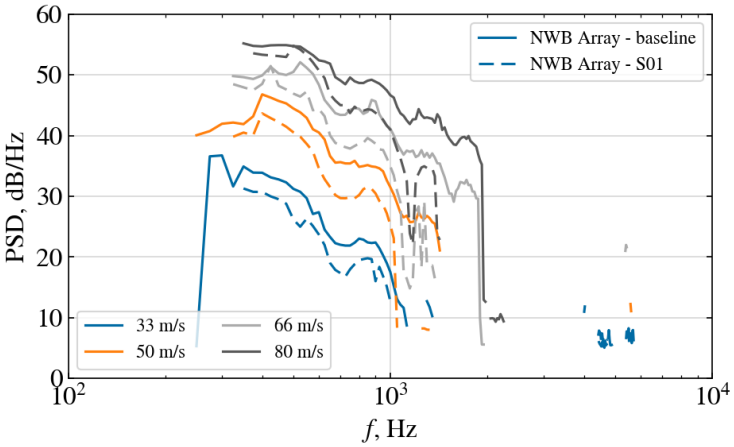

DTU-Array, VT-Array

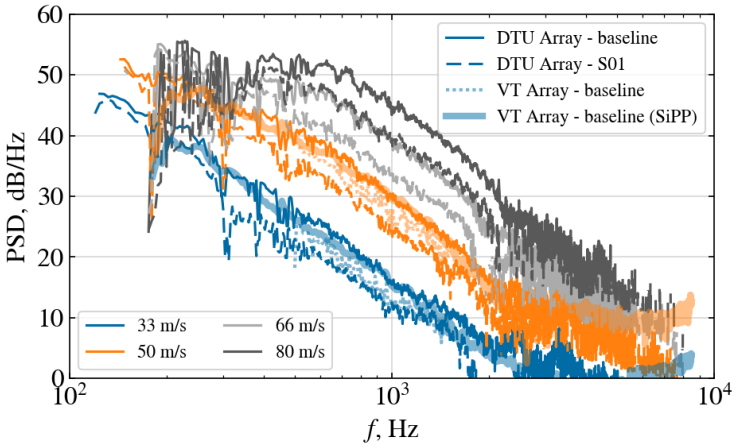

Noise Reduction, CL=0

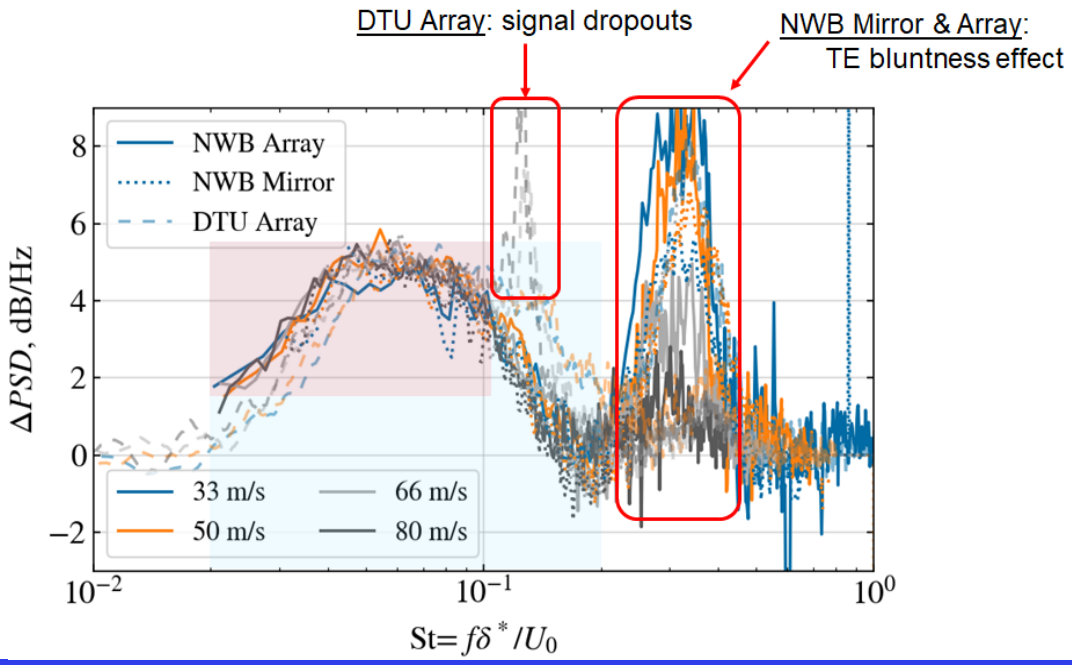

Source power integration area:

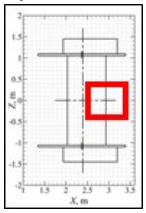

δ*: suction side displacement thickness (XFOIL)

NWB: Classical beamforming after BGN removal

DTU: Classical beamforming

Noise Reduction, CL=0.5

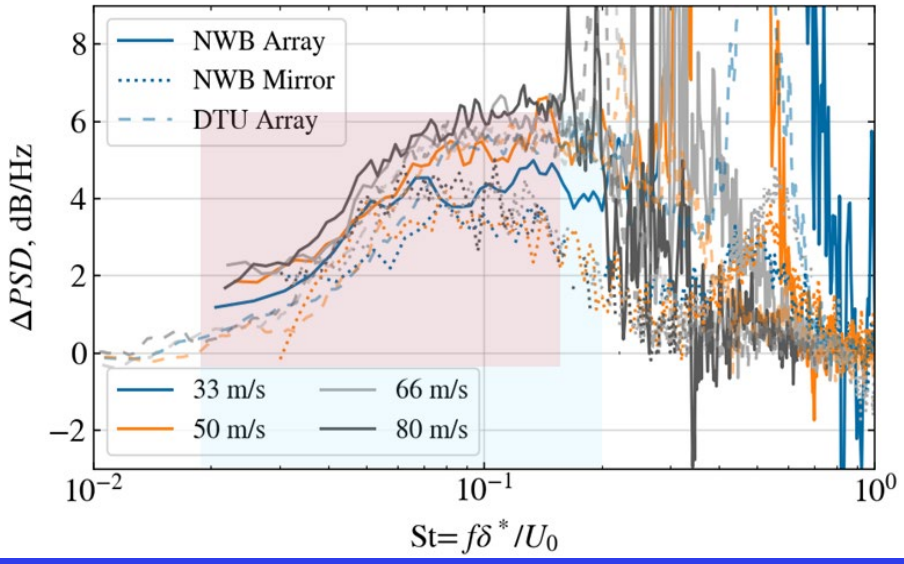

Source power integration area:

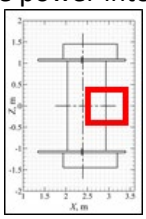

δ*: suction side displacement thickness (XFOIL)

NWB: Classical beamforming after BGN removal

DTU: Classical beamforming

Conclusions

- New high quality validation data for Reynolds numbers up 6 million and Cl = 0.5
- Maximum deviation of the SPL below 3 dB using delay and sum beamforming, but better in a large frequency range
- Clean-SC further decreases deviations
- Scalability of the noise reduction through serrations
- TU Berlin joined the benchmark team (now 6 institutions)
- New participants are welcome
- The teams is working towards a (or several) publications

Funding sources

- The current work is part of Task 39 "Quiet Wind Turbine Technology", an initiative within the Technology Cooperation Programme (TCP) by the International Energy Agency (IEA).

- The authors would like to thank the German Federal Ministry for Economic Affairs and Climate Action (BMWK) for supporting the operation of this task.

- The authors would like to thank the Danish Energy Agency for funding the participation of the Technical University of Denmark in the IEA Task 39 under the programme "Energiteknologiske Udviklings- og Demonstrationsprogram (EUDP)", Journal number 134-21022.

9 WP2 / Annex 5 - Conference proceedings on measurement of tip noise

INCEEUROPE

10th International Conference
on
Wind Turbine Noise
Dublin – 21st to 23rd June 2023

Experimental investigation of noise from a wall-mounted swept tip blade in a wind tunnel

Oliver Lylloff, Department of Wind and Energy Systems, Technical University of Denmark (DTU), Frederiksborgvej 399, DK-4000 Roskilde: ollyl@dtu.dk
Andreas Fischer, Department of Wind and Energy Systems, Technical University of Denmark (DTU), Frederiksborgvej 399, DK-4000 Roskilde.

Summary

A wall-mounted swept tip segment of a wind turbine blade (tip model) is tested in an acoustic Kevlar-walled wind tunnel at free stream velocities ranging from 20 to 80 m/s (corresponding to chord-based Reynolds numbers $4.9 \cdot 10^5$ to $2.0 \cdot 10^6$). The tip model used is the result of a design optimization focused on tip extensions for wind turbine blade upscaling. The trailing edge and tip vortex noise spectra are determined by integration of acoustic images generated with a microphone array using beamforming techniques. Aerodynamic lift and drag coefficients are determined from 128 surface pressure tabs on the model and related to the acoustic results. The results indicate, that tip vortex noise is dominant at high angles of attack (corresponding to high lift coefficients) and low flow-speeds. At higher flow speeds, trailing edge noise is the dominant source of acoustic output. This suggests, that tip vortex noise is important to take into account when wind turbines are operating in low wind speeds or noise curtailment. Additionally, the acoustic spectra dependence on velocity is estimated for trailing edge and tip vortex noise. The results indicate, that trailing edge noise scales with a power between 5 and 6, and similar for tip vortex noise, but only at high lift coefficients. Despite the special model used, the presented methodology clearly shows the benefit of using acoustic imaging techniques to distinguish noise sources in a wind tunnel, and can pave way for improved tip vortex noise models in the future.

1 Introduction

Wind turbine noise is comprised of different noise generation mechanisms, but the main contributing source is generally considered to be aerodynamic noise from the trailing edge

of the blades. The dominating sources are located at about 80% to 95% of the blade radius, where flow velocities are highest [1]. Therefore, much of the research conducted on wind turbine noise has focused on two-dimensional trailing edge noise, where the noise is considered to scale with the flow speed to a power of 5. Trailing edge serrations are nowadays widely used in the industry to decrease the overall sound emission of a wind turbine [2].

Tip vortex noise (tip noise) was not considered as a dominant noise mechanism on modern wind turbines. It was already in the 1990s demonstrated that it could be reduced by gradually reducing the chord length towards the tip [3], [4] as shown in Figure 1. However, since trailing edge noise is mitigated more and more successfully, tip noise might become relevant again for modern wind turbine designs. As it has not been relevant in the last 20 years there are not many engineering models to predict tip noise available (one example of such a model is the one by Brooks, Pope, and Marcolini [5]) and relevant data sets to develop such a model for modern wind turbines are rare. Hence, the goal of this study is to provide an experimental methodology based on wind tunnel tests, that can lead to tip noise model validation.

Early experimental work on airfoil tip noise and models was done in refs. [6], [7] on a NACA0012 airfoil at low Reynolds numbers. The studied flow conditions are insufficient for modelling modern day wind turbines [8], but the experimental methodology has proven very useful. In the study by Brooks and Marcolini [7], tip noise was obtained by 'subtracting' 2D and 3D airfoil noise spectra (both should produce similar TE noise). At zero-lift ($\alpha = 0$), tip noise was assumed to be negligible, hence 2D and 3D noise spectra should be similar, and a fair agreement was observed, when corrected for different span-lengths. An interesting outcome of the study was, that the noise power scaling law, known for trailing edge noise, was not observed for tip noise [7]. These early studies was later included in the so-called BPM model [5], which is well-know for predicting trailing edge noise. In a more recent study [9], also on a NACA0012 airfoil, the BPM model predictions for tip noise are found to agree with measurements at higher Reynolds numbers, but only at low frequencies. The study proposed an empirical model extension to BPM that agrees better with measurements. A tip noise scaling law of flow speed to power 7.5 was found but a physical interpretation was not evident [9]. An extensive study on different airfoil tip models are given in refs. [10], [11], which couples noise measurements with flow visualizations (PIV). A summary of studies on tip noise in wind tunnels are given in Table 1.

This paper is structured as follows. In Section 2, the wind tunnel, experimental setup, post-processing techniques, and the tip model are described. In Section 3, the aerodynamic and acoustic results are shown. Aerodynamic lift and drag coefficients are determined, and the acoustic spectra, images and scaling properties are studied. The results and methodology are discussed in Section 4 and conclusions are given in Section 5.

2 Methods

In this section, a description of the wind tunnel and measurement methods are given.

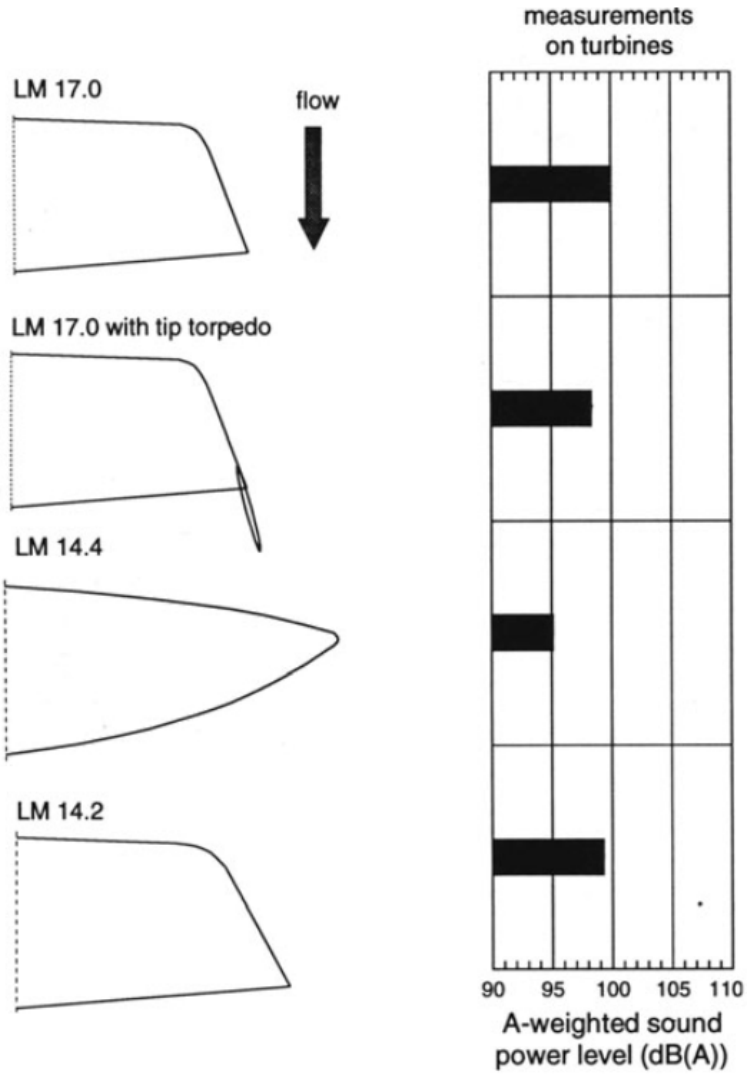

Figure 1: Illustration from [3].

2.1 Poul la Cour Tunnel

The Poul la Cour Tunnel (PLCT, Technical University of Denmark (DTU), Risø Campus, Roskilde, Denmark), is a university-owned wind tunnel dedicated to wind energy research. It was commissioned in 2018 and is capable of both aerodynamic and aeroacoustic measurements. The wind tunnel is comprised of a closed-loop airline with acoustic absorbent treatment and a fan with a nominal power of 2.4 MW. A maximum flow speed of 105 m/s can be achieved in the test section. The test section dimensions are $2 \times 3 \times 9$ m (H$\times$W$\times$L) and it has interchangeable side walls: Hard walls in aerodynamic configuration, and tensioned Kevlar walls in acoustic configuration. The later is utilized in this study. The design of the acoustic setup was inspired by the Virginia Stability wind tunnel [14]. The benefit of the Kevlar-walled configuration is that sound from the test item can transmit almost unhindered through the Kevlar wall and be captured by acoustic equipment, while the flow

Airfoil(s)	Tip shape	Re [-]	U_0 [m/s]	Ref.
NACA0012	Flat & round		40, 70	[7]
NACA0012	Flat & round		?	[5]
NACA0012	Flat	$8.0 \cdot 10^5 - 1.6 \cdot 10^6$	$30 - 60$	[9]
NACA0012 & NACA0018	Flat	$2.3 \cdot 10^5 - 3.3 \cdot 10^5$	35,50	[12]
Unknown type	Flat	$3.0 \cdot 10^5 - 1.1 \cdot 10^6$	$30 - 100$	[13]
8 different NACA	Flat and round	$1.0 \cdot 10^5 - 2.3 \cdot 10^5$	$5 - 50$	[11]
Custom design	Round	$4.9 \cdot 10^5 - 2.0 \cdot 10^6$	$20 - 80$	This study

Table 1: Previous work on tip noise in wind tunnels.

is retained inside the test section, and only small corrections are needed compared to an open-jet configuration [15]. Surrounding the test section is an anechoic room with a free-field condition that was tested according to ISO 3745 [16]. It is close to an ideal free field above frequencies of 125 Hz. However, in the frequency range between 200 Hz and 3150 Hz the deviation from ideal free field conditions is $\pm$ 2 dB which is slightly higher than allowed according to ISO 3745.

2.2 Microphone array methods

Acoustic measurements are conducted with an 84-channel microphone array (1/4" B&K Type 4985) situated in the anechoic room, outside the test section at a distance of 2.3 m from the tip model. Acoustic images are computed with conventional frequency-domain beamforming [17], denoted Delay-and-sum (DAS), and Clean-SC [18]. Source integration is used to extract acoustic spectra from three different spatial regions (see Fig. 2). The trailing edge and tip integration regions are 0.5 m wide (chord-wise) and 0.8 m high (span-wise). The airfoil integration region is 1.5 m by 1.6 m. The integration regions are positioned 0.2 m from ceiling and floor to reduce the influence of junction noise and reflections from the floor. The resulting integrated spectra from each of the regions are normalized to 1 m span.

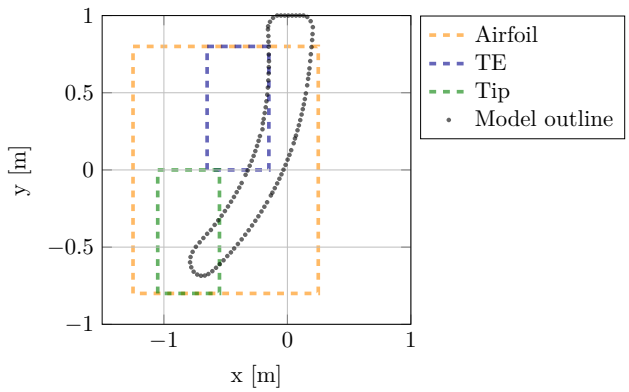

Figure 2: Integration regions used in the study. Flow direction is right to left.

The two different post-processing techniques, DAS and Clean-SC, have different use-cases. To illustrate this, an example of the spectra produced by the two methods (using the trailing edge integration region shown in Fig. 2) are shown in Fig. 3. In a broad frequency range, between 800 Hz and 3000 Hz, there is good agreement. At lower frequencies, DAS produces higher levels, due to a poor resolution of the acoustic images. The spectral shape, however, is very smooth compared to Clean-SC. At higher frequencies (above 4000 Hz), Clean-SC shows a fluctuating behavior, that is likely due to background noise. In the following, Clean-SC is used for computing integrated spectra, while DAS is used to show acoustic images.

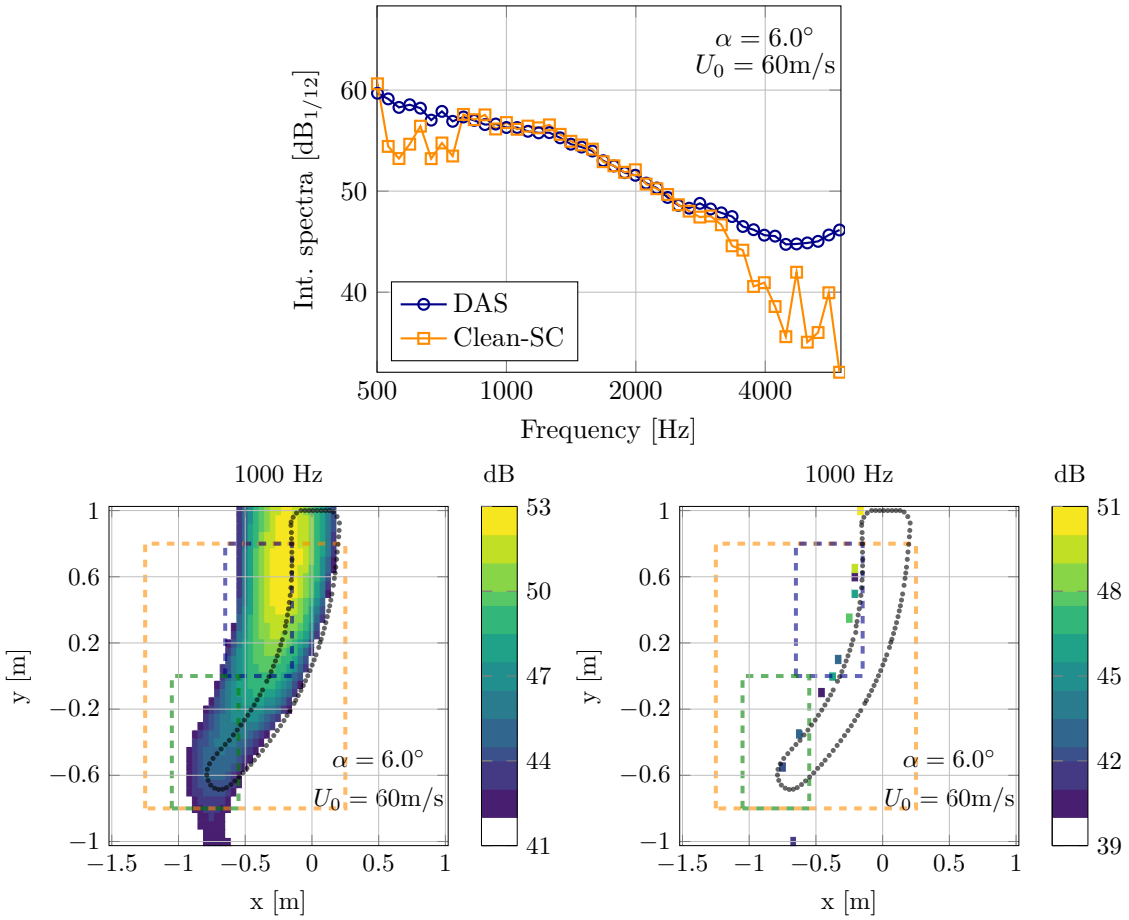

Figure 3: Comparison of post-processing techniques. Top: Integrated spectra. Bottom left: DAS acoustic image. Bottom right: Clean-SC acoustic image.

2.3 Blade tip model

The swept blade tip model [19] (See Fig. 4), was chosen because of its availability. The swept design was the result of an aeroelastic optimisation within load constraints. It is not representative of the blade tip of modern wind turbines, but the tip noise mechanism is the same as for a more traditional design.

The root section of the model was covered by a fairing (see Fig. 4b) to reduce the noise source at the junction of the model and the wind tunnel ceiling, because such a noise source would not be present on a wind turbine blade. Additionally, if the junction noise source was not reduced, it might influence the tip noise levels at low frequencies when the resolution of the microphone array is poor.

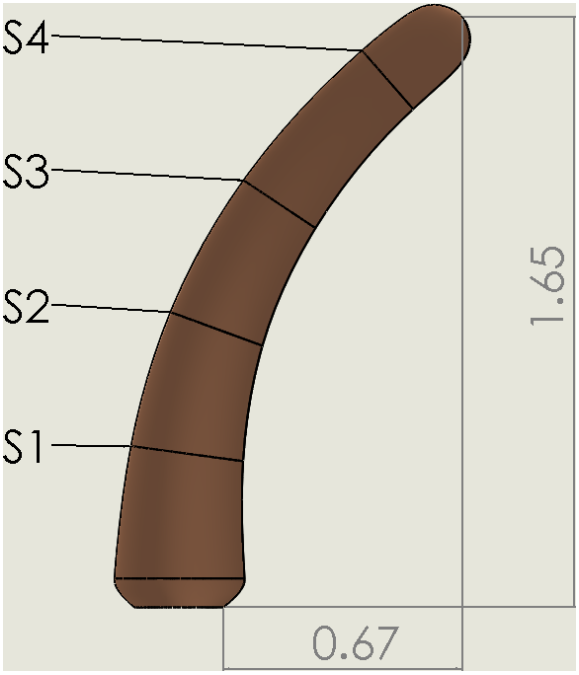

(a) Model sketch of airfoil. The model was mounted in the ceiling of the wind tunnel, hence it appears upside-down in subsequent figures. Flow direction is left to right.

(b) Picture of airfoil model in tripped configuration mounted in wind tunnel test section with fairing at root.

Figure 4: Swept blade tip model.

3 Results

In this section, the aerodynamic and acoustic results of the tested configurations are presented. In Table 2 an overview of the experimental data collected is given. The angle-of-

Configuration	AoA [deg.]	Re [-]	U_0 [m/s]
Tripped	$-20:2:20$	$4.9 \cdot 10^5$	20
Tripped	$-20:2:20$	$9.7 \cdot 10^5$	40
Tripped	$-14:2:20$	$1.4 \cdot 10^6$	60
Tripped	$-14:2:18$	$2.0 \cdot 10^6$	80

Table 2: Tested configurations in this study.

attack and aerodynamic coefficients presented in the following are uncorrected and computed only for the root-segment of the blade (the section below the ´S1´ line in Fig. 4a). A standard 2D aerodynamic Kevlar-wall correction [20] is insufficient for the analysis the swept tip blade used in this study. For future work, a 3D correction as the one described in ref. [21] would be relevant for this use case.

3.1 Aerodynamic results

The lift coefficient as function of angle-of-attack (AoA) and lift over drag are shown in Figure 5. In the following results, three particular cases are chosen to couple the acoustic

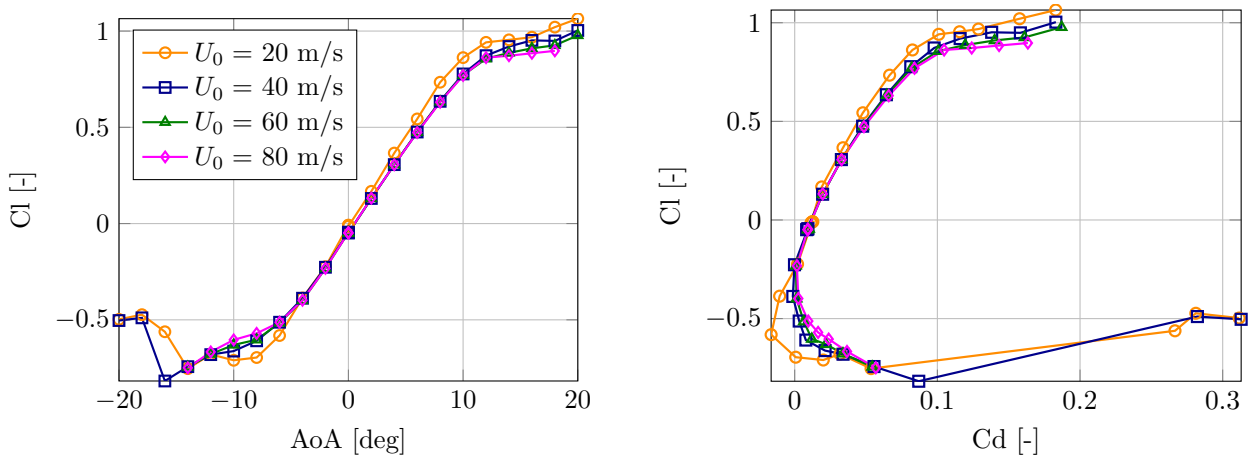

(a) Lift coefficient C_l as function of angle-of-attack (AoA).

(b) Lift over drag.

Figure 5: Aerodynamic results.

and aerodynamic results: A case with attached flow ($C_l = 0.5$, AoA $= 6°$), a case with partly stall behavior ($C_l = 0.8$, AoA $= 10°$), and a case in deep stall ($C_l = 1.0$, AoA $= 14°$).

3.2 Acoustic results

Acoustic images are shown in Figs. 6 to 8 and noise spectra captured from spatial integration of the acoustic images are shown in Figs. 9 to 11.

The three cases considered are: Attached flow $C_l = 0.5$ (shown in Fig. 6), partly stall $C_l = 0.8$ (shown in Fig. 7), and deep stall $C_l = 1.0$ (shown in Fig. 8). Comparing the different acoustic images, it is clear, that in the attached flow case, trailing edge noise is becoming increasingly dominant for increasing flow speed. However, one exception is at $U_0 = 20\,\mathrm{m/s}$, where the tip noise source is pronounced at higher frequencies. This is also observed in the integrated spectrum in Fig. 9. At increasing angle-of-attack, going into partly stall, the tip noise source is more prominent in the acoustic images (Fig. 7), particularly towards higher frequencies. Although at 1000 Hz, trailing edge noise is still dominant at $U_0 = 80\,\mathrm{m/s}$. Moving to deep stall (Fig. 8), the noise sources are more evenly distributed along the airfoils trailing edge, except at $U_0 = 20\,\mathrm{m/s}$, where a tip noise source is still present. The same trends are observed in the integrated spectra in Fig. 10 and

Fig. 11. Interestingly, in the case for partly stall, the cross-over frequency where tip noise becomes more dominant than trailing edge noise is moving as function of flow speed. At $U_0 = 20\,\mathrm{m/s}$ it is 700 Hz, at $U_0 = 40\,\mathrm{m/s}$: 1200 Hz, $U_0 = 60\,\mathrm{m/s}$: 2000 Hz, and at $U_0 = 80\,\mathrm{m/s}$ it is 3000 Hz (see Fig. 10).

3.2.1 Overall Integrated Spectrum Level

The general trends observed in the acoustic images and integrated spectra, in the previous section, can be summarized by computing overall integrated spectrum levels (OAISL) by a summation of integrated spectra (from Clean-SC) of the three difference spatial regions (airfoil, trailing edge, and tip) in the frequency range 0.5 kHz-5 kHz. Results are shown in Fig. 12 as function of C_l. This metric allows for a direct coupling between aerodynamic and acoustic observations, but lacks the frequency dependence that was described in the previous section. In general, tip noise is only dominant at $U_0 = 20\,\mathrm{m/s}$ and $C_l > 0.7$. However, when going into deep stall, trailing edge noise again dominates. At $U_0 = 40\,\mathrm{m/s}$ this tendency is vaguely observed, but tip noise is generally $3 - 5$dB lower. At higher flow speeds, tip noise is more than 10 dB lower than trailing edge noise.

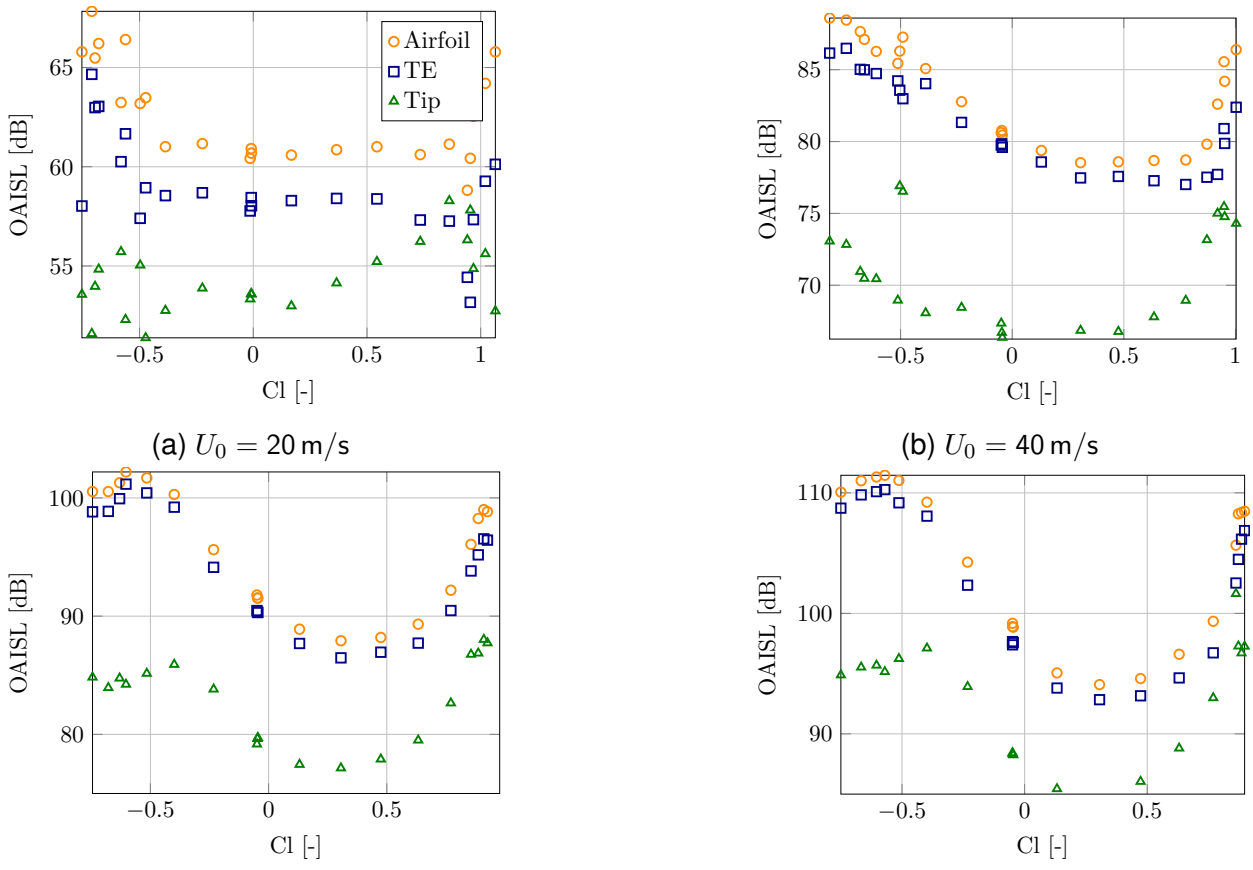

(a) $U_0 = 20\,\mathrm{m/s}$ (b) $U_0 = 40\,\mathrm{m/s}$

(c) $U_0 = 60\,\mathrm{m/s}$ (d) $U_0 = 80\,\mathrm{m/s}$

Figure 12: Overall Integrated Spectrum Level (OAISL) computed from integrated spectra using Clean-SC in frequency range 0.5 kHz-5 kHz.

3.2.2 Velocity scaling

Using the overall integrated spectrum level (OAISL), computed above, the velocity scaling is assessed. Results and regression lines for the three flow cases considered, are shown in Fig. 13.

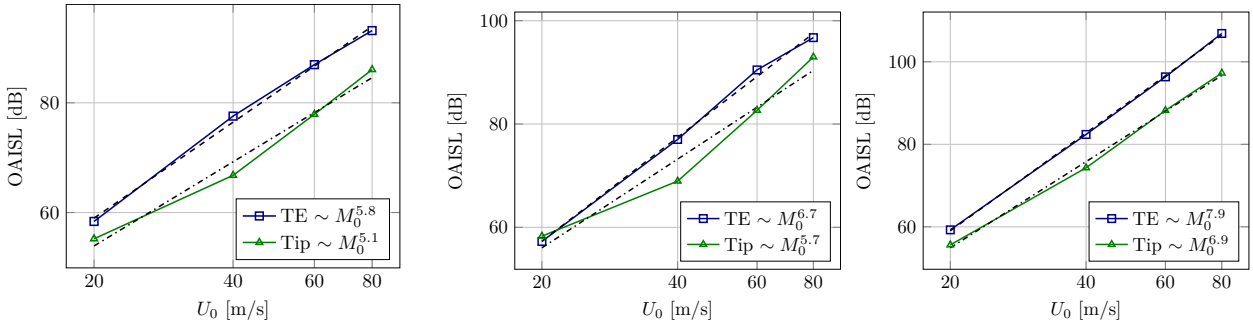

(a) Scaling at $C_l = 0.5$. (b) Scaling at $C_l = 0.8$. (c) Scaling at $C_l = 1.0$.

Figure 13: Velocity scaling at three different C_l values and regression lines as function of free-stream Mach number M_0.

With a limited set of data points, regression lines are subject to large uncertainty, but the observed tendency is an increase in power coefficient as function of C_l. The trailing edge noise of a extruded aerofoil section scales with the Mach number to the power of 5 under the assumption that the boundary layer turbulence scales with the flow speed to a power of 2 [22]. Brooks and Marcolini [7] empirical found a scaling of the mach number to the power of 5 for tip noise which is in line with our results for attached flow ($C_l = 0.5$). Three dimensional flow effects along the swept trailing edge might cause the difference in scaling of the trailing edge noise compared to classical literature. At $C_l = 0.8$ and $C_l = 1.0$ the flow is partially or fully detached from the model. The high values of the scaling exponent might be caused by this flow condition.

4 Discussion

The acoustic imaging technique has proven to be a useful tool for identifying different noise generation mechanisms on a blade tip model. Developments in wind tunnel design and post-processing methods, over the last couple of decades, have improved the acoustic image resolution greatly, to an extent where small details can be studied with high precision. These developments also put extra weight on the choice of acoustic imaging technique. In this study, DAS and Clean-SC was chosen, which are two well-known and established methods within the acoustic imaging community, and their mutual benefits and disadvantages were briefly described. But there are other methods available, that might be relevant for this particular use case, e.g., [13]. One issue is the poor resolution at lower frequencies, which is somewhat solved by using Clean-SC. In the acoustic images, e.g., Fig. 6 at 1000 Hz, reflections from the floor is seen to extend into the tip integration region. This effect is even stronger at lower frequencies, which can lead to overestimated levels.

The choice of integration regions is another point that could be relevant to study in future work. In this study, equally-sized rectangular regions were placed approximately over the trailing edge and tip sections, but smaller regions shaped to the curvature of the model is another possibility. The effects of such regions have not been studied in the literature, and it is unclear if it has a benefit over the conventional rectangular regions. One possible future development could be a more direct coupling between the acoustic integration regions and aerodynamics of individual sections of the model, e.g., using the segments shown in Fig. 4a.

The aerodynamic properties of the root segment of the tip model was used throughout this study. It is quite certain, that the flow properties on the segment near the tip is different than the segment at the root, and therefore the coupling between the aerodynamic and acoustic results are subject to some degree of uncertainty. To eliminate this uncertainty, future wind tunnel work on blade tip noise should use a more representative wind turbine blade tip, such as the design ”LM 14.4” shown in Fig. 1.

In the section about velocity scaling, a simple power law regression line was used to estimate the power coefficient, under the assumption that the Mach number is the only dependent variable. This might be true for trailing edge noise, but it is not evident that this is also the case for tip noise. For instance, the empirical model developed in ref. [9] has additional dependent variables.

5 Conclusion

An experimental wind tunnel methodology for investigation of blade tip noise was presented. Acoustic images produced with a microphone array and state-of-the-art post-processing techniques were used to extract noise from the trailing edge and tip regions of the blade. The acoustic spectra were compared at different flow velocities and angles of attack and related to the aerodynamic flow properties. It was found, that tip noise is dominant at low flow speeds, and at high angles of attack, corresponding to lift coefficients above 0.7. At higher flow speeds, tip noise is only dominant in the high frequency range. The coupling between acoustic results and the aerodynamic properties could be further improved in future work by implementing a 3D Kevlar-wall corrections, as described in ref. [21], and computing flow properties on individual segments of the blade tip model. Knowledge of the boundary layer properties could shed further light on the complex coupling between aerodynamics and acoustics, and be investigated with, e.g., a hot-wire probe.

With the increasingly successful mitigation of trailing edge noise, tip noise might be the next dominant noise source to tackle in future wind turbine design, and with the presented methodology in this study, the development of new and more precise tip noise models are within reach.

Acknowledgements

The present work is conducted as a sub-task of the IEA Wind TCP research Task 39 (Quiet Wind Turbine Technology). DTU participation was supported by the EUDP project

Jr. nr. 134-21022 funded by the Danish Energy Agency (Energistyrelsen).

References

[1] S. Oerlemans, P. Sijtsma, and B. Méndez López, "Location and quantification of noise sources on a wind turbine," *Journal of Sound and Vibration*, vol. 299, no. 4, pp. 869–883, 2007. DOI: https://doi.org/10.1016/j.jsv.2006.07.032.

[2] S. Oerlemans, "Wind Turbine Noise Mitigation," in *Handbook of Wind Energy Aerodynamics*, B. Stoevesandt, G. Schepers, P. Fuglsang, and Y. Sun, Eds., Cham: Springer International Publishing, 2022, pp. 1447–1462. DOI: 10.1007/978-3-030-31307-4{_}73.

[3] H. Klug, T. Oston, M. V. Lowson, *et al.*, "Aerodynamic noise from wind turbines and rotor blade modification," English, in *International European Union wind energy conference, Gothenburg, Sweden*, 1996, pp. 782–784.

[4] S. Wagner, R. Bareiß, and G. Guidati, *Wind Turbine Noise*. Berlin, Heidelberg: Springer Berlin Heidelberg, 1996. DOI: 10.1007/978-3-642-88710-9.

[5] T. F. Brooks, D. Pope, and M. A. Marcolini, "Airfoil self-noise and prediction," *Nasa Reference Publication*, no. 1218, 1989.

[6] A. R. George and S. T. Chou, "BROADBAND ROTOR NOISE ANALYSES.," *NASA Contractor Reports*, 1984.

[7] T. F. Brooks and M. A. Marcolini, "Airfoil tip vortex formation noise," *AIAA journal*, vol. 24, no. 2, pp. 246–252, 1986.

[8] P. Fuglsang and H. Aagaard Madsen, "Application of aeroaccoustic models to design of wind turbine rotors," English, in *Aero-acoustic noise of wind turbines noise prediction models*, B. Maribo Pedersen, Ed., Technical University of Denmark. Department of Fluid Mechanics, 1997, pp. 39–47.

[9] D. J. Moreau, C. J. Doolan, W. N. Alexander, T. W. Meyers, and W. J. Devenport, "Wall-Mounted Finite Airfoil-Noise Production and Prediction," *AIAA Journal*, vol. 54, no. 5, pp. 1637–1651, May 2016. DOI: 10.2514/1.J054493.

[10] T. Zhang, T. Geyer, C. de Silva, J. Fischer, C. Doolan, and D. Moreau, "Experimental Investigation of Tip Vortex Formation Noise Produced by Wall-Mounted Finite Airfoils," *Journal of Aerospace Engineering*, vol. 34, no. 6, Nov. 2021. DOI: 10.1061/(asce)as.1943-5525.0001315.

[11] T. Zhang, D. Moreau, T. Geyer, J. Fischer, and C. Doolan, "Dataset on tip vortex formation noise produced by wall-mounted finite airfoils with flat and rounded tip geometries," *Data in Brief*, vol. 28, p. 105 058, Feb. 2020. DOI: 10.1016/j.dib.2019.105058.

[12] T. F. Geyer, D. J. Moreau, J. Giesler, P. M. Hall, E. Sarradj, and C. J. Doolan, "Measurement of the noise generated by wall-mounted airfoils of different thickness," in *2018 AIAA/CEAS Aeroacoustics Conference*, American Institute of Aeronautics and Astronautics Inc, AIAA, 2018. DOI: 10.2514/6.2018-3796.

[13] G. R. Yakhina, M. Roger, A. Finez, *et al.*, "Localization of swept free-tip airfoil noise sources by microphone array processing," *AIAA Journal*, vol. 58, no. 8, pp. 3414–3425, 2020. DOI: 10.2514/1.J058231.

[14] W. J. Devenport, R. A. Burdisso, A. Borgoltz, *et al.*, "The Kevlar-walled anechoic wind tunnel," *Journal of Sound and Vibration*, vol. 332, no. 17, pp. 3971–3991, Aug. 2013. DOI: 10.1016/j.jsv.2013.02.043.

[15] S. Glegg and W. Devenport, *Aeroacoustics of low mach number flows: Fundamentals, analysis, and measurement*. 2017, pp. 1–537.

[16] "Acoustics – Determination of sound power levels and sound energy levels of noise sources using sound pressure – Precision methods for anechoic rooms and hemi-anechoic rooms," International Organization for Standardization, Geneva, CH, Tech. Rep., 2012.

[17] D. H. D. H. Johnson and D. E. Dudgeon, *Array signal processing: concepts and techniques*. PTR Prentice Hall, 1993, pp. 1–533.

[18] P. Sijtsma, "CLEAN based on spatial source coherence," *International journal of aeroacoustics*, vol. 6, no. 4, pp. 357–374, 2007.

[19] T. Barlas, G. R. Pirrung, N. Ramos-García, *et al.*, "Wind tunnel testing of a swept tip shape and comparison with multi-fidelity aerodynamic simulations," English, *Wind Energy Science*, vol. 6, no. 5, pp. 1311–1324, Oct. 2021. DOI: 10.5194/wes-6-1311-2021.

[20] A. Fischer, C. Bak, O. Lylloff, *et al.*, "Cross validation of the aerodynamic and acoustic measurements in two Kevlar-walled wind tunnels," *Journal of Physics: Conference Series*, vol. 2265, no. 2, p. 022 103, May 2022. DOI: 10.1088/1742-6596/2265/2/022103.

[21] H. Ura, M. Shigemi, T. Hirotani, and T. Homma, "Wall Interference Correction Method for Kevlar Wall Test Section," *Journal of Aircraft*, vol. 57, no. 5, pp. 889–900, Sep. 2020. DOI: 10.2514/1.C035864.

[22] J. E. F. Williams and L. H. Hall, "Aerodynamic sound generation by turbulent flow in the vicinity of a scattering half plane," *Journal of Fluid Mechanics*, vol. 40, no. 04, p. 657, Mar. 1970. DOI: 10.1017/S0022112070000368.

IEA Wind Task 49
Final Technical Report

APPENDIX - WP3
Noise propagation modelling

Contents

1 Introduction **2**

2 Benchmarking of noise propagation prediction codes for complex terrain **2**
- 2.1 Definition of test-cases . . . 3
- 2.2 Code-2-code comparisons of noise propagation models in complex terrain . . . 3
  - 2.2.1 Results of comparison benchmark between PE and Nord2000 . 3
  - 2.2.2 Publication by DLR/DTU on codes comparison benchmark . . 3
  - 2.2.3 Preliminary comparison with field measurement at Perdigão (DLR dataset) . . . 3

3 Benchmarking of noise propagation prediction codes for flat terrain and offshore conditions **5**
- 3.1 Definition of test-cases . . . 5
- 3.2 Results of the benchmark . . . 5
  - 3.2.1 Effect of low-level jet on noise propagation over water . . . 5
  - 3.2.2 Comparisons between models and offshore noise propagation measurements (KTH dataset) . . . 9
  - 3.2.3 Comparisons between models and onshore noise propagation measurement (Akzeptanz dataset) for flat terrain . . . 12

4 WP3 / Annex 1 - Definition of noise propagation codes benchmark for complex terrain **13**

5 WP3 / Annex 2 - Report on noise propagation code benchmark for complex terrain **21**

6 WP3 / Annex 3 - Conference proceedings on noise propagation codes benchmark for complex terrain **42**

7 WP3 / Annex 4 - Definition of noise propagation codes benchmark for flat terrain and offshore conditions **51**

8 WP3 / Annex 5 - Conference proceedings on noise propagation codes benchmark on flat terrain **58**

1 Introduction

WP3 deals with the benchmark validation of the noise propagation models.

Two main benchmark are defined, but it was extended to additional comparison cases as part of the Task 39 activities.

Firstly, a benchmark case over a complex land is defined and conducted together with other participants. benchmark.

Secondly, a benchmark case of propagation over water at long distances will be defined and carried out where the modelling of water impedance, the discontinuity of impedance from water to land, and wind flow are critical for the prediction of multiple reflections. Possible flow and noise measurement data from IEA participants will be used for the benchmark. Third, after benchmarking validation, an improvement of engineering models, such as the Danish BEK-135 and ISO 9613-2, will be carried out. WP3 is primarily dedicated to the benchmarking and improving of wind turbine noise simulation codes, which was initiated in the 1st phase of the Task 39 (in collaboration with Task 29 - Aerodynamics), and for which a number of unsolved issues remain. In addition, this WP introduces activities related to the prediction of Low-Frequency Noise. Indeed, even if this is a sensitive topic for the public, few thoroughly validated modelling models and publicly available validation data exist.

This report summarizes the results obtained in WP3. It is divided into 2 main activities:

- Benchmarking of noise propagation prediction codes for complex terrain.
- Benchmarking of noise propagation prediction codes for flat terrain and offshore configurations.

2 Benchmarking of noise propagation prediction codes for complex terrain

During this activity, four approaches for noise propagation were considered:

1. The widely used software Nord2000 based on ray tracing theory (developed by FORCE Technology).
2. The Parabolic Equation (PE) method implementation by DTU (Technical University of Denmark).
3. The wave-based model (AKU3D) by DLR (German Aerospace Center).
4. The particle-based model (AKUMET) developed by DLR.

The results of these different activities are reported below either by a technical report, a conference publication, or by a short summary of the activities.

2.1 Definition of test-cases

A document is drafted in order to define the computational conditions for the benchmarking of codes in complex terrain. This document describing the benchmark can be found in Section 5/Annex 2.

2.2 Code-2-code comparisons of noise propagation models in complex terrain

2.2.1 Results of comparison benchmark between PE and Nord2000

A number of commputations were conducted on multiple complex terrain configurations (as defined in Section 4/Annex 1) using the Parabolic Equation method developed by DTU and the well-known Nord2000 software developed by FORCE Technology.

2.2.2 Publication by DLR/DTU on codes comparison benchmark

The reporting for this part of the activities takes the form of a conference publication presented at the Forum Acusticum 2023 conference. The article can be found later in this report (see Section 6/Annex 3) and constitutes one part of the overall project goals.

2.2.3 Preliminary comparison with field measurement at Perdigão (DLR dataset)

In order to investigate the behavior of noise propagation prediction codes in complex terrain for real situations, DLR proposed to share their dataset acquired during the so-called Perdigao experiment. The overarching project is partially funded by the European Union (EU) ERANET+ to provide the wind energy sector with more detailed resource mapping capabilities in the form of a new digital EU wind atlas. A major goal of the Perdigão field project is to quantify errors of wind resource models against a benchmark dataset collected in complex terrain. It included a noise propagation experiment which was conducted by DLR.

DLR provided information concerning the terrain and a database of wind turbine noise measurement is now available online. In order to start a qualitative assessment of the noise propagation, DTU initiated calculation with their Parabolic Equation framework. However, the calculations were rapidly faced with numerical challenges. Indeed, the PE does not behave well for terrain with high slopes, which is one of the characteristics of the Perdigão topography. A solution was found by articifially rotating the calculation domain when considering the actual terrain. This is illustrated in Fig. 1 and it can be observed that inteference patterns are better captured when the calculation domain is rotated. Ultimately, the idea would be to compare the above results with the predictions calculated by DLR in Fig. 2.

Unfortunately, it proved difficult to conduct more qualitative comparisons between models and measurement data. DLR is still working on the processing of the data in order to be able to do this type of comparisons.

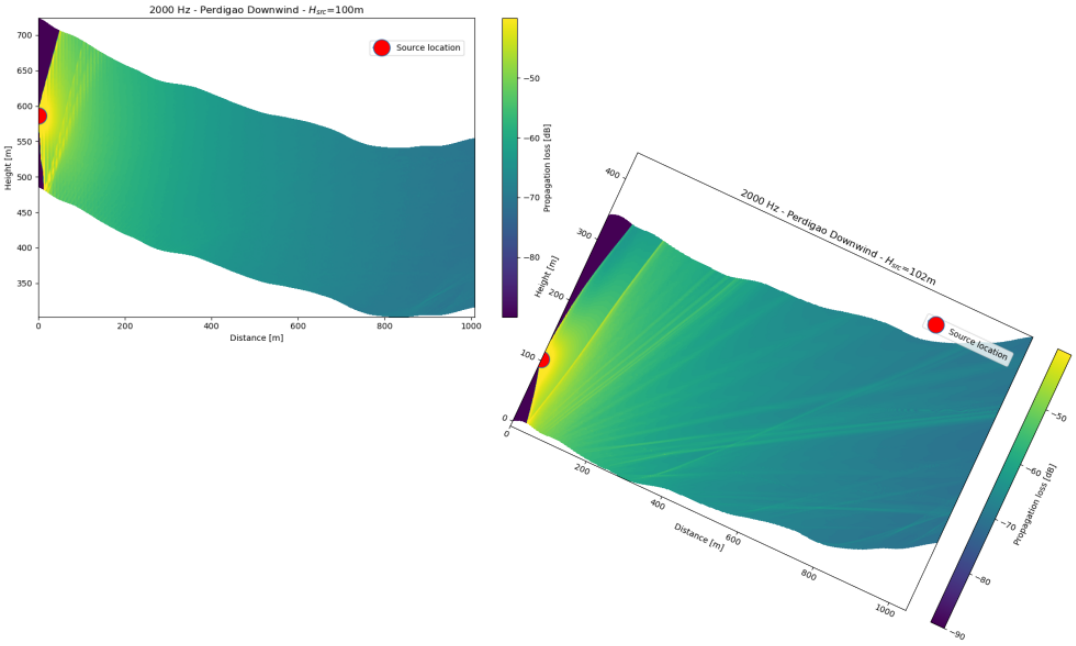

Figure 1: Noise propagation loss map at the Perdigão test site as computed with the PE method for a frequency of 2000 Hz. The map on the left is done with the calculation domain following the actual horizontal condition, while the map on the right is conducted by rotating the caculation domain by 24 degs in order to better align the numerical horizontal direction with the terrain slope and reduce numerical errors.

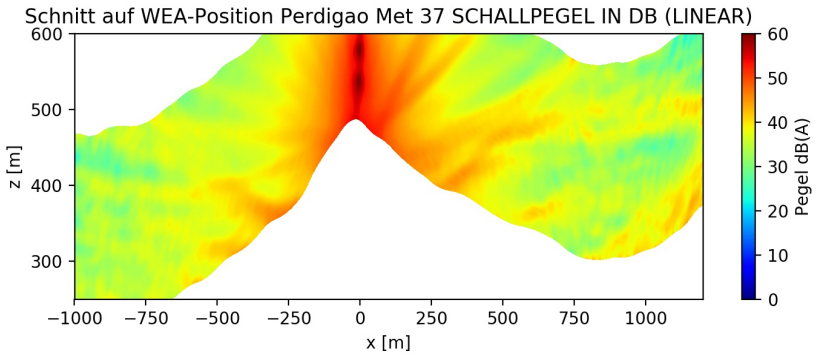

Figure 2: Noise propagation loss map at the Perdigão test site as computed by DLR prediction framework, including turbulence.

3 Benchmarking of noise propagation prediction codes for flat terrain and offshore conditions

During this activity, four approaches for noise propagation were considered:

1. The widely used software Nord2000 based on ray tracing theory (developed by FORCE Technology).
2. The Parabolic Equation (PE) method implementation by DTU (Technical University of Denmark).
3. The Parabolic Equation (PE) method implementation by LUH (Leibniz University Hannover).
4. The Parabolic Equation (PE) method implementation by KTH (Royal Institute of Technology Stockholm).
5. The LEE method implementation by Aachen.

3.1 Definition of test-cases

This activity consists in drafting a document defining the computational conditions for the benchmarking of codes for flat terrain and offshore condition. The document corresponding to this work, corresponding to a technical report, can be found in Section 7/Annex 4.

3.2 Results of the benchmark

3.2.1 Effect of low-level jet on noise propagation over water

As defined in Section 7/Annex 4, a series of wind speed profiles are defined in order to investigate their effect on long range propagation (over water). The different wind speed profiles are displayed in Fig. 3, three of them are intended to reproduce extreme weather conditions, with a phenomenon named low-level jet.

The transmission losses for four specific frequencies (250, 500, 1000 and 2000 Hz) up to 5 kms are displayed in Fig. 4. It can be seen that the effect of the low-level jets are quite similar to each other and only differ at very large distances. The differences with a classical power-law profile are also relatively modest.

However, a recent publication shown that much more extreme low-level jet conditions should be chosen in order to observe their impact on noise propagation as illustrated in Fig. 5. Such more extreme conditions should be considered for future calculations.

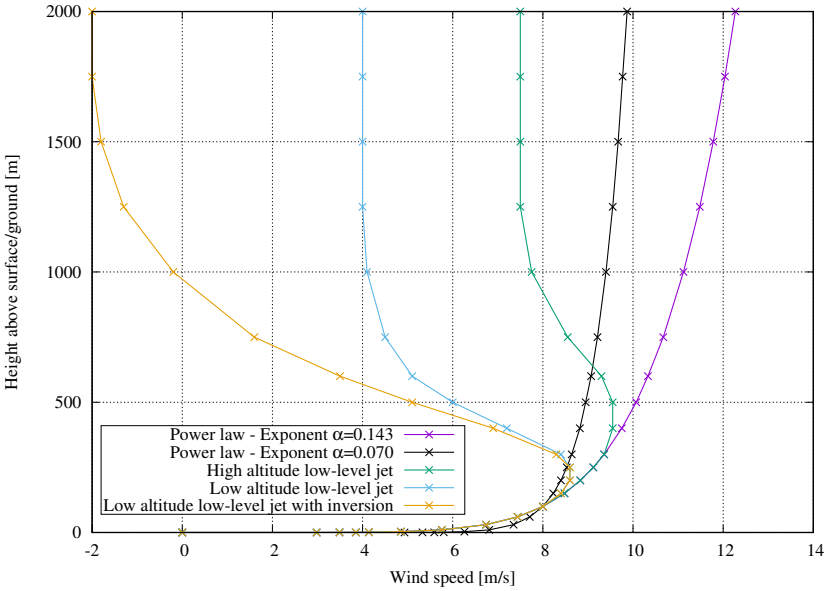

Figure 3: Wind speed profiles.

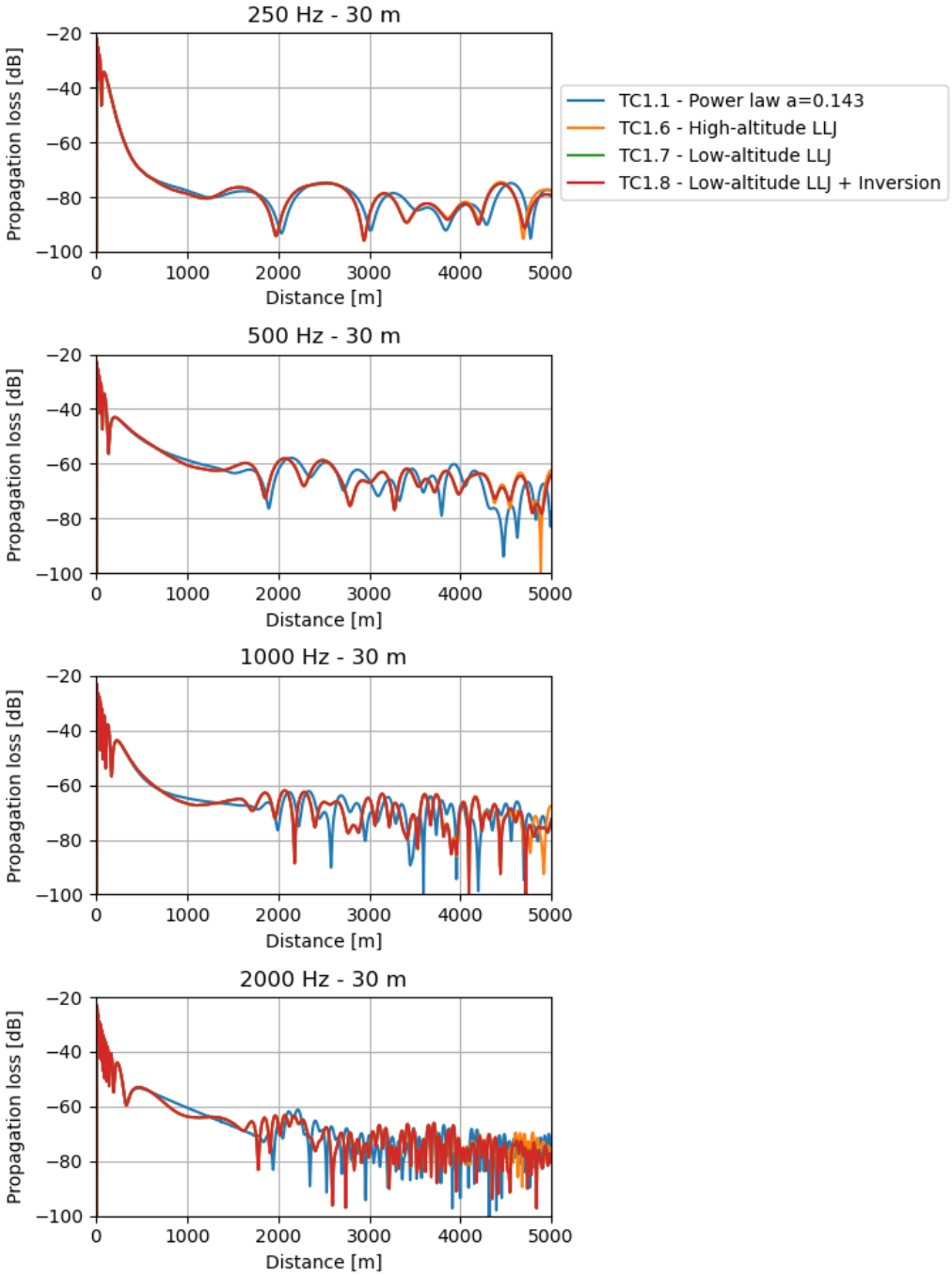

Figure 4: Transmission losses for various wind speed profiles.

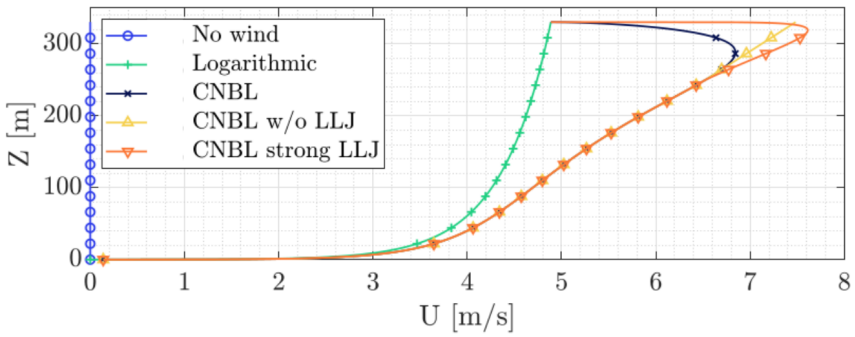

Figure 5: Wind speed profiles with more extreme low-level jet conditions (Reproduced from Libianchi et al, "Sensitivity of the pressure field to the wind and temperature profiles in a conventionally neutral boundary layer", JASA, Vol 154(2), 2023).

3.2.2 Comparisons between models and offshore noise propagation measurements (KTH dataset)

This work is based on the offshore noise propagation experiment conducted by KTH (Royal Institute of Technology, Sweden). The experiment is conducted in Kalmar straight. A loudspeaker is placed at 30 m height on a light-house in the middle of the straight, and a microphone array is located at 9.7 kms inland on the island of Öland. The atmospheric conditions were monitored with a weather balloon from which the effective speed of sound could be evaluated. The set-up is illustrated in Fig. 6. The noise was emitted at three different (tonal) frequencies: 80, 200 and 400 Hz.

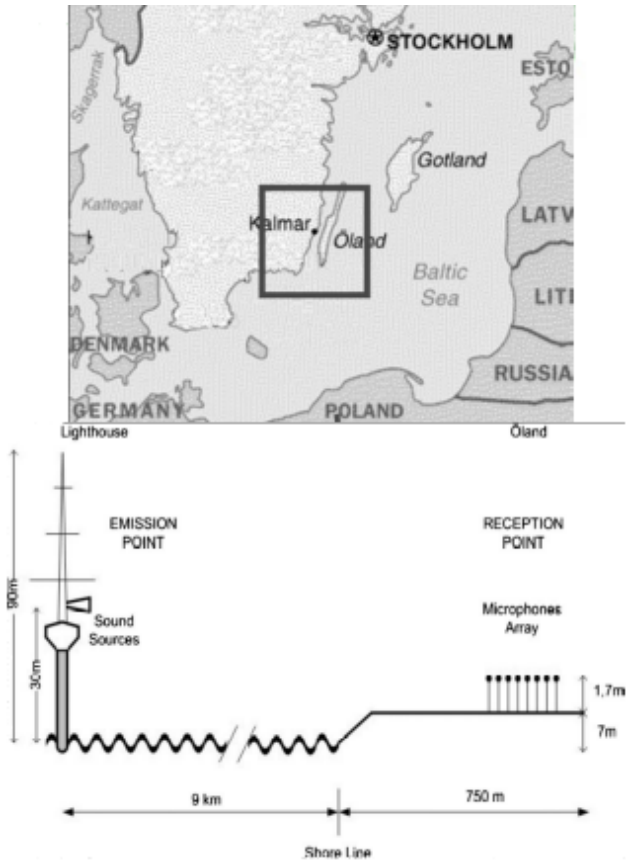

Figure 6: Experimental set-up of noise propagation experiment in offshore conditions by KTH.

In parallel, KTH conducted Parabolic Equation model in order to compare propagation losses with measurements. In the present study, the Parabolic Equation as implemented by DTU is compared with KTH results and the measurement data. The results of these comparisons are displayed in Figs. 7, 8 and 9 for the three considered frequencies, respectively.

It appears that DTU PE results has a tendency to underestimate the measured data, as well as KTH results.

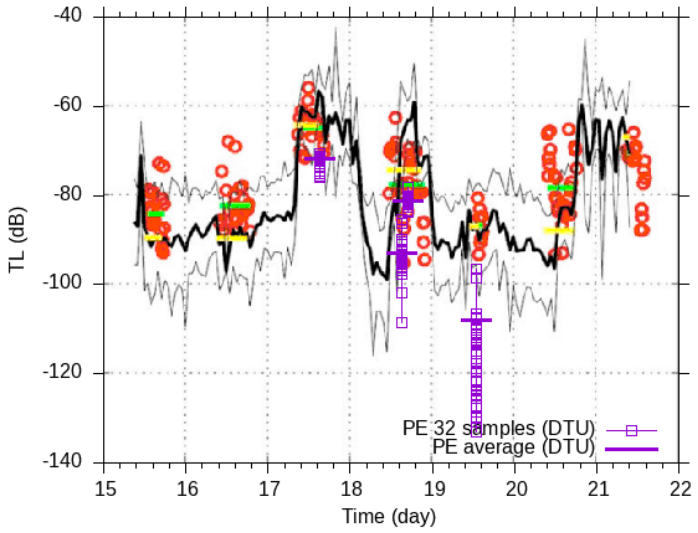

Figure 7: Measured and predicted propagation losses for KTH experiment with a source emission at 80 Hz. Measured (red circles) and predicted (black lines) propagation losses for the laminar calculations. Daily averages of measured and predicted TLs are shown as horizontal lines. DTU turbulent results are in purple.

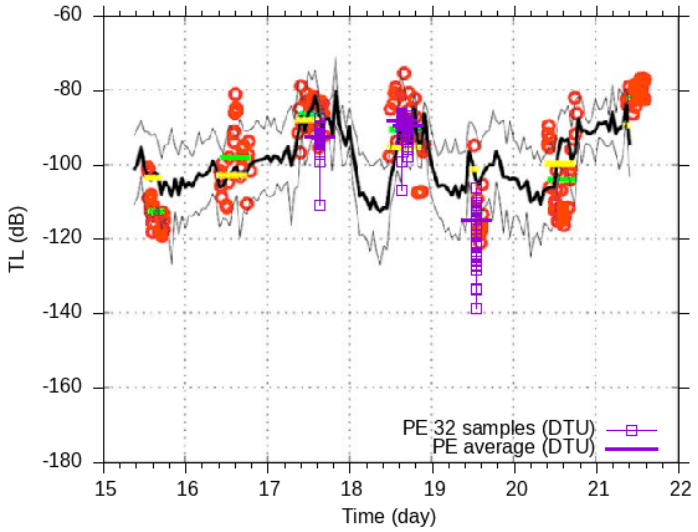

Figure 8: Measured and predicted propagation losses for KTH experiment with a source emission at 200 Hz. Measured (red circles) and predicted (black lines) propagation losses for the laminar calculations. Daily averages of measured and predicted TLs are shown as horizontal lines. DTU turbulent results are in purple.

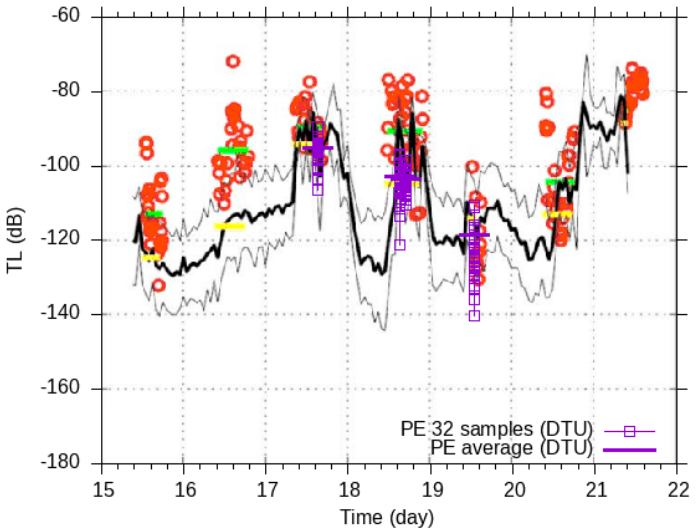

Figure 9: Measured and predicted propagation losses for KTH experiment with a source emission at 400 Hz. Measured (red circles) and predicted (black lines) propagation losses for the laminar calculations. Daily averages of measured and predicted TLs are shown as horizontal lines. DTU turbulent results are in purple.

3.2.3 Comparisons between models and onshore noise propagation measurement (Akzeptanz dataset) for flat terrain

This study gave rise to a conference publication at the DAGA 2024 (Annual German Conference on Acoustics) in Hannover. The results for this part of the activities can be found in Section 8/Annex 5.

4 WP3 / Annex 1 - Definition of noise propagation codes benchmark for complex terrain

International Energy Agency
IEA Wind Technology Collaboration Program (TCP)

IEA Wind Task 39 – Quiet Wind Turbine Technology (Phase 2)

BENCHMARK FOR NOISE PROPAGATION MODELS
Definition of a benchmark exercise

Contact: Franck Bertagnolio (DTU Wind and Energy Systems, email: frba@dtu.dk)

July, 2022

Introduction

The aim of this benchmark is to compare and validate various sound propagation models for **onshore** conditions, in the context of wind turbine noise.

The benchmark comparison exercise is divided into 2 main parts: 1) a series of academic idealized test-cases focusing mainly on the effect of terrain, and 2) real-life test-cases where model results will be compared with field noise measurements. The latter will probably be considering a case with flat terrain from the WEA-Akzeptanz project with 3 relatively flat measurement test-sites in Germany [Martens2020], and then a complex/hilly terrain configuration from the joint-project conducted in Perdigao, Portugal, focusing on atmospheric wind in complex terrain and including with noise measurements conducted by DLR [Schady2020]. The idealized and real-life cases will be addressed iteratively in two separate rounds of comparisons.

Note that a second benchmark focusing on *offshore* conditions is conducted in parallel. It focuses more on the atmospheric effects on propagation models, which is not thoroughly investigated here. Nevertheless, the influence of wind and turbulence will be included in the present study.

The benchmark definitions and the results to be provided for the 1st round are described in the present document.

Definition of terrain, ground characterictics and atmospheric conditions

The main interest of this benchmark is sound propagation in onshore conditions with the definition of terrains of variable complexity.

Test-cases round 1 definition (idealized)

In this first part of the benchmark, a number of idealized test-cases are defined. The goal is to investigate the influence of terrain for different types of models. A *reference* test-case with flat terrain is considered. Then, a series of test-cases using a single and double Gaussian hills of given heights (approx. 80 m) are defined. The double Gaussian hill is also used to investigate "Valley" effects. For all cases, the noise propagation model should successively consider a case with no-wind, and a case with

a wind profile with a power-law for downwind propagation, both with and without atmospheric turbulence for the latter. The ground should always be considered as representative of grassland with a fixed ground impedance. Frequencies from 16 Hz up to 4 kHz are considered. Further details are provided below.

Four different terrain test-case configurations are defined:

1. Flat terrain
2. Single Gausssian hill
3. Double Gaussian hill
4. Valley (using the same double Gaussian hill terrain definition as in 3.)

For each of these test-cases, the terrain definition, the sources locations, and the receptor/receiver locations are defined in separate files, as specified in Table 1. These files can be retrieved from the IEA Wind Task 39 SharePoint website following this link:
https://share.dtu.dk/sites/IEA_WIND_T39_459100/WP3%20Noise%20propagation/Forms/AllItems.aspx?RootFolder=%2Fsites%2FIEA%5FWIND%5FT39%5F459100%2FWP3%20Noise%20propagation%2FNoisePropagation%5FAnalysis%5Fand%5FBenchmark%2FBenchmark%5FRound1&FolderCTID=0x01200006BC6AACDCAEC14692A74AECBBECF8BC&View=%7BFC427970%2D9CAB%2D43E9%2D8181%2D30C28187D6E3%7D&InitialTabId=Ribbon%2ERead&VisibilityContext=WSSTabPersistence

Test-cases \ Files for…	Terrain definition	Source position	Receptor positions
1. Flat terrain	terrain_flat.dat	source_flat.dat	receiver_flat.dat
2. Single Gaussian hill	terrain_1hill.dat	source_12hill.dat	receiver_1hill.dat
3. Double Gaussian hill	terrain_2hill.dat	source_12hill.dat	receiver_2hill.dat
4. Valley	terrain_2hill.dat	source_valley.dat	receiver_valley.dat

Table 1 – Names of file containing source and receptor positions for each test-case.

The influence of atmospheric conditions are considered as follows. Each terrain test-case considered should include **a case with no-wind and no-turbulence, and a case with a wind velocity profile** using a power low as: $U(h) = U_H\,(h/H)^{\beta}$, where $H = 100$ m is the reference height, $U_H = 8$ m/s is the wind speed at reference height, and the power coefficient $\beta = 1/7 = 0.143$ is characteristics of neutral atmospheric condition. The wind direction should be in the direction from the sources toward the receptors, i.e. the receptors are located downwind of the sources. In the latter **case with a wind velocity profile, both cases without and with atmospheric turbulence** should be considered. The manner to define and implement the effect of the atmospheric turbulence is left to the participants, but **turbulence intensities TI = 5 and 10%** (i.e. a standard deviation equal to σ_u = 0.4 m/s and 0.8 m/s, respectively, for a hub-height velocity here fixed at 8 m/s) for the longitudinal component should be chosen. If possible/available as an option of the model, **a fixed length scale of 100 m** and **neutral** atmospheric conditions should be enforced. Isotropic turbulence should be preferred if this can be enforced. In any case, some basics about the implementation of the turbulence (e.g. which model is used) should be provided when delivering the results. No temperature gradient effect should be considered.

For each test-case, the calculations should be conducted with **3 source heights: 30, 100 m and 300 m**. The sources should be considered as monopoles. The reference source is located at x = 0 m in the longitudinal direction. However, note that in the cases of the single and double Gaussian hill, sources located at x = -1000 m should also considered.

The **receptor** positions should be equally spaced **every 1 m from emission location up to 5 km** (starting at and relatively to the reference point at x = 0 m). However, if for some reason the participant is limited (e.g. by computational resources), **at least receptors equally spaced by 1 km between 1 km and 5 km** in the longitudinal direction relatively to the source (at x = 0) should be considered (as provided in the Task 39 SharePoint link above). All receptors should be placed at a height of **2 m above ground level**. Note also that additional receptor locations are defined **for the Valley case**. Their longitudinal 'x'-locations are reported in the file 'receiver_valley.dat' in the SharePoint (see also Fig. 4), and at each of these locations 4 receptor heights at: **0.5 m, 1.5 m, 2 m, and 4 m** (above ground level) should be considered.

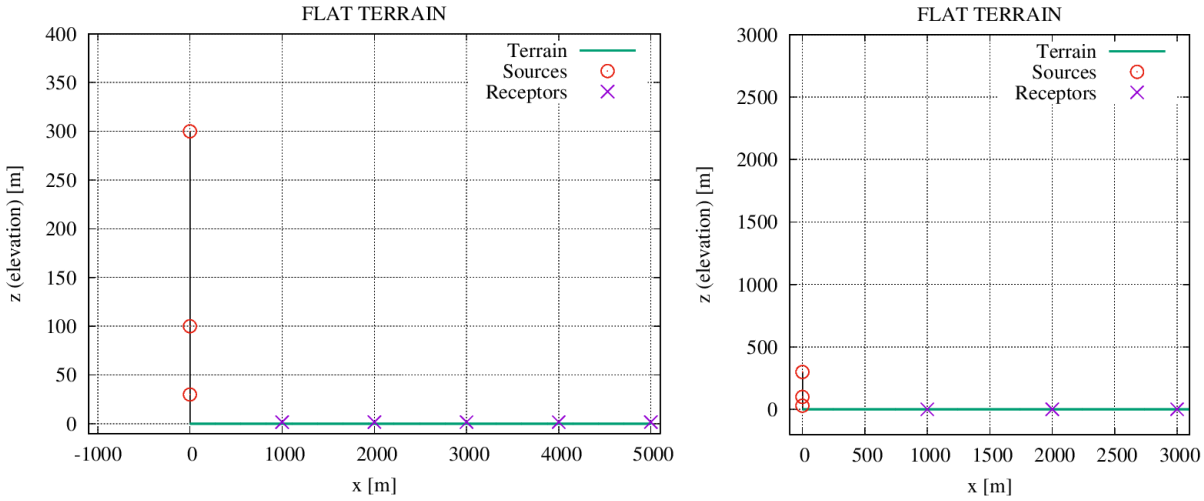

Figure 1 – Sketch of terrain, source and receptor positions, for the Flat Terrain case (Left: All features - Not to scale; Right: Zoom to scale).

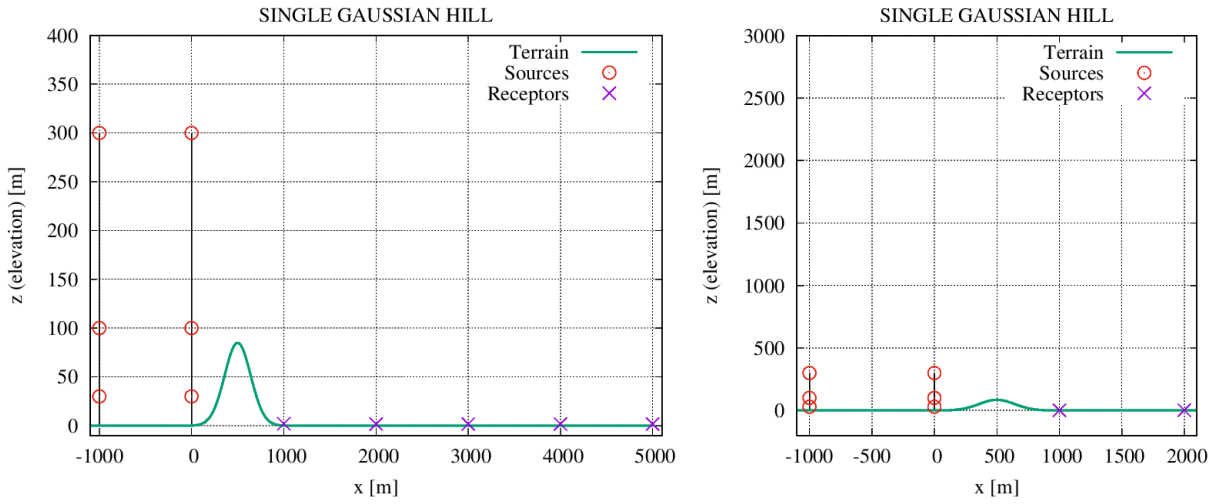

Figure 2 – Sketch of terrain, source and receptor positions, for the Single Gaussian Hill case (Left: All features - Not to scale; Right: Zoom to scale).

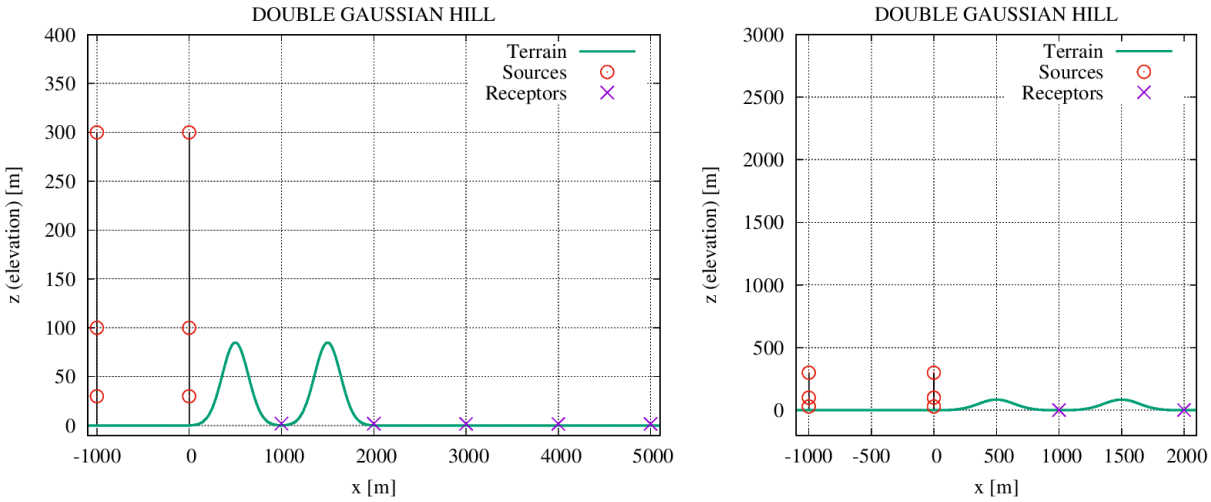

Figure 3 – Sketch of terrain, source and receptor positions, for the Double Gaussian Hill case (Left: All features - Not to scale; Right: Zoom to scale).

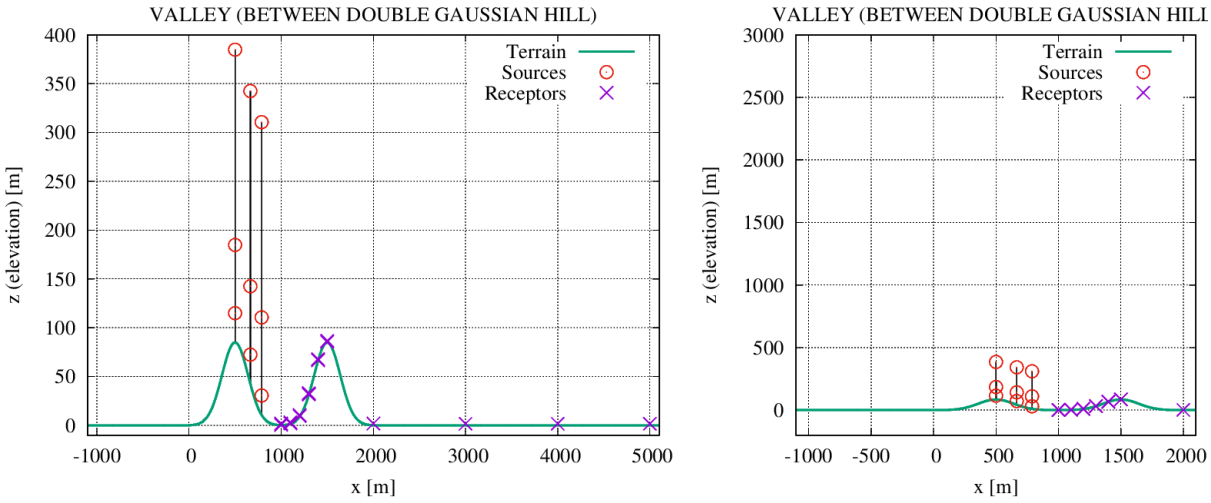

Figure 4 – Sketch of terrain, source and receptor positions, for the Valley case (Left: All features - Not to scale; Right: Zoom to scale).

Quantity	Value	Unit
Reference wind speed at 100m U_H	8	m/s
Wind shear profile power law coefficient	1/7=0.143	-
Turbulence intensity (longitudinal component)	10	% (rel. U_H)
Turbulence integral length scale	100	m
Temperature at all height	15	deg.C
Atmospheric pressure at all height	1013	hPa
Rel. Humidity at all height	70	%-RH
Air density at all height ρ_0	1.22	kg/m^3
Speed of sound c_0 (using O. Cramer, JASA, 93, p. 2510, 1993)	341	m/s
Ground surface effective flow resistivity σ (of grass-type cover)	250	kPa.s/m^2

Table 2 – General atmospheric and ground conditions for the noise propagation calculations.

Regarding the ground surface acoustic characteristics, it is recommended to use the Delany and Bazley model [Delany1970] providing the characteristic impedance:

$$Z_c = \rho_0 c_0 \times [1 + 9.08 \times (10^3 \times f/\sigma)^{-0.75} - \boldsymbol{i} \times 11.9 \times (10^3 \times f/\sigma)^{-0.73}]$$

where σ (with unit: N.s.m^{-4}, corresponding to Pa.s.m^{-2}) is also called the airflow resistance or the static air flow resistivity in some references, but it is the same quantity that is referred to in Table 2.

In case the participant does not wish to conduct all test-cases (e.g. if computational resources are limited), a priority order for the test-cases to be calculated is provided in Table 3. Nevertheless, the participants may provide the results for the test-cases of his/her choice, or as the modeling approach itself allows.

Priority order	Test-Cases	Atmospheric conditions
1	TC1.1 (Flat Terrain)	No wind
2	TC1.2	Wind – No turbulence
3	TC1.3	Wind – With turbulence (TI=5 & 10%)
7	TC2.1 (Single Hill)	No wind
4	TC2.2	Wind – No Turbulence
8	TC2.3	Wind – With turbulence (TI=5 & 10%)
11	TC3.1 (Double Hill)	No wind
6	TC3.2	Wind – No Turbulence
12	TC3.3	Wind – With turbulence (TI=5 & 10%)
9	TC4.1 (Valley)	No wind
5	TC4.2	Wind – No Turbulence
10	TC4.3	Wind – With turbulence (TI=5 & 10%)

Table 3 – Detailed list of test-cases and their order of priority.

The noise propagation losses should be provided for 1**/1 octave bands** at the center frequencies from 16 Hz to 4 kHz. Note that for certain solution methods (e.g. Parabolic Equations), it does make sense to **average** several calculations results **over several frequencies** distributed within each frequency band in order to be compared with simpler methods (e.g. ray tracing or ISO standard). Please provide information about how the model calculation results have been processed.

Test-cases round 2 definition (real-life – To be considered later as part of a 2nd round of comparisons)
In this part of the benchmark exercise, several specific conditions acquired during existing measurement campaigns will be reproduced. The definition of these test-cases will be handled in a 2nd round of this benchmark project.

Results and Formats

The results to provide for the different test-cases, as well as their preferred formatting, are described in this section.

Noise propagation losses should be provided as **non-weighted** (although A-weighted is also acceptable – Remind to specify this when providing your results) **Sound Pressure Levels (SPL) calculated at the 9 center frequencies of the 1/1 octave bands** from 16 Hz to 4 kHz. In other words, the calculations should be made using the center frequency of each band, i.e. 16, 31.5, 63, 125, 250, 500, 1000, 2000 and 4000 Hz. If possible (and meaningful), the SPL integrated over the 1/1 octave

bands frequencies should also be provided. Please do specify how the SPL are calculated (in term of frequency band integration).

The **preferred** format for delivering the results is ASCII text files organized as follows:

[start of file]
Possibly several header lines here (starting with "#" as leading character)
f [Hz], SPL [dB$_{1/1}$] at position 1, SPL [dB$_{1/1}$] at pos. 2, SPL [dB$_{1/1}$] pos. 3, … **for source at 30 m**
f_1 $SPL_{1,P1}$ $SPL_{1,P2}$ $SPL_{1,P3}$ … $SPL_{1,PN}$
f_2 $SPL_{2,P1}$ $SPL_{2,P2}$ $SPL_{2,P3}$ … $SPL_{2,PN}$
…
f_Q $SPL_{Q,P1}$ $SPL_{Q,P2}$ $SPL_{Q,P3}$ … $SPL_{Q,PN}$

f [Hz], SPL [dB$_{1/1}$] at position 1, SPL [dB$_{1/1}$] at pos. 2, SPL [dB$_{1/1}$] pos. 3, … for source at **100 m**
f_1 $SPL_{1,P1}$ $SPL_{1,P2}$ $SPL_{1,P3}$ … $SPL_{1,PN}$
f_2 $SPL_{2,P1}$ $SPL_{2,P2}$ $SPL_{2,P3}$ … $SPL_{2,PN}$
…
f_Q $SPL_{Q,P1}$ $SPL_{Q,P2}$ $SPL_{Q,P3}$ … $SPL_{Q,PN}$

f [Hz], SPL [dB$_{1/1}$] at position 1, SPL [dB$_{1/1}$] at pos. 2, SPL [dB$_{1/1}$] pos. 3, … for source at **300 m**
f_1 $SPL_{1,P1}$ $SPL_{1,P2}$ $SPL_{1,P3}$ … $SPL_{1,PN}$
f_2 $SPL_{2,P1}$ $SPL_{2,P2}$ $SPL_{2,P3}$ … $SPL_{2,PN}$
…
f_Q $SPL_{Q,P1}$ $SPL_{Q,P2}$ $SPL_{Q,P3}$ … $SPL_{Q,PN}$
[end of file – More "blocks" can be added if more source locations are calculated (see details below)]

where Q is the number of considered frequencies (Q = 9, here), and P1, P2, … to PN denotes the receptor positions number 1 to number N for the different test-cases. If more source locations are considered (e.g. Gaussian hill cases or Valley case), the files can be extended by increasing the number of "blocks" (1 block includes all frequencies and all receiver positions for one single source location). The actual source position for each block should be clearly indicated in the comment lines starting with a leading character "#". Note that the receptor positions may differ from one test-case to another, and from one participants to another. Therefore, it should be indicated/specified by the participants how the receptor positions are defined (e.g. in a header line of the file starting with "#" as a leading character).

The output files should be preferably be named "tcX.I.S_NAME.dat" where:

- "X" stands for the terrain test-case number (1 to 4) as defined earlier in this document, and corresponding to Figs. 1 to 4.
- "I" should be set to "0" for the no-wind case, "1" for the wind and no-turbulence case, "2" for the wind and with-turbulence case with TI=5%, and "3" for the wind and with-turbulence case with TI=10%.
- "S" can be used to denote the sources locations (e.g. to distinguish x = -1000 and x = 0 m, see Figs. 2 & 3). However, "S" can be omitted and the different results with different source 'x'-locations can be included in a single file (with more "blocks", see definition above). This should be clearly specified when providing the results (e.g. in header/comment lines of the files starting with "#" as a leading character).
- Finally, "NAME" is the name of the institution delivering the results. Note that if the participant/institution delivers results with different propagation models, these should be made clear with appropriate names or acronyms here.

If a different file content format and/or file name convention are used, please provide a detailed description about how the results should be interpreted. In addition, note that ASCII text files are strongly preferred, but MS-Excel files are also accepted.

Timing for delivery of results

The results would ideally be provided on:

- *September/October, 2022 ???*

References

[Martens2020] Susanne Martens, Tobias Bohne and Raimund Rolfes, “An evaluation method for extensive wind turbine sound measurement data and its application”, Proc. Mtgs. Acoust. 41, 040001 (2020); doi: 10.1121/2.0001326

[Schady2020] Arthur Schady, and Katharina Elsen, “On the detectability of a wind turbines noise under different meteorological conditions”, Proc. Mtgs. Acoust. 41, 040002 (2020); doi: 10.1121/2.0001331

[Delany1970] Delany M. E. and Bazley E. N., “Acoustical properties of fibrous absorbent materials”, Applied Acoustics, 3, pp.105-116 (1970); doi: 10.1016/0003-682X(70)90031-9

5 WP3 / Annex 2 - Report on noise propagation code benchmark for complex terrain

IEA Wind Task 39 - Phase 2

WP3 - Wind turbine noise propagation

Report on noise propagation code benchmark for complex terrain

Contents

1 Introduction **2**

2 Test-case definitions **2**

3 Numerical models used for cross-validations **4**

4 Benchmarking of noise propagation prediction codes **4**

5 Flat terrain **4**

6 One-hill case **7**

6.1 Noise levels at 2 m height 7

6.2 Noise maps 11

7 Double-hill case **15**

8 Valley case **17**

9 Conclusions **20**

1 Introduction

WP3 includes several validation benchmarks of noise propagation models. As part of this WP, a sub-task consisted in investigating noise propagation over complex terrain, and in particular compare and assess different noise propagation codes in a benchmark exercise.

The benchmark test-cases were defined as a separate sub-task. In the present report, the results of the study are collected and conclusions are drawn.

2 Test-case definitions

This section is a reminder of the main elements of test-cases to be considered.

The various configurations for the terrain on which to calculate the noise propagation effects are illustrated in Fig. 1. The hill height in all cases is 80 m and its shape is defined with a Gaussian function. Note that all receivers are located at 2 m height, while the sources are located at 30, 100 and 300 m for each horizontal position where they are defined (see Fig. 1).

Reference atmospheric conditions for the simulations are reported in Fig. 2. Furthermore, three different wind conditions were defined:

1. No wind
2. Wind - No turbulence
3. Wind - With turbulence

All calculations are assumed to investigate downwind noise propagation only.

The above definitions result in a total of 12 test-cases. However, the participants were given the choice to compute less cases, but respecting a priority order as indicated in Fig. 3.

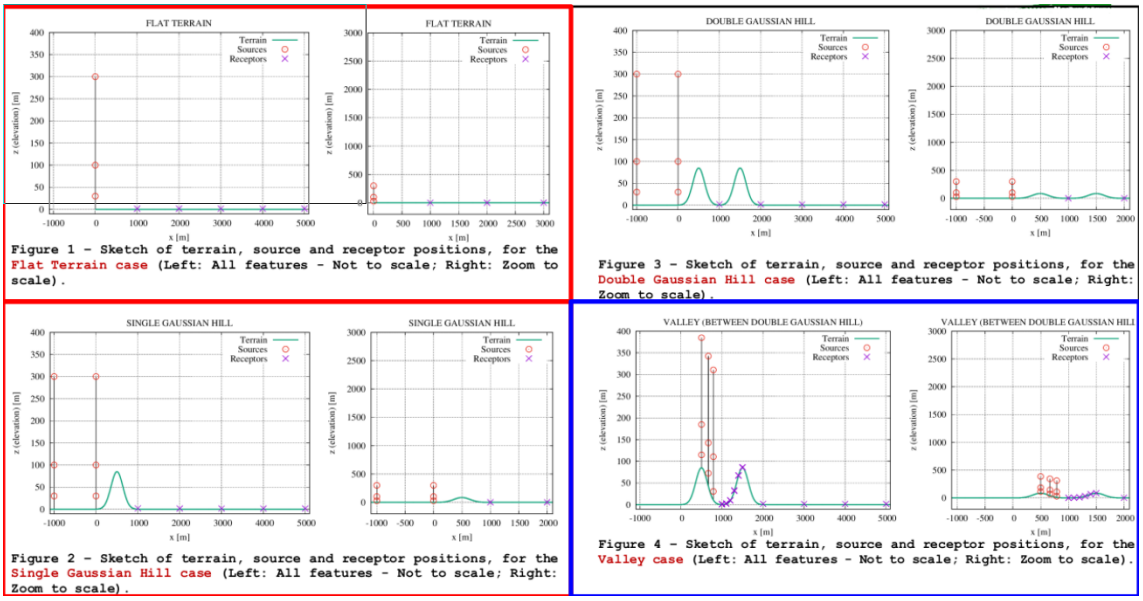

Figure 1: Various terrain configuration for code benchmarking: Flat terrain (top-left), One single hill (bottom-left), Two hills (top-right), Valley (bottom-right). The sources are indicated by red circles. The receiver positions (at 2 m height) are indicated by purple crosses. The ground is indicated by a green line. The sketches are not to scale with respect to horizontal distance x and elevation z.

Quantity	**Value**	**Unit**
Reference wind speed at 100m	8	m/s
Wind shear profile power law coefficient	1/7=0.143	-
Temperature at all height	15	deg.C
Atmospheric pressure at all height	1013	hPa
Rel. Humidity at all height	70	%-RH
Ground surface effective flow resistivity (grass)	250	kPa.s/m^2

Figure 2: Atmospheric conditions for the present benchmark.

Priority order	Test-Cases	Atmospheric conditions
1	TC1.1 (Flat Terrain)	No wind
2	TC1.2	Wind – No turbulence
3	TC1.3	Wind – With turbulence (TI=5 & 10%)
7	TC2.1 (Single Hill)	No wind
4	TC2.2	Wind – No Turbulence
8	TC2.3	Wind – With turbulence (TI=5 & 10%)
11	TC3.1 (Double Hill)	No wind
6	TC3.2	Wind – No Turbulence
12	TC3.3	Wind – With turbulence (TI=5 & 10%)
9	TC4.1 (Valley)	No wind
5	TC4.2	Wind – No Turbulence
10	TC4.3	Wind – With turbulence (TI=5 & 10%)

Figure 3: Definition of test-cases.

3 Numerical models used for cross-validations

The comparisons were restricted to comparing two codes:

- Nord2000: Ray tracing method developed by FORCE Technology.
- WindSTAR: Parabolic Equation (PE) method developed by DTU.

Note that further cross-validations between models were conducted as part of this WP5 using the Akzeptanz measurement data from LUH (Leibniz Universität Hannover). These comparisons can be found elsewhere in this report.

The test-case definitions in the previous section result in many figures. The following analysis concentrates only on relevant cases that could lead to better understanding of the respective code behaviors.

4 Benchmarking of noise propagation prediction codes

5 Flat terrain

In order to get a better sense of the basic differences between the two codes introduced in Section 3, a flat terrain configuration is considered. A first comparison of the transmission losses (TL), for observer at 2 m height from the ground, as a function of the distance from the source (at 100 m height only, here) for various frequencies (ranging from 16 Hz to 2000 Hz) is displayed in Fig. 4(a). Note that for case TC1.3 (with turbulence), the PE calculations become prohibitely expensive at high frequencies and results are not shown for 1000 Hz and 2000 Hz.

However, Nord2000 predictions are assumed averaged in each (1/3 oct.) frequency bands. Therefore, it appears natural to process the PE data in the same way as displayed in Fig. 4(b).

Some discrepancies are observed between the two modelling approaches. But, the scale of this discrepances relatively to the actual TL levels used for the figure makes it difficult to evaluate them precisely. As the geometric losses and atmospheric absorption should be identical for both approaches, these are removed from the calculation results, and the comparisons are displayed Fig. 5.

In this last case, it is clearly visible that including wind as an effect at all frequencies. There exists some bias between the Nord2000 and PE methods which can only be explained by systemic errors, which are difficult to attribute to one model or another. This latter issue can probably only be determined by comparisons with experimental data, as done elsewhere in this report.

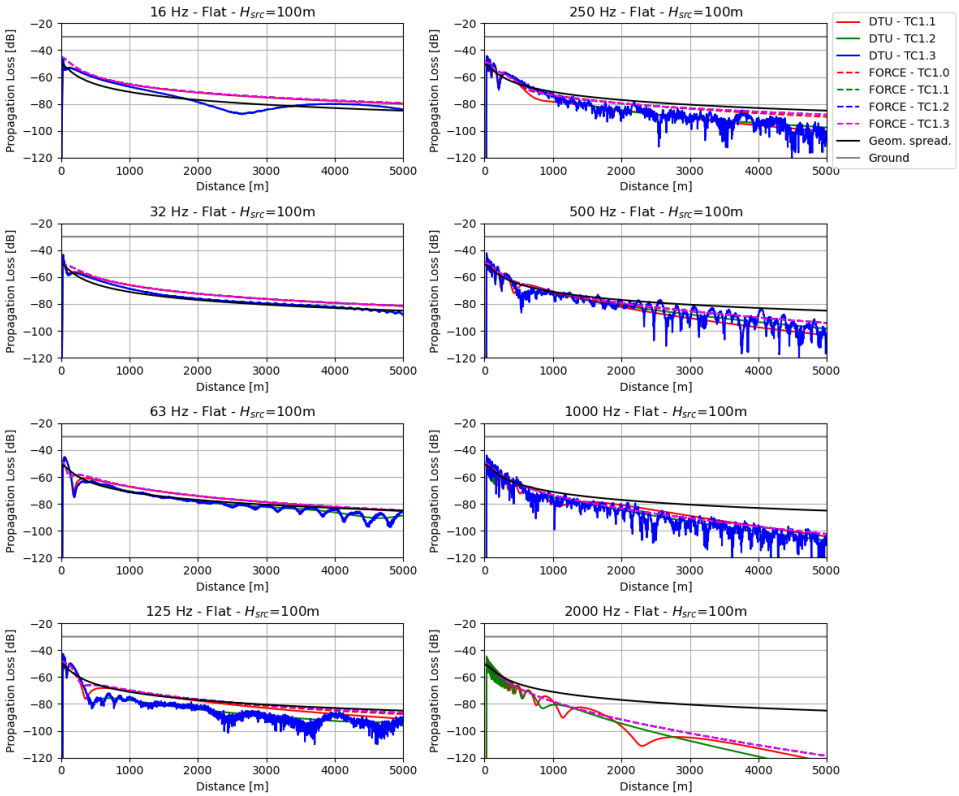

(a) PE calculations at center frequency

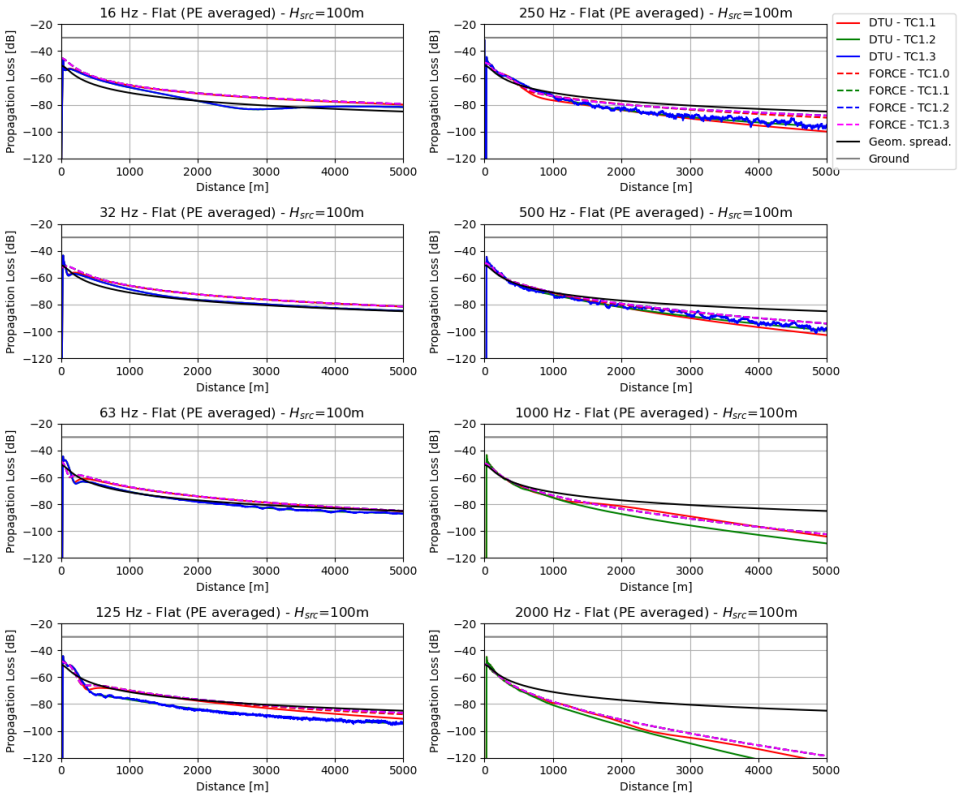

(b) PE calculations averaged in frequency bands

Figure 4: Transmission loss as a function of distance from source for flat terrain.

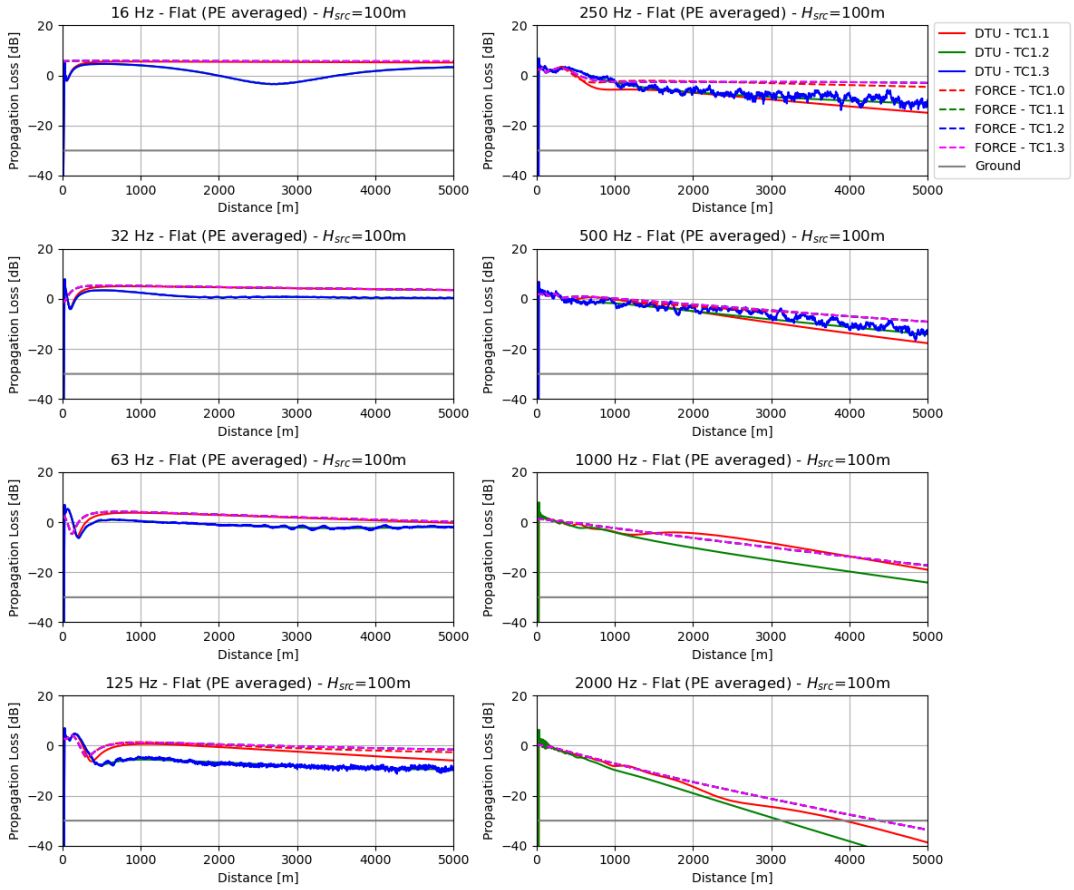

Figure 5: Transmission loss as a function of distance from source for flat terrain, without geometric losses and atmospheric absorption.

6 One-hill case

The main conclusions for this study stems from the comparisons in the case of a single hill configurations, although the case of the double-hill is also shortly considered. The noise source is placed either at the foot of the hill (upwind relatively to it) or at 1 km upwind of the hill foot. Prediction results do not include geometric losses and atmospheric absorption.

6.1 Noise levels at 2 m height

The TL at 2 m heights as a function of horizontal distance from the source are displayed in Figs. 6(a) and 6(b) for the two noise source positions upwind of the hill, respectively, both at a 30 m height. For sources at 100 m and 300 m height, the results are displayed in Figs. 7(a-b) and 8(a-b), respectively.

Both models predict a shadow zone in the downwind side of the hill as expected. This is observed irrespectively of the position of the source, although much less pronounced when the source is highre (say at 300 m).

Howver, the most noticeable inconsistency between the two calculation methods is an interference pattern that is only observed fot the PE method. Nevertheless, in some cases the Nord2000 software also predicts peculiar behavior at the same region. This interference pattern is clearly observed in the range 700 to 1000 m downwind from the hill top. It is present at all frequencies and for all source heights. It appears to be sometimes an constructive interference, sometimes a destructive one, depending on frequency.

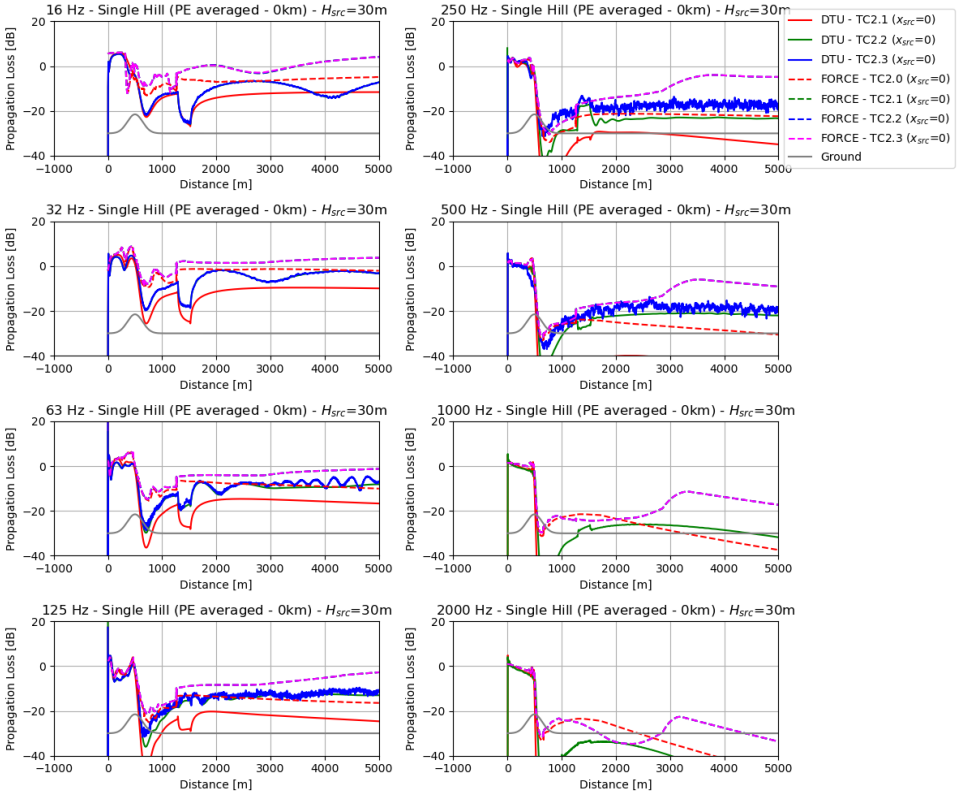

(a) Source at the foot of the hill

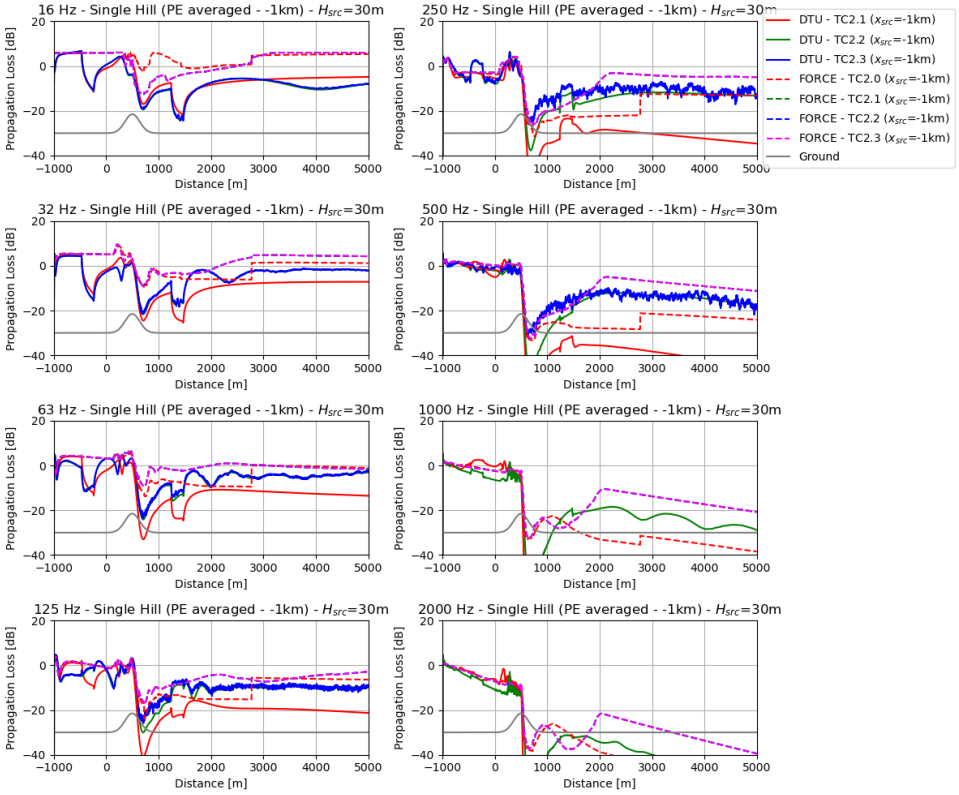

(b) Source at 1 km upwind the foot of the hill

Figure 6: Transmission loss as a function of distance from source for a single hill - Source height is 30 m.

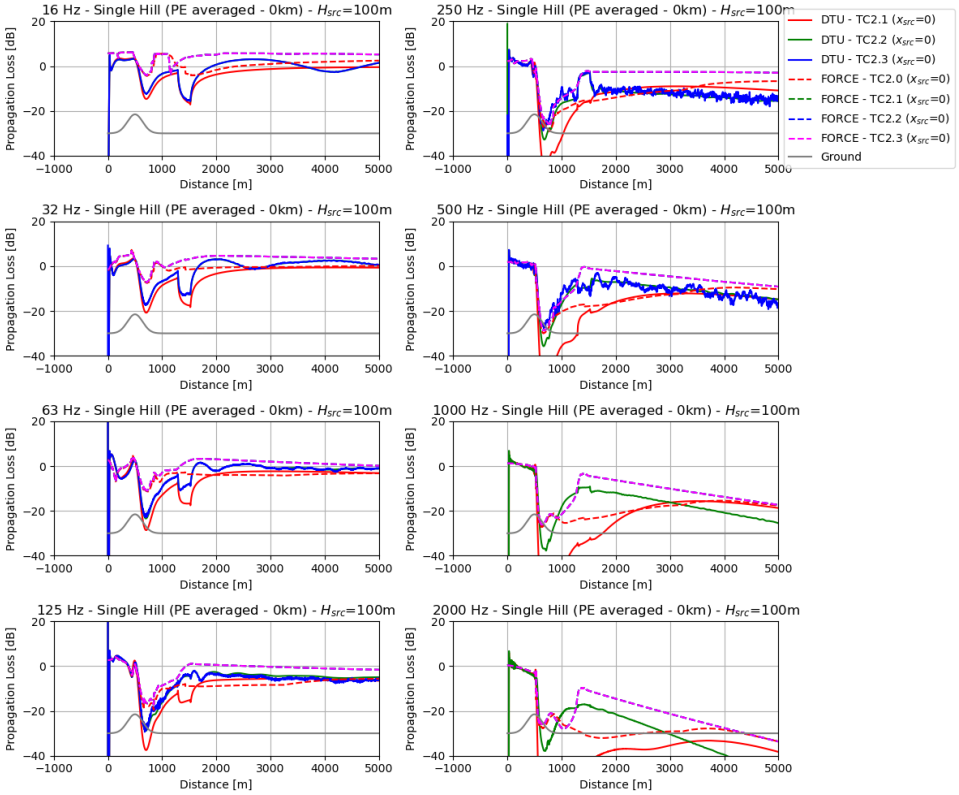

(a) Source at the foot of the hill

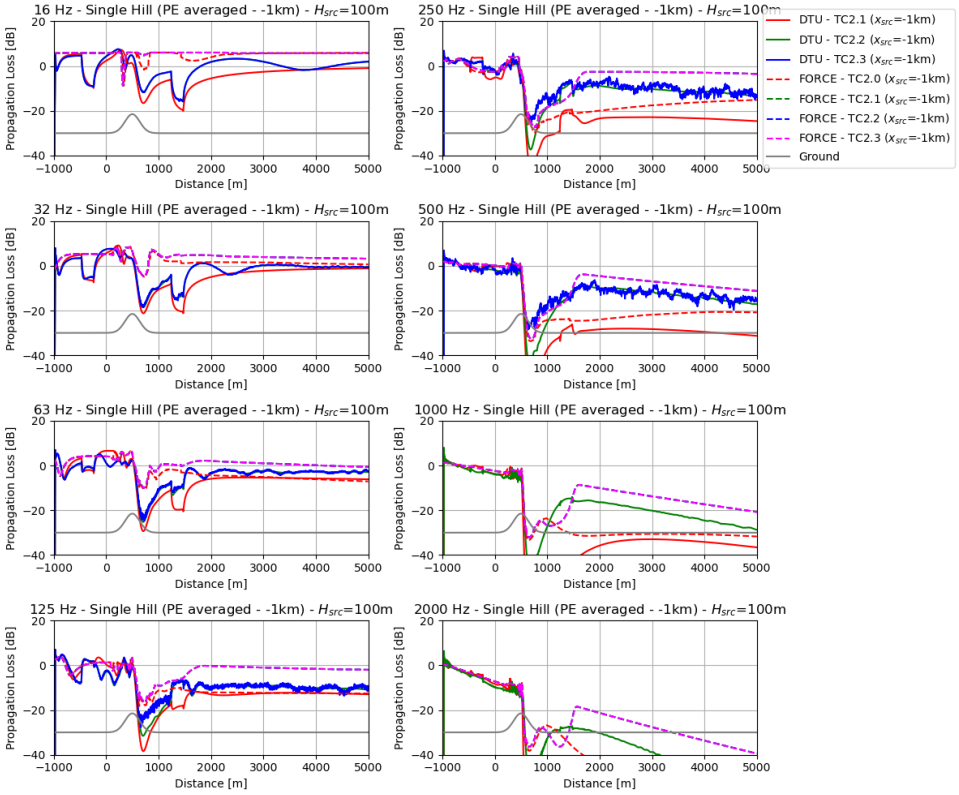

(b) Source at 1 km upwind the foot of the hill

Figure 7: Transmission loss as a function of distance from source for a single hill - Source height is 100 m.

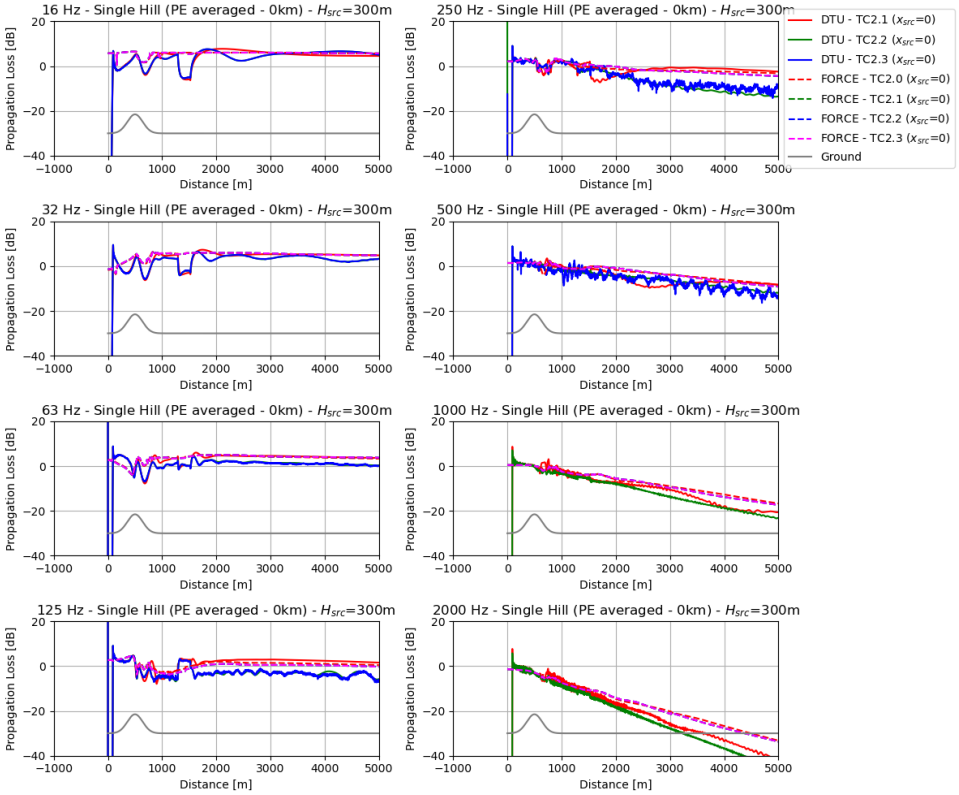

(a) Source at the foot of the hill

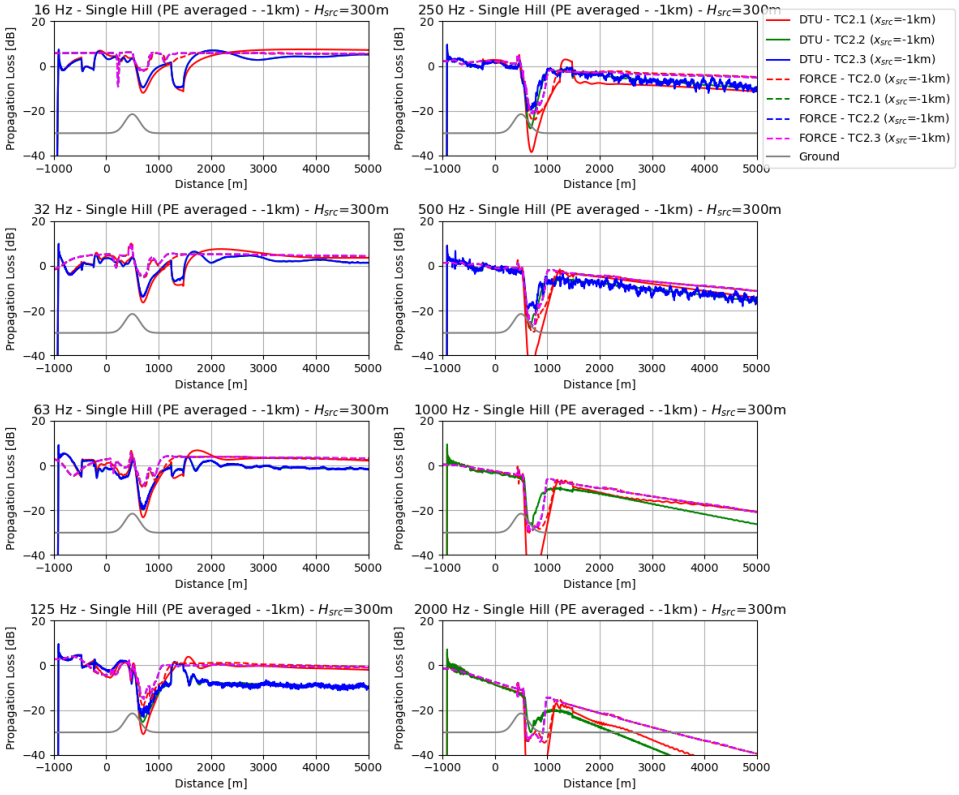

(b) Source at 1 km upwind the foot of the hill

Figure 8: Transmission loss as a function of distance from source for a single hill - Source height is 300 m.

6.2 Noise maps

In order to investigate, this interference pattern in more details, noise maps of the noise TL are displayed, for the source at the foot of the hill, for frequencies equal to 32 Hz and 250 Hz in Figs. 9 and 10.

Finally, the same noise maps as above, but for the noise source located at 1km upwind of the foot hill, are displayed in Figs 11 and 12

The same interference pattern is observed at the same distance of the top of the hill. It is surmised that the observed interference pattern is caused by the noise wave interacting with the hill shape sufficiently downstream of the latter.

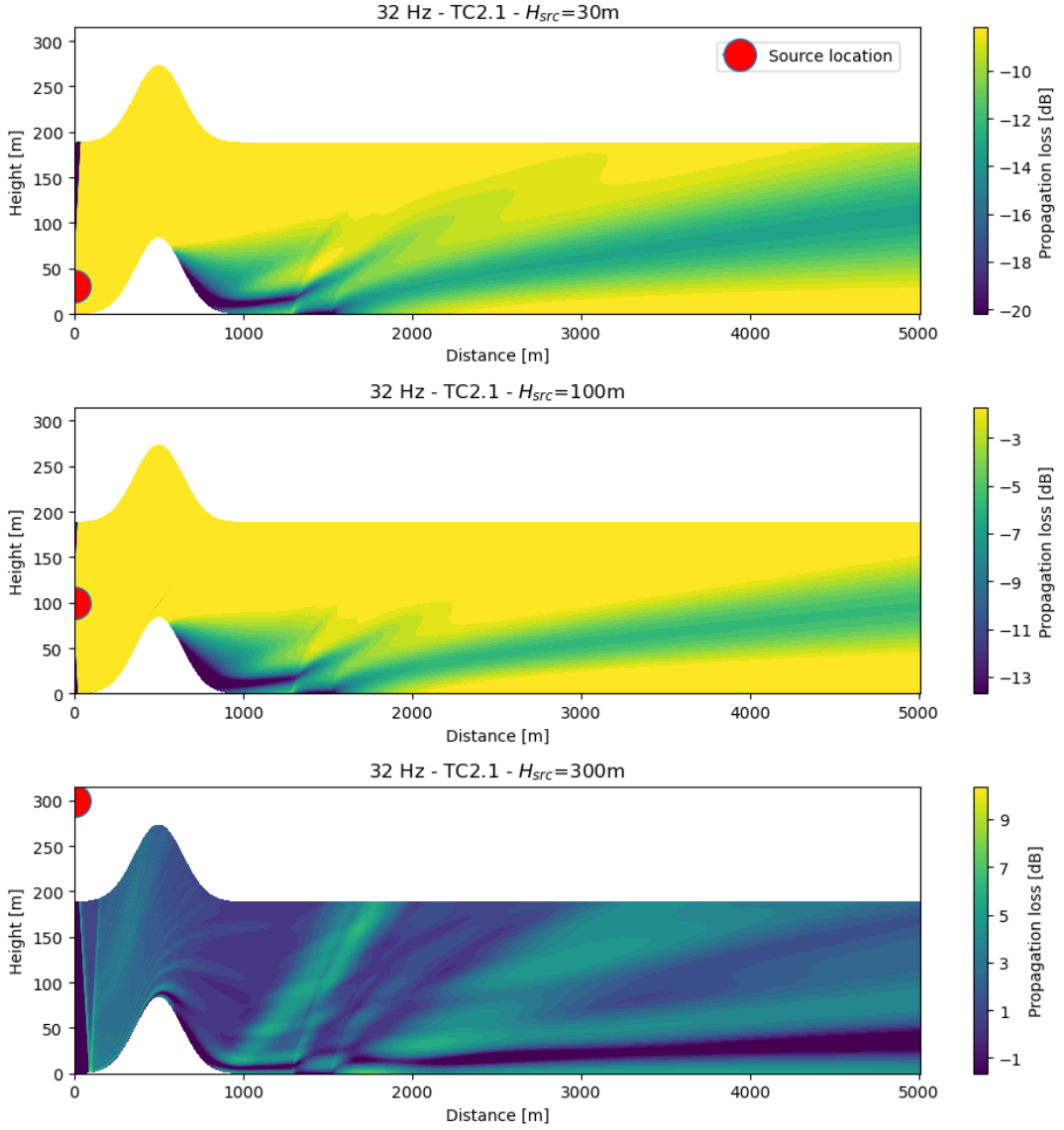

Figure 9: Transmission loss map for a single hill with source at foot of the hill at a frequency 32 Hz (Top: source at 30 m height, Middle: source at 100 m height, Bottom: source at 300 m height).

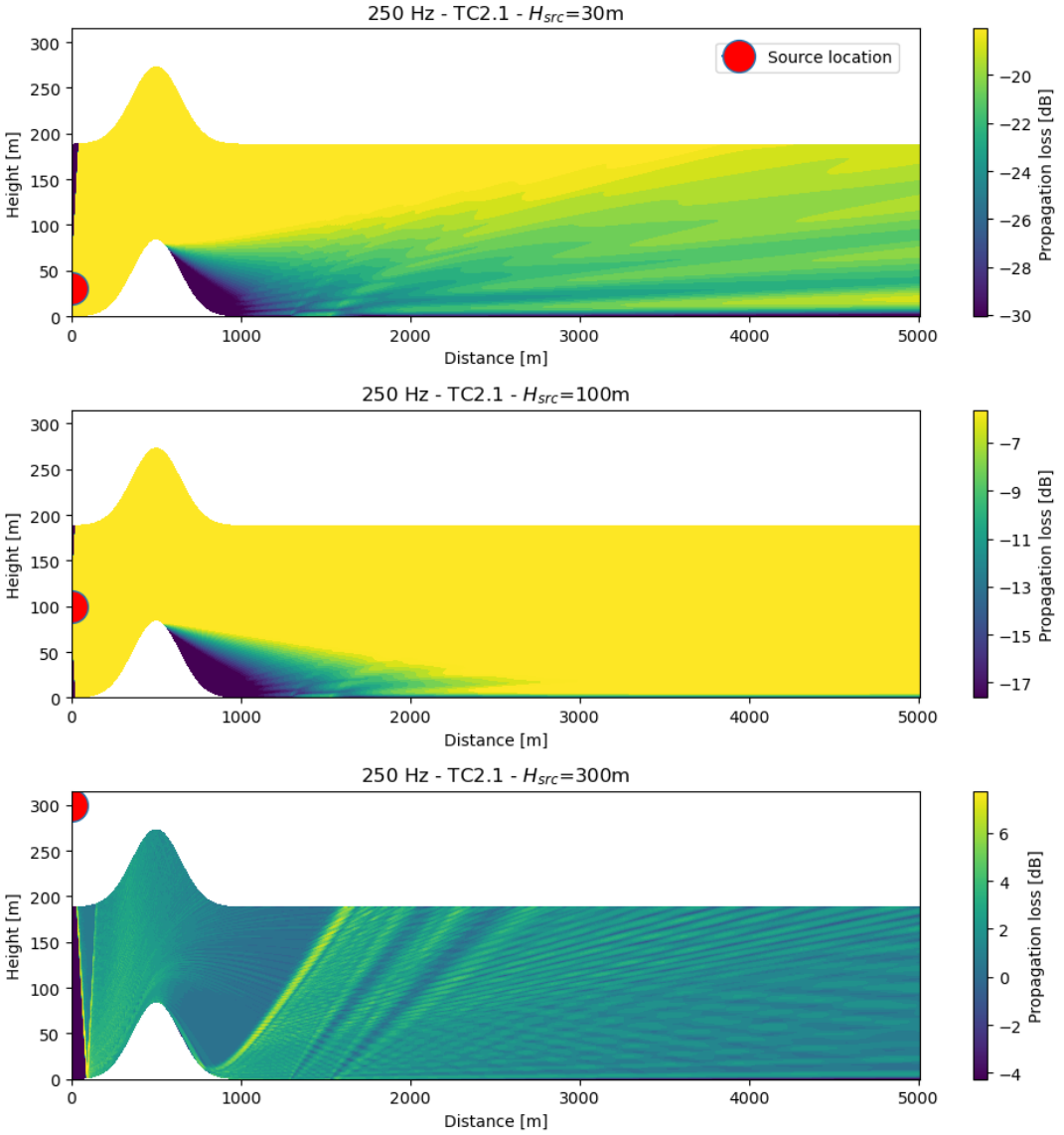

Figure 10: Transmission loss map for a single hill with source at foot of the hill at a frequency 250 Hz (Top: source at 30 m height, Middle: source at 100 m height, Bottom: source at 300 m height).

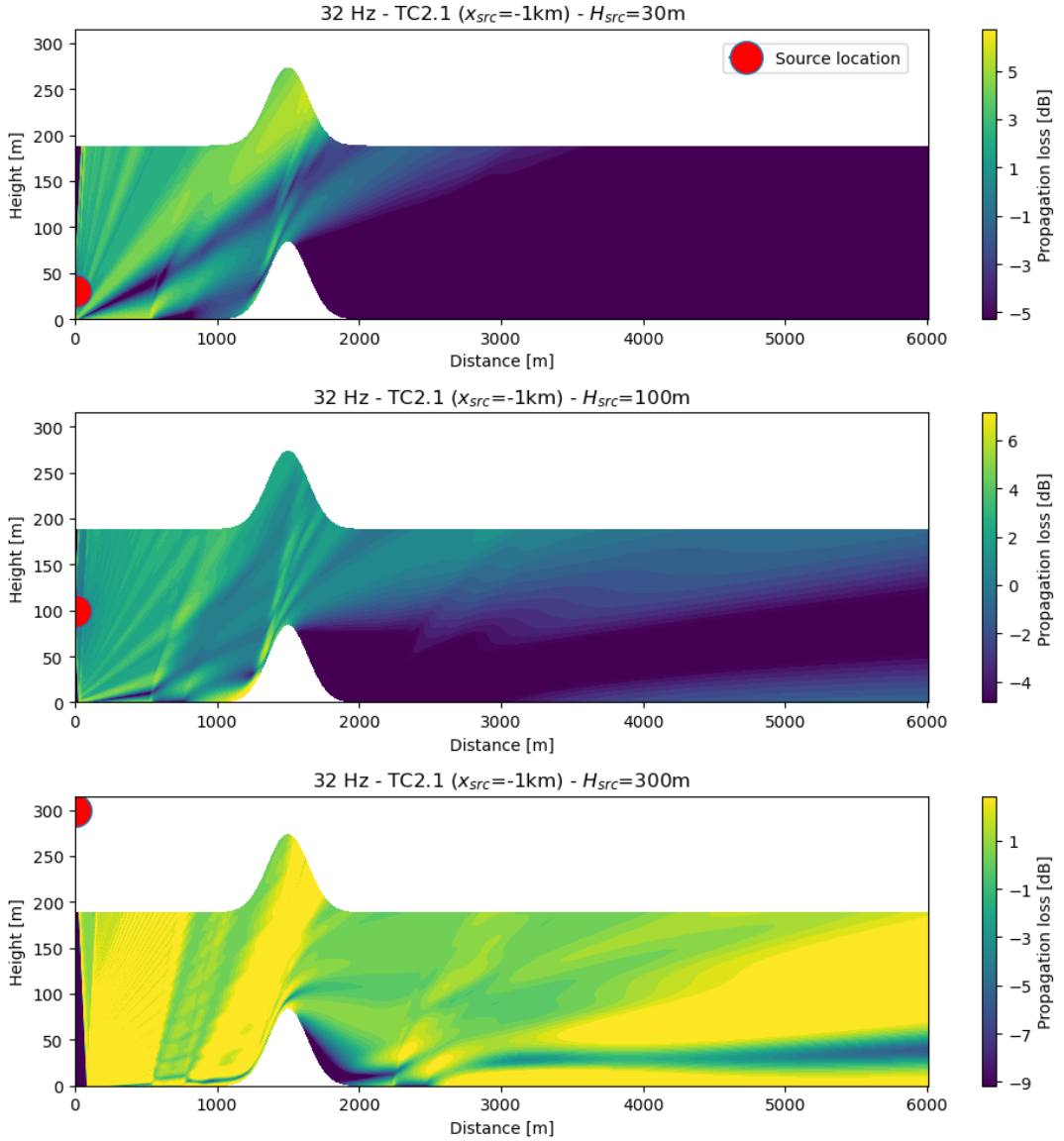

Figure 11: Transmission loss map for a single hill with source 1 km upwind for the foot of the hill at a frequency 32 Hz (Top: source at 30 m height, Middle: source at 100 m height, Bottom: source at 300 m height).

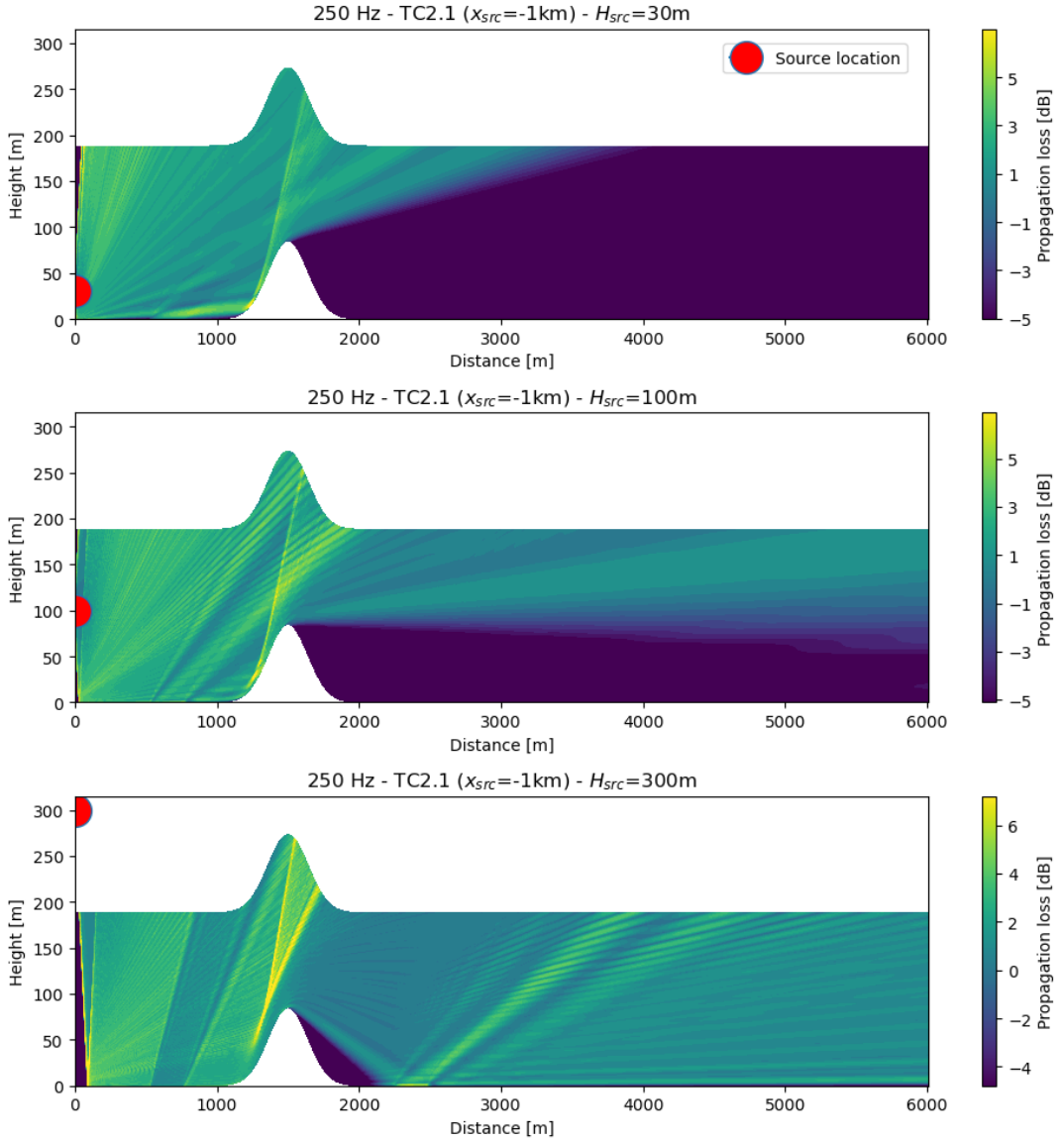

Figure 12: Transmission loss map for a single hill with source 1 km upwind of the foot of the hill at a frequency 250 Hz (Top: source at 30 m height, Middle: source at 100 m height, Bottom: source at 300 m height).

7 Double-hill case

In order to further investigate the interference pattern observed in the previous section, the case of the double-hill is considered here.

Noise maps of the noise TL are displayed, for the source at the foot of the most upwind hill, for frequencies equal to 32 Hz and 250 Hz in Figs. 13 and 14.

Once again the interference pattern is observed in the range 700 to 1000 m from the top of the second downwind hill.

It is concluding that the observed interference pattern is caused by the noise wave interacting with the hill shape sufficiently downstream of the latter.

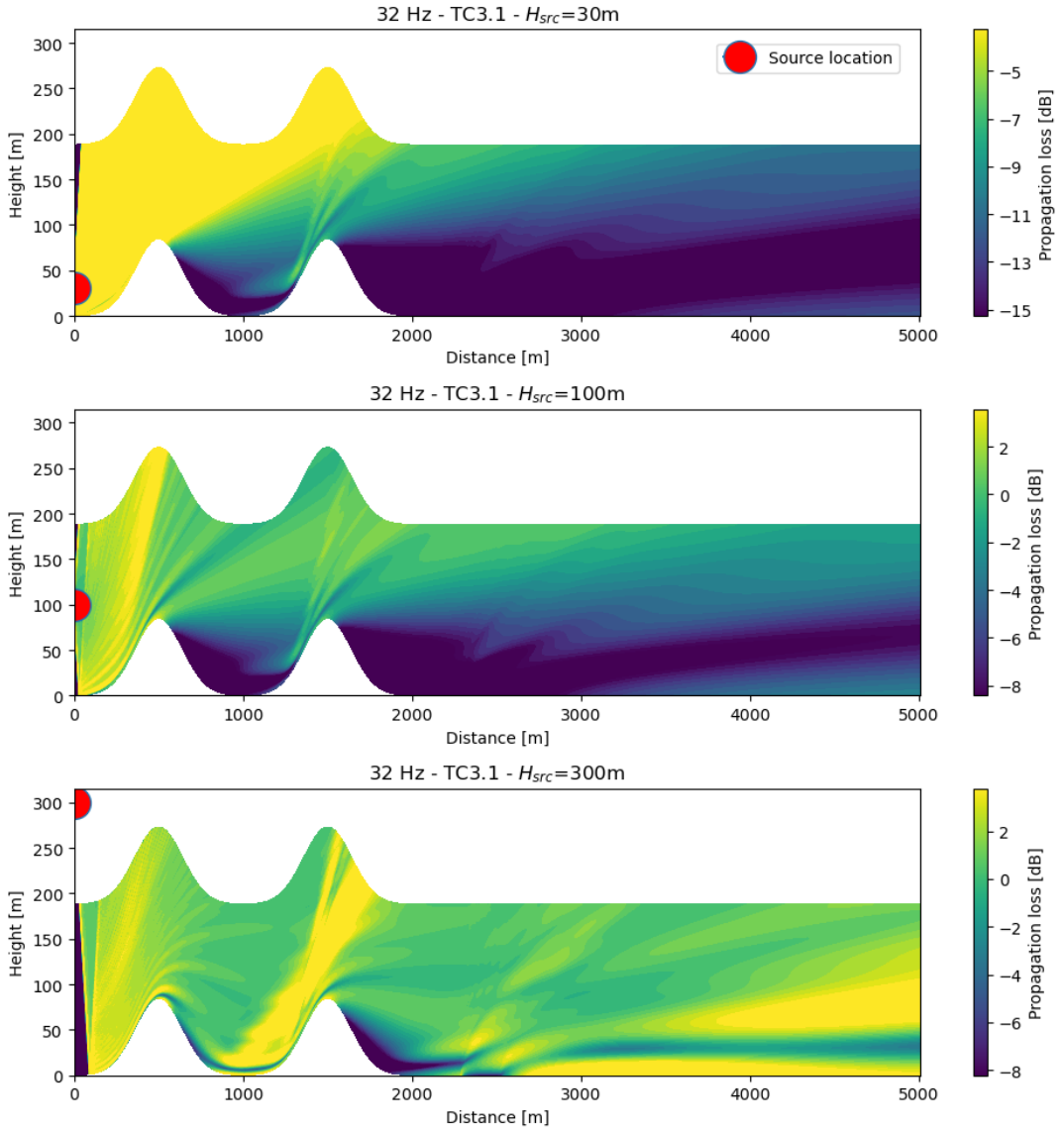

Figure 13: Transmission loss map for a double-hill with source at foot of the upwind hill at a frequency 32 Hz (Top: source at 30 m height, Middle: source at 100 m height, Bottom: source at 300 m height).

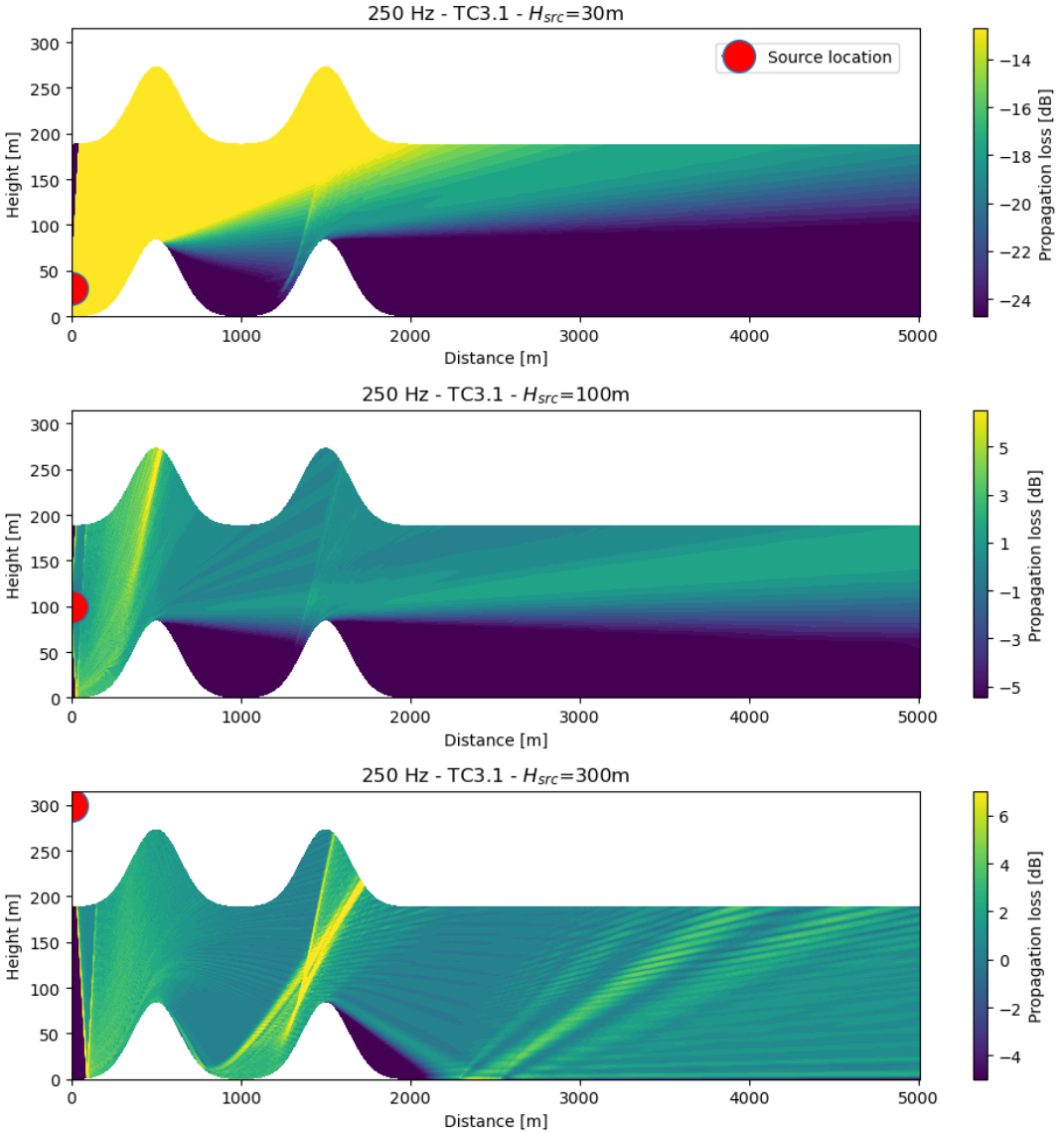

Figure 14: Transmission loss map for a double-hill with source at foot of the upwind hill at a frequency 250 Hz (Top: source at 30 m height, Middle: source at 100 m height, Bottom: source at 300 m height).

8 Valley case

This section focuses on a valley configuration as illustrated in Fig. 1 (bottom-right sketch). The main idea is to verify a specific good practice from applying the ETSU-R-97 according to the IOA (UK) for multiple reflection in a valley. The modification to the standard are reported in Fig. 15.

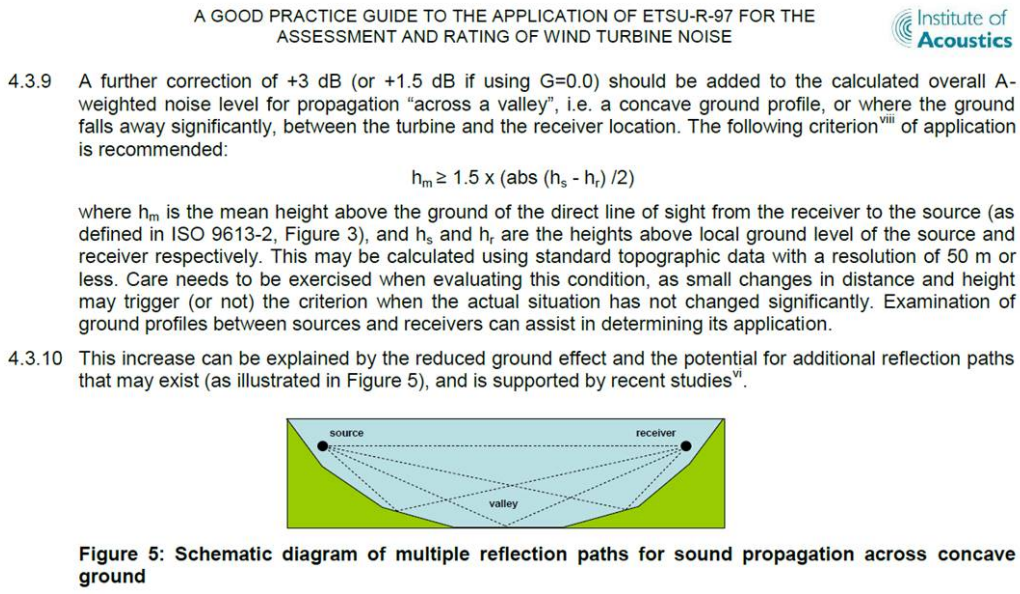

A GOOD PRACTICE GUIDE TO THE APPLICATION OF ETSU-R-97 FOR THE ASSESSMENT AND RATING OF WIND TURBINE NOISE

Institute of Acoustics

4.3.9 A further correction of +3 dB (or +1.5 dB if using G=0.0) should be added to the calculated overall A-weighted noise level for propagation "across a valley", i.e. a concave ground profile, or where the ground falls away significantly, between the turbine and the receiver location. The following criterion[viii] of application is recommended:

$$h_m \geq 1.5 \times (\text{abs}\ (h_s - h_r)\ /2)$$

where h_m is the mean height above the ground of the direct line of sight from the receiver to the source (as defined in ISO 9613-2, Figure 3), and h_s and h_r are the heights above local ground level of the source and receiver respectively. This may be calculated using standard topographic data with a resolution of 50 m or less. Care needs to be exercised when evaluating this condition, as small changes in distance and height may trigger (or not) the criterion when the actual situation has not changed significantly. Examination of ground profiles between sources and receivers can assist in determining its application.

4.3.10 This increase can be explained by the reduced ground effect and the potential for additional reflection paths that may exist (as illustrated in Figure 5), and is supported by recent studies[vi].

Figure 5: Schematic diagram of multiple reflection paths for sound propagation across concave ground

Figure 15: Good practice for applying the ETSU-R-97 in a valley configuration.

Both the PE and Nord2000 methods are confronted to the ISO 9312-2 standard in the valley configuration defined in Section 2. The considered receiver heights are 0.5, 2 and 4 m. The source heights are 30, 100 and 300 m.

Comparisons for the case without wind are displayed for the sources at an horizontal position of 500, 666 and 788 m (from upwind foot of the hill, the top being at 500 m) in Figs 16(a-b-c), respectively. The case with wind are displayed in Figs 17(a-b-c).

From these figures, it seems that the results for the ISO standard are nearly almost in between the Nord2000 and PE results. Therefore, it seems that the correction invoked earlier does not apply, at least in the cases considered in the present study.

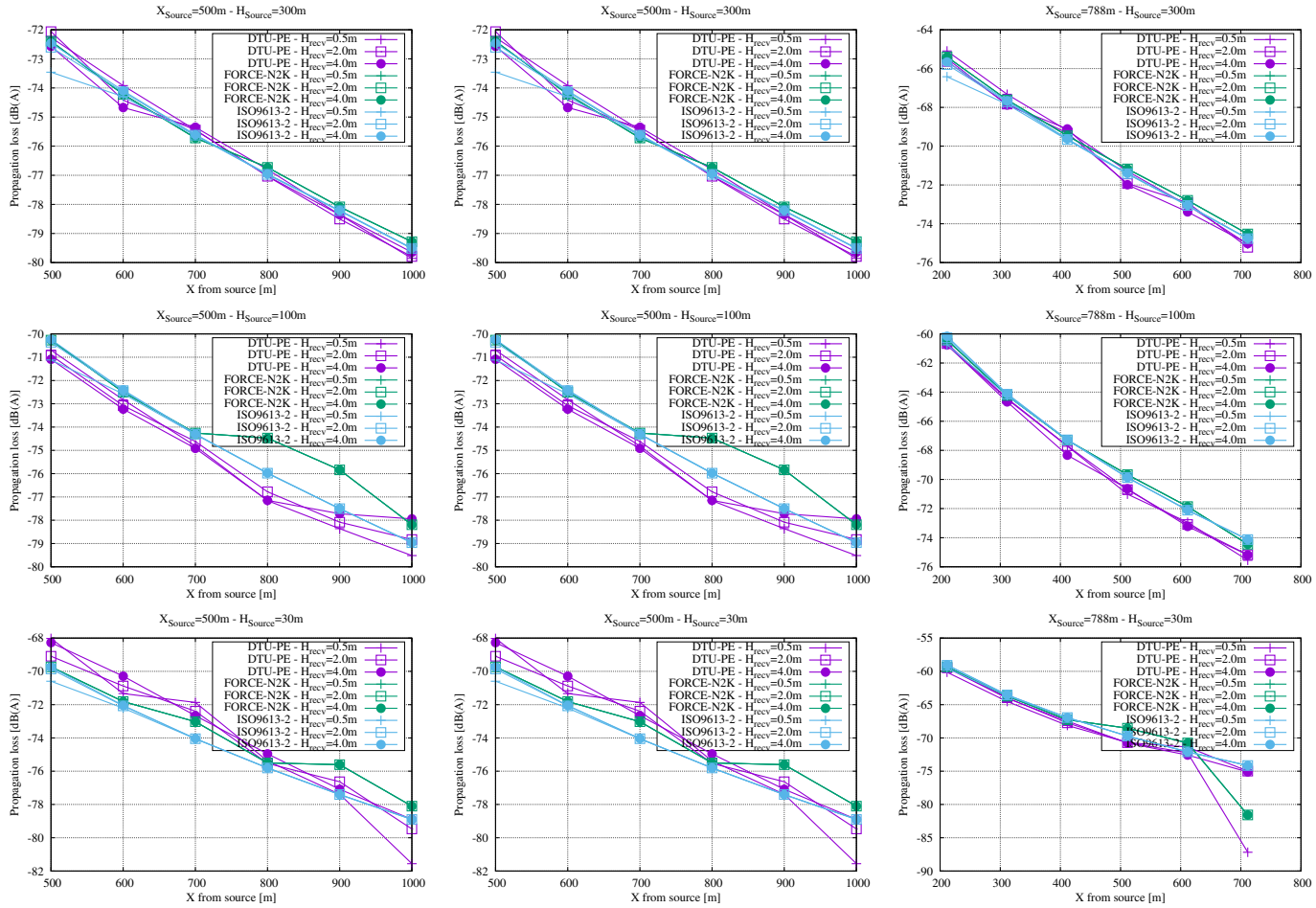

(a) Source at 500 m (b) Source at 666 m (c) Source at 788 m

Figure 16: Transmission loss as a function of distance from source in valley - No wind case.

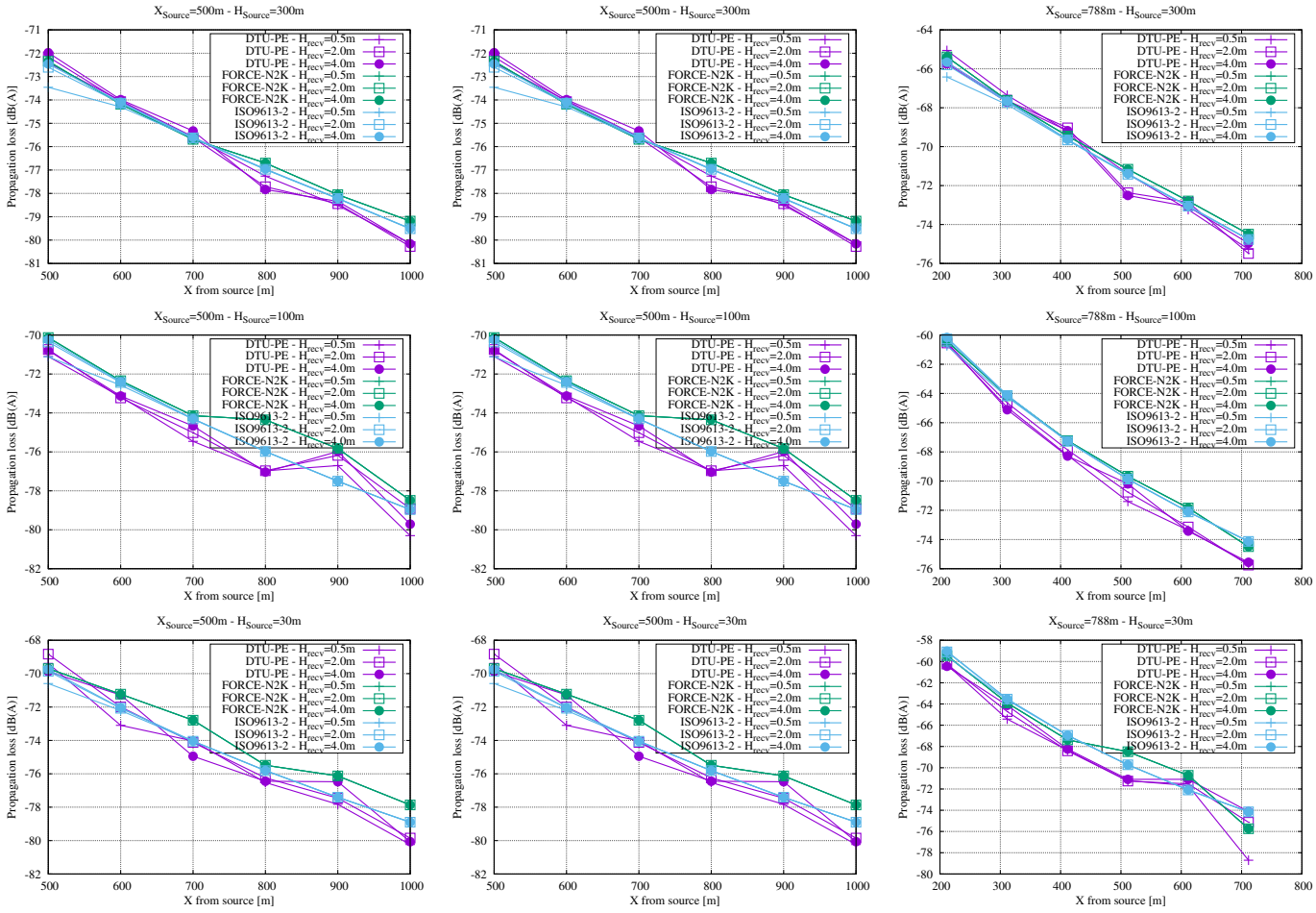

(a) Source at 500 m (b) Source at 666 m (c) Source at 788 m

Figure 17: Transmission loss as a function of distance from source in valley - With wind.

9 Conclusions

In this report, a number of calculations for academic terrain configurations are conducted. Two prediction method for noise propagation are compared: Nord2000 ray method and the PE method.

Some bias between the two predictions method are observed. However, it can not be concluded from the present study which method is the most representative of actual noise propagation.

The main important conclusion from the present study is the prediction of interference patterns for the noise propagating waves downwind of a hill. It appears that irrespectively of frequency and the noise sources heights considered here (30, 100 and 300 m), the interference patterns starts at the ground at approximately 700 m and terminates around 1000 m from the top of the hill.

6 WP3 / Annex 3 - Conference proceedings on noise propagation codes benchmark for complex terrain

forum acusticum 2023

SOUND-PROPAGATION-MODELS IN WIND-ENERGY: A CODE2CODE-COMPARISON

Katharina Elsen[1*] **Franck Bertagnolio**[2] **Arthur Schady**[1]

[1] German Aerospace Center, Oberpfaffenhofen, Germany
[2] Technical University of Denmark, Roskilde, Denmark

ABSTRACT

Within the framework of IEA wind Task 39 different benchmark-tests are performed. Here we are presenting a comparison of a particle-based model, a wave-based model and a PE-model with respect to two different test cases. They are of theoretical nature, addressing the influence of a simple meteorology in the first case and a simple topography in the second case.

Some non-intuitive behaviour of the models can be observed that is compared for the different models. We will show in particular, how the source (physics or model) of such a behaviour can be analysed and understood. This is important, as some models can create non-physical behaviour – like caustics – whilst at the same time, not all physical effects are captured by different models.

Keywords: *sound propagation simulation, wind energy, code comparison*

1. INTRODUCTION

There are several models currently being used in simulating sound propagation of wind turbine noise, starting from relatively simple standard engineering methods which are also used throughout the planning process of wind parks, up to computationally expensive high fidelity models. Whilst they are all meant to model the same physical process, they can be very different in terms of their physical background, accuracy and computational cost. Most of the models are falling in one of the following categories, which are ray-tracing (or particle tracking), parabolic equations (PE) or Linearized-Euler-Equations (LEE). However, these models do not only differ in terms of their accuracy, they also differ with respect to the sound propagation effects, like refraction or diffraction, that they are able to simulate. Furthermore, one might have to consider peculiarities that come along with the model, like caustic curves in Ray-tracing approaches and a limited propagation angle like in the PE-model. DNS-simulations like the solution to the LEEs on the other hand have the drawback of easily becoming computationally very expensive as the grid width and time resolution have to be adjusted to the wavelength of the highest frequency that is to be modelled. In the following we are presenting three different sound propagation models as well as two theoretical, wind energy related, test cases that were showing interesting and unexpected results. We will then compare the outcome of the simulations and analyse the origin of the effects we are observing.

**Corresponding author*: *katharina.elsen@dlr.de.*

2. DESCRIPTION OF THE 3 MODELS

2.1 Wave-Based Model (*AKU3D*)

The sound propagation model *AKU3D*, described in Blumrich et al [1] and Heimann et al [2], is based on the governing equations of a compressible and adiabatic gaseous medium in a non-rotating system, which are the equation of motion, the equation of continuity and the first law of thermodynamics for adiabatic processes (gravity is

neglected), resulting in the following set of equations:

$$\frac{\partial \mathbf{u}}{\partial t} + (\mathbf{u} \cdot \nabla)\,\mathbf{u} = -\frac{1}{\rho}\nabla p, \tag{1}$$

$$\frac{\partial p}{\partial t} + \mathbf{u} \cdot \nabla p = -\kappa p \nabla \cdot \mathbf{u}, \tag{2}$$

with $\kappa = c_p/c_v$. The atmospheric variables $\phi = (\mathbf{u}, p, \rho)$ are then split up into their meteorological, turbulent and acoustic parts:

$$\phi = \bar{\phi} + \phi' + \phi'', \tag{3}$$

where the overbar ($\bar{\phi}$) denotes the mean variables, a single prime (ϕ') indicates the turbulent deviations from the mean meteorological values and the double prime (ϕ'') describes the deviations from the mean field according to acoustic waves (in particular sound pressure p'' and particle velocity $\mathbf{u}''$).

The sound propagation model is based on prognostic equations of $\mathbf{u}''$ and p''. The model equations are deduced from (1) and (2) with $\mathbf{u} = \bar{\mathbf{u}} + \mathbf{u}''$, $p = \bar{p} + p''$ and $\rho^{-1} = \alpha = \bar{\alpha} + \alpha''$. The equations are then linearized with respect to the mean state where the turbulent parts are disregarded as the atmosphere is seen to be stationary in time. Finally a diffusion term was added in order to simulate the effect of atmospheric absorption.

The prognostic model equations are numerically solved on an orthogonal staggered grid. The numerical scheme conforms to that of the flow model except that the explicit forward-in-time scheme is also used for the diffusion term. The spatial distribution of the meteorological field is taken from the results of a flow model.

2.2 Particle-Based Model (*AKUMET*)

The idea behind the particle-model *AKUMET*, described in Heimann et al [3], is distributing the sound energy on a given number of sound particles and propagating those particles through the atmosphere. The paths of the particles are hereby describing the propagation of the wavefront. *AKUMET* was designed to simulate the propagation of sound over hilly terrain in an inhomogeneous atmosphere. Therefore a frequency-dependent fraction of sound pressure amplitude:

$$p_i(f) = \frac{1}{N}\sqrt{2\rho_s c_s J_0(f)} \tag{4}$$

is assigned to each particle $j (j = 1, \ldots, N)$, where ρ_s and c_s are the air density and sound speed at the source, respectively. The sound intensity at the distance s_0 from the source is given by:

$$J_0(f) = \frac{P_s(f)}{a_1 \triangle \psi s_0^{a1}}. \tag{5}$$

Depending on the type of source, a_1 is set to 2 (point source) or 1 (line source).

The path of the j-th particle is given by the ray vector $\vec{x}_j(t)$ and the unit vector normal to the wavefront $\vec{n}_j(t)$. Differential equations for both vectors are given by Pierce et al [4]:

$$\frac{d\vec{x}_j}{dt} = \vec{v} + c\vec{n}_j, \tag{6}$$

$$\frac{d\vec{n}_j}{dt} = -\vec{\nabla}c - \sum_{i=1}^{3} n_{ji}\vec{\nabla}v_i, \tag{7}$$

with the speed of sound $c = \sqrt{\kappa R_L T}$. $\vec{v}$ is the three dimensional wind vector, whereas κ and R_L are the ratio of specific heat capacities and the gas constant of dry air, respectively. Equations (6) and (7) are numerically integrated for all particles using forward time integration until the particle has left the computational domain.

At the end of the simulation a sound pressure level is computed, based on the particles that have passed through a grid cell during the simulation. The model considers reflection on the ground, air absorption, refraction and obstacles of arbitrary shape. The spatial distribution of the meteorological field is taken from the results of a flow model. The model has already been used in several wind turbine noise applications (e.g. Heimann et at [5])

2.3 Parabolic Equation (PE) Model

The WindStar-Pro model implements the Generalized Terrain Parabolic Equation (GTPE) as described and tested in Barlas et al [6]. The Helmholtz wave equation is solved for the acoustic pressure in the frequency domain (i.e. independently for each frequency). In the present study, the two-dimensional, wide-angle, Crank-Nicholson, parabolic equation is used with a starter function for modelling a point source. An effective speed of sound, which is the parameter driving sound wave refraction, is used to account for temperature and wind velocity gradients in the atmosphere. The ground impedance is calculated using the classical Delany-Bazley model, which uses the ground flow resistivity as an input. Further implementation details about the PE and GTPE methods are provided in West et al [7] and Salomons [8], respectively.

3. DESCRIPTION OF THE TEST CASES

All together three test cases with different topography and meteorology are studied. These are introduced in the following, in order of their overall complexity.

3.1 Test case 1: Flat topography with generic meteorology

The first test case is characterised by a flat topography and a simple meteorological profile as shown in Fig. 1.

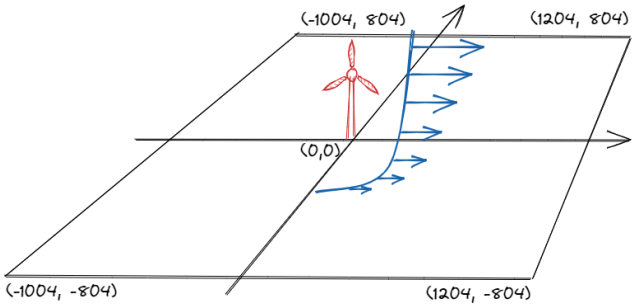

Figure 1. Sketch of computational domain, wind profile and wind turbine position for test case 1.

3.1.1 Topography:

The domain is defined as $[x_{min}, x_{max}] \times [y_{min}, y_{max}] = [-1004\ m, 1204\ m] \times [-804\ m, 804\ m]$ and z ranges from $0\ m$ to $700\ m$. The grid width x/y-direction is given by $d_x = d_y = 8\ m$ and is variable in z-direction (increasing with height).

3.1.2 Meteorology

The parameters of the meteorological profile are given in table 1. The profile is assumed to be constant for all x/y and thus only varies in z. To retrieve the logarithmic wind profile, given a roughness length z_0, the wind speed $u(h)$ for any given height $h > 0$ is calculated from the reference height $h_r > 0$ and reference wind speed u_r as follows:

$$u(h) = u_r \frac{\ln\left(\frac{h}{z_0}\right)}{\ln\left(\frac{h_r}{z_0}\right)} \tag{8}$$

3.1.3 Source:

The wind turbine is located at $(x_0, y_0) = (0, 0)$ and is defined as a single point source at $78\ m$ over ground, with a sound power level of $107\ dB$. Simulations with a spectrum of frequencies from $20\ Hz$ to $20\ kHz$ as well as single frequency simulations were performed. For this paper, frequencies of 16 Hz and 100 Hz are used.

3.1.4 Model setup:

The simulation was performed without turbulence, using standard air absorption (ISO 9613) and totally even ground. The ground itself was considered using complex impedance and diffraction at the ground was enabled.

3.2 Test case 2: Single hill with meteorology

The second test case is a 2D-domain characterised by a hill and a simple meteorological profile as shown in Fig. 2.

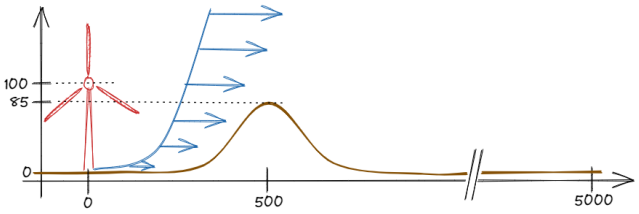

Figure 2. Sketch of topography, wind profile and wind turbine position for test case 2.

3.2.1 Topography:

The domain is defined by $[x_{min}, x_{max}] = [0\ m, 5000\ m]$ and z ranges from $0\ m$ to $1500\ m$. The height of the hill itself is defined in (9).

$$h(x) = 84.9 \cdot \exp\left(-\left(\frac{x - 500}{200}\right)^2\right). \tag{9}$$

The grid width depends on the model. In case of the particle-model $d_x = 8\ m$ was sufficient, whereas it is variable in z-direction (increasing with height). For the wave-based-model $d_x = d_z = 1.5$ was chosen. PE-model?

3.2.2 Meteorology

The parameters of the meteorological profile are given in table 1 on the right. The profile is assumed to be constant for all x and thus only varies in z. The wind profile with

Case 1			Case 2		
parameter		value			
sound speed	$[m/s]$	340.0	sound speed	$[m/s]$	340.0
temperature	$[°C]$	20.0	temperature	$[°C]$	15.0
vertical temp. grad.	$[K/100m]$	0.0	vertical temp. grad.	$[K/100m]$	0.0
humidity	$[\%]$	70.0	humidity	$[\%]$	70.0
wind speed in 10 m	$[m/s]$	(0.0/2.5/)5.0	wind speed in 100 m	$[m/s]$	8.0
wind profile		log. prof.	wind profile		power law
roughness length	$[m]$	0.2	power coefficient		0.143
wind direction	$[°]$	270.0	wind direction	$[°]$	270.0
ground resistivity	$[kPas/m^2]$	absorption	ground resistivity	$[kPas/m^2]$	250.0

Table 1. Meteorology for test cases 1 (left) and 2 (right).

wind speed $u(h)$ at a given height h was calculated using the power law:

$$u(h) = u_r \left(\frac{h}{h_r} \right)^{\beta} \tag{10}$$

with power coefficient β, reference height $h_r > 0$ and reference wind speed u_r.

3.2.3 Source:

The source is located at $x_0 = 0$ and is defined as a single point source. Three simulations where performed with the respective height of the source at $z = 30, 100, 300$ m. Several frequencies have been tested, here we will concentrate on 16 Hz.

3.2.4 Model Setup:

4. SIMULATION RESULTS

In the following three subsections we are showing the simulation results of the test cases described above, i.e. describing the initial problem, explaining the thought-process to narrow down the problem and finally comparing the results obtained using the different models.

4.1 Flat topography with generic meteorology

4.1.1 Description of the problem

The Problem was initially found during *AKUMET*-Simulations for wind-turbine noise. A 2D-plot of the associated sound pressure level on the ground is shown in Fig. 3. The wind direction is 270°, i.e. the wind is blowing in positive x-direction. As can be expected, the

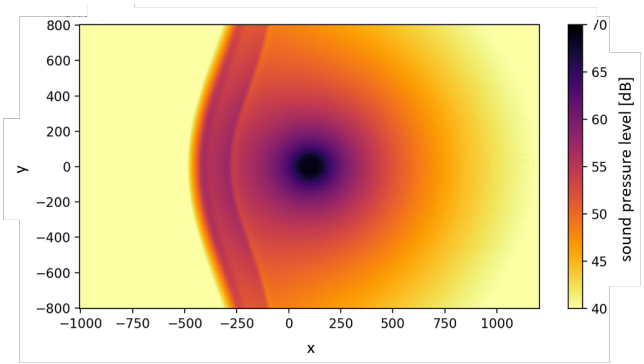

Figure 3. 2D-plot of the sound pressure level simulated on the ground using *AKUMET* for the first test case.

sound pressure level in the downwind-domain is generally higher than in the upwind-domain. The shadow-zone in the upwind-domain is clearly visible. However, there is also a strong increase in sound pressure level visible directly before the beginning of the shadow zone whose origin is not obvious.

4.1.2 Solution strategies

To narrow down the problem, we first reduced it to the 2D-domain and disabled several subroutines connected to weighting and smoothing the sound pressure level. Further we switched to fully absorbing ground conditions to eliminate reflections. As the problem is obviously dependent on the wind field, we then performed simulations

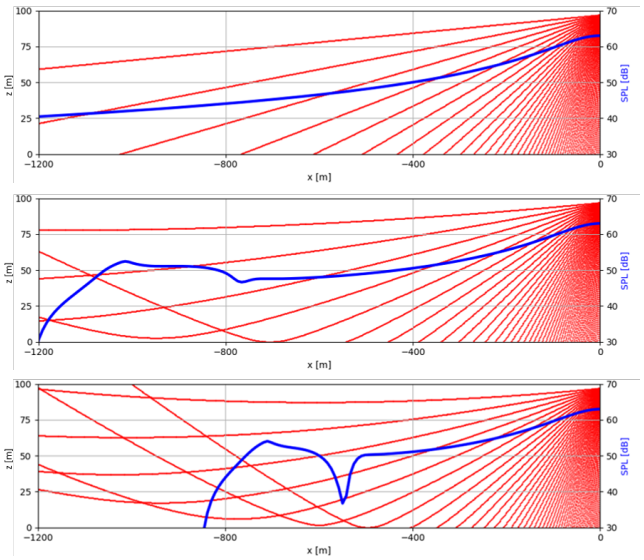

Figure 4. Results for test case 1, computed using *AKUMET* for three different wind speeds (top: 0 m/s, middle: 2.5 m/s, bottom: 5/s) with a grid width of 8 m for a frequency of 100 Hz. Sound pressure level is given in blue, sound rays are shown in red.

with different wind speeds. The main goal was to understand whether the origin of the effect was physical, numerical or model-related. As *AKUMET* is basically a Ray-tracing-model, we were able to plot those rays, which are essentially the paths that the particles are travelling. The results, restricted to the upwind-domain, for different wind speeds are shown in Fig. 4. The sound pressure level is shown in blue whereas selected sound rays are plotted in red. No wind speed is given in the top figure, lower wind speed (2.5 m/s) was chosen in the middle figure and the original wind speed (comp. table 1) was used for the bottom figure.

4.1.3 Explanation of the effect

From Fig. 4 can be seen that the increase of sound pressure level is preceded by a sudden drop of it. The effect, including the depth of the drop, clearly increases with the wind speed and it occurs earlier on in the domain the higher the wind speed is while it is absent in the absence of wind. This is easily explained by the stronger downwards refraction of the sound rays in higher wind speeds. It shall however been mentioned that the effect is not exactly related to the wind speed itself but to the wind speed

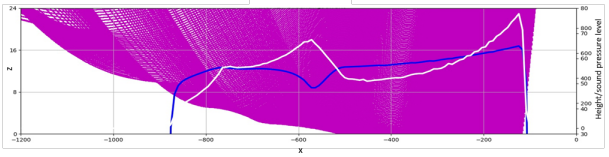

Figure 5. Results for test case 1, computed using *AKUMET* with a grid width of 8 m for a frequency of 100 Hz. Sound pressure level is given in blue, sound rays are shown in purple and the number of particles per grid cell in white.

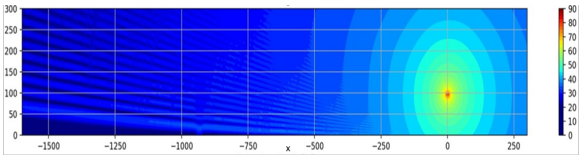

Figure 6. Sound pressure level field for test case 1, computed using *AKU3D* for a frequency of 100 Hz and a wind speed of 5 m/s.

gradient.

Looking more closely at the sound rays we find that the drop occurs in the area where the first sound rays, those still moving downwards and those already been refracted upwards, are intersecting. This leads, on one hand, to a higher number of particles in that area, and on the other hand, to destructive interference (resulting in the sound pressure level to drop, blue curve). This can be seen in Fig. 5 (sound rays are shown in purple to indicate the beginning of the shadow zone), where the number of particles is indicated by the white curve, the sound pressure level is again shown in blue. Further downwind the number of particles decreases again but so do the effects of interference, leading to an increase in sound pressure level. The number of particles is, due to the additional, upwards refracted sound rays in that area, still higher than it was before the drop, and therefore is the sound pressure level. Finally, the maximum in sound pressure level (around x=-700 in Fig. 4, bottom) is caused by constructive interference. These results are obtained under the assumption of a coherent source.

4.1.4 Comparison with other model results

The input parameters of *AKUMET* cannot be matched exactly on the wave-based model *AKU3D*, as, one being a

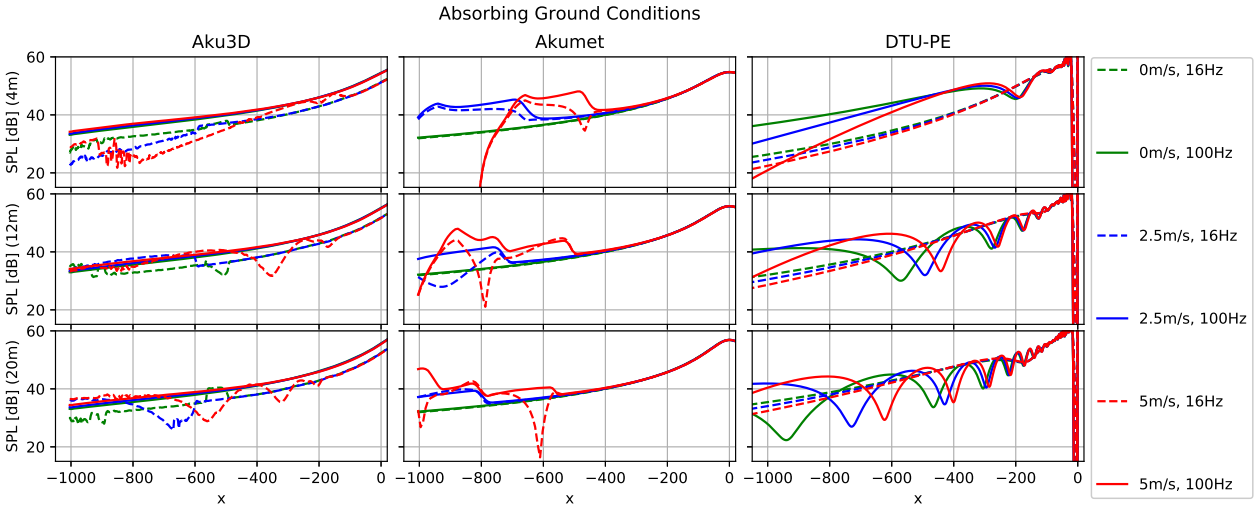

Figure 7. Test Case 1, absorbing ground conditions: left: Aku3d, middle: Akumet, right: PE; from top to bottom: 4m, 12m and 20m above ground; dashed and solid line: 16 Hz and 100Hz respectively; green, blue and red: 0m/s, 2.5m/s and 5m/s wind speed

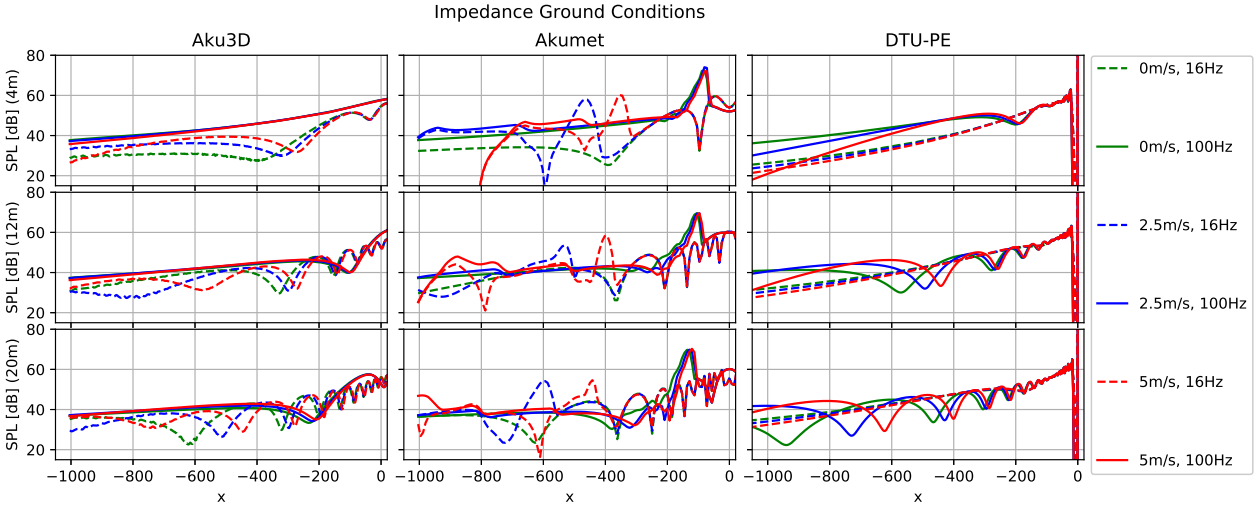

Figure 8. Test Case 1, impedance ground conditions: left: Aku3d, middle: Akumet, right: PE; from top to bottom: 4m, 12m and 20m above ground; dashed and solid line: 16 Hz and 100Hz respectively; green, blue and red: 0m/s, 2.5m/s and 5m/s wind speed

Lagrangian approach and the other a Eulerian approach that directly simulates the wave propagation, they have different requirements concerning e.g. grid width and time stepping. The same holds for the PE-model. Therefore the input parameters were adapted to fit the model. Due to the high computational cost the domain was restricted to 2D. The resulting sound pressure level field of the *AKU3D*-simulation is shown in Fig. 6. One can nicely see the interference pattern, as well as the formation of a shadow zone in the upwind domain. Fig. 7 shows the behaviour for 3 different wind speeds (0 m/s, 2.5 m/s and 5 m/s) and two different frequencies (16 Hz and 100 Hz) for all three models using absorbing boundary conditions. Fig. 8 shows the same test case for impedance boundary conditions. Clear differences can be observed between the models, for different frequencies, but also between impedance and absorbing ground conditions. Generally, the results of *AKU3D* and *PE-DTU* are more similar to each other, while in case of *AKUMET* the wave can be observed more clearly. Simulations with absorbing ground are strongly helping in understanding the origin of the problem, as in case of impedance boundary conditions – due to the single frequency – reflection patterns can be observed. Nonetheless, the wave can be observed with all three models. The reason why the wave is more pronounced in case of the *AKUMET*-simulation is most likely explained by the formation of a shadow zone, leading to sharper edges (comp. Fig. 4).

4.2 Single hill with simple meteorology

In Fig. 9 the original findings of test Case 2 for 16Hz and a source in 30m of height are shown for different models (PE, Nord2000) as well as for different turbulence settings, geometric spreading is shown in grey (solid). No legend is given in this plot as we only want to point out the initial problem, which is the second drop in sound pressure level, followed by a rise in the sound pressure level. Whilst the first drop is easily explained by the shadow zone, formed by the hill (shown in light grey), the explanation of the second drop is less obvious. There are also significant differences between the different models. Fig. 10 shows a comparison of the simulations results for the three models compared in this paper. From left to right we find the results of *AKU3D* *AKUMET* and *PE-DTU* each for three different source heights, 30m (dashed, green), 100m (solid, blue) and 300m (dotted, red) and all for a frequency of 16 Hz. It shall be noted that the results are still preliminary and only a qualitative comparison can be made between the models. The three models are showing significant differences but also some similarities. The largest differences are found for the 30m source, as here the influence of the hill is strongest, due to the formation of a shadow zone. Due to computational limitations, only the domain up to 1350m is shown here, however, this includes the area of the second drop of the *PE-DTU*-model. Such a drop could not be found in case of *AKU3D* for neither of the source heights. In case of *AKUMET* we find some oscillations in the far field of the 100m source that result from numerical limitations. Only the *AKUMET*-simulation is showing the building of a sharp shadow-zone in case of the 30m source. Comparing the results to test case 1, one could assume that the drops in the *PE-DTU*-simulation result from interference-effects. Also in test case 1, interference and reflection effects where varying significantly in all three simulations. However, we can not yet prove this assumption and further analysis has to be done to fully explain the effect.

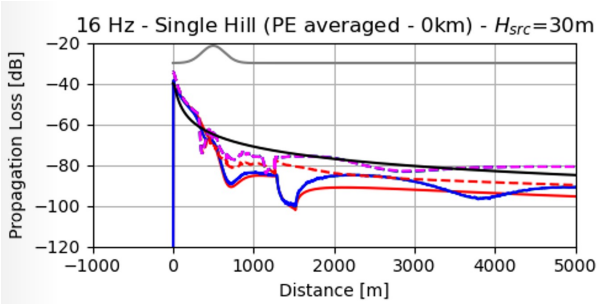

Figure 9. Test Case 2, 16Hz, original findings: comparison of the results of the 30m source height for different models (PE, Nord2000) and different turbulence settings, geometric spreading is shown in grey (solid)

5. SUMMARY

We were presenting two theoretical test cases and comparing the according simulation results of three different sound propagation models. In particular in test case 1, the questionable behaviour could be observed – from a qualitative point of view – in all three models, also significant differences were found among the respective simulations. It was shown how the origin of a specific behaviour can be traced down using the specific characteristics (i.e. sound rays) of the different sound propagation

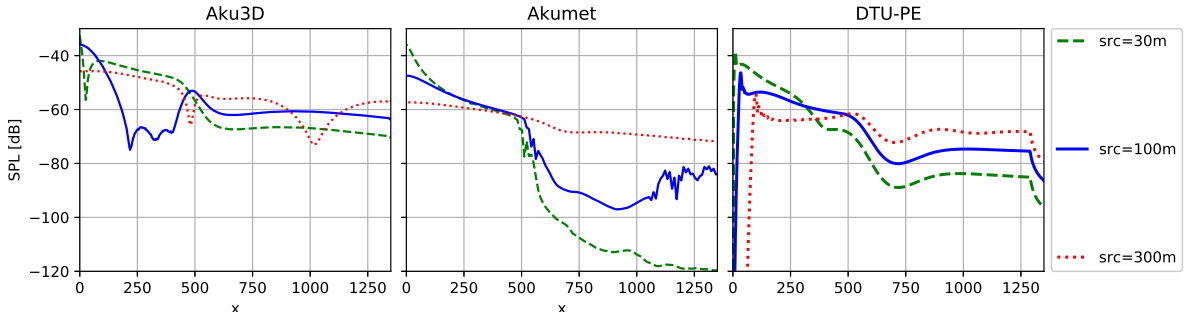

Figure 10. Test Case 2, impedance ground conditions, 16Hz: left: Aku3d, middle: Akumet, right: PE; dashed (green), solid (blue) and dotted (red) line: source height of 30m, 100m, and 300m respectively

models. With respect to the second test case more detailed analysis of the problem has to be done to fully understand the origin of the problem. Generally speaking, all models do have their advantages and disadvantages and our findings are showing that it can be beneficial to use different model-approaches to simulate a specific problem. This can strongly help the investigation whether a problem is really physical or model related.

6. ACKNOWLEDGEMENT

7. REFERENCES

[1] R. Blumrich and D. Heimann, "A linearized eulerian sound propagation model for studies of complex meteorological effects," *JASA*, vol. 112, no. 2, pp. 446–455, 2002.

[2] D. Heimann and R. Karle, "A linearized euler finite-difference time-domain sound propagation model with terrain-following coordinates," *JASA*, vol. 119, no. 6, pp. 3813—-3821, 2006.

[3] D. Heimann and G. Gross, "Coupled simulation of meteorological parameters and sound level in a narrow valley," *applied acoustics*, vol. 56, pp. 73–100, 1999.

[4] A. D. Pierce and P. W. Smith, "Acoustics: An introduction to its physical principles and applications.," *Physics Today*, vol. 34, no. 12, pp. 56–57, 1981.

[5] D. Heimann, Y. Käsler, and G. Gross, "The wake of a wind turbine and its influence on sound propagation," *MetZet*, vol. 20, no. 4, pp. 449–460, 2011.

[6] E. Barlas, W. J. Zhu, W. Z. Shen, K. O. Dag, and P. Moriarty, "Consistent modelling of wind turbine noise propagation from source to receiver," *J. Acoust. Soc. Am.*, vol. 142, no. 5, pp. 3297–3310, 2017.

[7] M. West, K. Gilbert, and R. A. Sack, "A tutorial on the parabolic equation (pe) model used for long range sound propagation in the atmosphere," *Appl. Acoust.*, vol. 37, no. 1, pp. 31–49, 2017.

[8] E. M. Salomons, *Computational Atmospheric Acoustics*. Netherlands: Springer Dordrecht (Publisher), 2002.

7 WP3 / Annex 4 - Definition of noise propagation codes benchmark for flat terrain and offshore conditions

International Energy Agency
IEA Wind Technology Collaboration Program (TCP)

IEA Wind Task 39 – Quiet Wind Turbine Technology (Phase 2)

BENCHMARK FOR SOUND PROPAGATION MODELS IN OFFSHORE CONDITIONS
Definition of a benchmark exercise

Contact: Franck Bertagnolio (DTU Wind and Energy Systems, email: frba@dtu.dk)

July, 2022

Introduction

The aim of this benchmark is to compare and validate various sound propagation models for **offshore** (and *offshore-to-onshore*) conditions, in the context of wind turbine noise.

The benchmark comparison exercise is divided into 2 main parts: 1) a series of idealized test-cases to evaluate the effects of some physical parameters, mainly related to atmospheric conditions and sea-to-shore transition, and 2) a real-life case derived from a measurement campaign conducted in Sweden in 2009 using loudspeakers placed on a lighthouse at sea (at 9.04 km from the shore in the direction of the propagation of interest) and a microphone array located onshore (560 m further away from the shoreline). More details about the actual test-site can be found in [Bolin2009] in the references. The idealized and real-life test-cases will be addressed iteratively in two separate rounds of comparisons.

The benchmark definitions and the results to be provided for the 1st round are described in the present document.

Sea/Ground Surfaces and Atmospheric conditions

The main interest of this benchmark is sound propagation in offshore conditions, but the transition from sea-to-land and its effect on the noise immission levels are also investigated. The overall study and analysis of the results will focus on low-frequency noise since it should be the dominant part of the spectrum for large distances from source to receiver typical of offshore wind farm conditions. However, frequencies up to 4 kHz are considered.

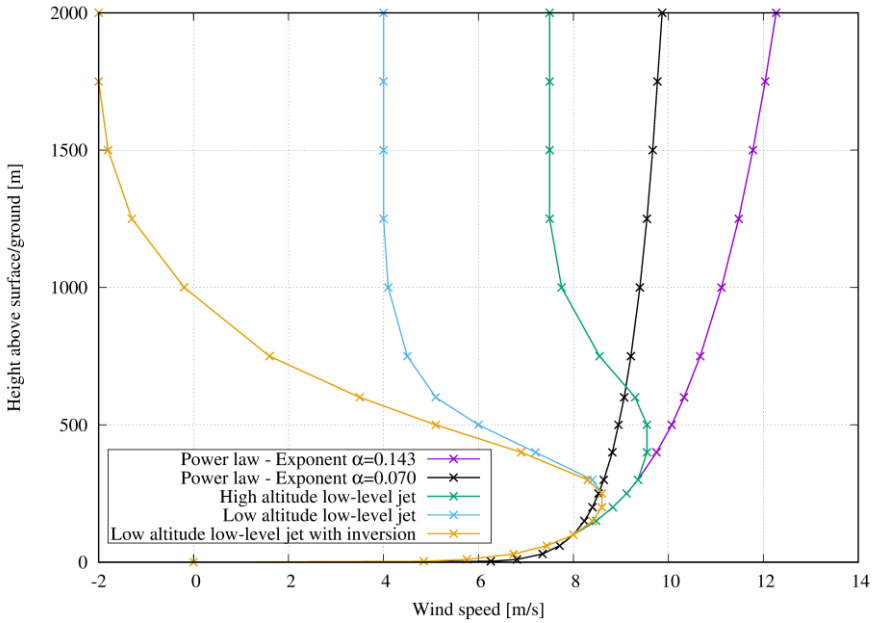

Figure 1 - Various wind shear profiles (all such that the wind speed at 100m is equal to 8m/s).

Test-cases round 1 definition (idealized)

In this first part of the benchmark comparison, a number of 'idealized' test-cases (without ground, i.e. only a flat sea surface) are defined. The goal is to investigate the influence of various physical parameters on the different model results. Since the sea surface is considered as flat and uniform, the study concentrates on the atmospheric conditions with various wind profiles (see Fig. 1 and test-cases TC1.0 to TC1.8 definitions as defined below), e.g. with the definition of various low-level jet (LLJ) conditions. Thereafter, the sea-to-land transition is also investigated (TC1.10 and higher).

Sea-surface only:

- TC1.0: No wind, constant atmospheric conditions with height, sea surface (flat) from source to all receiver
- TC1.1: As TC1.0 but with positive wind shear (Power law – Exponent α=0.143=1/7)
- TC1.2: As TC1.0 but with positive wind shear (Power law – Exponent α=0.07)
- TC1.3: As TC1.1 but with negative velocity (i.e. upwind propagation configuration)
- TC1.4: As TC1.1 but with atmospheric turbulence
- TC1.5: As TC1.3 but with atmospheric turbulence
- TC1.6: As TC1.1 but with 'high' altitude LLJ as a velocity profile
- TC1.7: As TC1.1 but with 'low' altitude LLJ as a velocity profile
- TC1.8: As TC1.1 but with 'low' altitude LLJ with inversion as a velocity profile

Sea-to-land cases:

- TC1.10: As TC1.1, but with the last part of the noise path (beyond the shoreline located at 9.04 km) is ground (grassland-type) without elevation
- TC1.11: As TC1.10, but with the last part of the noise path including terrain elevation (see details below)
- TC1.12: Same as TC1.10, but the sources are moved to the position of receptors #6, #7 and #8
- TC1.13: Same as TC1.11, but the sources are moved to the position of receptor #6, #7 and #8

For each test-case, the calculations should be conducted with **3 source heights: 30, 100 m and 300 m**. The sources should be considered as monopoles.

The **receptors** should be located **every 1 m from the emission location up to 12 km**. However, if the participant is limited (e.g. by computational resources), results can be provided only at **12 receptor** positions which should be equally spaced **every km between 1 km and 9 km,** with the **last points at 9.600 km, 11 km and 12 km** (as described in Table 1). **All receptors** should be placed at a **height of 2 m above ground** (or above sea, when at offshore locations) **level**.

The manner to define and model the effect of the atmospheric turbulence is left to the participants, but a **turbulence intensity TI = 10%** should be chosen, and if possible a **length scale of 100 m**, and **neutral conditions**. In any case, basics details about the implementation of the turbulence should be provided when delivering the results.

For the additional **'sea-to-land' test-cases**, the land ground elevation is either ignored (TC1.10) or included (TC1.11). Additional source locations are also considered (still using the 3 considered source heights) in test-cases TC1.12 and TC1.13. In these latter cases, the source positions should be placed closer to the shore at the receptor positions #6, #7 and #8 (i.e. at 3.04, 2.04 and 1.04 km from the shore, respectively).

No temperature gradient should be considered.

Note that the participants are free to choose and conduct the calculations for some selected or all test-cases at their discretion. However, they are strongly encouraged to conduct all of them for the sake of completeness for comparisons with other participants.

A number of files defining the test-site are available in various format (ESRI, xyz in ASCII, kml) on the Task 39 Sharepoint that can be retrieved using the following link:
https://share.dtu.dk/sites/IEA_WIND_T39_459100/WP3%20Noise%20propagation/Forms/AllItems.aspx?RootFolder=%2Fsites%2FIEA%5FWIND%5FT39%5F459100%2FWP3%20Noise%20propagation%2FOffshoreNoisePropagation%5FHighFidelityModels%2FBenchmark%5FRound1&FolderCTID=0x01200006BC6AACDCAEC14692A74AECBBECF8BC&View=%7BFC427970%2D9CAB%2D43E9%2D8181%2D30C28187D6E3%7D&InitialTabId=Ribbon%2ERead&VisibilityContext=WSSTabPersistence

Receptor number #	Distance from source [m]	UTM coordinate Latitude in Datum UTM 33 V [m]	UTM coordinate Longitude In Datum UTM 33 V [m]	Elevation from ground/sea level [m]
Light-house	*0*	*577721.01*	*6248343.24*	*30, 100, 300*
1	1000	578700.59	6248545.92	0
2	2000	579680.17	6248748.59	0
3	3000	580658.83	6248951.08	0
4	4000	581638.41	6249153.75	0
5	5000	582617.99	6249356.43	0
6	6000	583596.65	6249558.91	0
7	7000	584576.23	6249761.58	0
8	8000	585555.81	6249964.26	0
9	9000	586534.47	6250166.74	0
Shore	*9040*	*586569.5*	*62501734.0*	*0*
10	**9600**	**587123.32**	**6250288.58**	**4.48**
11	11000	587857.77	6250440.53	25.5
12	12000	588779.30	6250631.20	36.4

Table 1 – Source and receptor positions, as well as ground elevation for the sea-to-shore test-cases.

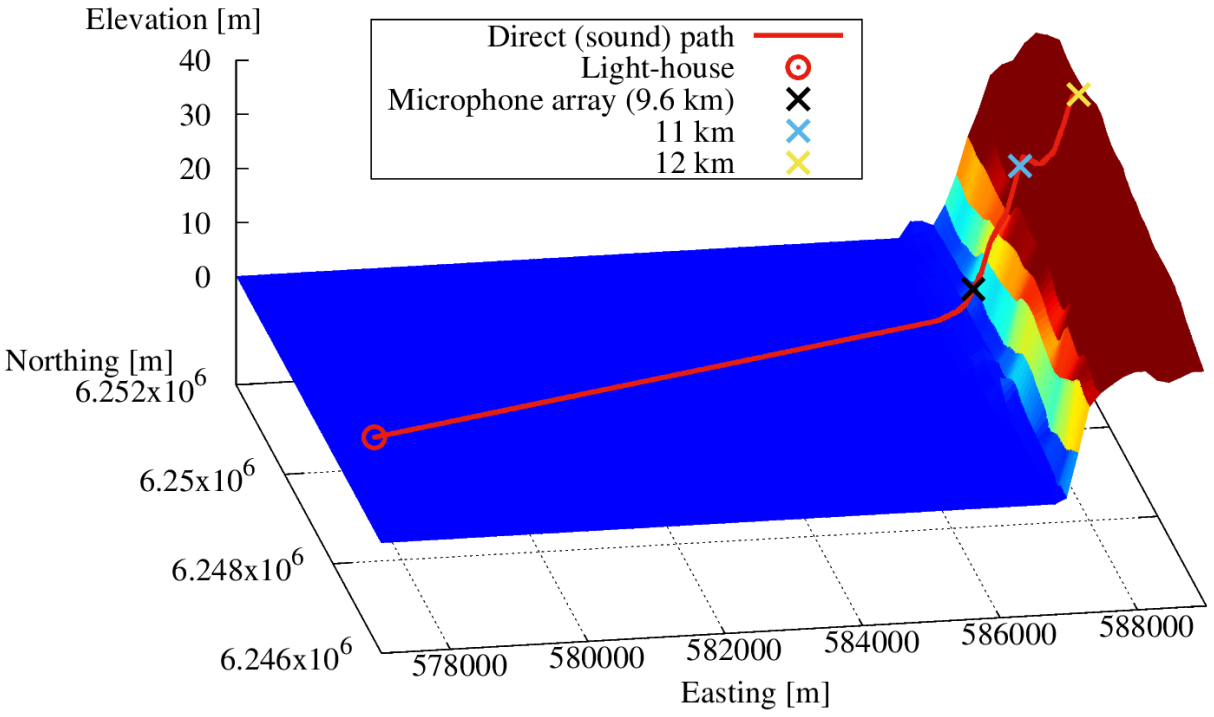

Figure 2 – Sketch of propagation environment with source, microphone array (receptor number #10), and receptors at 11 and 12 km positions.

Quantity	Value	Unit
Reference wind speed at 100m [m/s]	8	m/s
Temperature at all height [deg.C]	15	deg.C
Atmospheric pressure at all height [hPa]	1013	hPa
Rel. Humidity at all height [%]	70	%-RH
Sea surface effective flow resistivity [kPa.s/m^2]	10^6	kPa.s/m^2
Ground surface effective flow resistivity (grass) [kPa.s/m^2]	250	kPa.s/m^2

Table 2 – General atmospheric and ground conditions for the noise propagation calculations.

Test-cases round 2 definition (real-life – To be considered later as part of a 2nd round of comparisons)
In this part of the benchmark exercise, several specific conditions recording during the measurement campaign will be reproduced. The definitions of these test-cases will be handled in a 2nd round of this benchmark project with more detailed inputs from KTH in order to reproduce the conditions observed in [Bolin2009].

Results and Formats

The result to provide for the different test-cases, as well as their preferred formatting, are described in this section.

Noise propagation losses should be provided as **non-weighted** (although A-weighted is also acceptable – Remind to specify this when providing your results) **Sound Pressure Levels (SPL) calculated at the 9 center frequencies of the 1/1 octave bands** from 16 Hz to 4 kHz. In other words, the calculations should be made using the center frequency of each band, i.e. 16, 31.5, 63, 125, 250, 500, 1000, 2000 and 4000 Hz. If possible (and meaningful), the SPL integrated over the 1/1 octave bands frequencies should also be provided. Please do specify how the SPL are calculated (in term of frequency band integration).

The **preferred** format for delivering the results is ASCII text files organized as follows:

Possibly several header lines here (starting with "#" as leading character)
f [Hz], SPL [dB$_{1/1}$] at position 1, SPL [dB$_{1/1}$] at pos. 2, SPL [dB$_{1/1}$] pos. 3, … **for source at 30 m**
f_1 $SPL_{1,P1}$ $SPL_{1,P2}$ $SPL_{1,P3}$ … $SPL_{1,PN}$
f_2 $SPL_{2,P1}$ $SPL_{2,P2}$ $SPL_{2,P3}$ … $SPL_{2,PN}$
…
f_Q $SPL_{Q,P1}$ $SPL_{Q,P2}$ $SPL_{Q,P3}$ … $SPL_{Q,PN}$

f [Hz], SPL [dB$_{1/1}$] at position 1, SPL [dB$_{1/1}$] at pos. 2, SPL [dB$_{1/1}$] pos. 3, … for source at **100 m**
f_1 $SPL_{1,P1}$ $SPL_{1,P2}$ $SPL_{1,P3}$ … $SPL_{1,PN}$
f_2 $SPL_{2,P1}$ $SPL_{2,P2}$ $SPL_{2,P3}$ … $SPL_{2,PN}$
…
f_Q $SPL_{Q,P1}$ $SPL_{Q,P2}$ $SPL_{Q,P3}$ … $SPL_{Q,PN}$

f [Hz], SPL [dB$_{1/1}$] at position 1, SPL [dB$_{1/1}$] at pos. 2, SPL [dB$_{1/1}$] pos. 3, … for source at **300 m**
f_1 $SPL_{1,P1}$ $SPL_{1,P2}$ $SPL_{1,P3}$ … $SPL_{1,PN}$
f_2 $SPL_{2,P1}$ $SPL_{2,P2}$ $SPL_{2,P3}$ … $SPL_{2,PN}$
…
f_Q $SPL_{Q,P1}$ $SPL_{Q,P2}$ $SPL_{Q,P3}$ … $SPL_{Q,PN}$

[end of file – More “blocks” can be added if more source locations are calculated (see details below)]

where Q is the number of considered frequencies (Q = 9), and P1, P2, … to PN denotes the receptor positions number 1 to number N for the different test-cases. If more source locations are considered (i.e. in TC1.12 and TC1.13), the files can be extended by increasing the number of “blocks” (1 block includes all frequencies and all receiver positions for one single source location). The actual source position for each block should be clearly indicated in the comment lines starting with a leading character “#”.

The output files should be preferably be named “tcX_NAME.dat” where:

- “X” stands for the test-case number (1.0 to 1.13) as defined earlier in this document.
- Finally, “NAME” is the name of the institution delivering the results. Note that if the participant/institution deliver results with different propagation models, these should be made clear with appropriate names or acronyms here.

If a different file content format and/or file name convention are used, please provide a detailed description about how the results should be interpreted. In addition, note that ASCII text files are strongly preferred, but MS-Excel files are also accepted.

Timing for delivery of results

The results would ideally be provided on:

- *September/October, 2022 ???*

References

[Bolin2009] Bolin K., Boué M., and Karasalo I., ”Long range sound propagation over a sea surface”, J. Acoust. Soc. Am., Vol. 126, No. 5, pp. 2191-2197 (2009).

8 WP3 / Annex 5 - Conference proceedings on noise propagation codes benchmark on flat terrain

Comparing Wind Turbine Noise Measurements to Multiple Sound Propagation Models

Susanne Könecke[1], Franck Bertagnolio[2], Karl Bolin[3], Erik Thysell[4], Tobias Bohne[1], Raimund Rolfes[1]

[1] *Leibniz University Hannover - Institute of Structural Analysis/ ForWind, Email: s.koenecke@isd.uni-hannover.de*

[2] *Technical University of Denmark - Department of Wind Energy*

[3] *KTH Royal Institute of Technology Stockholm, Engineering Mechanics*

[4] *FORCE Technology*

Introduction

Wind TCP Task 39 of the International Energy Agency (IEA) aims to accelerate progress in the technology of quiet wind turbines and to improve the understanding and practices for noise emissions, their propagation and perception by residents. Work package 3 deals with the propagation of wind turbine noise. Here, different models are compared with each other along with measurement data [1]. The first results of these comparisons are presented in this article. In the beginning, the measurements and the individual models, namely WindSTAR, Nord2000 and the models of the KTH Royal Institute of Technology (KTH) and the Leibniz University Hannover (LUH), are briefly presented. The models are then compared regarding individual attenuation factors and post-processing steps. Finally, the models are validated using two sets of measurement data.

Measurements

As part of the project "WEA acceptance", extensive measurements were carried out in the area of wind turbines to validate a sound propagation model. Acoustical, meteorological and wind turbine operational data were acquired under different environmental conditions. By processing and analyzing the measurement data, ten validation cases and respective input parameters for sound propagation models were derived. In the validation cases, different propagation directions were considered. The measurements, the derivation of the input data for models and all validation cases and their application for model validation are presented in [2]. The measured data used in the validation are freely accessible [3].

In this contribution, case 1 and 3 from the validation cases are used. The data of those cases originate from a measurement campaign performed in a wind farm in northern Germany. The landscape is flat and grassy and, therefore, represents a simple propagation scenario. The measurement environment and the position of the measurement instruments are shown in Fig. 1. As can be recognized, several wind turbines are located in the area of the acoustic measurements. However, for the validation cases, only one turbine is operating.

During the campaign, data were collected from three acoustic measurement stations, capturing sound pressure levels, 1/3 octave bands, and audio samples at a sampling rate of 51 kHz. Synchronously, comprehensive meteorological measurements were conducted to characterize the lower atmosphere. A 100-meter-high measuring mast, situated permanently within the wind farm, continuously monitored temperature, humidity, wind speed, and wind direction at various heights. Moreover, operational data from wind turbines close to acoustic measurement stations were gathered. For more information on the measurements, see [2] and [4].

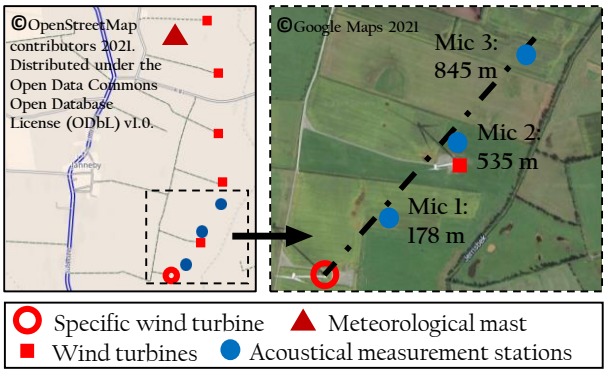

Figure 1: Overview map of the wind farm and measurement plan including the positions of devices.

Prediction Models

In [5], the sound pressure level L_p at the place of immission is formulated as a function of the frequency f:

$$L_p^n(f) = L_W^n(f) \underbrace{- 10 \cdot \log 4\pi (R^n)^2 - \alpha_L(f) \cdot R^n + \Delta L^n(f)}_{\textit{Attenuation terms}}. \quad (1)$$

Here, attenuation terms are subtracted from the sound power level L_W^n of the source n. The attenuation terms contain the geometrical spreading (first term) and the air absorption (second term), both dependent on the distance to the source R^n. Furthermore, the air absorption relies on the atmospheric coefficient α_L, which can be calculated as a function of frequency, temperature and humidity. The last attenuation term ΔL^n encompasses the sound propagation loss due to ground effects, atmospheric refraction, and scattering. ΔL^n can be determined using different approaches.

In this work, four approaches are compared - the models of the universities KTH and LUH, WindSTAR from the Technical University of Denmark (DTU) and the Scandinavian engineering model Nord2000.

The LUH and KTH model as well as WindSTAR are based on parabolic equation methods. The LUH model is based on the Crank Nicholson Parabolic Equation (CNPE) method [5]. In WindSTAR, the CNPE-method was adapted to consider non-uniform terrain following

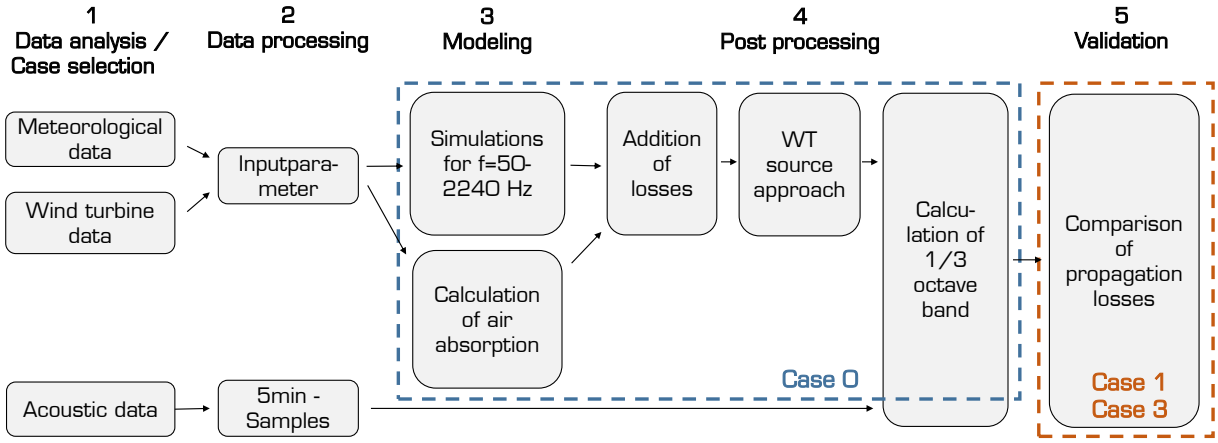

Figure 2: Procedure for validating a sound propagation model with wind turbine noise measurement data.

the work of [6]. This method is called Generalized Terrain Parabolic Equation (GTPE). In the KTH model, the Beilis-Tappert Parabolic Equation (BTPE) method is applied. Here, fourier-based algorithms are used so that long distances can be calculated with low computing resources. The PE-methods mentioned have many similarities, but also differences with regard to their numeric implementations. A comprehensive comparison of the GTPE- and BTPE-method is performed in [7]. Lastly, Nord2000 is a curved ray-tracing-based model.

To model a wind turbine as a source, the approach outlined in [8] is used. In a two-dimensional field, three point sound sources are located at hub height h and at $\pm 85\%$ of the rotor length l:

$$h_s = h \pm 0.85\, l. \tag{2}$$

This simplified representation of a wind turbine entails one simulation for each sound source [8]. Assuming that the point sources are incoherent, the simulation results are logarithmically summed afterwards.

Procedure

The validation procedure is visualized in Fig. 2. Validation cases were selected based on an analysis of the acoustic, meteorological and turbine-specific measurement data. To obtain the acoustic validation data, 5 minute samples were examined in detail (see [2]). The input parameters for the models were derived from meteorological measurements and turbine-specific data. Regarding the individual validation steps, first of all the atmospheric attenuation terms are determined and the additional attenuation are calculated using the models mentioned the previous section. Here, frequencies from 50 to 2240 Hz are considered in 5 Hz steps. In the post-processing, the calculated losses are added, the wind turbine source approach is applied and finally the 1/3 octave bands are calculated.

In this contribution, a very simplified case 0, characterized by the absence of wind, is used to check the determination of the air absorption and the excess attenuation as well as the post-processing of the modeled data, i.e. the complete validation chain. Model data are then compared with measured data. Here, cases 1 and 3 in [2] are considered, which differ in the direction of sound propagation. The effective sound speed profiles of cases 0,1 and 3 are shown in Fig. 3.

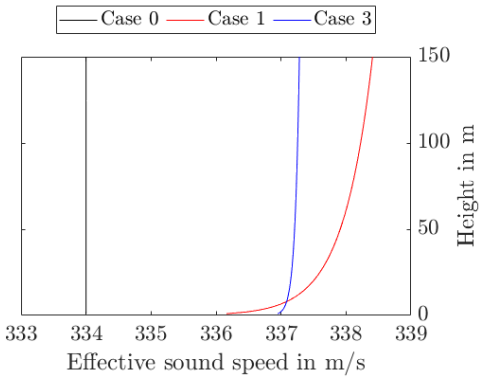

Figure 3: Profiles of effective sound speed for case 0,1 and 2.

It is important to note that different rotor lengths were considered in the model and measurement data. The turbine in the field has a rotor diameter of 114 m. In the modeling, a rotor diameter of 93 m was used. However, the following investigations show that the effects are not decisive for the general results.

Comparison - Case 0

In case 0, the effective sound speed is constant over the height. First, the excess sound losses $\Delta L^n(f)$ from equation 1 were calculated with a monopole sound source at hub height, i.e. at a height of 119 m, using the PE methods for 1/3 octave center frequencies. In Fig. 4 A, the calculated propagation loss between 535 and 845 m is shown. The Delany and Bazley model [9] with a flow resistance of 200 $kPasm^{-2}$ was selected as the standard ground model. The results of the three PE methods agree very well. If the Miki ground model [10], which is an extension of Delany and Bazley, is used, slight deviations are visible. In addition to $\Delta L^n(f)$, the calculation of atmospheric air absorption is verified. The LUH model and WindSTAR use the method of [11]. A comparison of the results with DIN ISO 9613-2 is shown in Fig. 4 B, where the calculated atmospheric attenuation is plotted for 1/3

octave center frequencies between 535 and 845 m. The calculated attenuation values agree.

Finally, the validation chain shown in Fig. 3 was checked. Here, only the final result is presented. In Fig. 4 C, the propagation losses between 535 and 845 m calculated with the LUH model and WindSTAR are plotted. All source heights and frequencies, i.e. all frequencies from 50 to 2240 Hz in 5 Hz steps, as well as all validation steps, i.e. the addition of the losses, the application of the wind turbine source and the calculation of 1/3 octave bands are taken into account in the calculation. The results agree well so the complete chain was successfully checked using the simplified case 0.

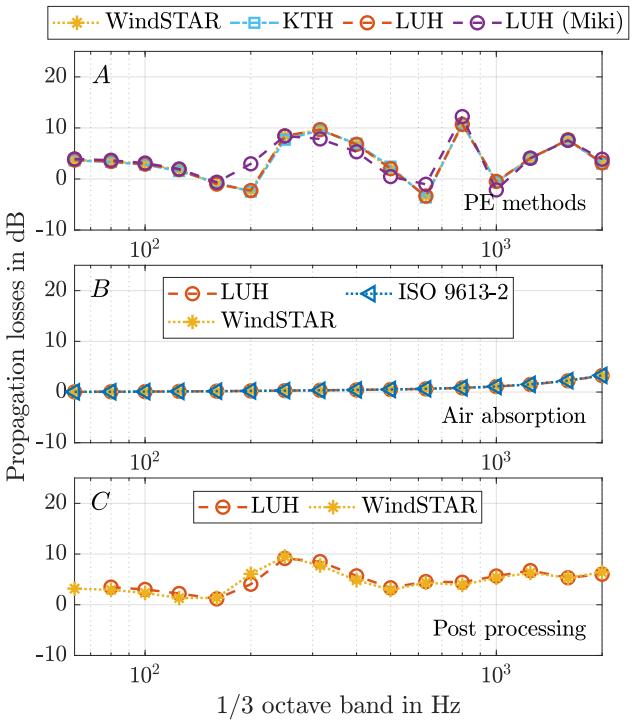

Figure 4: Comparison of modeled sound propagation losses per 1/3 octave band for case 0. **A**: Comparison of the results obtained with the different PE methods. **B**: Comparison of calculated air absorption values. **C**: Comparison of the results considering the complete validation chain shown in Fig. 3.

Comparison - Case 1

Case 1 is characterized by light downwind conditions and a slightly stable atmosphere. In Fig. 5 A and B, the comparisons of modeled and measured propagation losses per 1/3 octave band between 178 and 535 m, respectively, between 178 and 845 m, are shown. Since there is an angle restriction of 30 in the PE methods, a comparison of the propagation losses between 535 and 845m is also given in Fig. 5 C.

Two results are shown for the WindSTAR model - one for a rotor diameter of 93 m and one for a diameter of 114 m. The deviations of the calculated losses are small, so that a qualitative comparison between measurement and model data is possible - even if different rotor diameters have been taken into account.

If the microphone at a distance of 178 m is used as a reference (Fig. 5 A and B), a good agreement between modeled and measured data is achieved. The broad propagation peaks caused by interference are well reproduced by the models. With regard to the model results of WindSTAR, the first interference peaks is shifted towards lower frequencies by a one 1/3 octave band. Nord2000, in particular, predicts the losses between 178 and 845 m well (Fig. 5 B). The predicted losses are at the same level as the measured ones. At greater distances, the losses generally increase with greater frequency. This is due to the frequency-dependent air absorption. Despite the angle restriction, the LUH model and WindSTAR perform well at short distances. The KTH model does not provide meaningful results at distances of 178 m, so these are not shown in Fig. 5 A and B.

A less good agreement between the measured and modeled data is observed when looking at the propagation losses between 535 and 845 m (Fig. 5 C). The peaks modeled are shifted to lower frequencies. As a result, the level of modeled losses in the mid-frequency range (200-500 Hz) is 2 to 5 dB below the measured data. The KTH results show more pronounced interference peaks at 200, 400 and 630 Hz.

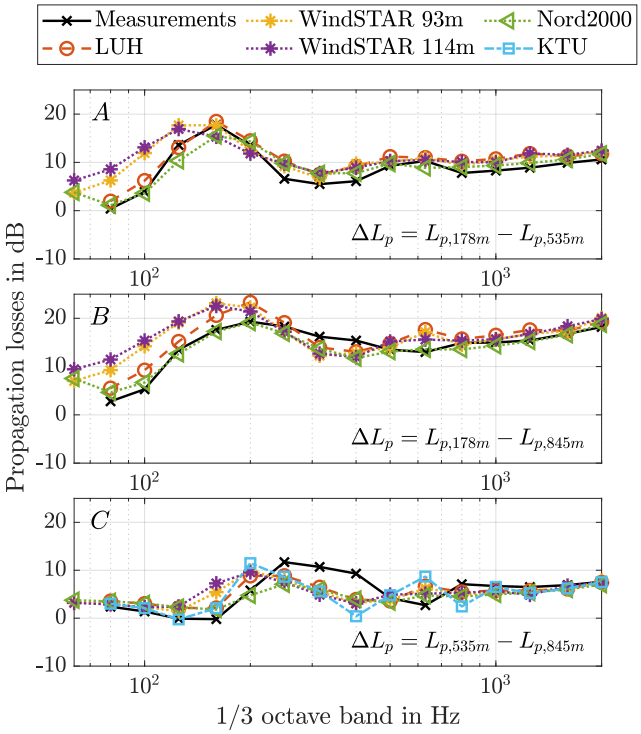

Figure 5: Comparison of measured and modeled sound propagation losses per 1/3 octave band for cases 1.

Comparison - Case 3

Case 3 is characterized by crosswind-downwind conditions and a moderately stable atmosphere. In Fig. 6 A to C, the propagation losses per 1/3 octave band between given distances are presented.

In Fig. 6 A and B, where the first microphone at 178 m is taken as reference, the agreement between modeled

and measured data above 300 Hz is good. As expected, the losses are higher with increasing frequencies. Below 300 Hz, the models predict higher losses. Here, the measured data is 3-8 dB below the modeled losses. In addition, the measured values show distinct peaks, for example in Fig. 6 A at 160 and 500 Hz. The models do not reproduce these peaks. In contrast, the agreement of the modeled and measured propagation losses between 535 and 845 m is better (Fig. 6 C). Especially with the LUH model and WindSTAR, the measured losses are modeled very well. At approx. 250 Hz, Nord2000 predicts 2-3 dB lower losses. As before, the results of the KTH model display strong interference.

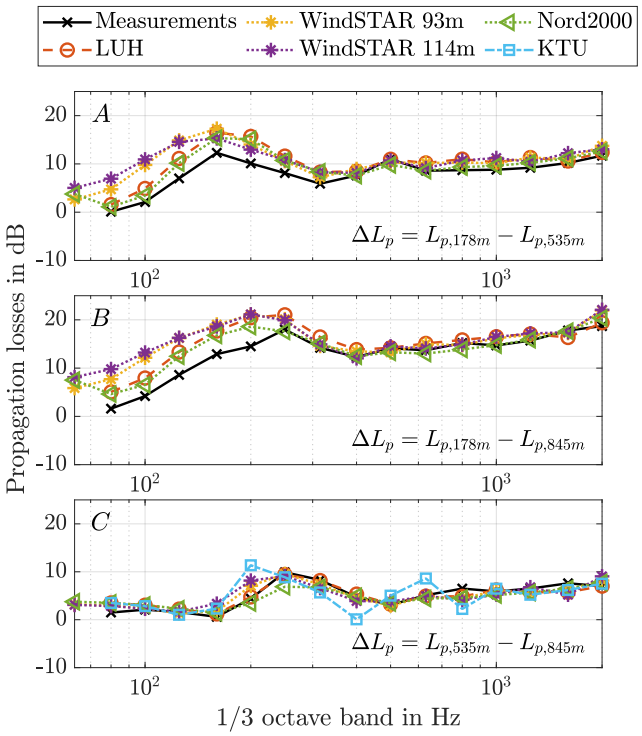

Figure 6: Comparison of measured and modelled sound propagation losses per 1/3 octave band for cases 3.

Conclusion and Outlook

In this contribution, a first comparison between measurement data and different models for predicting the sound propagation of wind turbines was shown. Here, the models of the LUH and the KTH, WindSTAR from the DTU and Nord2000 were applied.

Using a simple case characterized by a constant effective sound speed over height, the calculated attenuation terms and the validation chain were first checked. The individual steps were successfully verified for the LUH model and WindSTAR. The measured and modeled propagation losses were compared using two cases characterized by light downwind and crosswind-downwind conditions. A generally good agreement between measured and modeled data was achieved. The results of the KTH model showed higher dynamics at the 200, 400 and 630 Hz. These interference peaks are most likely an artifact of the way the ground reflection is treated.

In addition to the two cases, further propagation directions will be considered in the future. Here, in particular the comparison of situations with upwind is of interest. The measurement data used for the comparison was recorded in a flat grassy landscape in northern Germany. As part of the Wind TCP Task 39, models will be compared with measurement data from a complex terrain.

References

[1] Wind TCP Task 39 of the International Energy Agency, accessed on 4.4.2024 URL: `https://iea-wind.org/task39/`

[2] Könecke, S.; Hörmeyer, J.; Bohne, T.; Rolfes, R. (2023): A new base of wind turbine noise measurement data and its application for a systematic validation of soundpropagation models. Wind Energ. Sci., 8, 639–659. `https://doi.org/10.5194/wes-8-639-2023`

[3] Könecke, S.; Hörmeyer, J.; Bohne, T.; Rolfes, R. (2021): Dataset: Wind Turbine Sound Propagation Data for the Validation of Models. `https://doi.org/10.25835/0012136`

[4] Martens, S.; Bohne, T.; Rolfes, R. (2020): An evaluation method for extensive wind turbine sound measurement data and its application. Proceedings of Meetings on Acoustics, Acoustical Society of America (41). `https://doi.org/10.1121/2.0001326`.

[5] Salomons, E. M.(2001): Computational Atmospheric Acoustics, Springer Science+Buisness Media B.V., Dordrecht, New York. `https://doi.org/10.1007/978-94-010-0660-6`.

[6] Sack, R. A.; West, M (1995): A parabolic equation for sound propagation in two dimensions over any smooth terrain profile: The generalised terrain parabolic equation (GT-PE), Applied Acoustics, Volume 45, Issue 2, Pages 113-129.

[7] Nyborg, C. M.; Bolin, K., Karasalo, I.; Fischer, A. (2023): An inter-model comparison of parabolic equation methods for sound propagation from wind turbines, J. Acoust. Soc. Am. 154, 1299–1314. `https://doi.org/10.1121/10.0020562`.

[8] Barlas, E.; Zhu, W. J.; Shen, W. Z.; Kelly, M. (2017); and Andersen, S. J.: Effects of wind turbine wake on atmospheric sound propagation, Appl. Acoust., 122, 51–61. `https://doi.org/10.1016/j.apacoust.2017.02.010`.

[9] Delany, M. E.; Bazley, E. N. (1970): Acoustical properties of fibrous absorbent materials, Appl. Acoust., 3, 105–116.

[10] Miki, Y. (1990): Acoustical properties of porous materials – Modifications of Delany-Bazley models, Journal of the Acoustical Society of Japan, 11, 19–24.

[11] Bass, H. E.; Sutherland, L. C.; Zuckerwar, A. J.; Blackstock, D. T.; Hester, D. M. (1995): Atmospheric absorption of sound: Further developments, J. Acoust. Soc. Am., 97, 680–683.

IEA Wind Task 49
Final Technical Report

APPENDIX - WP4
Assessing and Managing the Noise Effects on Health, Wellbeing and Consent

APPENDIX - WP5
Characterising Non-Noise Influences on Perception and its Effects

Contents

1 Introduction **2**

2 Review article **2**

3 WPs 4 and 5 / Annex 1 - Summary of WPs 4 and 5 online discussions **3**

1 Introduction

WPs 4 and 5 focus on acceptance and psychological aspects related to wind turbine noise.

In this document, the output documents from this WP are provided.

2 Review article

A number of meetings and workshops were held during Phase 2 of the Task 39 period. A summary of the discussions was presented at the WTN 2023 conference, together with an associated conference paper. The latter can be found in the Section 3/Annex 1.

3 WPs 4 and 5 / Annex 1 - Summary of WPs 4 and 5 online discussions

INCEEUROPE

10th International Conference
on
Wind Turbine Noise
Dublin – 21st to 23rd June 2023

Socio-psychological effects of wind turbine noise: Research activities of IEA Wind TCP Task 39 (Work Packages 4 & 5)

E. A. King, University of Galway, Ireland: eoin.king@universityofgalway.ie
Eugene McKeown, University of Galway, Ireland
Denis O'Hora, University of Galway, Ireland
Lars Sommer Søndergaard, Department of Acoustics, Noise and Vibrations, FORCE Technology, Denmark: lss@forcetechnology.com
Erik Thysell, Department of Acoustics, Noise and Vibrations, FORCE Technology, Denmark: erth@forcetechnology.com
Tom Cronin, Danmarks Tekniske Universitet (DTU), Denmark
Daphne Schössow, Leibniz University Hannover, Germany: schoessow@ikt.uni-hannover.de
Stephan Preihs, Leibniz University Hannover, Germany: preihs@ikt.uni-hannover.de
Jürgen Peissig, Leibniz University Hannover, Germany: peissig@ikt.uni-hannover.de
Gundula Hübner, Martin-Luther-University Halle-Wittenberg + MSH Medical School Hamburg, Germany: gundula.huebner@psych.uni-halle.de
Johannes Pohl, Martin-Luther-University Halle-Wittenberg + MSH Medical School Hamburg, Germany: johannes.pohl@psych.uni-halle.de
Florian Johannes Yanic Müller, MSH Medical School Hamburg, Germany: florian.mueller@medicalschool-hamburg.de
Esther Blumendeller, University of Stuttgart, Germany: blumendeller@ifb.uni-stuttgart.de
Niels Adema, Hanze University of Applied Sciences Groningen, The Netherlands: ni.c.adema@pl.hanze.nl

Summary

This paper presents a report of some of the activities of the International Energy Agency's (IEA) Wind TCP Task 39. By identifying best practices in an international collaboration, Task 39 hopes to provide the scientific evidence to inform improved regulations and standards, increasing the effectiveness of quiet wind turbine technology. Task 39 is divided into five separate work packages, which address the broad wind turbine noise topic in successive steps; from wind turbine noise generation (WP2), to airborne noise propagation over large distances (WP3). The assessment of wind turbine noise and its impact on humans is addressed in WP4, while WP5 is dealing with other aspects of perception and acceptance, which may be related to noise. All WPs contribute to a dedicated Work Package on dissemination (WP1). This paper provides an update

of activities primarily associated with the socio-psychological aspects of wind turbine noise (WP4 and WP5). Through the consideration of a wide variety of factors, including measurement technologies, auralisation and psychology, the effects on noise perception, annoyance and its impact on wellbeing and health is being further investigated. This paper presents a discussion of the activities of each member country and highlights some of the key research questions that need to be further considered.

1. Introduction

The IEA Wind Technology Collaboration Programme (TCP) is an international co-operation of 23 countries and sponsor members that share information and research activities to advance wind energy deployment. The goal of IEA Wind TCP Task 39 is to mitigate the generation of negative wellbeing, prevent health effects and consent effects by consolidating the understanding of wind turbine sound emission, propagation and noise perception, in order to accelerate the development and deployment of quiet wind turbine technology.

The integration of wind turbines in the energy system is subject to several environmental, societal and regulatory constraints. An important impact of wind turbines on the community derives from the emission of wind turbine noise. In many jurisdictions, there are concerns about the potential impacts of wind turbine noise on health and wellbeing. Perceptions of wind turbine noise can also negatively affect societal acceptance, a key to the successful adoption of new technologies, both at the local and global levels.

Developing noise mitigation technologies and recommending best practices for regulatory and siting processes is regarded as an important step toward public acceptance. IEA Wind TCP Task 28 (on the Social Science of Wind Energy Acceptance) has advanced the potential for enhanced community engagement to address that particular issue. One goal of Task 39 is to work with Task 28 to align research to reduce the non-acoustic influences on wind turbine acceptance. This combination of effort should eventually facilitate the wider deployment of wind energy. Work to increase the collaboration between these Tasks is ongoing.

The Task 39 work programme is summarised in Figure 1 and includes 5 Work Packages. The overall approach is to address the broad wind turbine noise topic in successive steps, from wind turbine noise generation (WP2), to airborne noise propagation over large distances (WP3). The assessment of wind turbine noise and its impact on humans is addressed in WP4, while WP5 is dealing with other aspects of perception and acceptance which may not be related directly to noise itself. Cross-cutting topics (e.g. amplitude modulation, low-frequency noise, etc) can be used as vectors for interactions between engineering and social/psychological sciences. WP1 is about dissemination and will be also considered in each of the WPs.

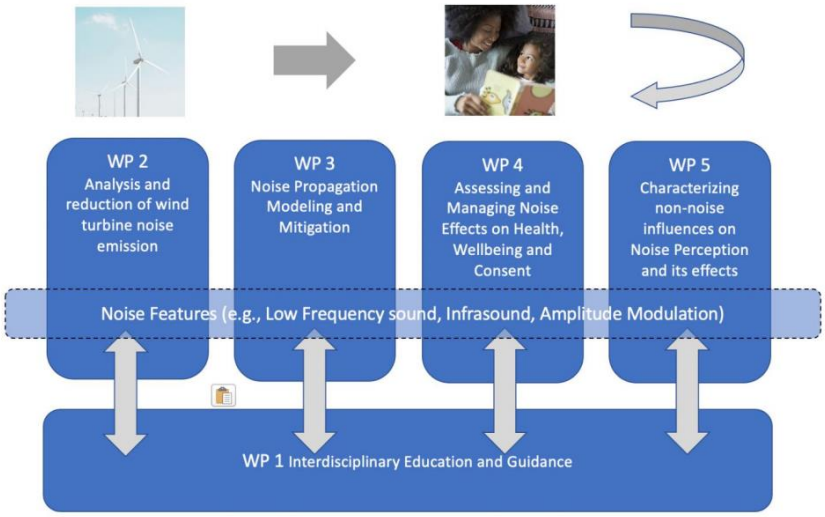

Figure 1: Task 39 Work Programme

Task 39 was initiated in October 2017 and its 1st Phase officially finalised after 3 years at the end of 2020. Phase #2 was approved by the Executive Committee around mid-2021, and a 2nd Phase kick-off meeting was held in September 2021. While the 1st Phase concentrated on engineering models, in the 2nd Phase, the objective is to propose a work programme with a more balanced approach for addressing both engineering and socio-psychological aspects.

1.1 Goals of Task 39 WP4

This WP includes a programme of activities designed to assess the contribution of wind turbine sound to noise perception, annoyance and the effects of these on health, wellbeing and consent. Proposed activities in this task include both lab and field-based psycho-acoustic annoyance testing as well as exploring the possibility of using auralization and stimulus synthesis in annoyance assessments.

1.2 Goals of Task 39 WP5

Social acceptance of wind turbines is driven to some extent by noise produced by wind turbines, but there is evidence of an effect in the reverse direction. That is, sensitivity to wind turbine sound/noise[1] may be driven partly by social acceptance with lower acceptance driving greater sensitivity to such noise. These complex iterative interactions require detailed research to investigate and interactions with Task 28 are likely to be a great benefit to this activity. Regulations in some countries impose a 'penalty' on audible characteristics of wind turbine sound such as tonality. Development of penalty schemes for amplitude modulation is ongoing. Such penalty schemes are predicated on the concept that annoyance is related to a sound level (measured in decibels). A further step assumes that a penalty in decibels can equate the annoyance of a sound with an audible feature with a higher sound level without the audible feature. The annoyance concept is a complex issue, and an investigation is required to validate this principle and estimate penalties if appropriate

2. Activities of Task Participants

WPs 4 and 5 activities have been ongoing since March 2022, with an online meeting gathering experts from different scientific horizons (engineering, noise assessment, psychology). It was

[1] The terms 'noise' and 'sound' are often (incorrectly) used interchangeably. Indeed in preparing this paper we considered the difference between objective 'sound' and perceived 'noise'.

highlighted at an early point that the group might need develop an efficient knowledge exchange program, so experts from different backgrounds could communicate effectively. For example, annoyance is an important concept to both fields, but depending on one's background the discussions on annoyance might deviate into one field. To address this issue, a seminar featuring presentations from experts in both Engineering and Psychology was held, and followed by an open discussion forum. Early meetings also indicated a desire to develop an effective knowledge sharing platform, and it has been proposed that this will be through a shared working documents (hosted on the Open Science Framework) to facilitate the joint definition of technical concepts (from multiple fields). These actives are ongoing and are informed/supported by the collaborative activities of partners, described below.

2.1 Denmark

The department of Acoustics, Noise and Vibration at FORCE Technology focus on some of the unanswered questions from the DecoWind project in the EUDP project "Participation to IEA Wind Task 39" (grant 134-21022). DecoWind was a 3-year Danish research project whose goal was to devise advanced control strategies for wind turbines and farms for minimizing their acoustic impact. It was a collaboration between FORCE Technology, DTU, Siemens-Gamesa Renewable Energy, and EMD International.

In Denmark and several other countries noise is regulated as absolute levels, hence the audibility of the noise source is not directly handled. In the rural areas some of the common sources of noise is vegetation or waves, which masks other environmental sound/noise sources. The effect of masking from vegetation and/or waves has not been studied in much detail in Denmark. The aim of this work package in the EUDP project is to gather data from vegetation and wave sound/noise and use this to form simple models for both vegetation and wave sound/noise. The models are used to estimate the audibility of wind turbines erected in rural areas, considering both temporal effects, spectral effects and effects of wind turbine size, distance and wind shear.

In parallel, the auralization of wind turbine sound/noise is studied, both in the EUDP project with a focus on auralization of offshore wind turbines, and in a Performance Contract with a focus on the auralization of onshore wind turbines.

Separately, the Science, Technology & Innovation (STI) group at DTU Wind and Energy Systems is working on a project called Co-Green, funded by the Independent Research Fund Denmark, using the case of wind turbine noise to explore how different scientific disciplines understand noise, how and to what extent they work together, and how regulations and policies are impacted by their work. Working with Danish wind farm case studies, the project takes lay knowledge of the environment seriously and considers conventional experts as part of the network surrounding the issue of how wind turbine sound is perceived as noise, and what the regulations do about it. The results of the project are envisaged to help towards a more inclusive and co-created approach to wind turbine siting, and to the subject of wind turbine noise, in particular.

2.2 Germany

The Stuttgart Chair of Wind Energy (SWE) at the University of Stuttgart is involved in the interdisciplinary Project Inter-Wind (grants 03EE2023A-D), together with the Karlsruhe Institute of Technology (KIT), Center for Solar Energy and Hydrogen Research Baden-Württemberg (ZSW) and the MSH Medical School Hamburg (MSH). Within the framework of this project, the relation of meteorological, acoustic and ground motion measurements with annoyance reports from residents of a wind farm in southern Germany is being investigated (see Gaßner et al., 2022; Müller et al., 2023).

Since 2020, three measurement campaigns have been carried out at a wind farm on the Swabian Alb in southern Germany. The SWE is has carried out acoustic measurements. One microphone

was placed close to a wind turbine (WT) of the wind farm, two other microphones outside and inside residential buildings in the municipality at a distance of 1km from the wind farm. In parallel, the KIT assed ground motions, the ZSW added meteorological and operation data from the turbines. A field experiment on how different operations modes result in annoyance mitigation measures is in progress. Findings from the measurement campaigns and the combined data analyses in relation to reported annoyance will be discussed with the IEA Task.

Additionally, in cooperation the Delft University of Technology and the MSH conducted a first acceptance analyse by residents of the Klixbüll test side in northern Germany. This work of linking sound emission of established and airborne wind energy and social acceptance benefits from intensive exchange with the IEA Tasks 28 and 48.

The Institute of Communications Technology (IKT) at Leibniz University Hannover is working on the publication of sound recordings of wind turbines from our former Project WEA-Akzeptanz (Wind Turbine Acceptance) (see Schössow et al., 2022). The collected extensive data set will be published open-access considering the FAIR-principle. Within the dataset there is meteorological, sound pressure and turbine-specific data. The dataset published initially will hold the recordings of one month of three wind turbines, three microphones and one meteorological mast. Spatial audio and 360° videos will be available on request for some days of the measurement campaign and could be used as stimuli in laboratory studies or as ground truth for auralisation purposes.

In terms of laboratory studies in the course of a student thesis the influence of the presentation format of visual stimuli was investigated (Schössow et al., 2023). For this study the presentation of 360° videos on three projection screens surrounding the participant in the real lab, the same situation but build in VR as well as the pure 360° video were chosen as presentation modes. The results from the study show that the annoyance ratings and distance estimation of the turbine are unaffected by the visual presentation mode. However, the overall immersion and feeling of interaction was significantly better for the 360° video than for the two “flat” presentations.

2.3 Ireland

Since Ireland’s first wind farm development in 1992, wind farms have been regulated in terms of noise exposure-response guidelines, in which exposure is measured in terms of a sound pressure level. Since then, the supporting science has improved and the psychoacoustics of wind turbine noise has identified features other than noise that induce annoyance. However, the prevalence and impact of these features on Irish wind farm communities has not been assessed.

In 2022, under the Irish Research Council COALESCE (Collaborative Alliances for Societal Challenges) funding call, the interdisciplinary project ‘Wind Sense’ was commissioned. The COALESCE call was designed to support the development of interdisciplinary and intersectoral collaboration/capacity in the context of national or global challenges. It is hoped awardees would expand their research activities and build the sustainability of their research agenda through enhanced competitiveness for future success in European or international collaborative funding programmes. The Call supports researchers to form new connections and to consolidate existing national and international knowledge networks as part of a challenge-based approach. A challenge-based approach will bring together resources and knowledge across different fields, technologies, and disciplines, including social sciences and the humanities, and indeed beyond academia, into new sectors. A key component of the COALESCE grant is that it is led by a PI from AHSS, but includes a Co-PI from a STEM field. Given the interdisciplinary goals of the Wind Sense project, concerning the psychoacoustics of wind turbine noise, the project aligns with the strategy of the COALESCE call.

The aim of the 'Wind Sense' project, (led by O'Hora and King at the University of Galway) is to generate WTN annoyance maps for Irish wind farms based on novel sound quality models of the prevalence of WTN features around candidate wind farms and the impact of these features on annoyance. Wind turbine noise annoyance maps will be generated for the candidate wind farms and will allow for the development of a national wind turbine noise annoyance map in Ireland, to inform turbine developers and policy makers. The project sees collaboration with IEA Task 39 Members, and activities are ongoing.

3. Key Research Questions

The following key research questions have been identified by Task 39 participants, and might be considered as research topics in need of further interdisciplinary investigation:

- Health vs Well-Being. These terms are often used interchangeably, but they mean different things. For example, stress due to wind turbine noise may result in an elevated stress experience and thus will impact well-being, but this may not result in health issues in every case.
- Annoyance – what is 'annoyance'? The scientific community needs a robust definition for better understanding of annoyance and associated impacts. If the scientific community does not have an accepted definition, then the general public impacted by developments may become irritated, e.g., different understandings result in different amount of strongly annoyed residents (see Hübner et al., 2019).
- Benchmarks. There is some debate on the developments of benchmarks for annoyance; while some standards are under development/revision as well as other factors (such as a technical specification for 'non-acoustic' factors related to annoyance) being considered by ISO Technical Committees, there appears to be no formally accepted benchmarks for annoyance.
- Mitigation measures. There are a limited number of studies that have performed assessments of (validated) mitigation measures (including, for example, any experiments that quantify how many people are less annoyed following mitigation measures). This could be further complicated by varying planning restrictions across countries; for example, oftentimes once wind turbines are operational it is difficult to assess low-noise operations if such measures were not included in the original planning process. It may be that more flexibility is needed in planning processes in order to allow for the assessment of mitigation measures.
- International cooperation. It would be interesting to examine in detail the different approaches to the management and control of wind turbine noise in different countries. For example, Germany has different noise settings during day/night period, but such an approach is not possible in Denmark, while set-back distances can vary widely from country to country. It would be beneficial to perform cross-country comparisons between planning conditions/restrictions to determine the pros and cons of various approaches in practice.
- Set-back distances. It is unclear if set-back distances have a discernible effect on annoyance; contradictive findings exist. When based on GIS-data, it would seem that distance does not have a significant impact (if emission regulations are applied)
- New sources. Innovative technologies (AWE) will lead to new noise sources. The scientific community will need to adapt to these new sources and assess the potential impact on annoyance. For Task 39, this could lead to potential collaborative opportunities with Task 48 (on Airborne Wind Energy).

4. Conclusions

This paper presents an overview of the activities of IEA Wind TCP Task 39 that are primarily associated with the socio-psychological aspects of wind turbine sound/noise (WP4 and WP5). We would encourage industry to consider these aspects in more detail, as any solutions that address socio-psychological aspects will need industry support. There is a real value on engagement and working with communities, both in terms of engaging the community for solutions, but also preparing them for actual impacts.

Task 39 is working on science-based solutions to these issues, but it is recognised that the issues we are trying to address are very much a transdisciplinary issues. These will require collaborative research transcending individual disciplines to construct knowledge beyond the scope of any single discipline.

References

Gaßner, L., Blumendeller, E., Müller, F. J. Y., Wigger, M., Rettenmeier, A., Cheng, P. W., Hübner, G., Ritter, J., & Pohl, J. (2022). Joint analysis of resident complaints, meteorological, acoustic, and ground motion data to establish a robust annoyance evaluation of wind turbine emissions. Renewable Energy, 188, 1072–1093. https://doi.org/10.1016/j.renene.2022.02.081

Hübner, G., Pohl, J., Hoen, B., Firestone, J., Rand, J., Elliot, D. & Haac, T. R. (2019). Monitoring annoyance and stress effects of wind turbines on nearby residents: A comparison of U.S. and European samples. Environment International, 132. (Doi.org/10.1016/j.envint.2019.105090).

Müller, F.J.Y., Leschinger, V., Hübner, G. & Pohl, J. (2023). Understanding subjective and situational factors of wind turbine noise annoyance. Energy Policy, 173, 113361, https://doi.org/10.1016/j.enpol.2022.113361.

Schössow, D., Bergner, J., Preihs, S. & Peissig, J. (2022). Concept for an open database of acoustical wind turbine measurements. Wind Europe Technology Workshop 2022, Brussels.

Schössow, D., Kawczynski, D., Preihs, S., Peissig, J. (2023). Der Einfluss visueller Präsentationsmodi auf die Wahrnehmung von WEA-Stimuli in Probandenstudien. Fortschritte der Akustik - DAGA 2023, 49. Jahrestagung für Akustik, Hamburg.

Bertagnolio, F et all (2022). DecoWind: Development of low-noise and cost-effective wind farm control technology. Inter-noise 2022. https://az659834.vo.msecnd.net/eventsairwesteuprod/production-inconference-public/3889aefd315848d6bf9656a24c0a820d

Søndergaard, L. S. et all (2021). Wind farm neighbourship investigated by a daily app questionnaire combining weather, noise, and annoyance. 9th International Conference on Wind Turbine Noise